Czech University of Life Sciences, Prague

Faculty of Forestry and Wood Sciences

Ph.D. Thesis

"Mapping selected forest structural indicators by means of terrestrial and mobile laser scanning"

Ph.D. Student: Ing. Arunima Singh

Study Programme: Applied Geoinformatics and Remote Sensing in Forestry

Department: Forest Management and Remote Sensing

Supervisor: Ing. Martin Mokroš, Ph.D.

Author's Declaration

I hereby declare that this Doctoral Thesis (Mapping selected forest structural indicators by means of terrestrial and mobile laser scanning) is my own work and quoted only according to the references listed within. Neither part of this thesis has been submitted as fulfillment to award a degree to any other institution. This thesis was written under the guidance of Ing. Martin Mokroš, Ph.D.

I agree to the publication of the thesis according to Act No. 111/1998 Coll. on universities as amended, regardless of the outcome of its defense.

Prague, 2024 Signature……………………

Acknowledgment

I would like to express my gratitude to my supervisor, Ing. Martin Mokroš, Ph.D. for the opportunity and trust in me to work with him. I am grateful for his valuable guidance and support during my doctoral study. My acknowledgment also goes to the Czech University of Life Sciences Prague, particularly IGA (A_21_23), IGA (A_08_23), and Reforest, EVA 4.0, No. CZ.02.1.01/0.0/0.0/16_019/0000803 for financial and material support that made everything possible during my studies. I would also like to extend my gratitude to COST Action CA20118, supported by COST (European Cooperation in Science and Technology), for the support and collaboration opportunity in some of the published articles related to this thesis. The thesis was also supported by the Slovak Research and Development Agency APVV-20-0391.

I am also grateful to all my colleagues for their support.

Annotation

In the last two decades, novel terrestrial-based laser scanning technologies have been introduced for the three-dimensional capture of forest states. These technologies allow us to measure and reconstruct different parts of forest ecosystems in a three-dimensional space on a sub-twig scale. Achievable high accuracy and details provide us with many possibilities for forestry research and practice. However, the accuracy of mapping selected forest structural indicators by means of terrestrial and mobile laser scanning is needed to investigate and understand the benefits of these technologies.

Terrestrial laser scanning (TLS) and mobile laser scanning (MLS) have shown potential in mapping individual tree dimensions (diameter at breast height (DBH), tree height, biomass) of living, standing trees. Automated tools are available for mapping individual trees at maximum accuracy. However, the benchmarking of these tools needs to be done to encompass various output parameters related to the application in forestry. The 100 % tree detection rate using TLS and MLS is also in the queue to be solved, especially concerning the different forest structures and complexity levels. The total time and cost associated with TLS and MLS devices have a lot of impact on the quality and quantity of the data. There is a lack of protocol for the data acquisition and processing using TLS and MLS in the forest ecosystem. Also, TLS has been proven to solve the biomass saturation problem at the plot level by integrating with other datasets.

Therefore, this study focused on different aspects of data acquisition using TLS and MLS. Automated point cloud processing tools were compared, and a user guide and manual were prepared. A methodology was developed to create a database of existing processing solutions and benchmark their accuracy regarding forest parameters extraction. A comparative analysis was also conducted on the TLS and MLS devices. Later, a methodology was developed to showcase the significance of DBH and different tree species. Further analysis was done to overcome the biomass saturation problem with integrating TLS and ALOS PALSAR data and achieved the promising accuracy for above-ground biomass mapping.

Further research is needed to explore more complex forest environments to check the applicability of the developed methodologies on a larger scale. The benchmarking of automated point cloud processing tools needs to be revised timely as new tools will be developed. Other forest structural indicators should be checked with the developed approaches, and further analysis and relations need to be finalized to see the effect of modern technology on forest ecosystem monitoring and management.

Keywords: terrestrial laser scanning, mobile laser scanning, diameter at breast height, tree species, tree height, biomass, occlusion, point cloud.

Table of Contents

List of Figures

List of Tables

List of Abbreviations

DBH: Diameter at Breast Height

TLS: Terrestrial Laser Scanner

MLS: Mobile Laser Scanner

SAR: Synthetic Aperture Radar

ALOS: Advanced Land Observing Satellite

PALSAR: Phased Array Type L-Band Synthetic Aperture Radar

SLAM: Simultaneous Localization And Mapping

RHT: Randomized Hough Transform

RANSAC: Random Sample Consensus

RF: Random Forest

ANN: Artificial Neural Network

Lidar: Light Detection And Ranging

GPS: Global Positioning System

IMU: Inertial Measurement Unit

WGS: World Geodetic System

BA: Bundle Adjustment

LOAM: Lidar Odometry And Mapping In Real-Time

RMSE: Root Mean Squared Error

rRMSE: Relative Root Mean Squared Error

UAV: Unmanned Aerial Vehicle

ALS: Airborne Laser Scanner

Contribution of the thesis

The thesis was contributed to original publications and can be summarized as follows:

1. Paper **I**: LiDAR data fusion for forest observation-A review. http://dx.doi.org/10.1007/s40725-024-00223-7 (Current Forestry Reports).
2. Paper **II** : Novel low-cost mobile mapping systems for forest inventories as terrestrial laser scanning alternatives. http://dx.doi.org/10.1016/j.jag.2021.102512 (International Journal of Applied Earth Observation and Geoinformation).
3. Paper **III**: An approach for tree volume estimation using RANSAC and RHT algorithms from TLS dataset. http://dx.doi.org/10.1007/s12518-022-00471-x (Applied Geomatics).
4. Paper **IV**: Aboveground Forest biomass estimation by the integration of TLS and ALOS PALSAR data using machine learning. http://dx.doi.org/10.3390/rs15041143 (Remote Sensing)
5. Paper **V**: Qualitative analysis of tree canopy top points extraction from different terrestrial laser scanner combinations in forest plots. http://dx.doi.org/10.3390/ijgi12060250 (ISPRS International Journal of Geo-Information).
6. Paper **VI**: Tree Parameter Extraction with iPhone Point Cloud Data Using Algorithms at Multiple Platforms (accepted) https://doi.org/10.1080/01431161.2024.2409996 (International Journal of Remote Sensing)
7. Paper **VII**: A review of point cloud processing software solutions in forest applications http://dx.doi.org/10.1007/s40725-024-00228-2 (Current Forestry Reports).

1. Introduction

1.1 State of the art and motivation

Forest resource information is collected at various scales, i.e., stand level, regional level, and countrywide, to plan and manage various ecosystem services and improve forest management (Toivonen et al., 2023). Potential information on timber harvesting is also important for the regional and forest levels. Also, understanding terrestrial ecosystems functioning and physical changes due to climate change and monitoring leads to the quest for 3D information on forest structure (Verbeeck et al., 2019). Forest structural indicators are measures used to describe the distribution and arrangement of vegetation and the physical attributes within the forest (Korom et al., 2022). The forest structural indicators are tree height, diameter at breast height (DBH), canopy cover, basal area, stem volume, biomass, species composition, etc. Forest structure as a 3D complex can be described in two sections: vertical and horizontal structures. The vertical structure describes the vertical distribution of vegetation in the forest ecosystem. The vertical profile of the forest provides very in-depth information on the inter-relation of forest ecosystems and biodiversity, whereas horizontal structure defines the horizontal profile of the vegetation in the forest ecosystem (Palace et al., 2016).

Forest structural indicators play an important role in the regulation and presence of biodiversity and in maintaining the microclimate of the forest ecosystem. They provide approximately 80% of global terrestrial biodiversity and fundamental ecosystem services to society, such as recreation, climate regulation, and timber (Balvanera et al., 2014). Forest structure also significantly regulates the occurrence and distribution of species and provides breeding sites. Also, it provides resources, niches, and shelter from predators (Melin et al., 2014). However, the more significant number and variability of niches are directly proportional to the presence of a greater diversity of species present in the forest (Stein et al., 2014). Extracting such detailed and fine scale information requires a high precision of measurement.

The measurement of such a large scale and fine scale is critical and time-consuming. The ground sampling method for the reconstruction of 3-D vegetation characteristics is a cumbersome and resource-demanding procedure; furthermore, it may compromise precision due to the possibility of manual measurement errors. However, current remote sensing methods include both active and passive sensors, which provides a possibility to measure the assessment of biodiversity of forests at a large scale (Turner et al., 2003). Light detection and ranging (LiDAR), as an active sensor, provides the measurement of vertical and horizontal vegetation structure of the forest at the landscape scale (Bergen et al., 2009). Previously, the qualitative representation of 3D forest structures was explicitly available. The hand-drawn tree archetypes were used as a representation (Hallé et al., 1978), and the conventional methods for the tree measurements were performed using tools such as calipers and clinometers. The traditional methods are labor-intensive and cumbersome.

Later, the development of the terrestrial laser scanner (TLS) provided 3D information on trees and forests, which provides in-depth information. Initially, the research was focused on tree parameter retrievals, such as tree height and DBH. However, the focus later diverted to tree volumetric assessment and aboveground biomass estimation (Gonzalez de Tanago et al., 2018). Currently, the applications also include the modeling aspects of branch architecture (Lau et al., 2018), habitat assessment (Ashcroft et al., 2014), forest fire modeling, or the quantification of fuel load (Y. Chen et al., 2016).

The forest structural indicators are an inseparable entity in forest management and protection. The ecological insights from the 3D measurements challenge the potential of TLS and mobile laser scanner (MLS). A study by (Verbeeck et al., 2019) showed that TLS can be used as a structural information source to understand the descriptive orientation of the axis of structural traits in woody plants. LiDAR has also been used to profile forests to understand stratification and its role in the balance of the forest ecosystem. LiDAR application is of wide ranges. Starting from habitat selection, such as the specific pattern and ecological niche decided by the mammals in the forest ecosystem. It has also been used to resolve the unsaid truth about the habitat requirements of mammals (Stobo-Wilson et al., 2021). Also, biodiversity population monitoring can be done using TLS. In this regard, a study has been done on butterfly population monitoring (Hristov et al., 2019). Due to pollution, slight changes have been observed in the physiological patterns of the plants and trees. So, (Hofman et al., 2014, 2016) have done modeling of particulate deposition on the leaf and its consequences.

The multi-temporal TLS or MLS data can also provide the 4D data for canopy structural dynamics to understand the canopy structure of the tree. Combining real-time monitoring with spectral information can be used to analyze relationships between structural and functional trait-based analysis (Calders et al., 2020).

The environmental changes can be assessed using continuous monitoring of different ecological indicators, helping to identify actual ecosystem conditions and changes that can potentially lead to irreversible transformation (Dale & Beyeler, 2001; Ratajczak et al., 2018). Here, the role of modern data acquisition technologies has started to be increasingly recognized and appreciated. For example, forest "health" and resilience were correlated with species and structural and functional diversity of the ecosystem (Espelta et al., 2020), and many of these features can be derived using advanced data acquisition methods such as TLS and MLS. The use of TLS and MLS in forestry is a revolution in lidar technology. This technology is more affordable and faster. It can provide autonomous observations which creates a possibility of forest inventory from stand level to regional level. It also identifies the state-of-the-art methods for various applications in ecology and projects on their various current issues and bottlenecks. The Spectral Variation Hypothesis says that spectral heterogeneity over the different pixel units of a spatial grid reflects a higher niche heterogeneity, allowing more organisms to coexist (Rocchini et al., 2021), suggesting an interesting link between remote sensing-based data and ecological properties. The well-recognized relationship between an indicator and indicandum (e.g., the indicated characteristics of biodiversity; Bastianoni et al. (2012)) suggests that, for example, deadwood volume and diversity and saproxylic beetle species richness are closely correlated (Gao et al., 2015). However, options for high-resolution mapping of deadwood parameters remain largely unresolved (Marchi et al., 2018). Therefore, research is required to understand the complexity of the interaction between forest dynamics, ecosystem services, and human well-being (Carpenter et al., 2009).

Generally, three fundamental aspects are considered to shape the adaptation of any new technology. Firstly, the overall time requirement for the data acquisition, equipment cost, and data post-processing. Secondly, the significance of the data collected from the field should be similar, surpass the conventional method, or provide some added advantages. Lastly, the tree attribute information should be precise enough to support the decision-making in forest management (Knoke et al., 2010). There is an intimate relation between these three aspects. The question remains regarding the potential use of MLSs in forest ecosystem applications. But it also has shown the possibility of improving the quality and quantity of the reference data collection in the forest inventories because it is faster and provides a level of detail of tree structure. A thorough literature review was done considering all the sections of this chapter, and the statistics on the number of publications focused on forestry and tree metrics using TLS and MLS are shown in Figure.1 and Figure.2. The keywords used to search in the Web of Sciences are mentioned in Table 1.

Table 1: The Keywords used to search in Web of Sciences

Technology	**Search code**	**Focused area**	**No. of Publication**
MLS	TS = ("mobile laser scann*" OR "personal laser scann*" OR "hand-held laser scann*" OR "backpack laser scann*" OR "backpack lidar" OR " mobile lidar")AND TS= ("forest" OR "tree" OR "forestry")	Forestry	334
TLS	TS = ("terrestrial laser scann*" OR "terrestrial lidar" OR "TLS") AND TS = ("forest" OR "tree" OR "forestry")	Forestry	1637
TLS	(TS = ("terrestrial laser scann*" OR "terrestrial lidar" OR "TLS") AND TS = ("diameter at breast height" OR "dbh" OR "tree height")	Tree metrics	392
MLS	TS = ("mobile laser scann*" OR "MLS" OR "personal laser scann*" OR "hand-held laser scann*") AND TS = ("diameter at breast height" OR "dbh" OR "tree height")	Tree metrics	86

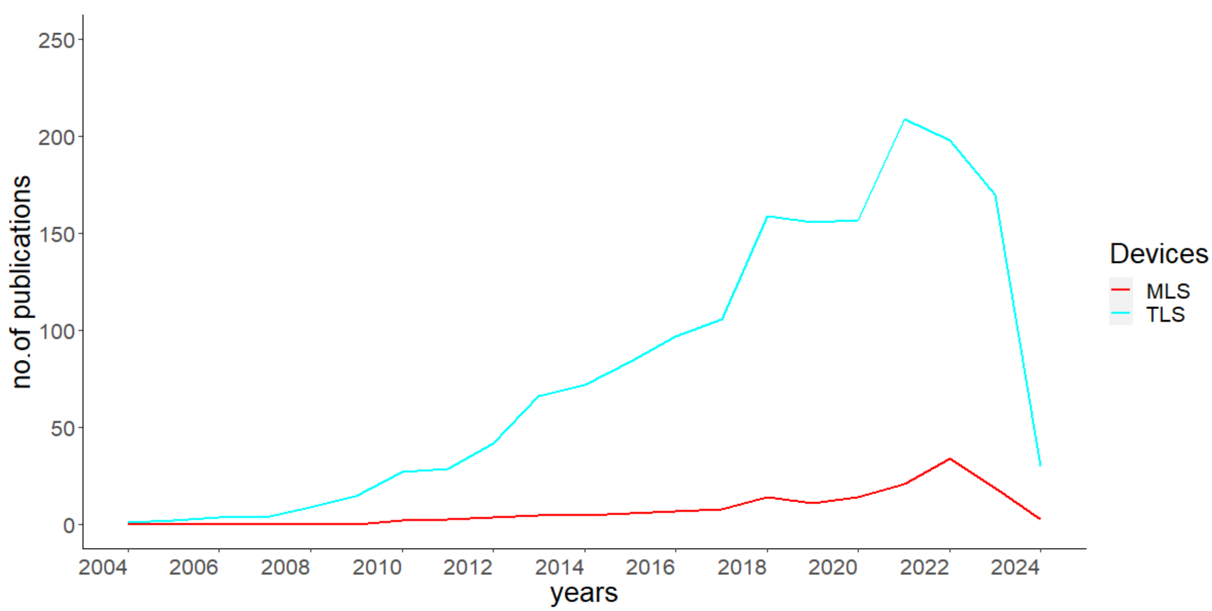

Figure 1: No. of publications in the preceding years between January 2004 to January 2024 focused on forestry using TLS and MLS

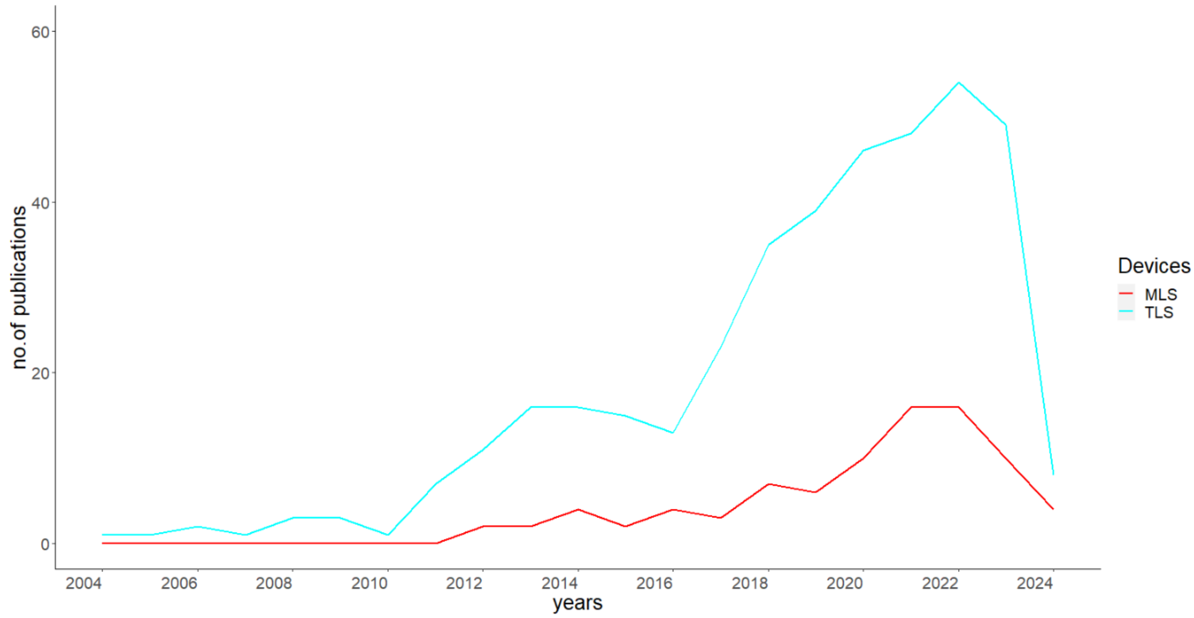

Figure 2: No. of publications in the preceding years between January 2004 to January 2024 focused on tree metrics retrieval in forestry using TLS and MLS

1.2 Hypothesis

The study focused on the following hypothesis:

1. The use of static and mobile laser scanning will significantly advance mainly in the field of mapping trees' positions and dimensions. In contrast, mapping of features such as tree parameters remains understudied.
2. Options for mapping the parameters can be substantially improved by the fusion of different data sources (e.g., point clouds with images)
3. Terrestrial laser scanning will provide more accurate and reliable data with lower estimation errors when compared to mobile laser scanning.
4. Mobile laser scanning will be more efficient during the data acquisition and will provide the required accuracy.

1.3 Objectives

This dissertation aims to develop new methodologies for measuring different trees and stand parameters, which can be instrumental in further forest ecology research. We mainly focus on using Terrestrial and a mobile laser scanner and the fusion of acquired data with other data sources. The following objectives will be addressed:

1. To review existing scientific literature and synthesize the current option for mapping variables of forest parameters using terrestrial and mobile laser scanners and identify the major knowledge gaps.
2. To establish experiments focusing on extraction of individual tree dimensions of living and standing trees from point clouds of terrestrial and mobile laser scanners and fusion with other data sources.
3. To create a database of existing processing solutions and benchmark their accuracy regarding the forest parameters extraction.
4. To explore options for estimating tree heights and diameters, aboveground forest biomass, and other parameters and formulate recommendations for integration into forest practice and research.

1.4 Thesis structure

The structure of the thesis is compiled in the form of chapters. The first chapter is a literature review and consists of an in-depth description of the previous and current work done using TLS and MLS. The second chapter is a methodology that entails brief information on the study areas used in this thesis and a description of the basic conceptual and methodological framework. This chapter also includes an overview of the statistical methods used for the evaluation of the results in all the papers related to this thesis. This chapter is further elaborated in the individual sections where each paper is described in detail. The other chapter includes results, all the papers included as an output of this thesis objectives are mentioned and described in detail sequence. There is another chapter on the discussion; this chapter includes an overall discussion of all the paper outcomes focusing on the key findings, knowledge gaps, and methodology limitations. Furthermore, the thesis also comprises sub-chapters on international collaborations and additional achievements during the study. Lastly, the Conclusion and recommendation is included to summarize the overall concept, findings, and future scope of the thesis.

2. Literature Review

This chapter includes the basic principle of TLS and MLS devices in section 2.1.1, and different data acquisition methods are explained in section 2.1.2. The processing of point cloud data is divided into two subsections; section 2.1.3 describes the pre-processing and data analysis of TLS, whereas the pre-processing and data analysis of MLS is described in section 2.1.4. The post-processing steps are explained in section 2.1.5 and its sub-sections. Thereafter, LiDAR data technology at various scales is explained in section 2.2. Furthermore, an emphasis is done on the LiDAR data fusion with other data; later, it is focused on the potential of synthetic aperture radar (SAR) data fusion with TLS.

2.1 TLS and MLS principle, Sensors, and Systems

TLS is based on the laser range measurement technique and measures its surroundings using LiDAR and angular measurements using the optical beam deflection method to acquire 3D points from the surface of the tree in the forest and other objects. Unlike TLS, MLS is used for mobile data collection fitted with LiDAR, cameras, and other remote sensors. The principle for range detection is based on two principles. The two main techniques involved in the measurement of range using a laser are time-of-flight (TOF) and phase shift (PS). The main difference between these two distance measurement technologies is that PS measures distance more accurately; however, it is subject to noise in the data, whereas TOF provides a greater data measurement range (Małaszek et al., 2022).

In the PS technique, the range is discerned at high frequency through amplitude modulation and the continuous illumination of the laser. In contrast, the TOF measures the range with the precise timing from the pulse time of flight and speed of light. In TOF, the emitted radiation is backscattered and recorded as a single return at the receiver end, but it could be recorded as several returns (single, last, and intermediate) by exceeding the detection threshold. A single return provides less information about the interacted object. In contrast, the multiple returns provide dense point cloud data and information, especially in the vegetation, because the backscattered signal interacted with the target inside or behind vegetation. The signal returns are in discrete form, but they could be digitized at the receiver end resulting in waveform data. The waveform includes additional information on the interaction between the target and the laser pulse concerning the discrete form (Petrie & Toth, 2017).

In MLS, there are terrestrial and airborne laser scanners. Most terrestrial-based laser scanners are enabled with the SLAM (Simultaneous Localization and Mapping). SLAM is explained in detail in section 2.1.1. It offers precise positioning of the scanner in the forest because global navigation satellite system (GNSS) is inaccurate inside the forest. MLS system is often associated with one or more laser scanners, an inertial measurement unit (IMU), and GNSS, which offers the real-time positioning of the scanner (Forsman et al., 2016; Kukko et al., 2017; Pierzchała et al., 2018). Several types of MLS have been used to estimate forest parameters, such as phone-based scanning, vehicle-based scanning, backpack MLS, unmanned aerial vehicle (UAV)-based, hand-held mobile laser scanner, etc.

In hand-held mobile laser scanner (HMLS), various other terms were used, such as hand-held laser scanning (HLS), hand-held personal laser scanner (H-PLS), wearable laser scanning (WLS), or personal laser scanning (PLS) (Gollob et al., 2020). Furthermore, the vehicles need more access due to inaccessible areas in the forest, which hinders data acquisition. This limitation motivates the invention of something that can be carried by humans as operators and referred to as PLS. So, the first PLS was invented and was large and heavy (~30 kg) (Kukko et al., 2012; Liang et al., 2018)There are several HMLS systems available in the market (ZEB1, ZEB-REVO, ZEB-REVO-RT, ZEB-HORIZON) and evaluated in forest conditions.

In backpack MLS, there are different methods for data collection. Hyyppä et al. (2020) demonstrated a method based on a pulse-based 2D laser scanner tilted from the vertical and mounted on a backpack. However, there is a major drawback with MLS, which is mapping the point cloud that has already been mapped in the previous steps, thereby increasing the positioning errors. So, SLAM corrections were also used to reduce positioning errors. Basically, in the forest area, the tree occlusion often deteriorates the GNSS signal and causes an interruption in forest mapping. So, the SLAM problem arises due to the requirement of estimation of the location of the MLS point clouds while mapping in the forest (Shao et al., 2020).

2.1.1 Simultaneous Localization and Mapping (SLAM)

A SLAM is a complex algorithm used for the mapping of an unknown environment and localizing and mapping a device in that environment. SLAM was initially incorporated in robotics; the movement guess was initially based on wheel odometry, and the corrections were made with the help of cameras and lidar sensors (Zheng et al., 2023).SLAM technique was incorporated into the MLS mapping system to compensate for the mapping issues in the forest ecosystems (Guan et al., 2013). There are various types of SLAM algorithms and approaches available, such as Graph SLAM, EKF SLAM, Fast SLAM, Topological SLAM, Visual, 2D LiDAR, 3D LiDAR, and ORB SLAM. Also, the filter-based and graph-based methods are common SLAM techniques. In the filter-based method, the common filters used are the extended Kalman filter (EK) (Kohlbrecher et al., 2011) and the Particle filter (PF) (Grisetti et al., 2007). The examples are Hector SLAM and G-mapping, respectively. The two methods are related and rely on the assumptions of the robot motion model and sensor noise and usually, consider the motion relationship between adjacent data.

There are a few issues with the filter-based methods while violating the assumption and execution of loop closure. There is difficulty in addressing this method. Additionally, it also increases memory consumption and computation. So, another method called the graph method became very popular, which works by combining all the poses of the scanner at different times and executing loop closure and then the elimination of cumulative error is done by optimization of poses. For example, Karto-SLAM (Konolige et al., 2010) and Cartographer (Hess et al., 2016). It also resolves memory consumption and computational issues by combining poses and optimization in real-time. Apart from this, it also has some limitations in providing highly accurate positioning and mapping results which makes it unfit for a mapping environment like forest. However, the bundle adjustment (BA) method has also been widely used to correct SLAM problems. In this method, nonlinear optimization is performed to optimize the features and poses of the scanner simultaneously.

The nonlinear optimization relies on the matched features and produces maps of high accuracy. The lidar odometry and mapping in real-time (LOAM) method is a very good example in this context (J. Zhang & Singh, 2014), which selects the line and plane features on object surfaces that consist of stable and distinct features to estimate the motion of a scanner and obtains highly accurate mapping results indoor and urban scenarios. However, there is uncertainty in the forest mapping because of the presence of highly similar objects, so it is difficult to extract reliable features from the object surface. Also, the scan match can fall into the local optimum due to inaccurate corresponding pairs. Moreover, the challenges are never-ending as another hurdle in SLAM occurs while data acquisition by considering global optimization, and it is challenging to avoid error accumulation. However, there are other methods available that work on multiple loop-closure detections to maintain global positioning accuracy (Mur-Artal et al., 2015). Also, in other studies related to graph-based SLAM to correct the GNSS-IMU trajectory drift, the initial movement guess is made with the trajectory calculated from GNSS and IMU measurements. In this technique, the GNSS maintains the global position accuracy, whereas the IMU provides altitude information, which is helpful for the orientation of the laser scanner. The drift is gradual and can be measured or corrected using the initial trajectory to extract tree stems from the point cloud whenever the trajectory drifts away from the real trajectory that is measured in a short period. The initial trajectory could also have an error, so the trajectory loops enable the correction options as trees are static objects (Kukko et al., 2017).

2.1.2 Data Acquisition Methods

In the TLS instrument scanning mechanism, the instrument scans stepwise in a horizontal and vertical direction. The instrument measures vertically using a fast mirror rotation and slow horizontal instrument movement. The instrument starts the laser beam in a vertical direction from the scanner zenith and rotates to the lowest scanning position below the horizontal plane of the instrument. Then, the instrument scans continuously to the scanner zenith on the other side. The instrument scans at 180° in the horizontal plane on both sides simultaneously. The scanning mechanism and the point cloud of the forest are shown in Figure 3 (Liang et al., 2016).

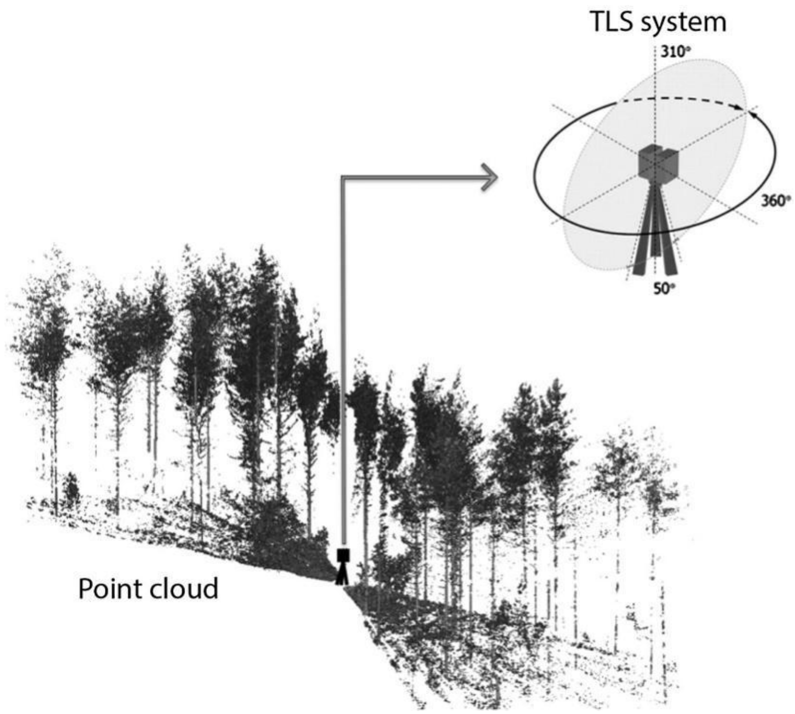

Figure 3: The TLS data acquisition mechanism and point cloud data. Source: (Liang et al., 2016)

TLS has been used to acquire tree attributes and forest parameters. The data acquisition scheme is reliable on the two basic principles, i.e., TOF and PS. The scheme encompasses the three types of data-acquiring methods, i.e., single scan, multi-scan, and multi-single scan, shown in Figure 4. The single scan approach is performed to place the scanner at the center of the plot and acquire the full (360 x 310) view of the plot. In the multi-scan, the scanner is placed at the center and the different corners of the plot to acquire the point cloud at every direction and, therefore, minimizes the occlusion effect. The multi-single-scan approach relies on multiple single scans performed in all plot directions. Acquiring a plot using a multi-scan or multi-single-scan approach leads to very good data quality, but it is time-consuming. All the mentioned approaches are shown in Figure 4.

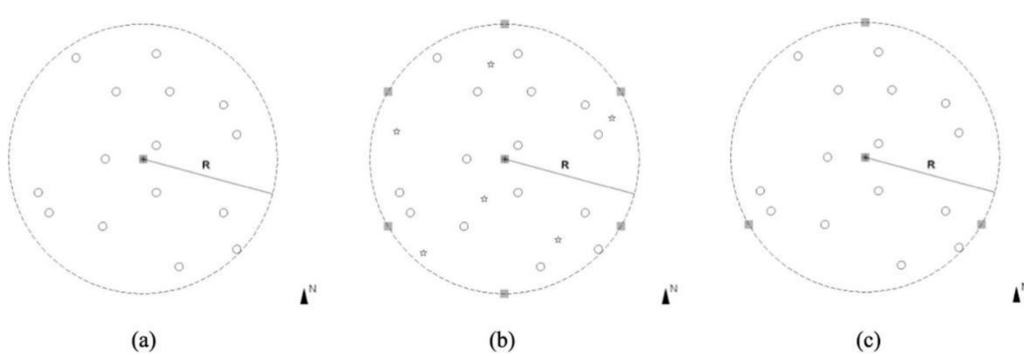

Figure 4: Scanning scheme of the plots (a) single scan approach, (b) multiple scan approach, (c) multi-single scan approach (Liang et al., 2016).

In MLS, the acquisition of 3D data is possibly done by employing several laser scanners mounted on a mobile platform. The main goal of mobile laser scanning is to record the 3D data of object surfaces. The expected requirements could be the high resolution and high accuracy of the registered data, automatic registration of 3D data in a common coordinate system, and time-efficient data acquisition in expanded target areas. The MLS instrument is on-board with IMU or global positioning system (GPS). The IMU or GPS measures the exact position and orientation of the mobile platform within the geodetic system world geodetic system (WGS84). There are two main components of a differential GPS system, a stationary base station and a rover on the mobile platform. It also has at least one laser scanner, providing a 2D line scan mode. The platform should be rigid and shock-absorbing. It could have been mounted with an optional synchronized digital photo camera. The scanning scheme varies depending on the instrument and the type of forest. The most often scanning scheme used is the serpentine which is shown in Figure 5. The main purpose is to reduce the occlusion of the trees and solve the time constraint due to the mobility of the device (Hyyppä et al., 2020b).

Moreover, researchers have used different scanning schemes in previous studies to cover the entire plot and each tree. The serpentine scanning approach by (S. Chen et al., 2019) lasted approximately 5 minutes, including the system initialization. There are alternative approaches have been tested (Bauwens et al., 2016) have acquired an approach to scanning in a circular pattern and took 24 min per plot, and Ryding et al. (2015) acquired a free-walking approach to form a closed loop by starting and ending at the same point. It took them ~4m to complete the plot having a 15 m radius. The average time required to scan plots of 30m, 15m, and 10m was also estimated (Del Perugia et al., 2019). The description of scanning schemes is shown in Figure 5.

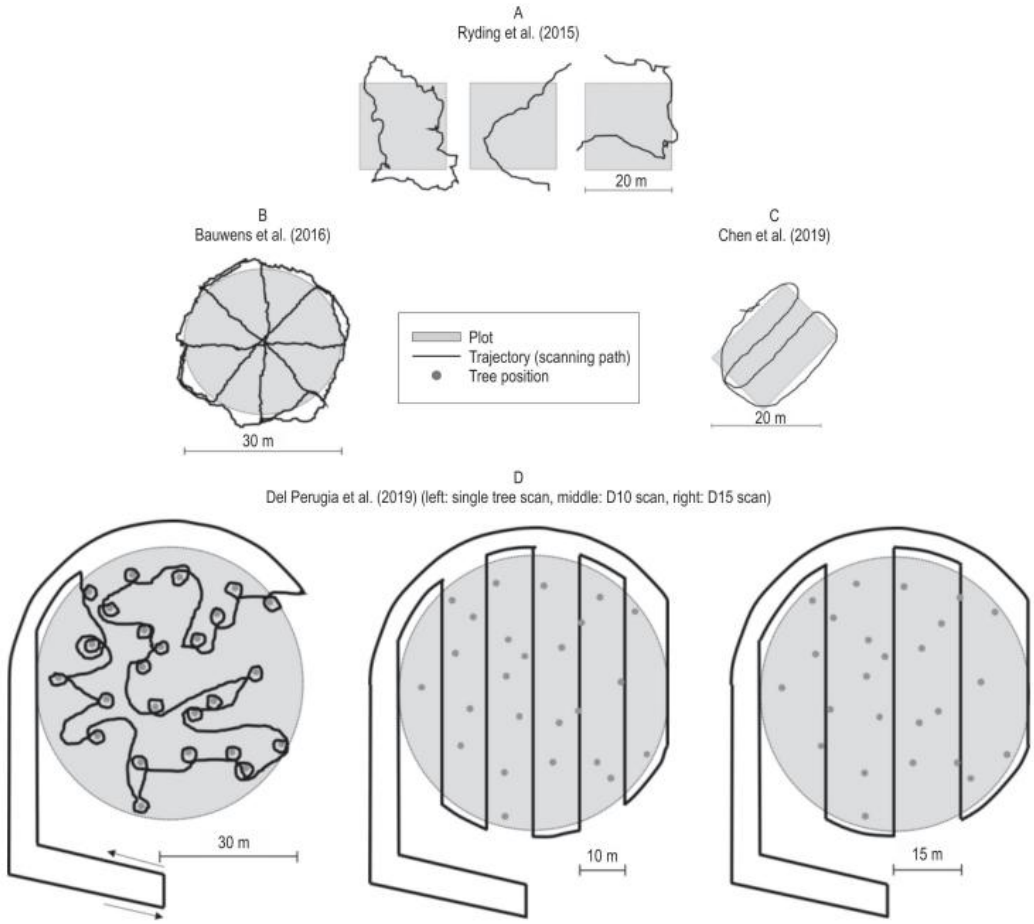

Figure 5: Examples of scanning trajectories acquired by recent studies using HMLS. Source: (Balenović et al., 2021)

2.1.3 Pre-processing and data analysis for TLS

Currently, the hour of need is the automation of the 3D data; due to the large size and time-consuming processing, new and robust algorithms are required to switch to automation in the 3D world from manual dependencies. The need for automating algorithms to extract structural information from an object is equally important, as is sensor development concerning forest monitoring from different perspectives. Generally, the plot is extracted from the merged plot, a co-registered point cloud of multiple scans in different directions. The co-registration is possible because of the available tie-points in different directions. These are highly reflective objects which are easy to differentiate. However, a new range of instruments, such as Leica BLK360 and RIEGL VZi-series, does not require this manual practice of co-registration. They provide onboard registration (Calders et al., 2020). Then, the individual tree is extracted from the merged plot, and noise filtration is done to avoid unwanted objects. Then, all the necessary post-processing is performed accordingly. TLS has also shown good potential in the crown vertical profile model in one study; the crown radius was measured and compared to the reference crown radius and found to be R^2 of 0.93, which shows a great potential to extract information at the crown level using TLS (F. Wang et al., 2023).

2.1.4 Pre-processing and data analysis approach for MLS

The pre-processing and data analysis for MLS is different from the TLS. The co-registration of point clouds is done using a SLAM algorithm where alignment and match of pair scans are done. This process is known as point cloud registration. The data drifting from the real trajectory is maintained in this step using SLAM. Since it is difficult to apply any automated modeling without further geometric improvement (Liang et al., 2012). The graph SLAM optimization method was implemented in detail by (Kukko et al., 2017); the graph represents the features (tree stems) and the trajectory. Furthermore, the positional accuracy of MLS was also tested under the forest canopy, and it was found that the SLAM algorithm integrated with IMU showed a planer positioning error of less than 15 cm and a vertical error of 10-30 cm. This concluded a need for a better GNSS-based global positioning inside the forest (Muhojoki et al., 2024).

2.1.5 Post-processing

Post-processing includes measuring the tree parameters in the forest regions with the Lidar technique, which is explained in the following sections:

2.1.5.1 DTM Generation

The DTM is the 3D representation of terrain elevation on the earth's surface. In the post-processing of Lidar data, the first step is generating DTM, an important information source in forest management planning and inventory. While measuring the forest parameters, the analysis also includes finding the ground level necessary as the reference level in further computation and analysis. DTM is considered the reference level. The generation of DTM is done successfully by using Airborne Laser scanning (ALS), but TLS and MLS are still emerging in this field (Murino & Puppo, 2015). The extraction of DTM in forestry involves several steps. Firstly, the separation of ground and canopy is required before fine DTM extraction in forested terrain. Then, detection of the ground points and interpolation of total ground points from neighboring ground points is done (Xi et al., 2016).

Additionally, different algorithms and methods are emerging using TLS to improve the generation of DTM. The accuracy of DTM in dense forests is questionable, but (Guarnieri et al., 2012) demonstrate the potential of TLS to provide DTM in dense vegetation using multi-target capability. Recently, there has been a trend of the fusion of datasets and the collective use of several devices for the improvisation of the results. So, in this context (Jurjevic et al., 2021) used TLS, hand-held personal laser scanning (PLShh, GeoSLAM Horizon), and other devices for DTM generation. The results proved to achieve < 15 cm of RMSE and a normalized median absolute deviation of <10 cm. Since TLS acquired data with more precision and accuracy, its spatial coverage is limited, which was improvised using MLS. In the other context, to improve the accuracy of stem detection, a voxel-based method was used for the generation of DTM using backpack MLS (Hyyppä et al., 2020). The study (Pirotti et al., 2013) showed that TLS has always been used extensively for the generation of terrain and surface models, since the research in the field of LiDAR started.

2.1.5.2 Automatic Tree reconstruction

The automatic tree reconstruction requires geometrical modeling. So, a single tree is modeled in steps, a small piece of a tree trunk is reconstructed, and the rest is modeled in the direction of the tree growth. Generally, tree modeling approaches include skeleton, circle, cylinder, or another geometric primitive (Liang et al., 2016). In this approach, the 3D structure of the tree is exploited. The software and algorithms are available to do the same. For example, Treeseg is used by (Burt et al., 2019) with a different approach, and they considered the stem points close to the ground instead of dividing it into clusters as a possible tree. Generic point cloud processing techniques such as principal component analysis, region-based segmentation, Euclidean clustering, shape fitting, and connectivity testing were followed to extract the tree. The segmented point cloud is shown in Figure 6. These methods generally require manual intervention and quality control. The more complex the ecosystem is, the more manual assistance will be required.

Moreover, the QSM algorithm can also be used to model the tree point cloud after extracting the tree. However, QSM quality depends on the quality of point clouds. In a few cases, the QSM fails, such as in buttressed trees in tropical forests (Disney et al., 2018), so instead of mesh-based models advised (Liski et al., 2014), QSM was also tested with the MLS, but the resolution was not sufficient to generate QSM, the QSM generated with TLS and MLS point clouds are shown in Figure 8. The estimation of DBH using cylinder fitting produced a 3.7 cm standard deviation for a tree, shown in Figure 7 (Bienert et al., 2018).

An automatic open-source package is available to determine basic tree structural metrics such as DBH, tree height, projected crown area, and diameter above buttresses. This tool works with QSMs (Terryn et al., 2023). The combination of point cloud acquisition sources and QSMs has shown great potential for understanding the forest structures; in this context, Tree QSM and AdQSM methods were used to make 3D tree models (Gan et al., 2024).

The extraction parameters also include leaf segregation from the tree point cloud. The current state-of-the-art for leaf-wood separation requires machine learning (ML) and other computer vision approaches (Béland et al., 2014; Belton et al., 2013). Wang (2020) tried unsupervised ML algorithms over supervised for the leaf wood separation or classification in a tree.

The skeletonizing method is also used to derive the tree structural metrics, which are mainly focused on the branching architecture. The method mainly derives a graph comprising geometric information of the vertices and edges from the point cloud (Bucksch & Lindenbergh, 2008). Other software and algorithms are available to deal with the same, such as TreeQSM (Calders et al., 2015) and Simpletree (Hackenberg et al., 2015) to extract tree structural metrics, tree volume, and topology. Both techniques rely on fitting the cylinders. Additionally, CloudCompare (Girardeau-Montaut, 2015) and 3D Forest (Trochta et al., 2017; Yurtseven et al., 2019) are also available and are open-source software to extract tree structural parameters.

There are various other algorithms available for tree skeletonization, such as DBSCAN, a clustering algorithm used to make tree skeletons using TLS data (You et al., 2023). To understand the physiological function of trees, it is important to segregate leaves and wood. Also, to measure accurate individual tree biomass. LWSNet was proposed in a study to segment leaves from the trees and found an F1 score of 97.29% (Jiang et al., 2023).

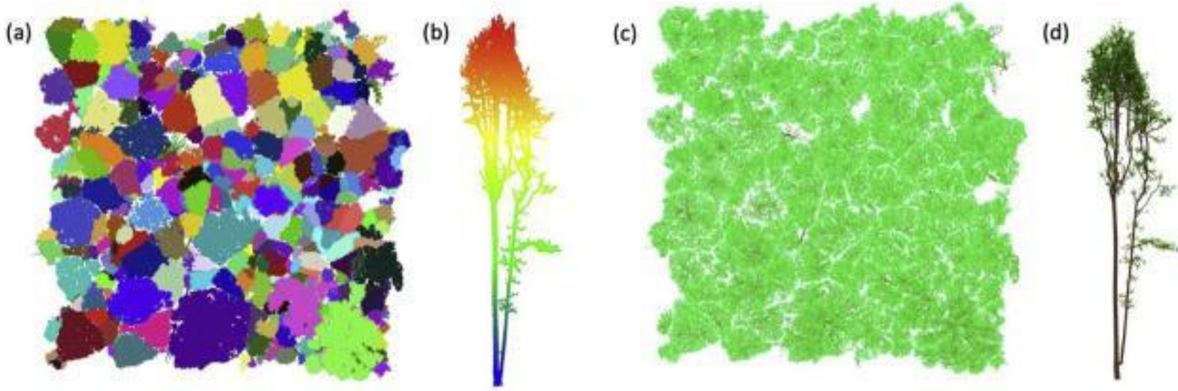

Figure 6: (a) and (c) show an above view of the forest point cloud, (b) and (d) show a side view of the tree point cloud. Source: (Calders et al., 2015)

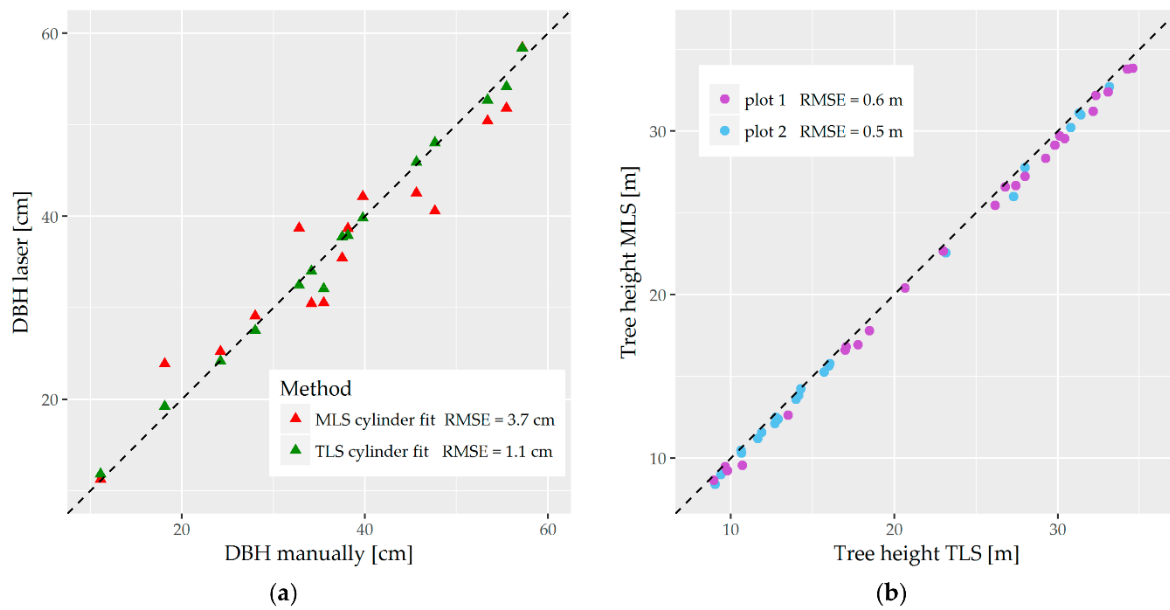

Figure 7: (a) A comparison of DBH measurement using TLS and MLS and DBH manually, (b) comparison of tree height using TLS and MLS. Source: (Bienert et al., 2018)

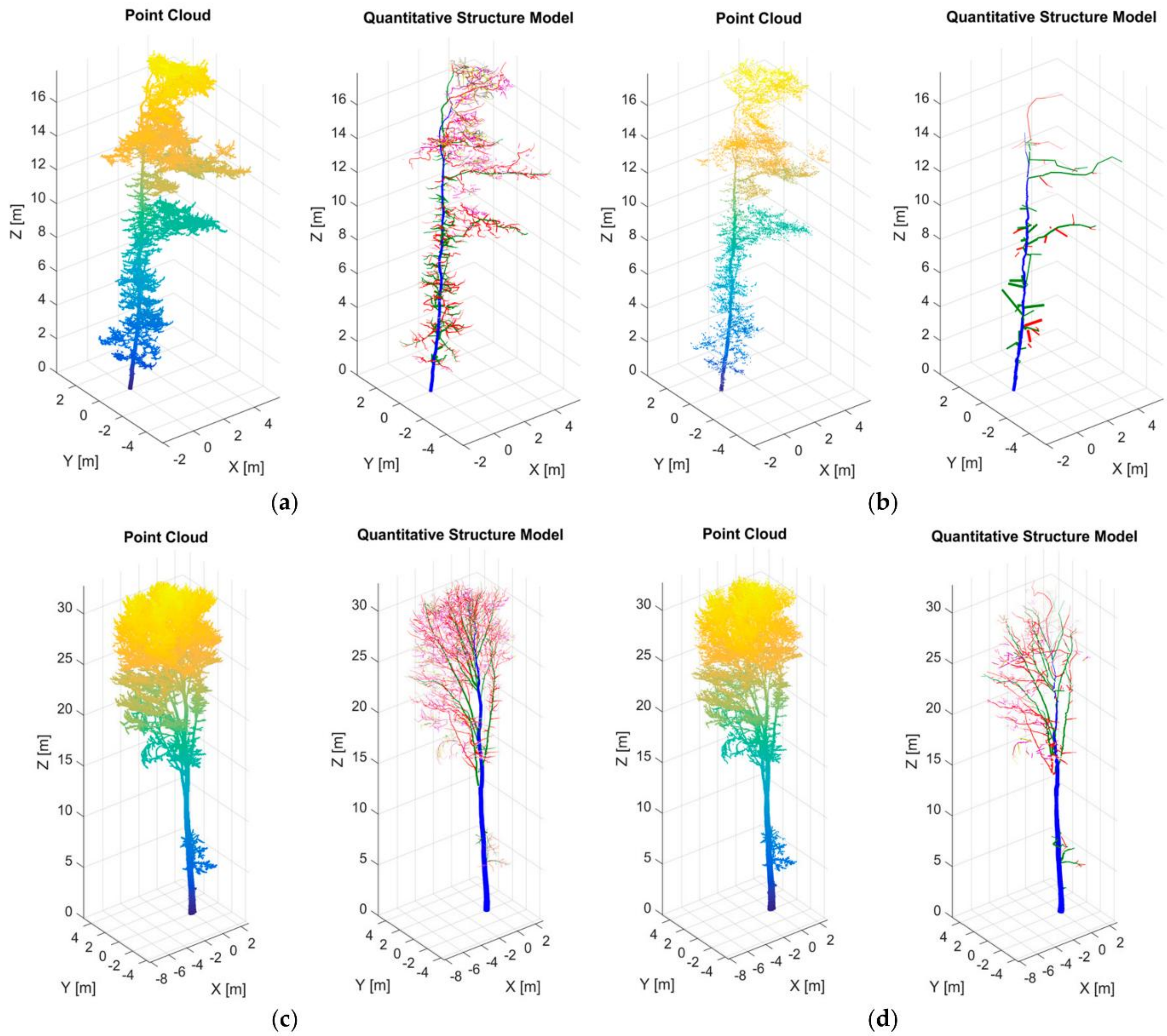

Figure 8: (a) and (c) point cloud of the leaf off and leaf on for *Carpinus betulus*, *Fagus sylvatica*, and QSM using TLS, respectively. (b) and (d) point cloud of the leaf off and leaf on for *Carpinus betulus*, *Fagus sylvatica*, and QSM using MLS, respectively. Source: (Bienert et al., 2018)

2.1.5.3 Forest Metrics Retrieval

Forest metrics consist of measurement of DBH, tree height, stem volume, stem quality, stem curve, stem detection, stem density, and biomass. Earlier, the focus of close-range device applications in the forest was to measure tree attributes. The measurement of tree attributes is performed with the TLS, MLS, and other related devices. However, tree species identification and change detection over time are equally important these days.

2.1.5.3.1 Stem detection, stem quality and density

The stem detection in a plot is an integral part of the plot measurements. Stem detection is highly correlated with steam density and forest type. The higher the density of the forest, the more uncertain the detection of the stem. So, it varies with the type of plot and its stem density. The type of forest could be generally of 3 types: sparse, dense, and very dense. In the sparse forest, the tree allocation probability could be 80 % with a stem density of 200-400 stems/ha. For the forest type of very high density, it may be around 70 % with a stem density of 1000 stems/ha. With the support of these tests, 28 circular plots with a radius of 20-25 m were performed. It has been concluded that the average stem detection rate was 42% (Yao et al., 2011). Liang, Litkey, Hyyppä, et al. (2012) have also done a test for 9 circular plots with a 10 m radius, and a 73 % stem detection rate was reported, and using a 5 m radius, it has been improved to 85 %. This concluded that stem detection accuracy is a function of range in the single scan. In another study, it has been proven that the most accurate range for stem detection is 6 m (Astrup et al., 2014). The detection rate decreased as we increased the distance of the scanner from the tree in a single scan (Olofsson et al., 2014). Hence, the range is a function of the stem detection rate. In the multiscan mode, the stem detection accuracy could be between 62.1% to 100%, provided the type of forest and scanning setup needs to be considered (Maas et al., 2008). MLS also proved to be an efficient device for stem detection. S. Xu et al. (2018) exhausted MLS data for stem detection in residential environments and achieved completeness of 94.2 % and correctness of 95.7 %.

Similarly, stem quality is also an important tree attribute. It shows the health status of the tree. The stem quality check can be regulated based on the status of fungal infection, i.e., presence of fungus, rotten branches, etc. TLS proved to be a fundamental device for this purpose and has shown its potential for the identification of stem form (taper, sweep, and lean) (Liang et al., 2013)and bark characteristics (Stängle et al., 2014). It can also be used for the classification of wood defects. The trees were also classified based on their timber quality into 3 classes, i.e., high-quality timber, timber, and pulpwood, with an accuracy of 95 % to 83.6% (Kankare et al., 2014)

The measurement of tree stems is important not only for commercial purposes but also for biological purposes. A comparative study was done using mobile and terrestrial laser scanners for the modeling of tree stem taper. The results showed that MLS was not efficient for taper models but worked well for sampling DBH and reconstruction of stem maps (Stovall, MacFarlane, et al., 2023).

2.1.5.3.2 DBH and Tree Height

DBH and tree height measurement is the most crucial part of tree attribute retrieval. There could be any possibility of error being commissioned during the measurement. The most reliable instrument needed to be deployed onboard to reduce this uncertainty. TLS and MLS proved to be the most accurate devices for this purpose. A lot of studies have been done to support this argument. In support of this, (Yao et al., 2011) have done the DBH estimation using TLS for 28 plots at tree level and mean plot level. The RMSE obtained for the estimation was 7.6 cm and 2.4 cm, respectively. Another study (Liang, Hyyppä, et al., 2012) was done at tree level and came up with the RMSE of 1.3 cm, and the bias recorded was 0.2 cm. There is the same process to measure DBH and stem curves. Stem curve detection is also a very significant part of forest inventory. In support of this context, (Henning & Radtke, 2006) studied 9 pine trees and the spruce tree. Different modes of scan play a very vital role in this context. The single scan TLS data has been used, and observed that the RMSE of the stem curve measurement was 4.7 cm (Maas et al., 2008). Regarding the tree height measurements, there is uncertainty with the accuracy because of the improper visibility of the treetops in the TLS data. The tree heights were measured, and the RMSE obtained was 0.75 m at the tree level (Moskal & Zheng, 2012) There is evidence for the accuracy improvement in the sparse forest (Fleck et al., 2011; Huang et al., 2011), perhaps it is still questionable in the dense forest because of the tall and dense canopy trees provide a hindrance to measure the treetops of short trees in dense forest accurately. Considering the slant range effect, there could still be some possibility for the argument. The reliable point spacing should be 1-2 cm level at the treetops to capture the smallest branches at the top. With the multiscan approach, the possibility can be enhanced to a remarkable point or with the integration of ALS data.

MLS is also used for the DBH measurement, and several studies have supported this new technology. So, a comparative study has been done to perform the field reference data collection using HMLS and backpack laser scanner in the boreal forests and compared the RMSE of MLS and UAV of 2-8 % for DBH measurements (Hyyppä et al., 2020). Also, a segmentation study was performed on an individual tree to extract biophysical information such as tree height, DBH, etc., using MLS and TLS (Zhong et al., 2017). An automatic approach was tried using algorithms (cylinder, circle, ellipse fitting) and machine learning models (e.g., random forest classifier) for the estimation of DBH and number of trees and found that 92.5% of 292 trunks were correctly classified (Zeybek & Vatandaşlar, 2021). The automatic processing algorithms save time and provide a better understanding of the analysis of point clouds. In the process of making automatic processing tools, deep learning plays a very important role, Pointnet ++ is a deep learning semantic algorithm that is used for the segmentation of the trees. A study was conducted using Pointnet++ segmentation and concluded that this algorithm works well with tree segmentation (Krisanski et al., 2021).

2.1.5.3.3 The estimation of stem volume

The stem volume estimation is very significant in terms of forest biomass estimation. Several studies focused on the automated and manual methods for stem volume estimation. The stem detection and its accuracy are highly dependent on the scan mode. A study was performed (Pueschel et al., 2013) to compare the multi-scan and single-scan approach; the multiscan approach on 6 beech trees for volume estimation reported deviations ranged from 2% to 6%, whereas with the single scan results observed deviation was 34 % to 44 %. Also, in a study (Astrup et al., 2014), a single scan was performed for spruce, pine, and birch trees, and the reported bias was 68.0, 14.9, and 24.1 dm^3. Stem volume was also estimated using allometric equations which are the function of DBH and tree height.

The studies performed using TLS showed that stem volume estimation is as accurate as destructive measurement methods and allometric volume models. TLS does not rely on any predictor variables for volume estimation. Also, the estimation of height at the plot level is difficult using conventional measuring devices. The DBH estimation model was developed using Airborne Laser Scanning (ALS) and TLS data. Allometric models were combined, and the spectral attributes were derived using Landsat and ALS data. The result was evaluated with four forest growth environments, and different regression models were used to compare accuracy (Y. Wu et al., 2023).

Moreover, the irregularity of the stem is usually ignored while the estimation of stem volume, the tetrahedron model was used with stem segments for the estimation of stem volume (Using et al., 2023). The tree species-specific allometric equation modeling was done using a non-destructive method using TLS, and the results concluded that TLS biomass estimates with RMSE ~ 19 % were more precise than the nation scale allometry (RMSE ~39%) (Stovall, Vorster, et al., 2023). Another study was conducted on a non-destructive approach for the estimation of individual tree volume using TLS data. Comparison of QSM with 60 trees references allometric models, TLS-based geometric parameters of the stem, coarse wood, and fine branches was considered. The results showed that the integration of crown parameters in allometric models can improve the branch wood volume (Bornand et al., 2023). Considering the MLS data, the speed and accuracy of the device make it more reliable for forest inventory. The device was tested for the estimation of hardwood volume and concluded that SLAM based MLS systems are suitable for forest inventory and support in-situ measurements of trees (Vandendaele et al., 2022). MLS devices are also capable of tree detection in complex forest environments such as the Mediterranean mixed forest region due to the variability in the tree allometries and spacing and the presence of natural regeneration (Tupinambá-Simões et al., 2023).

2.1.5.3.4 Biomass estimation

Biomass is a function of DBH, tree height, and tree species. Allometric models are extensively used for the estimation of biomass and completely rely on tree structure parameters. Most of the allometric models are species-specific. However there is a question to establish an automated method to estimate biomass that is completely based on the structure of the tree and not the species. TLS has been extensively used to automate this process. The research continuously approaches sharpening the aboveground biomass models. In this context, (Yu et al., 2013) developed a model to predict the stem biomass and compared it with the field-estimated values. The RMSE obtained for the prediction model using TLS was 12.5 %, whereas the RMSE obtained using the field-based biomass equation was 17.9 %. This study also says that the branch biomass can be evaluated in the same manner if the branch point cloud is dense.

Additionally, (Kankare et al., 2013) showed results for the branch biomass estimation using metrics derived from TLS point cloud data and obtained overall accuracy was 12.9 % and 11.9 %. Also, Hauglin et al. (2013) confirmed this finding. To further increase the accuracy of biomass estimation, integration of datasets and devices is required. So, another study is performed, which is focused on the integration of the TLS and ALS-derived biomass components to improve the accuracy of the biomass in the ALS-based branch biomass model. The outcome reveals a 3 % increase in the accuracy of the crown biomass. So, TLS can be used to assess tree biomass with high automation and increased accuracy . Consequently, a new method has been proposed to estimate tree attributes which are known as the concave hull by slices method. This is proven to obtain better accuracy than the existing methods, especially the backpack lidar scanner proved its flexibility to collect data in a definite time (Xu et al., 2021)

2.1.5.3.5 Change detection

Change detection of the forest structure is a major concern to researchers nowadays, considering the fluctuation in the environment. The losses in terms of insect attacks, degradation due to human intervention, etc., also leave a concern and quest for forest monitoring. The use of TLS data in change detection has not been reported in detail, but a study by (Liang, Hyyppä, et al., 2012) did a single scan of pine-dominated plots for a consecutive 3 years gap and estimated biomass using a national-level allometric equation with a function of DBH. Another study has also reported the change detection using the automated method over a time of forest structure and has accounted for 90 % of the tree stem changes in 5 plots using single scan TLS data. The bias for the estimated DBH was also calculated and found to be 0.2 cm, and the RMSE calculated was 1.3 cm (Srinivasan et al., 2014).

The total tree volume increment over the year can be assessed using TLS, and this has been proved in a study. The mean increase in the total tree volume was estimated and compared. They concluded that the difference in the average tree volume increment with the conventional measurement was 6.0 % (4.8 m^3 /ha) when only trees captured by the scanner were compared; it increased to 8.1% (7.0 m^3 /ha) when all the trees in the plot were considered (Mengesha et al., 2015). The multi-temporal TLS data is quite helpful for the study, which focuses on the change in forest productivity and structure. However, many more outcomes are still needed to support this hypothesis.

MLS is still in the pipeline to detect changes in the forest. Change detection requires static and continuous observation, and MLS is not static, and observations could be changed after a certain period. This is still on the list of challenges faced by MLS in forest inventory.

2.1.5.3.6 Tree Species Classification

Tree species classification is nowadays a vital topic among researchers, especially the hassle in the classification of tree species in tropical forests. It is important to better understand the functional behavior of the forest ecosystem. Initially, an expert was required to identify the tree species, which limited the field surveys. These days, researchers are trying and testing an automatic approach for this purpose. In this context, the pointNet++ model was used for tree species classification using a backpack laser scanner. The results showed that the tree height feature is not important for point cloud deep learning methods for tree species classification (Liu et al., 2022).

2.2 Role of active remote sensing methods in the mapping of forest structural indicators

The application of different remote sensing methods, such as close-range, satellite, and airborne, in forestry is depicted in Figure 9. The advancement of different remote sensing methods at various scales, from terrestrial to space-borne, introduces the possibility of observing forests from the stand to the global level. The global impact of ecology and biodiversity can be made possible by combining the large footprint space-borne GEDI missions (Marselis et al., 2018). In-situ measurement techniques are costly and labor intensive, and bias is more likely to be introduced in manual measurements. These biases propagate with the fusion or integration of reference data to other remote sensing data, increasing the error and bias level in the outcome. Therefore, close-range technology is more reliable because it can reach the level of detail in the forest, which is difficult to perform manually (Liang et al., 2022). Furthermore, the role of satellite remote sensing and the possibility of integrating different remote sensing technologies to get a fine level of observation is discussed here, with particular emphasis on SAR data.

SAR is an active remote sensing technology. It illuminates the objects on the ground by sending microwave signals from the sensor platform to the ground and receives backscattered signals from the ground object. It can also operate in any weather conditions. The potential role of SAR in assessing forest AGB has been proven in many previous studies—however, a detailed analysis of the possibilities needed to be considered. Various SAR datasets with X, C, P, and L band polarizations have been used for mapping AGB with different methodological approaches over the years (Cartus et al., 2022; Choi et al., 2021; Godinho Cassol et al., 2021; Ji et al., 2020; Karila et al., 2019; Khati & Singh, 2022; Narvaes et al., 2023; Santoro et al., 2019; Vatandaşlar & Abdikan, 2022; T. Zhang et al., 2023). SAR datasets such as ALOS PALSAR L-band have been analyzed and concluded to achieve the possible accuracy for estimating forest biophysical parameters such as forest height; hence, it was important to investigate the potential and correlation of different polarization of SAR datasets with the forest height. This approach was then extended with the fusion or integration of SAR datasets with other sensors, such as optical and LiDAR. While measuring the forest structure, the forest canopy density is highly affecting the sensitivity of the

L-band to the mean height of the forest, which was reported using TanDEM-X InSAR data that the vegetation density change is more correlated with the height change of forested area (de Jesus & Kuplich, 2020; Sinha et al., 2020; Tamiminia et al., 2022; Velasco Pereira et al., 2023)

The primary purpose was to investigate the variability in the accuracy while addressing AGB with or without the fusion of SAR to other sensors and come up with methodological advancement that can be used for the AGB estimation. The fusion of SAR with other sensors is further extended, incorporating LiDAR at different platforms (terrestrial, aerial, and space-borne), which enhances the performance of already established AGB models and opens the possibility of AGB estimation at a global scale. In this context, a study claims the increase in correlation (R^2) value from 0.64 to 0.74, whereas RMSE obtained was 39.3 Mg/ha (Mohite et al., 2024; Solberg et al., 2024; Z. Wu et al., 2024).

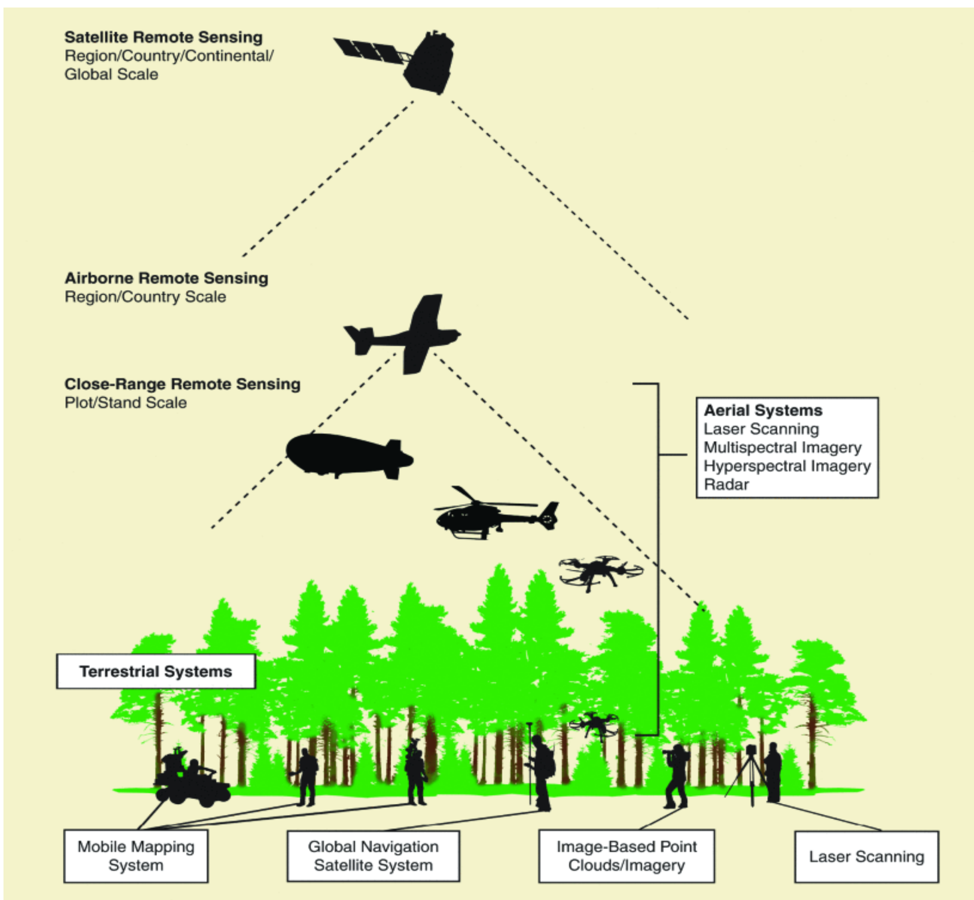

Figure 9: An overview of different remote sensing method application scenarios in forestry (Liang et al., 2022).

3. Material and Methods

In the following subchapters, we will establish the basis of the research experiments that were done by the PhD candidate. The experiments were done at three different locations in India, Slovakia, and Czechia. The details of the study sites and statistical analysis will be explained. However, the PhD candidate also did research work that was not dependent on a study size. These focused on reviews of processing solutions for forest point clouds and a review of LiDAR fusion. More details on these are within chapters 4.2.2 and 4.4.2

3.1 Study areas and materials

This dissertation aims at methodological advances, and it is not situated in one region. The field data collection covers a variety of forest stand structures.. The datasets used in the study were acquired at three places.

3.1.1 Barkot Forest (India)

The first study area selected from India was the Barkot Forest Range of the Dehradun Forest division. It lies at a latitude of 30°03’52” to 30°10’43” N and a longitude of 78°09’49” to 78°17’09” E. The total forest area is 84.96 km^2. We established 13 plots. The forest type is tropical, moist, and deciduous. It is dominated by *Shorea robusta* (Sal), with co-associated tree species such as *Mallotus philippensis* (Rohini). The study area is shown in Figure 10. The study is explained in detail in papers III and IV.

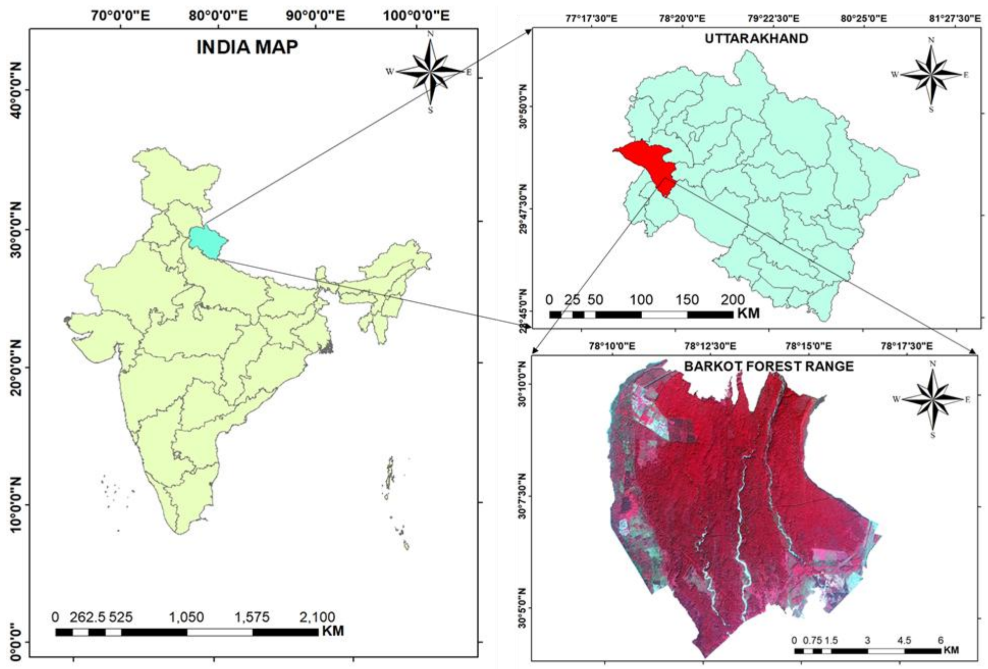

Figure 10: Study area 1

The field data was collected using a measuring tape, rangefinder, and handheld GPS. A total of 13 plots of 31.5 x 31.5 m area were selected. The field sampling was done at the LiDAR footprint with a stratified random sampling method. The tree parameters considered were tree height and DBH. DBH was calculated by measuring the circumference at breast height (CBH). The point cloud of the plots was acquired using TLS (Riegl VZ-400), and ALOS PALSAR L-band data was used for the spatial distribution of above-ground biomass (AGB). The ABG was estimated using the stem volume, specific wood gravity, and biomass expansion factor. The details of the datasets are mentioned in Table 2.

Table 2: Specification of the datasets used in the paper and III and IV

ALOS PALSAR		Terrestrial Laser Scanner (TLS)	
Product	ALOS2-HBQR1_1_A-ORBIT_ALOS2157270590-170421	**Product**	Riegl VZ-400
Product Type	HBQR 1.1	**Range**	Up to 600m
Mission	ALOS2	**Minimum Range**	1.5 m
Wavelength	23.6 cm	**Measurement rate**	122000 pts/sec
Frequency	1.27 Hz		
Orbit	15727	**Field of View**	100x360
Polarization	HH, HV, VH, VV	**Accuracy**	5 mm
SampleType	Complex	**Precision**	3 mm
Pass	Ascending	**Laser Type**	Class 1
		Laser Wavelength	NearInfrared (1553 nm)
		Laser Beam Divergence	0.35 m rad
		Weight	Approx. 9.6 kg

3.1.2 Kremnica Mountains (Slovakia)

The second study location was in Kremnica Mountains, Slovakia. This study area is explained in papers V and VI. The dominant tree species were European beech (*Fagus sylvatica)* with a mixture of European oak (*Quercus robur*), Silver fir (*Abies alba*), Norway spruce (*Picea abies*) and European hornbeam (*Carpinus betulus*). The study area is depicted in Figure 11.

The field data was collected using Topcon GPT3000M, and the tree's circumference was measured by measuring tape. We established eight research plots with varying tree densities of 25 x 25 m. The details of the field data inventory are explained in paper II. The point cloud was acquired using TLS (Faro Focus s70), a hand-held personal laser scanner (PLS_{hh}) (GeoSLAM Horizon Scanner), an iPad Pro 2020 tablet, and a multi-camera prototype. Data acquisition by mobile photogrammetry was done by the multi camera prototype (MultiCam). Sony a6300 cameras with

Sony 10-18 mm F4 OSS lenses were used. Further details are available in the paper II. The other devices used are described in detail in Table 3.

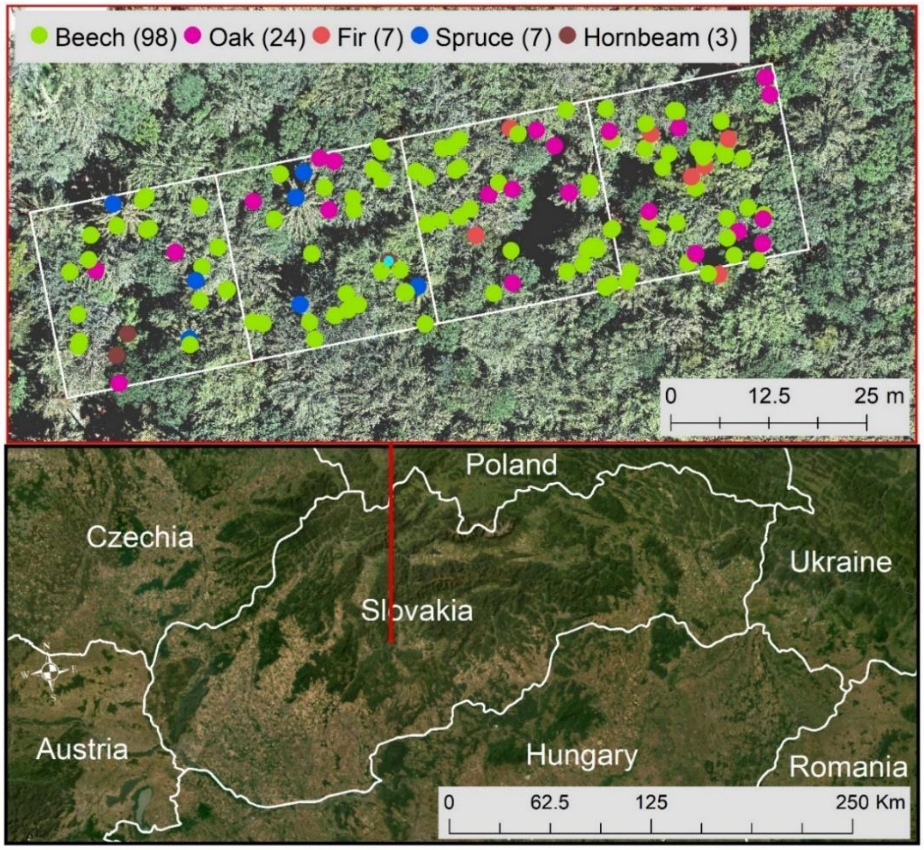

Figure 11: Study Area 2

Table 3: Specification of the devices used in the paper II

Specifications	**TLS (Faro Focus s70)**	**PLS_{hh} (GeoSLAM Horizon Scanner)**	**iPad Pro 2020 tablet**
Range	0.5 – 70 m	100 m	5 m
Accuracy	±2 mm on 10 m or ±3.5 mm on 25 m	1-3 cm	
Resolution (point spacing)	6.14 mm/10 m		
Scan time	2 min and 24 sec		
Laser Type	Laser Class 1	Laser Class 1	
Laser Wavelength	1550nm	903 nm	

Measurement rate	614m upto 500,000 pts/sec	300,000 pts/sec	
weight	4.2 kg	1.3 kg	495 gm

3.1.3 Czech University of Life Sciences (Czechia)

In the third research location, we scanned nearby trees on the campus of the Czech University of Life Sciences, Prague. We selected six tree species, and for each of them, 20 individual trees were selected. The following tree species were selected: *Pinus sylvestris* (Pine), *Fagus sylvatica* (Beech), *Quercus robur* (Oak), *Carpinus betulus* (Hornbeam), *Abies alba* (Fir), and *Picea abies* (Spruce). The study area used for paper VII. The tree species' bark image was captured using an iPhone 12 Pro; the range is 5 m and depicted in figure 12. Using a measuring tape, the DBH was estimated at 1.3 m above the ground for evaluation of the estimated DBH using three software tools. In total, 120 trees were selected for DBH estimation. The mean DBH varies between 24.7 and 42.4 cm, and the standard deviation varies between 6.08 and 10.27, as shown in Table 4. The detailed methodology considered in the research is explained in the paper VI.

Table 4: Statistical representation of BDH for each tree species

Tree species	Average_DBH (cm)	Range of DBH (cm)	Standard deviation
Pine	42.4	30.5 - 50.9	6.08
Oak	38.7	25.4 - 60.8	10.27
Beech	30.8	18.1 - 46.1	7.37
Hornbeam	24.7	14 - 44.5	6.67
Spruce	35	17.1 - 51.5	8.35
Fir	42.1	32.8 - 66.2	8.13

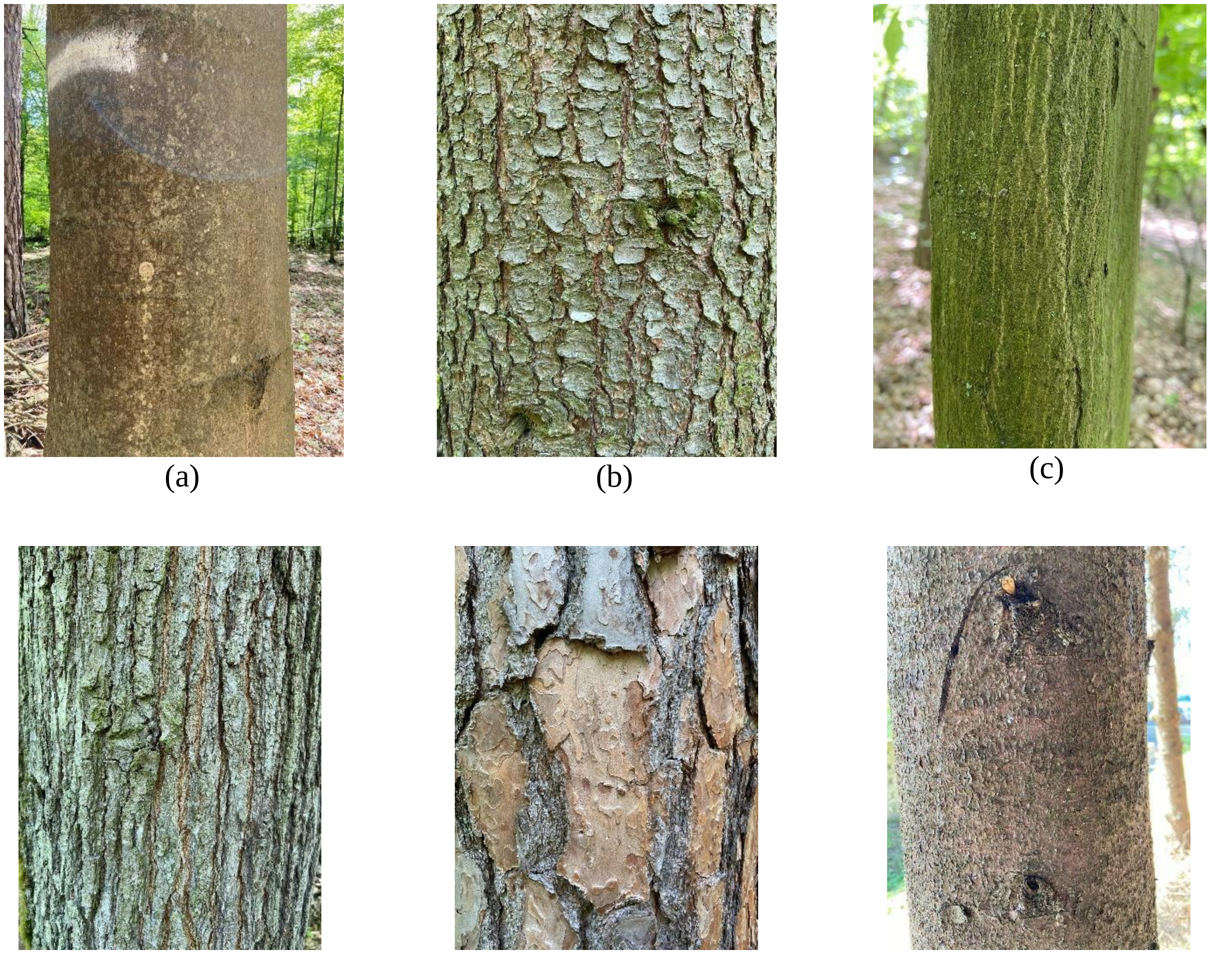

(a) (b) (c)

(d) (e) (f)

Figure 12: Bark images captured with iPhone 12 Pro of (a) Beech, (b) Fir, (c) Hornbeam, (d) Oak, (e) Pine, (f) Spruce

3.2 Statistical analysis

The diameter was estimated using all three different methods and was evaluated using two different statistical parameters: Root Mean Squared Error (RMSE) and relative Root Mean Squared Error (rRMSE). These statistical parameters were used to compare different methods for the estimation of DBH, as shown in equations 1 and 2.

$$\boldsymbol{RMSE} = \sqrt{\frac{1}{N}\sum_{i=1}^{N} (Y_i - \hat{Y})^2} \qquad \text{(Eq. 1)}$$

$$\boldsymbol{rRMSE} = \frac{\sqrt{\frac{1}{N}\sum_{i=1}^{N}(Y_i - \hat{Y})^2}}{\sum_{i=1}^{N} Y_i} \times \mathbf{100} \qquad \text{(Eq. 2)}$$

Where $\boldsymbol{Y_i}$ is the actual observation time series, Ŷ is the estimated time series, and N is the total number of observations.

The root mean square error of cross-validation ($\boldsymbol{RMSE_{cv}}$) was calculated to evaluate the predictive accuracy of the regression models (random forest (RF) and artificial neural network (ANN)). The mathematical expression is mentioned in equation 3.

$$\boldsymbol{RMSE_{cv}} = \frac{1}{k}\sum_{i=1}^{k} \sqrt{\frac{1}{n_i}\sum_{j=1}^{n_i} \left(y_j - \hat{y}_j\right)^2} \qquad \text{(Eq.3)}$$

Where $\boldsymbol{k}$ is the number of folds, $\boldsymbol{n_i}$ is the number of data points in the *i*-th fold, $\boldsymbol{y_j}$ and is the true value for the j-th data point in the *i*-th fold. $\boldsymbol{\hat{y}_j}$ is the predicted value for the j-th data point in the *i*-th fold.

A paired t-test was performed to check the statistical significance of ForestScanner and RANSAC for the measurement of DBH. To identify the significance of using different DBH measurement methods. This test was performed in R software. The formula for two-way ANOVA is mentioned in Equation 4. This test was performed in R software.

$$\boldsymbol{F} = \frac{\boldsymbol{MST}}{\boldsymbol{MSE}} \qquad \text{(Eq.4)}$$

Where F is the Anova coefficient, $\boldsymbol{MST}$ is the mean sum of squares due to treatment, and $\boldsymbol{MSE}$ is the mean sum of squares due to error. Then, the Tukey post-hoc test was performed using the formula mentioned in Equation 5.

$$\boldsymbol{T} = \boldsymbol{q} \times \sqrt{\frac{\boldsymbol{MSE}}{\boldsymbol{n}}} \qquad \text{(Eq.5)}$$

Where $\boldsymbol{T}$ is the HSD statistics $\boldsymbol{q}$ is critical value for the chosen significance level (often 0.05). $\boldsymbol{MSE}$ is the mean sum of squares due to error and $\boldsymbol{n}$ is the number of observations in each group.

4. Results

The results of the dissertation thesis are presented in the form of seven original publications. The publications are elaborated briefly in the subsections of this chapter. Subsection 4.1, entitled Revolutionary Devices for Measuring DBH, which comprises papers II and VI. This subsection is focused on the potential use of the application of iPhone/iPad devices in DBH measurement and its comparison with the other available devices such as TLS, MLS, and a multi-camera prototype).

This subsection focused on the objectives 2, 3, and 4. The sub-section 4.2 describes the benchmarking of algorithms for point cloud processing; this includes papers III and VII. This elaborates an approach for tree volume estimation using RHT and RANSAC algorithms and further an intense review of the point cloud processing software solutions. This subsection focused on objectives 3 and 4. The sub-section 4.3 comprises paper V and describes the methodology for the detection of canopy top points using different combinations of TLS scan positions and reveals the status of occlusion at the canopy top. The sub-section 4.4 is focused on LiDAR data fusion and future perspectives in forestry and encompasses papers I and IV. This subsection includes a thorough review of the LiDAR data fusion with other datasets and is followed by methodology for the estimation of AGB using the integration of TLS and ALOS PALSAR L-band datasets. This subsection focused on objective 1.

4.1 **Revolutionary devices (iPhone 12 Pro and iPad Pro) for measuring DBH**

4.1.1 Tree parameter extraction with iPhone point cloud data using multiple algorithms

published as: This paper is accepted in the International Journal of Remote Sensing and currently under publishing process.

Extended summary:

In this paper, the DBH was estimated using iPhone 12 pro point cloud using three software tools (rTLS- R package, RANSAC -CloudCompare plugin, ForestScanner). In this context, the scanning of 123 trees comprising six species: pine, oak, beech, hornbeam, spruce, and fir was done. The scanning of each tree was done with the iPhone 12 Pro. This smartphone has a time-of-flight sensor with a maximum range of 5 m. This sensor is incorporated in newer versions of iPhones within Pro and Pro Max and is also a part of the iPad Pro (2021 and newer). The ForestScanner application (Mapry) was used to collect the point clouds of trees. ForestScanner can estimate DBH directly in the application in real-time. It is based on a circle-fitting algorithm using a cross-section at a particular height. The detailed conceptual framework is shown in Figure 13.

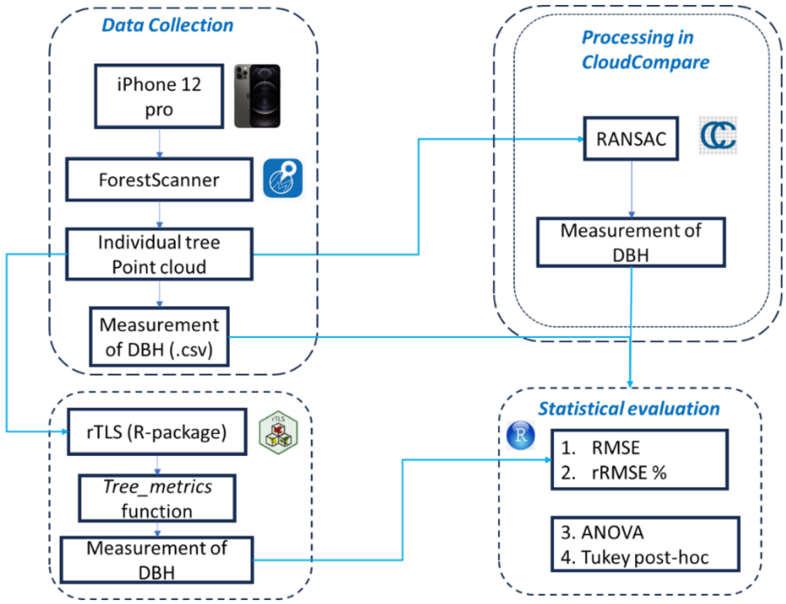

Figure 13: Conceptual workflow

The three software tools were compared and analyzed. In the first software tool, the iPhone 12 Pro-based application ForestScanner was used to estimate DBH, and statistical analysis was done to evaluate the DBH values obtained with the field-estimated DBH values. The RMSE value recorded for this method was 2.58 cm, and the rRMSE obtained 7.25 %. The R^2 value obtained for this method was 0.976. The other method used was the CloudCompare-based plugin- RANSAC. RMSE obtained for this tool was 2.19 cm, and the rRMSE obtained was 6.25 %. The R^2 value obtained was 0.976. This strongly correlates with the observed (field-estimated DBH) and predicted (RANSAC DBH, ForestScanner DBH) value of DBH. The scatter plot is shown in Figure 14.

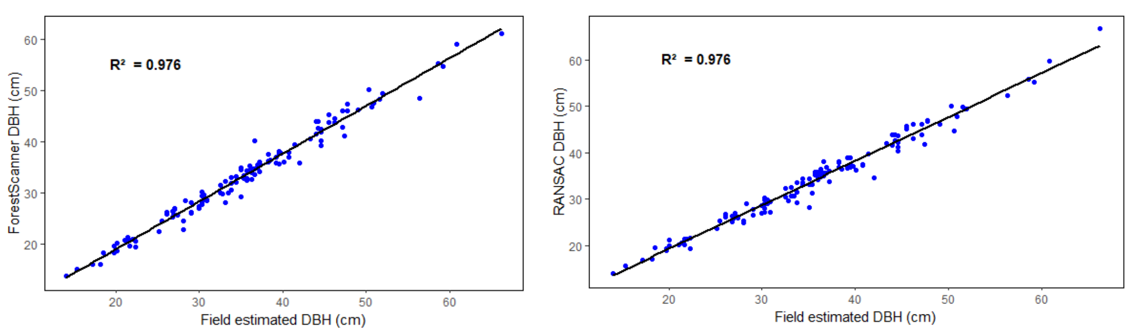

(a) **(b)**

Figure 14: Scatter plots of field-estimated DBH with (a) ForestScanner (Lidar DBH), (b) RANSAC DBH

Significance of DBH estimation for tree species

A comparative analysis of the ForestScanner and RANSAC algorithms was done to test the significance of the DBH estimation for different tree species. The statistical comparison was done using RMSE and rRMSE % for each tree species. The RMSE varies from 2.02 to 3.77 cm, whereas the rRMSE % varies within the range of 4.67 to 9.2 % for ForestScanner. The RMSE observed for RANSAC is in the range of 1.3 to 2.85 cm. The rRMSE % is observed to range from 5.15 to 7.82 %. The detailed information is mentioned in Table 5, and the graphical representation is depicted in Figure 15. The biases and outliers are shown in Figure 16.

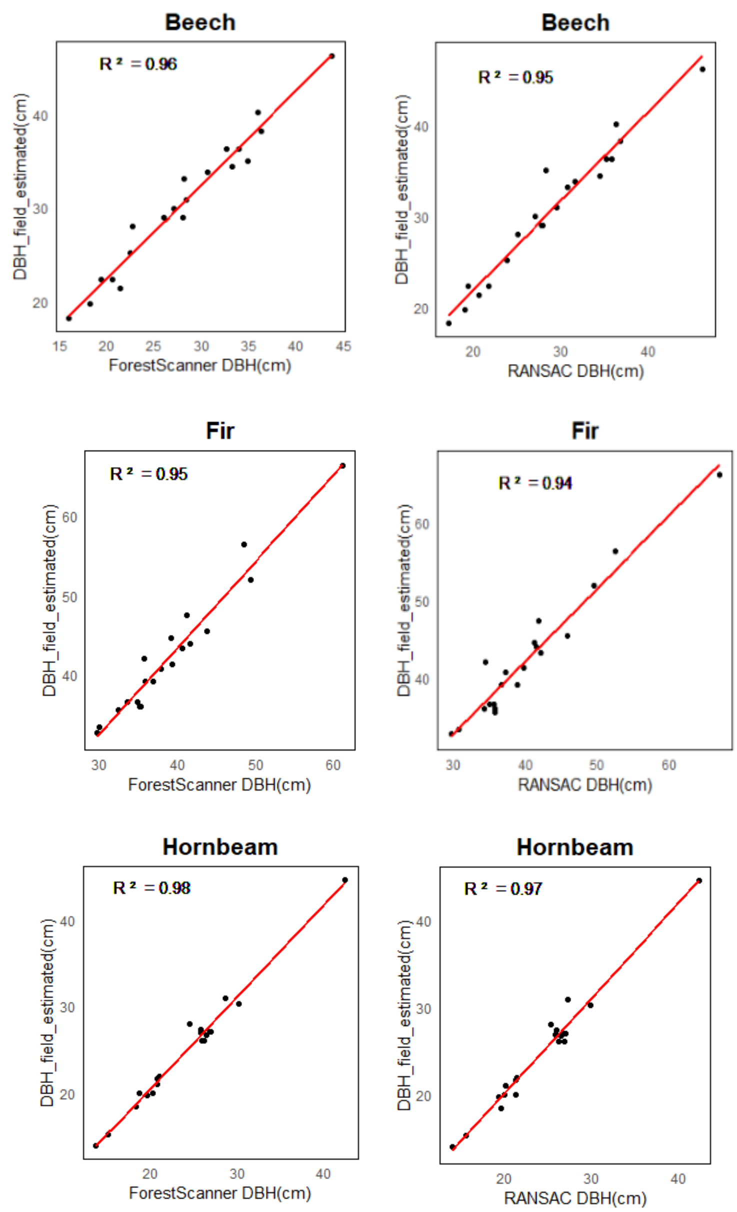

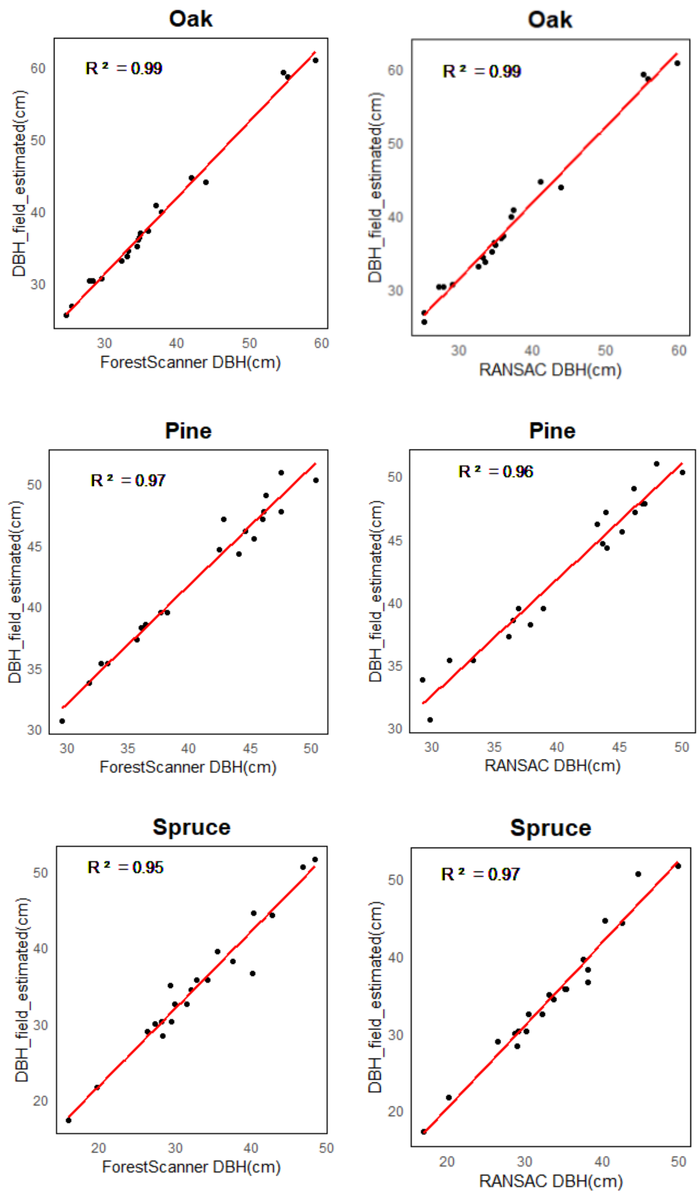

Figure 15: Comparison of the performance of iPhone 12 pro in estimating DBH among 6 tree species

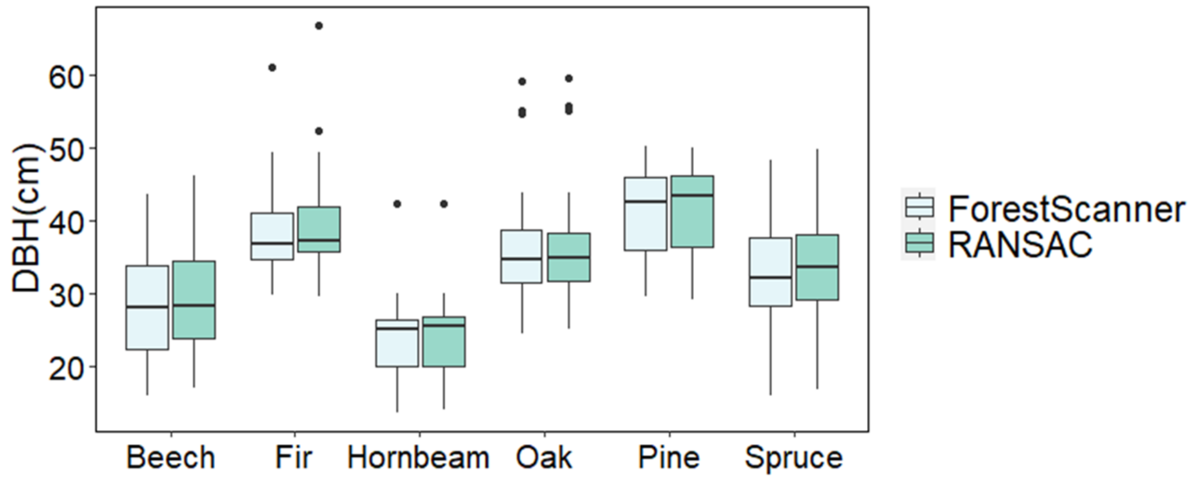

Figure 16: Boxplot of errors for each tree species and both approaches (ForestScanner and RANSAC)

Table 5: Comparing the statistical significance between ForestScanner and RANSAC in the context of tree species.

Tree_species	**ForestScanner RMSE (cm)**	**ForestScanner rRMSE%**	**RANSAC RMSE (cm)**	**RANSAC rRMSE%**
Pine	2.02	4.76	2.18	5.15
Beech	2.83	9.2	2.4	7.82
Oak	2.08	5.38	2.04	5.27
Hornbeam	1.22	4.95	1.3	5.28
Fir	3.77	8.94	2.85	6.77
Spruce	2.72	7.79	2	5.74

The Tukey post-hoc test was performed for the multiple comparisons of means for a two-way ANOVA with a confidence level of 95%. It shows the difference in means, the associated confidence intervals, and the p-value for different combinations of groups (Algorithm, species, and DBH). Inferences confirmed by ANOVA and Tukey post-hoc tests show that species significantly influence DBH. A more detailed analysis and description of the results is mentioned in the paper **VI**.

4.1.2 Novel low-cost mobile mapping systems for forest inventories as terrestrial laser scanning alternatives.

published as: Mokroš, M., Mikita, T., Singh, A., Tomaštík, J., Chudá, J., Wężyk, P., ... & Liang, X. (2021). Novel low-cost mobile mapping systems for forest inventories as terrestrial laser scanning alternatives. International Journal of Applied Earth Observation and Geoinformation, 104, 102512.

Extended summary:

A comparative analysis was done using low-cost devices (mobile laser scanning, personal laser scanning (hand-held or in a backpack), photogrammetry, or even smart devices with Time-of-Flight sensors) and TLS and conceptualized in paper II. The comparison was done to assess the performance of the capability of low-cost technologies to generate point clouds and their accuracy of tree detection and DBH estimation. A multi-camera prototype (MultiCam) was also tested.

The MultiCam prototype is capable of capturing images from four cameras simultaneously and with exact synchronization during mobile data acquisition. The focus was on individual tree detection and DBH estimation by cylinder-based algorithm across eight test sites with dimensions 25 x 25m. Altogether, 301 trees were located on test sites, and 268 were considered for the analysis and comparisons (DBH > 7 cm).

TLS provided the most accurate data. Across all test sites, we achieved the highest accuracy (rRMSE ranged from 3.7% to 6.4%) and tree detection rate (90.6–100%). When we considered only trees with DBH higher than 20 cm, the tree detection rate was 100% across all test sites (altogether 159 trees). When the threshold of trees considered in the evaluation was changed to 10 cm and then to 20 cm (from 7 cm), the accuracy (rRMSE) and tree detection rate increased for all devices significantly.

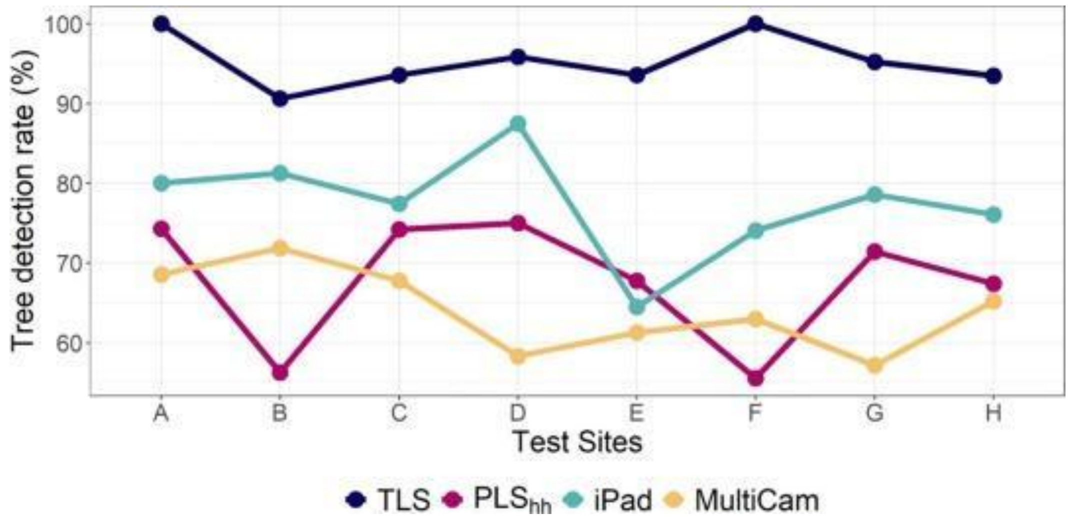

Figure 17: Tree detection rate of all devices used across eight plots

Results achieved (DBH > 7 cm) by iPad Pro were closest to TLS results. The rRMSE ranged across test sites from 8.6% to 12.9% and tree detection from 64.5% to 87.5%. PLS_{hh} and MultiCam, the rRMSE ranged from 13.1% to 24.9% and 14% to 38.2%, respectively. The tree detection rate ranged from 55.6% to 75% and 57.1% to 71.9%, respectively. The graphical representation is shown in Figure 17. The time needed to conduct data collection on a test site was fastest using MultiCam (approx. 8 min) and slowest using TLS (approx. 40 min). The DBH estimated from TLS, iPad and MultiCam underestimated the conventional DBH measurements. For TLS and iPad, the underestimation was statistically significant. In the case of PLS_{hh}, the DBH is significantly overestimated, as shown in Figure 18.

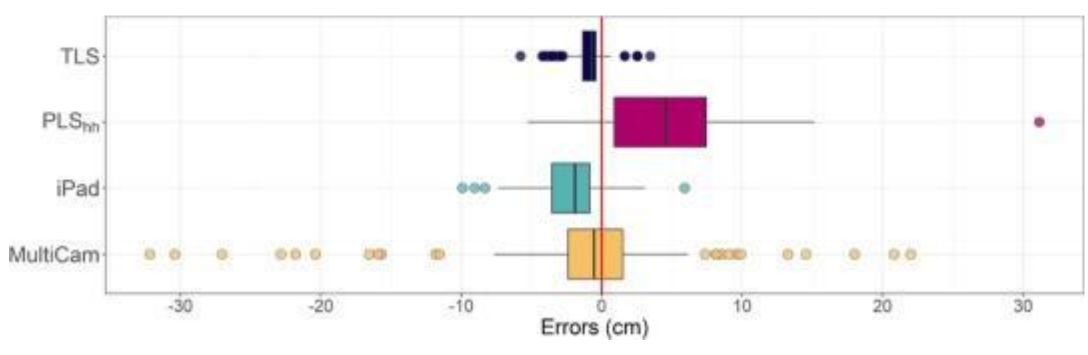

Figure 18: Boxplots of absolute errors (cm), where boxplots correspond to the 25th and 75th percentiles and whiskers are 1.5 * interquartile range. The line inside the box plots corresponds to the median. Dots represent outliers.

Results showed that DBH estimation from TLS point clouds is achieving the most accurate results with the highest tree detection rate across all test sites and overall, when compared to the other three mobile devices, as shown in Figure 19.

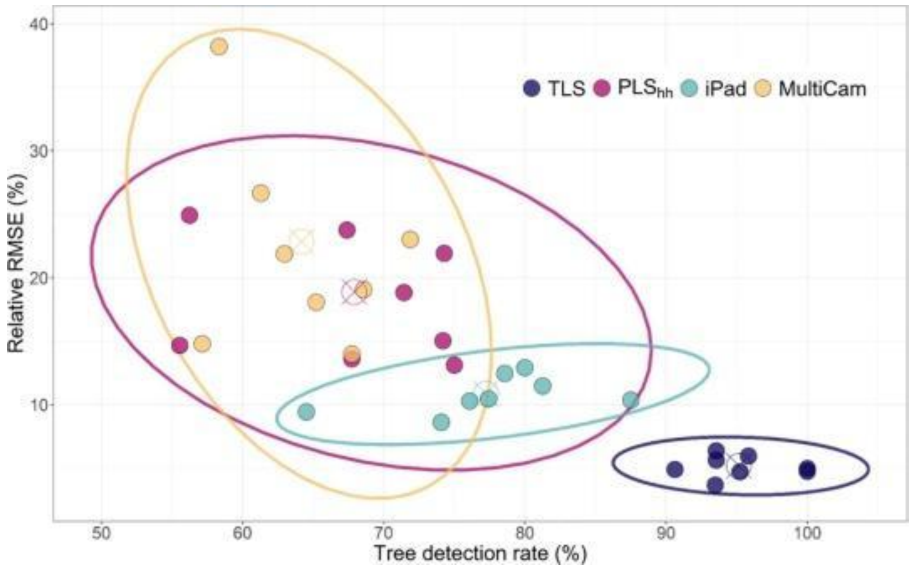

Figure 19: Scatter plot visualizing tree detection rate and rRMSE grouped by used devices. Each device has eight filled points (representing test sites) with one data ellipse and one crossed circle representing an overall tree detection rate and rRMSE of trees with DBH larger than 7 cm.

Conclusion:

The experimental analysis using iPhone 12 pro and iPad Pro was done in subsections 4.1.1 and 4.1.2. iPhone 12 pro and iPad Pro showed potential for the estimation of DBH and detection of trees in the forest. In subsection 4.1.1, The DBH estimated using ForestScanner and RANSAC showed same correlation value with the referenced DBH values. This shows that the ForestScanner application can be used for the estimation of DBH. Moreover, a significant relation was found between DBH, and tree species and inferences were confirmed by ANOVA and Tukey post-hoc tests. This shows that tree species significantly influence DBH. In subsection 4.1.2, iPad was tested against other devices for estimation of tree detection rate and DBH. And results showed that the TLS point clouds achieved most accurate results with the highest tree detection rate and DBH estimation accuracy, whereas iPad Pro showed the closet results accuracy to TLS.

Tree Parameter Estimation with iPhone Point Cloud Data Using Multiple Algorithms

Arunima Singh[1], Vladislav Pavlenko[1], Martin Mokroš[1,2]

Czech University of Life Sciences Prague, Faculty of Forestry and Wood Sciences, Kamýcká 129, Praha 6-Suchdol, 16500, Czech Republic

University College London, Gower Street, London, UK

Corresponding author email ID: **m.mokros@ucl.ac.uk**

Abstract: LiDAR technology introduced the possibility of indirectly estimating various tree parameters. In 2020, Apple incorporated LiDAR sensors into their iPhone 12 Pro. This brings an opportunity to make data collection and plot scanning incredibly convenient. The main aim is to search for a tool and software to estimate the most accurate Diameter at Breast Height (DBH) for individual trees. Therefore, this study focuses on using an iPhone 12 Pro for data collection of individual trees. The performance of three software tools (ForestScanner, rTLS, RANSAC) for the estimation of DBH with field-estimated DBH was compared. The investigation of the significance of the estimation of DBH for each tree species was performed using the three algorithms. In this context, the scanning of 123 trees comprising six species: pine, oak, beech, hornbeam, spruce, and fir was done. DBH was estimated of the scanned tree point cloud using a built-in algorithm of ForestScanner application in the iPhone 12 Pro, RANSAC (CloudCompare plugin), and rTLS (an R-based package). In this study, ForestScanner showed the best results. Therefore, ForestScanner can be used as a reliable tool for measuring DBH. Inferences confirmed by ANOVA and Tukey post-hoc tests show that species significantly influence DBH. Accurate DBH estimation is crucial, and using lightweight devices like the iPhone can revolutionize the forest inventory sector in terms of the estimation of DBH.

Keywords: DBH (Diameter at Breast Height), RANSAC (Random Sample Consensus), rTLS, tree parameters, iPhone.

1. Introduction

Conventional forest inventory measurements are costly, labor-intensive, and time-consuming. This motivated the forest researchers to focus on the applications of Close-Range Sensing as an alternative mode of forest inventory measurements. In recent years, with the modern developments and miniaturization of lidar sensors, they have become very compactly available. The latest iPhones and iPads have been integrated with LiDAR sensors. The range and accuracy of these LiDAR sensors are not comparable with high-end LiDAR systems; however, they are user-friendly and cost-effective ways of estimation and 3D data acquisition when the objects in focus are on shorter range (Liang et al., 2022).

In contrast, photogrammetry uses 2D images to create 3D point clouds using the structure from the motion algorithm, which is a low-cost alternative to costly LiDAR systems to produce 3D models. However, the post-processing is very demanding, especially for computational power. Also, the rate of failing to process the images to sufficient point cloud or model is relatively high in practice. Another alternative has been available recently using Time of Flight sensors within smartphones. Apple's iPhones (Pro and Pro Max) and iPads Pro have integrated ToF sensors since 2021. It is an opportunity to create 3D models using just a smartphone. The point cloud and model are ready right away onsite. It saves much time and is also great for quality checks directly in the field. Photogrammetry, on the other hand, requires images to be transferred from on-site to the lab and processed in high-end computers. This ease of 3D model generation has also helped in geometric research and reproduction of cultural heritage sites (Vlachos et al., 2022). The relative accuracy of the iPhone in 3D map generation by estimating its relative orientation, position, and navigation around the study area also needs to be studied thoroughly (Tamimi, 2022). iPhone 12 Pro LiDAR was also tested for its efficiency in measuring different roughness variations over 24 surface profiles. The results were also compared with photogrammetry-based Structure from Motion (SFM), and a significant correlation (R^2) of 0.70 was observed (Alijani et al., 2022).

The point cloud quality obtained is also important to test through these recently developed Lidar-integrated smartphones. The test used three smartphones (Huawei P30 Pro, iPhone 12 Pro, and iPAD 2021 Pro) based on planarity, surface variation, and omnivariance. Some issues were observed in the point cloud generated through these devices, such as loss of planarity, surface splitting, and drift problems with the Inertial Navigation System (INS) (Costantino et al., 2022).

Previous studies have proven that the point cloud derived from SfM is of little less quality than the high precision TLS. However, due to its cost efficiency, SfM is still deployed in many research studies. Recently developed iPhone LiDAR played a crucial role as an intermediate point cloud generation technology source. This also showed promising results in the rock mass characterization through geometrical analysis of the point cloud generated through iPhone-based LiDAR compared with TLS and SfM (Riquelme et al., 2021). Rapid scanning is essential when acquiring data at unstable surfaces of slopes and tunnels (Torkan et al., 2023).

iPhone 12 Pro's effectiveness was evaluated based on its geolocation accuracy, Inertial Measurement Unit (IMU), magnetometer for data collection orientation, and depth perception with its LiDAR sensor. The results demonstrated that the iPhone's geolocation is acceptable for geological and other field applications (Tavani et al., 2022). The reduction in the sensor size has allowed 3D to document the cultural heritage sites. Aslanlı fountain in İçkale of the Centre Sur district of Diyarbakır province was 3D documented using iPhone 13 Pro photographs and LiDAR data (Aslan & Polat, 2022). Three iOS-based point cloud-generating apps were tested with iPad Pro in the Cultural Heritage application. The apps were compared in different conditions because of overall accuracy, acquisition pattern, and operational limitations (Teppati Losè et al., 2022). An experiment was carried out to accurately monitor the snow depth variation over 75 days using iPhone LiDAR. Daily changes in the snow depth were compared with the snow ruler measurements, and a high correlation of 0.99 was observed with an RMSE of approximately 6mm. The authors also proposed that a mobile application can be developed to monitor the snow depth before, during, and after the snowfall. This can be handy and easy for all users (King et al., 2022) The research was conducted to evaluate the application of the iPhone 12 pro attached to a DJI Phantom 4 quadcopter for snow depth estimation. The iPhone 12 pro was attached to the UAV with a special 3D-printed mount for this specific purpose. The implementation was done on 3 study sites, and it was observed that the results were quite recommendable (King et al., 2023). Similarly, a study was conducted to test the iPhone 12 Pro LiDAR 3D modeling application and analysis of a coastal cliff in Denmark (Luetzenburg et al., 2021).

Moreover, researchers have already used Terrestrial Laser Scanners (TLS) in forest plots for accurate, detailed measurements and conveyed that TLS is very efficient in forest plot measurements (Kushwaha et al., 2022; A Singh et al., 2022; Singh et al., 2022). Tree parameters are crucial to calculate the Above Ground Biomass (AGB) and health of the tree growth (Singh et al., 2023). DBH is a vital forest inventory parameter with a very high correlation with tree height, volume, and biomass. Thus, the effective calculation of DBH is one of the main factors in forest measurements. Individual tree stem modeling is required to get the most accurate DBH. Tree stem modeling was done using an automated algorithm with a cylinder fit approach and found an accuracy better than 4 cm (Tarsha Kurdi et al., 2024). Modeling trees using point clouds could be difficult, so an algorithm was proposed to simulate tree models by rotating the surfaces. The test was evaluated with multiple trees with an overall accuracy between 0.3 to 0.89 m (Kurdi et al., 2024). The Lidar sensor generates the point cloud and estimates the depth using the motion sensors, camera exposure, and feature extractions. The maximum range of data acquisition is limited to 5 m. So, the operators must move closely around the tree stems to get sufficient points for DBH estimation. Multiple applications have been designed and made available on the online platform that estimates depth using these LiDAR sensors. A researcher has evaluated the use of iPad Pro 2020 to estimate the DBH of 101 urban trees. They compared three different scanning resolutions with two different confidence levels and two scanning modes (Wang et al., 2021). The availability and applicability of low-cost solutions such as the iPhone 12 Pro in the forest environment must be explored more. Evaluating the accuracy and efficiency of the iPhone 12 Pro for DBH estimation can be an easy and low-cost solution for forest inventory purposes. Also, it is important to see the significance of DBH measurement on individual tree species. So, in this research, 123 trees of different species were scanned using an iPhone 12 Pro. The stem regions were effectively acquired to estimate DBH. The DBH was estimated and compared through three different algorithms to evaluate the effective method for DBH estimation. An experiment was also done to find the significant relevance of tree species with DBH estimation using these three different algorithms.

2. Material and methods

2.1 Test Sites and Conventional in-situ measurements

The trees were collected within forest stands near the Czech University of Life Sciences, Prague, in the Czech Republic. In total, six tree species, and for each of them, 20 individual trees were selected. The following tree species were selected: *Pinus sylvestris* (Pine), *Fagus sylvatica* (Beech), *Quercus robur* (Oak), *Carpinus betulus* (Hornbeam), *Abies alba* (Fir), and *Picea abies* (Spruce). The tree species' bark image was captured using an iPhone 12 Pro and depicted in Figure 1 to show the different textures of the bark of each tree species. Using a measuring tape, the DBH was estimated at 1.3 m above the ground for evaluation of the estimated DBH using three software tools. In total, 120 trees were selected for DBH estimation. The mean DBH varies between 24.7 to 42.4 cm, and the standard deviation varies between 6.08 and 10.27 (Table 1).

Table 1: Statistical representation of DBH for each tree species

Tree species	Average_DBH (cm)	Range of DBH (cm)	Standard deviation
Pine	42.4	30.5 - 50.9	6.08
Oak	38.7	25.4 - 60.8	10.27
Beech	30.8	18.1 - 46.1	7.37
Hornbeam	24.7	14 - 44.5	6.67
Spruce	35	17.1 - 51.5	8.35
Fir	42.1	32.8 - 66.2	8.13

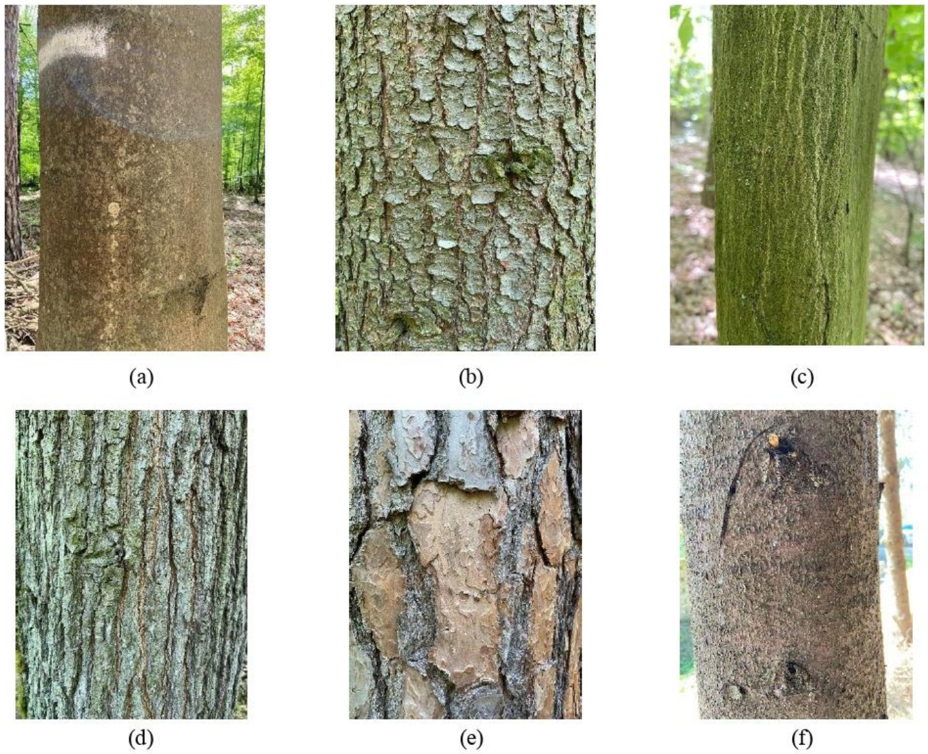

Figure 1: Bark images captured with iPhone 12 Pro of (a) Beech, (b) Fir, (c) Hornbeam, (d) Oak, (e) Pine, (f) Spruce

2.2 Data acquisition and pre-processing

The scanning of each tree with the iPhone 12 Pro was done. This smartphone has a time-of-flight sensor with a maximum range of 5 m. This sensor is incorporated in newer versions of iPhones within Pro and Pro Max and is also a part of the iPad Pro (2021 and newer). The ForestScanner application (Mapry) was used to collect the point clouds of trees. ForestScanner can estimate DBH directly in the application in real time. It is based on a circle-fitting algorithm using a cross-section at a particular height (Tatsumi et al., 2023). This application can collect the point clouds but also estimate the DBH right away in the application.

The data collection was done with the depicted trajectory (Figure 2). Each tree was acquired individually to avoid the unnecessary surrounding information. Forest Scanner scans the tree surfaces moving around the tree with the device. The real-time scanned surface recognition was done as it provides the point cloud and 3D triangle meshes on the phone screen in real-time. The point clouds were colorized with RGB information collected using the device's camera.

The relative coordinates were tracked from the starting point as it has IMU (Inertial Measurement Unit). The GNSS receiver built into the iPhone determined the starting point's absolute position. The real-time scanning and measurement of the tree stem were done, and the information was stored in the .csv file. This information was used for further statistical analysis. The scanned trees are shown in Figure 3.

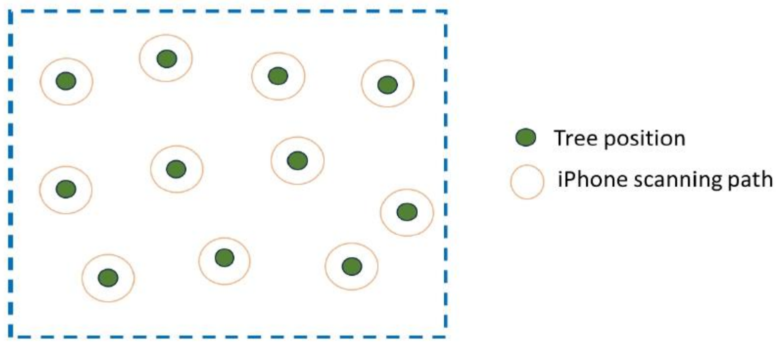

Figure 2: Trajectory of iPhone

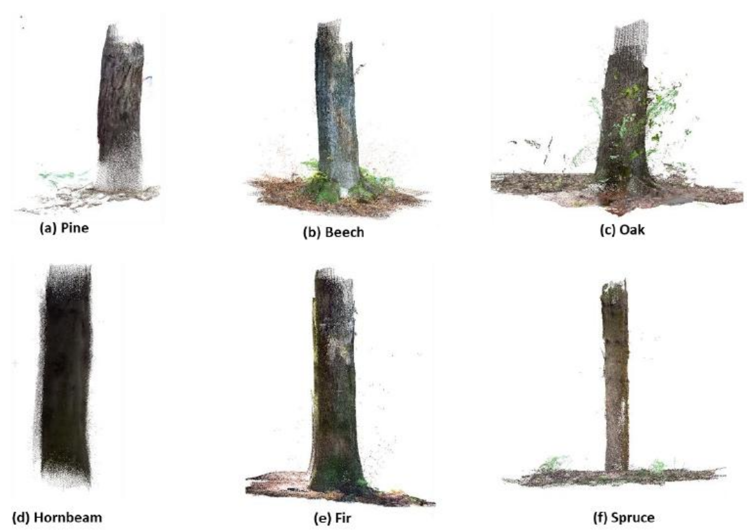

Figure 3: Point cloud of individual tree using iPhone 12 pro of (a) Pine, (b) Beech, (c) oak, (d) Hornbeam, (e) Fir, (f) Spruce (https://sketchfab.com/arunima92/models)

2.3 Post-Processing of Point Cloud

The DBH assessment was conducted using three software tools. The first was done using the ForestScanner application for iPhone 12 Pro directly on the iPhone in the field. For the Second, rTLS (R-based library) and the RANSAC algorithms (a plugin within CloudCompare) (Schnabel et al., 2007) was used as a third tool. For each approach, point clouds captured by the ForestScanner app were utilized, so the estimation by RANSAC and rTLS were based on the same data.

The point cloud obtained with the iPhone 12 pro contains noise. The point cloud was used without noise filtering in all three software tools to compare the potential of DBH estimation.

The iPhone 12 Pro-based ForestScanner application version 1.0.3 was used to estimate DBH. This application obtains single tree information and saves it to .csv file format. ForestScanner estimate DBH in real time using instance segmentation followed by the application of the Levenberg-Marquardt (LM) algorithm, which is used for the circle fitting method (Tatsumi et al., 2023). Secondly, an R-based rTLS library was used. The *tree_metrics* function was used to estimate DBH for each tree (Guzmán et al., 2021). The *tree_metrics* function incorporated the RANSAC algorithm for the estimation of DBH. This library only works with single tree point cloud input and not on the plot level.

Lastly, the RANSAC plugin is a CloudCompare (Girardeau-Montaut, 2015) based 2D circle fitting algorithm, which provides the best-fitted cylinder based on the random sample of the points on the tree trunk. The CloudCompare plugin provides the radius and height of the cylinder, which was later used to estimate the DBH for the individual trees. This algorithm was used in the CloudCompare-based plugin. After estimating the diameters of all the trees, statistical analysis was done to ensure the results' authenticity. The detailed workflow of the methodology used is depicted in Figure 4.

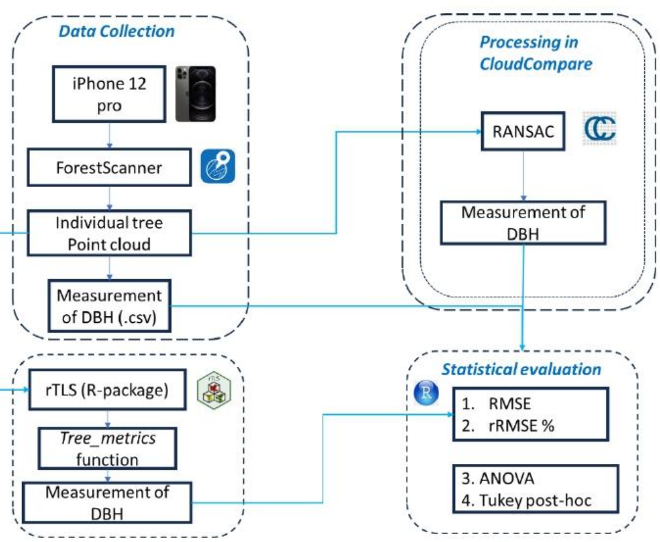

Figure 4: Workflow of the methodology

2.4 Statistical Analysis

The diameter was estimated using all three different methods and was evaluated using two different statistical parameters: Root Mean Squared Error (RMSE) and relative Root Mean Squared Error (rRMSE). These statistical parameters were used to compare different methods for the estimation of DBH, as shown in equations 1 and 2.

$$\boldsymbol{RMSE} = \sqrt{\frac{1}{N}\sum_{i=1}^{N}(\boldsymbol{Y_i} - \hat{Y})^2} \quad \text{(Eq. 1)}$$

$$\boldsymbol{rRMSE} = \frac{\sqrt{\frac{1}{N}\sum_{i=1}^{N}(Y_i - \hat{Y})^2}}{\sum_{i=1}^{N} Y_i} \times \mathbf{100} \quad \text{(Eq. 2)}$$

Where $\boldsymbol{Y_i}$ is the actual observation time series,
Ŷ is estimated time series,
N is the total number of observations.

A paired t-test was performed to check the statistical significance of ForestScanner and RANSAC for the measurement of DBH. To identify the significance of using different DBH measurement methods. This test was performed in R software. The formula for two-way ANOVA is mentioned in Equation 3. This test was performed in R software.

$$\boldsymbol{F} = \frac{\boldsymbol{MST}}{\boldsymbol{MSE}} \quad \text{(Eq.3)}$$

Where F is the Anova coefficient, $\boldsymbol{MST}$ is the mean sum of squares due to treatment, and $\boldsymbol{MSE}$ is the mean sum of squares due to error. Then, the Tukey post-hoc test was performed using the formula mentioned in Equation 4.

$$\boldsymbol{T} = \boldsymbol{q} \times \sqrt{\frac{\boldsymbol{MSE}}{\boldsymbol{n}}} \quad \text{(Eq.4)}$$

Where, $\boldsymbol{T}$ is the HSD statistics, $\boldsymbol{q}$ is Critical value for the chosen significance level (often 0.05). $\boldsymbol{MSE}$ is the mean sum of square due to error, and $\boldsymbol{n}$ is the number of observations in each group.

3. Results

The three software tools were compared and analyzed. In the first software tool, the iPhone 12 Pro-based application ForestScanner was used to estimate DBH and statistical analysis was done to evaluate the DBH values obtained with the field-estimated DBH values. The RMSE value recorded for this method was 2.58 cm, and the rRMSE obtained as 7.25 %. All the error values are shown in Table 2. The DBH obtained for all the trees using this method was correlated with the field-estimated DBH values to observe the accuracy of the method. So, the R^2 value obtained for this method was 0.976, which shows a promising correlation between the field-estimated DBH and DBH estimated using the ForestScanner application. The Scatter Plot is shown in Figure 5 (a).

The other method used was the CloudCompare-based plugin- RANSAC. The estimation of diameter using this tool was most accurate, precise, and close to the field-estimated DBH. The error value (RMSE) obtained for this tool was 2.19 cm, and the rRMSE obtained was 6.25 %. The error values are shown in Table 2. The DBH values estimated with this tool were visualized as scatter plots versus field-estimated DBH. The R^2 value obtained was 0.976. This strongly correlates with the observed (field-estimated DBH) and predicted (RANSAC DBH). The scatter plot is shown in Figure 5 (b).

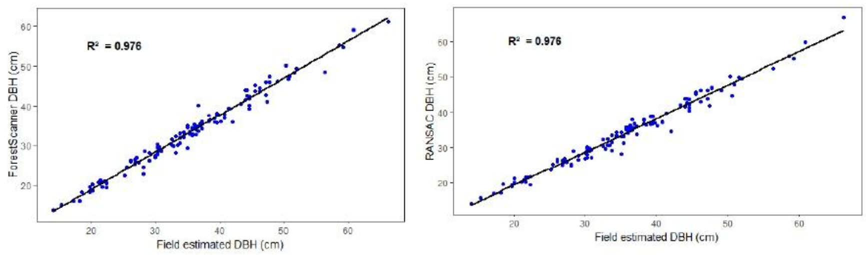

(a) (b)

Figure 5: Scatter plots of field-estimated DBH with (a) ForestScanner (Lidar DBH), (b) RANSAC DBH

In the R-based library rTLS, the diameter estimation was not promising. The error analysis depicted that the rTLS *tree_metrics* function is not accurate to estimate the diameter of the tree. The RMSE of the estimated diameter obtained using this tool was 132.61 cm, and the rRMSE obtained was 371.18 %. The results were visualized as scatterplots of field-estimated DBH versus rTLS-estimated DBH, and a weak correlation (R^2) of 0.025 was found. The results from rTLS were not promising enough to be included in further analysis. Therefore, it was excluded from further statistical analysis.

Table 2: Statistical error analysis

Type	rRMSE (%)	RMSE(cm)
Field estimated DBH & ForestScanner DBH	7.25	2.58
Field estimated DBH & RANSAC DBH	6.15	2.19

A comparative analysis of the ForestScanner and RANSAC algorithms was done to test the significance of the DBH estimation for different tree species. The statistical comparison was done using RMSE and rRMSE % for each tree species. The RMSE varies from 2.02 to 3.77 cm, whereas rRMSE % varies within the range of 4.67 to 9.2 % for ForestScanner. The RMSE observed for RANSAC is in the range of 1.3 to 2.85 cm. The rRMSE % is observed to range from 5.15 to 7.82 %. The detailed information is mentioned in Table 3. The biases and outliers are shown in Figure 7. The graphical representation of RMSE and rRMSE% for ForestScanner and RANSAC for each tree species is depicted in Figures 8 and 9.

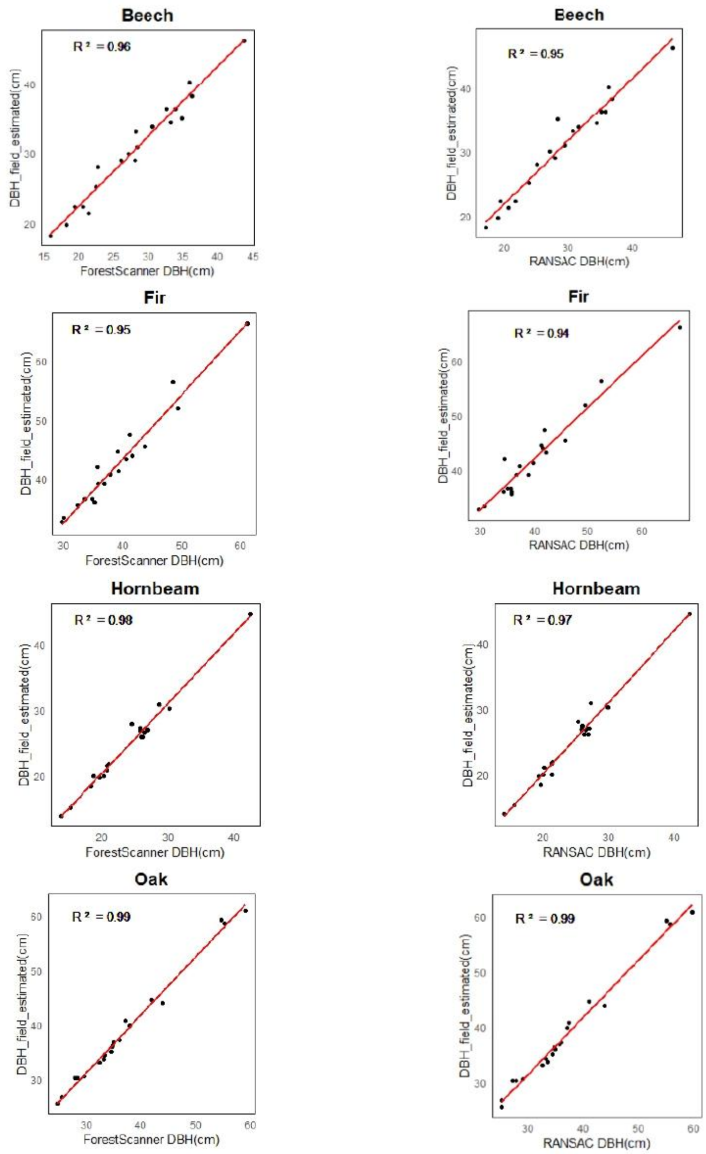

Beech
R² = 0.96
DBH_field_estimated(cm)
ForestScanner DBH(cm)
Beech
R² = 0.95
DBH_field_estimated(cm)
RANSAC DBH(cm)
Fir
R² = 0.95
DBH_field_estimated(cm)
ForestScanner DBH(cm)
Fir
R² = 0.94
DBH_field_estimated(cm)
RANSAC DBH(cm)
Hornbeam
R² = 0.98
DBH_field_estimated(cm)
ForestScanner DBH(cm)
Hornbeam
R² = 0.97
DBH_field_estimated(cm)
RANSAC DBH(cm)
Oak
R² = 0.99
DBH_field_estimated(cm)
ForestScanner DBH(cm)
Oak
R² = 0.99
DBH_field_estimated(cm)
RANSAC DBH(cm)

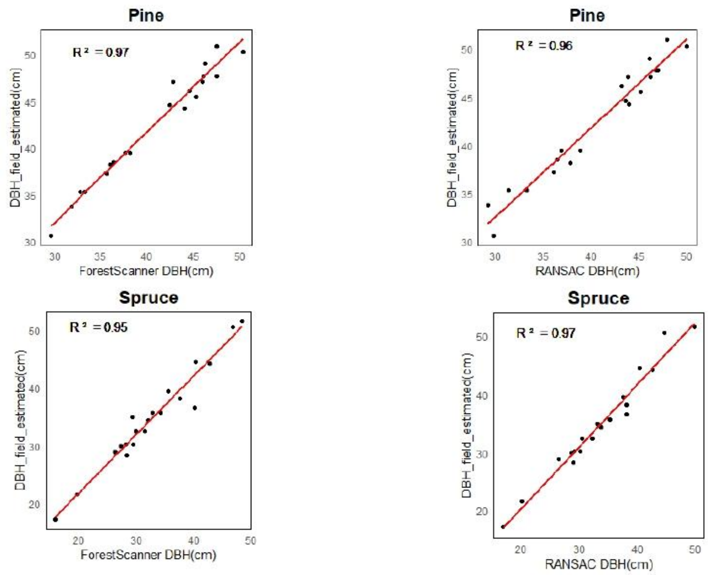

Figure 6: Comparison of the performance of iPhone 12 pro in estimating DBH among 6 tree species

Moreover, a comparative analysis was done between the estimated DBH of each tree species and the field-estimated DBH. The highest correlation (R^2) found for ForestScanner was for hornbeam, oak, and pine and ranged from 0.95 to 0.99. Whereas R^2 obtained for RANSAC was highest for hornbeam, oak, and spruce and range from 0.94 to 0.99. For visual interpretation, the correlation plots for all 6 species are shown in Figure 6.

Table 3: Comparing the statistical significance between ForestScanner and RANSAC in the context of tree species.

Tree_species	**ForestScanner RMSE (cm)**	**ForestScanner rRMSE%**	**RANSAC RMSE (cm)**	**RANSAC rRMSE%**
Pine	2.02	4.76	2.18	5.15
Beech	2.83	9.2	2.4	7.82
Oak	2.08	5.38	2.04	5.27
Hornbeam	1.22	4.95	1.3	5.28
Fir	3.77	8.94	2.85	6.77
Spruce	2.72	7.79	2	5.74

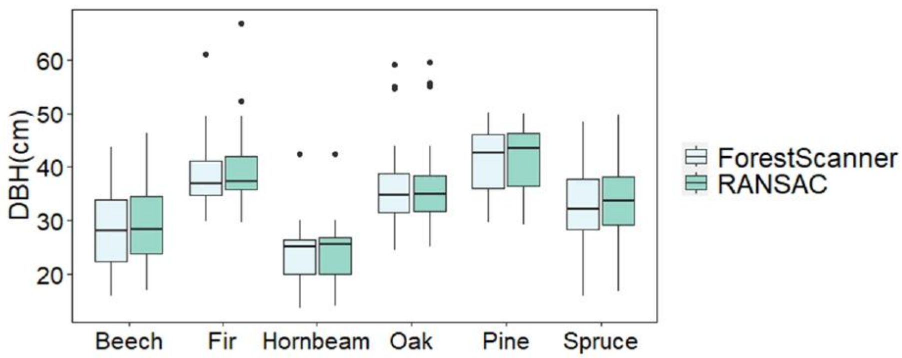

Figure 7: Boxplot of errors for each tree species and both approaches (ForestScanner and RANSAC).

The paired t-test results show a significant difference between the DBH measured with the ForestScanner and RANSAC. Out of the three algorithms used, RANSAC and ForestScanner application-based estimates were very close to the field-estimated DBH values. The statistical error evaluation was done. The RMSE obtained ranges from 2.19 to 132.61 cm, whereas rRMSE varies between 6.15 to 372.18 %. The higher variation in the error values is due to the rTLS algorithm. The estimated DBH values from the rTLS algorithm are insignificant and irrelevant to the field-estimated DBH values.

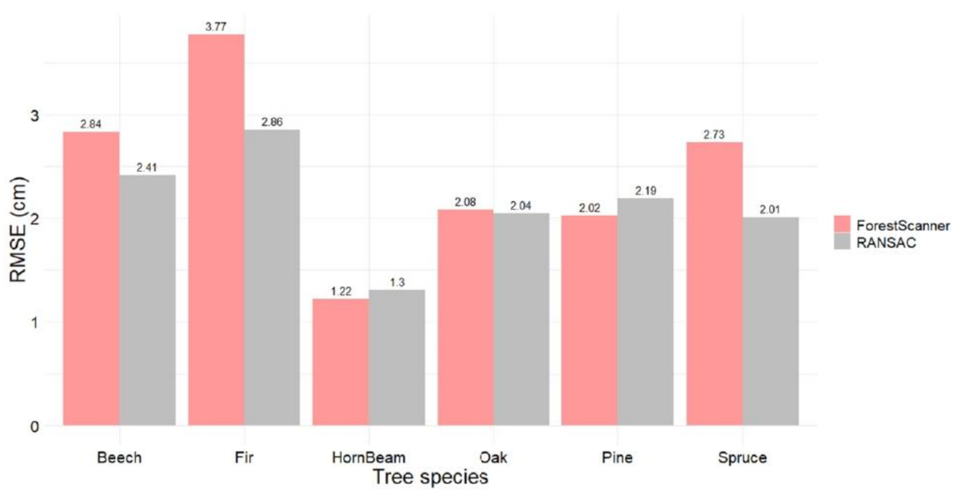

Figure 8: Graphical representation of RMSE (cm) for each tree species for ForestScanner and RANSAC

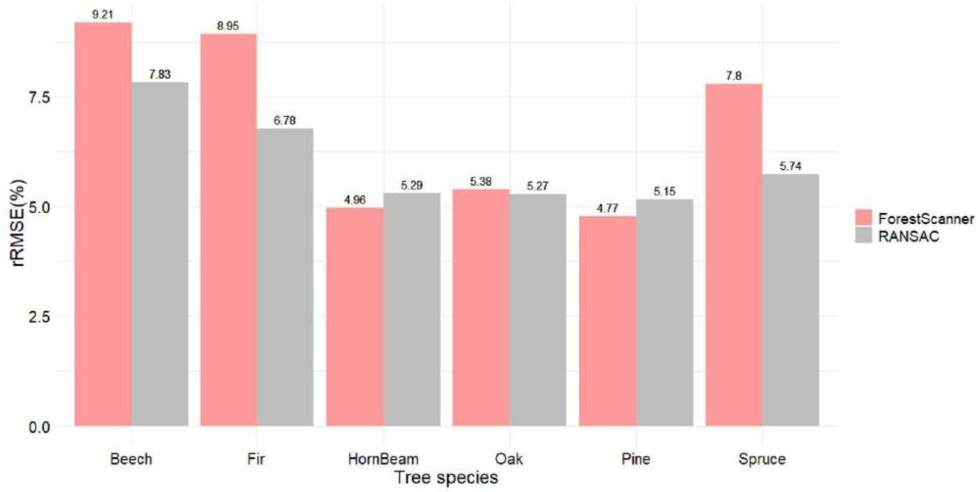

Figure 9: Graphical representation of rRMSE (%) for each tree species for ForestScanner and RANSAC

After the error calculation, a paired t-test was performed to see the statistical significance of the ForestScanner and RANSAC for the DBH estimation. The P-value is lower than the significance level, which is 0.05. This shows a significant difference between the means of ForestScanner and RANSAC. The summary of the t-test is shown in Table 4.

Table 4: Paired t-test observations

statistic	df	p_value	mean_difference	confidence_interval_lower	confidence_interval_upper
-4.15	122	6.14E-05	-0.512	-0.75	-0.26

Based on the RMSE and rRMSE % evaluation, a significant difference is observed in the tree species and DBH. So, the ANOVA test was performed, and the detailed analysis description is shown in Table 5. The F-value noted is 29.72, and the p-value obtained is close to zero (2.47E-23), indicating that the species factor is statistically significant. Meanwhile, the algorithm and interaction between the algorithm and species are not statistically significant. This shows that the species significantly impact DBH, and the data has a significant amount of variation. The interaction between the DBH, Algorithm, and species is clearly shown in Figure 10.

Table 5: ANOVA observations

	Df	Sum Sq	Mean Sq	F value	Pr(>F)
Algorithm	1	16.12936	16.12936	0.278	0.599
Species	5	8627.396	1725.479	29.72	2.47E-23
Algorithm:Species	5	12.07765	2.415531	0.0416	0.99
Residuals	234	13584.3	58.05255	NA	NA

Signif. codes: 0 '*' 0.001 '**' 0.01 '*' 0.05 '.' 0.1 ' ' 1**

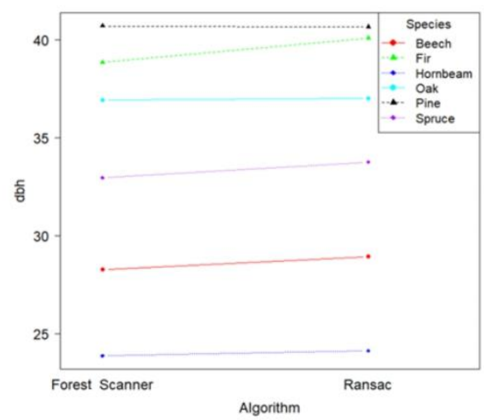

Figure 10: Interaction plot between the DBH, algorithm, and species

Tukey Post-Hoc test:

The Tukey Post-Hoc test was performed for the multiple comparisons of means for a two-way ANOVA with a confidence level of 95%. It shows the difference in means, the associated confidence intervals, and the p-value for different combinations of groups (Algorithm, species, and DBH). The analysis showed that the comparison RANSAC-Forest Scanner for the algorithm group does not show a significant difference (p adj = 0.598619), indicating no significant difference between these two algorithm levels. The graphical representation of the means of the species and interaction of algorithms is shown in Figure 11 and Figure 12. The further inferences are mentioned as:

1. For the Beech tree species, the p-value for the algorithm effect is 0.5986, which is greater than a typical significance level of 0.05. This suggests no significant difference between the algorithms (ForestScanner and Ransac) for the Beech tree species regarding their effects on the variable DBH.

2. However, when comparing different tree species for ForestScanner and Ransac, there are significant differences in some cases. For example, for the Fir tree species, there is a significant difference (p = 0.0006573), indicating that the choice of algorithm affects the DBH values. Significant differences are found for Oak, Pine, and Spruce tree species.
3. When looking at the interaction between Algorithm and Species, it's essential to note that the differences between ForestScanner and RANSAC vary depending on the tree species. For example, for Fir, the difference is significant (p = 0.000657), but for Beech, the difference is non-significant (p = 1.000000).
4. For individual comparisons between ForestScanner and RANSAC for specific tree species (e.g., Fir, Oak, Pine, Spruce), significant differences indicate that the choice of algorithm significantly affects DBH for those specific tree species.

Hence, Overall, it appears that the choice of algorithm significantly impacts DBH values for certain tree species but not for others. The significance of this impact varies by tree species. For the Beech tree species specifically, there is no evidence of a significant difference between ForestScanner and RANSAC regarding their effects on DBH.

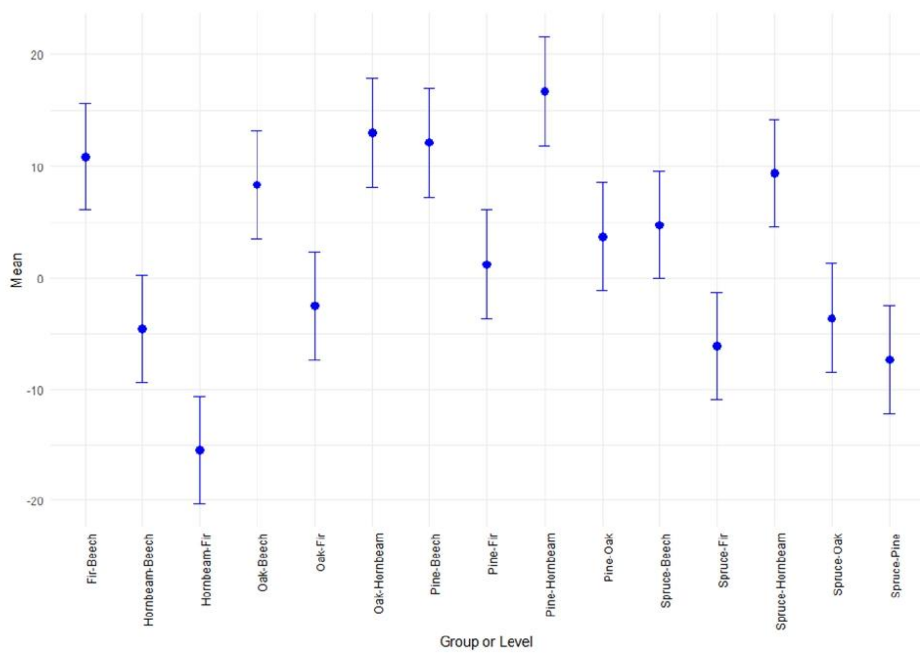

Figure 11: Graphical representation of mean of the interaction of species

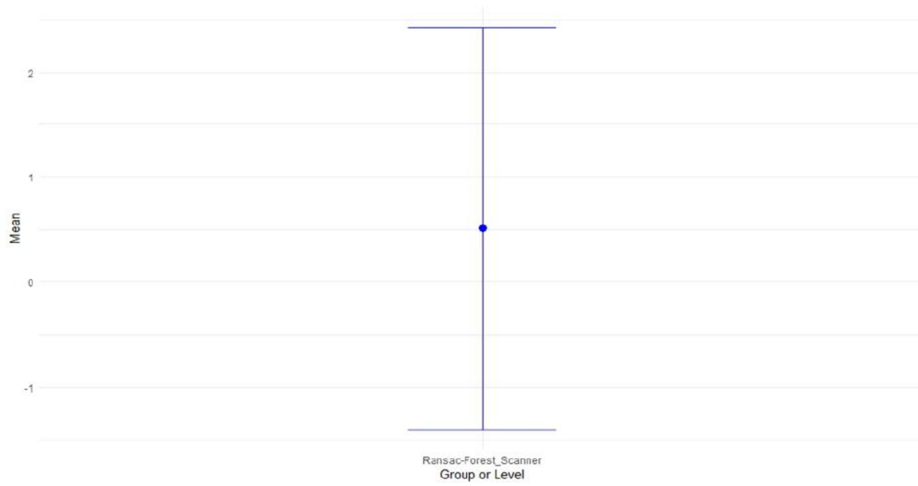

Figure 12: Graphical representation of mean of the interaction of Algorithm

For the Species, some comparisons show significant differences (p adj <0.05), while others do not. Fir-Beech has a highly significant difference (p adj = 0.000000), indicating a significant difference in the mean of Fir and Beech. On the contrary, Hornbeam-Beech shows no significance as the p adj observed is 0.072602, which can be marginally significant.

4. Discussion

This research used the iPhone 12 pro-based LiDAR application ForestScanner to estimate DBH, CloudCompare-based RANSAC plugin, and rTLS (R-package). The unfiltered point clouds acquired using iPhone 12 Pro were used. The potential use of ForestScanner and RANSAC in DBH estimation was found. However, rTLS did not show promising results. Although rTLS also works on the RANSAC algorithm, the results were not promising due to noise in the data. The problem was associated with the reading of the point cloud input file with rTLS library, and it also has issues while reading a post-processed point cloud. Due to noise in the point cloud, the estimates of DBH were vague, and the error was high. Consequently, we excluded rTLS from further statistical analysis. Instead, ForestScanner showed good results and accurately estimated DBH with unfiltered data.

The estimation of DBH is crucial for forest inventory. There are so many tools available for this purpose, so perhaps benchmarking of the tools is required to get the most robust tool for ease of estimation of DBH. Other studies focus on the estimation of DBH using MLS with the comparison of 3 algorithms, namely RANSAC, Monte Carlo, and optimum circle, and found good results with RMSE 5.31 cm and 1.23 cm of bias (Pérez-Martín et al., 2021). The other study on the DBH estimation was done using the RANSAC algorithm, which tested 71 trees and found a promising outcome. The RMSE calculated was 0.7 cm, and 2.27 % was the relative error. This shows the potential application of RANSAC in the estimation of DBH (Zhou et al., 2019). This study showed that the number of points fitting a circle does not affect the RANSAC algorithm.

Other studies support the robustness of the algorithms using real-time monitoring with mobile phones to estimate DBH. An algorithm was developed to detect tree position and measure

DBH. The RMSE observed was 0.33 cm for the DBH estimation and 0.12 m for tree position detection. The results showed that mobile phones with RGB-D SLAM could be a potential solution for real-time tree position detection and DBH estimation (Fan et al., 2018). The other methods, such as multi-height diameters for estimating DBH, are also accurate. This method also used RANSAC to estimate diameters at a certain height of the trees. The study shows RMSE of 3.17 cm and 2.5 cm as the mean absolute error for the estimation of DBH (Liu et al., 2021). To define the accurate estimation of DBH, a study reported the DBH thresholds of 7, 12, and 20 cm (Kükenbrink et al., 2022).

The research was carried out to test the performance of iPad Pro 2020 in different groups of tree species in urban forests. The evaluation was based on the Perimeter at Breast Height (PBH) and relative tree position. The estimation obtained from iPad Pro 2020 was compared with a measuring tape and Faro Focus 3D (TLS). After the analysis, it was observed that acquiring a 3D scan by going around the tree trunk twice improved the DBH estimation, and iPad Pro 2020 can deliver precise relative tree positions (Bobrowski et al., 2023; Pace et al., 2022). However, the time taken by the iPad Pro was approximately twice that of GeoSLAM ZEB Horizon and much less compared to TLS. In contrast, it is very cost-effective among all the LiDAR-based sensors. The tree detection rate was also very efficient in urban forest scenarios (Gollob et al., 2021). LiDAR-based iPad Pro efficiently estimated accurate DBH and distance between each tree. So, these low-cost technologies can accurately estimate a few tree parameters (Çakir et al., 2021).

Research was conducted to compare the performance of different low-cost technologies like Multicam photogrammetry, iPad Pro, hand-held, and Terrestrial Laser Scanner (TLS) to estimate Diameter at Breast Height (DBH). The authors observed that iPad Pro results were closest to TLS results when the trees with DBH > 7 cm were considered (Mokroš et al., 2021). TLS can generate 3D models in various applications with the required accuracy and precision. The point cloud density and distance measurement accuracy generated by the iPhone 12 Pro were tested on different surface materials like aluminum, plastic board, ceramic tile, canvas, and plywood. The results were compared with TLS, and it was observed that the iPhone 12 Pro could produce a point cloud with good density and proximate measurement values. The author concluded that the iPhone 12 Pro LiDAR is an efficient data acquisition source in 3D indoor building environments (Razali et al., 2022).

Apart from this, Wood log measurements are also a good application of LiDAR integrated iPhone 12 pro max and iPhone 13 pro max. It proved very efficient in measuring 267 and 200 spruce logs in two different test cases (Borz et al., 2022). A systematic review of 304 peer-reviewed papers is also presented for timber assortments using multi-source LiDAR platforms, which is done based on specific log dimensions, including log length and diameters at both ends. Promising results were obtained when airborne LiDAR was integrated with Terrestrial LiDAR. However, a high potential of smartphone-based LiDAR measurements was also presented (Alvites et al., 2022). A comparative analysis was done to measure the forest roads wearing with iPhone 13 Pro and was compared with the high Precision TLS and GeoSLAM ZEB Horizon. The results showed that the forest roads cross-section profile was being generated quite accurately. However, the estimates were not precise, and the error increased as the distance increased along the horizontal traverse of the path. The researchers did multiple analyses and observations and concluded that the iPhone 13 Pro LiDAR could not be exactly used for any design or calculation of materials required for forest road-wearing course repair (Mikita et al., 2022).

A free mobile application using an iPhone or iPad has been developed for forest inventory measurement: ForestScanner (Tatsumi et al., 2023). The application estimates the stem diameter by circle fitting and the relative position of each tree based on real-time instance segmentation. The application was tested on 672 trees and detected 100% of trees with DBH >5 cm. The application can be effectively used by non-experts; also, there is no need for manual analysis of 3D point clouds.

In this study, we have compared three algorithms and found that the ForestScanner is the best option when you have unfiltered data, and the CloudCompare-based RANSAC plugin is very good for the usage in the estimation of DBH when you have filtered data. We have also done statistical analysis to determine the significance of these devices for estimating DBH of different tree species and found a significant relation with the species. A significant relationship between species and DBH is also observed due to the variation in the bark texture of each tree species (Figure 1). The ANOVA and Tukey post-hoc test showed that the DBH estimation highly influenced the tree species. However, selecting algorithms between ForestScanner and RANSAC is an option, as it does not account much for the estimation of DBH and gives almost the same estimation.

5. Conclusion and Recommendation

The application of algorithms for estimating tree parameters is now in trend. There are a lot of algorithms and standalone software available for this purpose. However, benchmarking for the accuracy of the estimation of tree parameters is missing. In this study, we have tried to compare three methods using iPhone point cloud data. The comparison was based not only on the accuracy of the estimation of DBH by the algorithms but also on the impact of different methods on different tree species' diameters. Due to the different textures of the bark of different trees, the point cloud density and occurrence near the surface of the bark can be different. So, it can cause some differences while considering the surface point for fitting the algorithm. However, we found that ForestScanner and RANSAC can be used for the DBH estimation irrespective of the tree species; these algorithms are independent of noise in the data. Perhaps rTLS is highly dependent on noise in the data. The ForestScanner and the RANSAC algorithm demonstrate strong robustness in forestry applications, particularly for accurately estimating DBH considering the data quality. Future work will include more trees for the mentioned tree species in this study. Benchmarking of algorithms should be done to ensure the accuracy of the estimation of DBH. The algorithms should also be tested on the other tree species.

6. Acknowledgement

The authors thank the forestry and wood sciences faculty at the Czech University of Life Sciences, Prague, for providing the infrastructure. The work was supported by Internal Grant Agency grant no A_08_23 for providing funds ("Mobile Laser Scanning for precision forestry from data collection to tree parameter").

7. Declaration of Competing Interest

The authors declare that they do not have any known financial and personal interest that could appear to have a conflict in the work reported.

8. References

Alijani, Z., Meloche, J., McLaren, A., Lindsay, J., Roy, A., & Berg, A. (2022). A comparison of three surface roughness characterization techniques: photogrammetry, pin profiler, and smartphone-based LiDAR. *International Journal of Digital Earth*, *15*(1), 2422–2439. https://doi.org/10.1080/17538947.2022.2160842

Alvites, C., Marchetti, M., Lasserre, B., & Santopuoli, G. (2022). LiDAR as a Tool for Assessing Timber Assortments: A Systematic Literature Review. In *Remote Sensing* (Vol. 14, Issue 18). MDPI. https://doi.org/10.3390/rs14184466

Aslan, İ., & Polat, N. (2022). *Advanced LiDAR Availability of Iphone 13 Pro Laser Data in 3D Modeling*. http://publish.mersin.edu.tr/index.php/lidar/inde

Bobrowski, R., Winczek, M., Zięba-Kulawik, K., & Wężyk, P. (2023). Best practices to use the iPad Pro LiDAR for some procedures of data acquisition in the urban forest. *Urban Forestry and Urban Greening*, *79*. https://doi.org/10.1016/j.ufug.2022.127815

Borz, S. A., Toaza, J. M. M., Forkuo, G. O., & Marcu, M. V. (2022). Potential of Measure App in Estimating Log Biometrics: A Comparison with Conventional Log Measurement. *Forests*, *13*(7). https://doi.org/10.3390/f13071028

Çakir, G. Y., Post, C. J., Mikhailova, E. A., & Schlautman, M. A. (2021). 3D LiDAR Scanning of Urban Forest Structure Using a Consumer Tablet. *Urban Science*, *5*(4). https://doi.org/10.3390/urbansci5040088

Costantino, D., Vozza, G., Pepe, M., & Alfio, V. S. (2022). Smartphone LiDAR Technologies for Surveying and Reality Modelling in Urban Scenarios: Evaluation Methods, Performance and Challenges. *Applied System Innovation*, *5*(4). https://doi.org/10.3390/asi5040063

Fan, Y., Feng, Z., Mannan, A., Khan, T. U., Shen, C., & Saeed, S. (2018). Estimating tree position, diameter at breast height, and tree height in real-time using a mobile phone with RGB-D SLAM. *Remote Sensing*, *10*(11). https://doi.org/10.3390/rs10111845

Girardeau-Montaut, D. (2015). *CloudCompare version 2.6.1. user manual*. 181. http://www.danielgm.net/cc/

Gollob, C., Ritter, T., Kraßnitzer, R., Tockner, A., & Nothdurft, A. (2021). Measurement of forest inventory parameters with apple ipad pro and integrated lidar technology. *Remote Sensing*, *13*(16), 1–35. https://doi.org/10.3390/rs13163129

Guzmán, J. A., Hernandez, R., & Sanchez-Azofeifa. (2021). *rTLS: Tools to Process Point Clouds Derived from Terrestrial Laser Scanning*. https://cran.r-project.org/package=rTLS

King, F., Kelly, R., & Fletcher, C. G. (2022). Evaluation of LiDAR-Derived Snow Depth Estimates From the iPhone 12 Pro. *IEEE Geoscience and Remote Sensing Letters*, *19*. https://doi.org/10.1109/LGRS.2022.3166665

King, F., Kelly, R., & Fletcher, C. G. (2023). New opportunities for low-cost LiDAR-derived snow depth estimates from a consumer drone-mounted smartphone. *Cold Regions Science and Technology*, *207*. https://doi.org/10.1016/j.coldregions.2022.103757

Kükenbrink, D., Marty, M., Bösch, R., & Ginzler, C. (2022). Benchmarking laser scanning and terrestrial photogrammetry to extract forest inventory parameters in a complex temperate forest. *International Journal of Applied Earth Observation and Geoinformation*, *113*(March), 102999. https://doi.org/10.1016/j.jag.2022.102999

Kurdi, F. T., Lewandowicz, E., Shan, J., & Gharineiat, Z. (2024). Three-Dimensional Modeling and Visualization of Single Tree LiDAR Point Cloud Using Matrixial Form. *IEEE Journal of Selected Topics in Applied Earth Observations and Remote Sensing*, *17*, 3010–3022. https://doi.org/10.1109/JSTARS.2024.3349549

Kushwaha, S. K. P., Singh, A., Jain, K., & Mokros, M. (2022). Optimum Number and Positions of

Terrestrial Laser Scanner To Derive Dtm At Forest Plot Level. *International Archives of the Photogrammetry, Remote Sensing and Spatial Information Sciences - ISPRS Archives*, *43*(B3-2022), 457–462. https://doi.org/10.5194/isprs-archives-XLIII-B3-2022-457-2022

Liang, X., Kukko, A., Balenovic, I., Saarinen, N., Junttila, S., Kankare, V., Holopainen, M., Mokros, M., Surovy, P., Kaartinen, H., Jurjevic, L., Honkavaara, E., Nasi, R., Liu, J., Hollaus, M., Tian, J., Yu, X., Pan, J., Cai, S., … Hyyppa, J. (2022). Close-Range Remote Sensing of Forests: The state of the art, challenges, and opportunities for systems and data acquisitions. *IEEE Geoscience and Remote Sensing Magazine*, *10*(3), 32–71. https://doi.org/10.1109/MGRS.2022.3168135

Liu, L., Zhang, A., Xiao, S., Hu, S., He, N., Pang, H., Zhang, X., & Yang, S. (2021). Single Tree Segmentation and Diameter at Breast Height Estimation with Mobile LiDAR. *IEEE Access*, *9*, 24314–24325. https://doi.org/10.1109/ACCESS.2021.3056877

Luetzenburg, G., Kroon, A., & Bjørk, A. A. (2021). Evaluation of the Apple iPhone 12 Pro LiDAR for an Application in Geosciences. *Scientific Reports*, *11*(1). https://doi.org/10.1038/s41598-021-01763-9

Mikita, T., Krausková, D., Hrůza, P., Cibulka, M., & Patočka, Z. (2022). Forest Road Wearing Course Damage Assessment Possibilities with Different Types of Laser Scanning Methods including New iPhone LiDAR Scanning Apps. *Forests*, *13*(11). https://doi.org/10.3390/f13111763

Mokroš, M., Mikita, T., Singh, A., Tomaštík, J., Chudá, J., Wężyk, P., Kuželka, K., Surový, P., Klimánek, M., Zięba-Kulawik, K., Bobrowski, R., & Liang, X. (2021). Novel low-cost mobile mapping systems for forest inventories as terrestrial laser scanning alternatives. *International Journal of Applied Earth Observation and Geoinformation*, *104*. https://doi.org/10.1016/j.jag.2021.102512

Pace, R., Masini, E., Giuliarelli, D., Biagiola, L., Tomao, A., Guidolotti, G., Agrimi, M., Portoghesi, L., De Angelis, P., & Calfapietra, C. (2022). Tree Measurements in the Urban Environment: Insights from Traditional and Digital Field Instruments to Smartphone Applications. *Arboriculture & Urban Forestry*, *48*(2), 113–123. https://doi.org/10.48044/jauf.2022.009

Pérez-Martín, E., Medina, S. L. C., Herrero-Tejedor, T., Pérez-Souza, M. A., de Mata, J. A., & Ezquerra-Canalejo, A. (2021). Assessment of tree diameter estimation methods from mobile laser scanning in a historic garden. *Forests*, *12*(8). https://doi.org/10.3390/f12081013

Razali, M. I., Idris, A. N., Razali, M. H., & Syafuan, W. M. (2022). Quality Assessment of 3D Point Clouds on the Different Surface Materials Generated from iPhone LiDAR Sensor. *International Journal of Geoinformatics*, *18*(4), 51–58. https://doi.org/10.52939/ijg.v18i4.2259

Riquelme, A., Tomás, R., Cano, M., Pastor, J. L., & Jordá-Bordehore, L. (2021). Extraction of discontinuity sets of rocky slopes using iPhone-12 derived 3DPC and comparison to TLS and SfM datasets. *IOP Conference Series: Earth and Environmental Science*, *833*(1). https://doi.org/10.1088/1755-1315/833/1/012056

Schnabel, R., Wahl, R., & Klein, R. (2007). Efficient RANSAC for point-cloud shape detection. *Computer Graphics Forum*, *26*(2), 214–226. https://doi.org/10.1111/j.1467-8659.2007.01016.x

Singh, A, Kushwaha, S. K. P., Nandy, S., & Padalia, H. (2022). Novel Approach for Forest allometric eqaution modelling with RANSAC shape detection using Terrestrial Laser Scanner. *The International Archives of the Photogrammetry, Remote Sensing and Spatial Information Sciences*, *XLVIII-4/W*, 133–138. https://doi.org/10.5194/isprs-archives-XLVIII-4-W4-2022-133-2022

Singh, Arunima, Kushwaha, S. K. P., Nandy, S., & Padalia, H. (2022). An approach for tree volume estimation using RANSAC and RHT algorithms from TLS dataset. *Applied Geomatics*, *14*(4), 785–794. https://doi.org/10.1007/s12518-022-00471-x

Singh, Arunima, Kushwaha, S. K. P., Nandy, S., Padalia, H., Ghosh, S., Srivastava, A., & Kumari, N. (2023). Aboveground Forest Biomass Estimation by the Integration of TLS and ALOS PALSAR Data Using Machine Learning. *Remote Sensing*, *15*(4). https://doi.org/10.3390/rs15041143

Tamimi, R. (2022). Relative accuracy found within iPhone data collection. *International Archives of the Photogrammetry, Remote Sensing and Spatial Information Sciences - ISPRS Archives*, *43*(B2-2022), 303–308. https://doi.org/10.5194/isprs-archives-XLIII-B2-2022-303-2022

Tarsha Kurdi, F., Gharineiat, Z., Lewandowicz, E., & Shan, J. (2024). Modeling the Geometry of Tree Trunks Using LiDAR Data. *Forests*, *15*(2). https://doi.org/10.3390/f15020368

Tatsumi, S., Yamaguchi, K., & Furuya, N. (2023). ForestScanner: A mobile application for measuring and mapping trees with LiDAR-equipped iPhone and iPad. *Methods in Ecology and Evolution*, *14*(7), 1603–1609. https://doi.org/10.1111/2041-210X.13900

Tavani, S., Billi, A., Corradetti, A., Mercuri, M., Bosman, A., Cuffaro, M., Seers, T., & Carminati, E. (2022). Smartphone assisted fieldwork: Towards the digital transition of geoscience fieldwork using LiDAR-equipped iPhones. In *Earth-Science Reviews* (Vol. 227). Elsevier B.V. https://doi.org/10.1016/j.earscirev.2022.103969

Teppati Losè, L., Spreafico, A., Chiabrando, F., & Giulio Tonolo, F. (2022). Apple LiDAR Sensor for 3D Surveying: Tests and Results in the Cultural Heritage Domain. *Remote Sensing*, *14*(17). https://doi.org/10.3390/rs14174157

Torkan, M., Janiszewski, M., Uotinen, L., & Rinne, M. (2023). Method to obtain 3D point clouds of tunnels using smartphone LiDAR and comparison to photogrammetry. *IOP Conference Series: Earth and Environmental Science*, *1124*(1). https://doi.org/10.1088/1755-1315/1124/1/012016

Vlachos, A., Polyzou, A., & Economides, A. (2022). Photogrammetry With LiDAR IPAD Pro. *EDULEARN22 Proceedings*, *1*, 9555–9563. https://doi.org/10.21125/edulearn.2022.2308

Wang, X., Singh, A., Pervysheva, Y., Lamatungga, K. E., Murtinová, V., Mukarram, M., Zhu, Q., Song, K., Surový, P., & Mokroš, M. (2021). Evaluation of iPad Pro 2020 lidar for estimating tree diameters in urban forest. *ISPRS Annals of the Photogrammetry, Remote Sensing and Spatial Information Sciences*, *8*(4/W1-2021), 105–110. https://doi.org/10.5194/isprs-annals-VIII-4-W1-2021-105-2021

Zhou, S., He, G., Kang, F., Li, W., Kan, J., & Zheng, Y. (2019). Extracting diameter at breast height with a handheld mobile liDAR system in an outdoor environment. *Sensors (Switzerland)*, *19*(14). https://doi.org/10.3390/s19143212

International Journal of Applied Earth Observations and Geoinformation 104 (2021) 102512

Contents lists available at ScienceDirect

International Journal of Applied Earth Observations and Geoinformation

journal homepage: www.elsevier.com/locate/jag

Novel low-cost mobile mapping systems for forest inventories as terrestrial laser scanning alternatives

Martin Mokroš [a,b,*], Tomáš Mikita [c], Arunima Singh [a], Julián Tomaštík [d], Juliána Chudá [d], Piotr Wężyk [e], Karel Kuželka [a], Peter Surový [a], Martin Klimánek [c], Karolina Zięba-Kulawik [e], Rogerio Bobrowski [e,f], Xinlian Liang [g,*]

[a] Faculty of Forestry and Wood Sciences, Czech University of Life Sciences Prague, Kamycká 129, 16500 Prague, Czech Republic

[b] Department of Forest Harvesting, Logistics and Ameliorations, Faculty of Forestry, Technical University in Zvolen, T. G. Masaryka 24, 960 01 Zvolen, Slovakia

[c] Department of Forest Management and Applied Geoinformatics, Faculty of Forestry and Wood Technology, Mendel University in Brno, Zemědělská 3, 61300 Brno, Czech Republic

[d] Department of Forest Resources Planning and Informatics, Faculty of Forestry, Technical University in Zvolen, T. G. Masaryka 24, 960 01 Zvolen, Slovakia

[e] Department of Forest Resource Management, Faculty of Forestry, University of Agriculture in Krakow, 31-425 Krakow, Poland

[f] Department of Forest Engineering, Midwestern State University, 84.505-677 Irati, Brazil

[g] The State Key Laboratory of Information Engineering in Surveying, Mapping and Remote Sensing, Wuhan University, 430070 Wuhan, China

ARTICLE INFO

Keywords:
Terrestrial laser scanning
Mobile laser scanning
Photogrammetry
LiDAR
Forest

ABSTRACT

The development of devices capable of generating three-dimensional (3D) point clouds of the forest is flourishing in recent years. It is possible to generate relatively dense and accurate 3D data not only by terrestrial laser scanning but also mobile laser scanning, personal laser scanning (hand-held or in a backpack), photogrammetry, or even using smart devices with Time-of-Flight sensors. Each of the mentioned devices has their limits of usability, and different method to capture and generate 3D point clouds needs to be applied. Therefore, the objective of our experiment was to compare the performance of low-cost technologies capable of generating point clouds and their accuracy of tree detection and diameter at breast height estimation. We tested a multi-camera prototype (MultiCam) for terrestrial mobile photogrammetry constructed by authors. This device is capable of capturing images from four cameras simultaneously and with exact synchronization during mobile data acquisition. Secondly, we have designed and conducted a data collection with iPad Pro 2020 using the new built-in LiDAR sensor. Then we have used mobile scanning approach applied a hand-held personal laser scanning (PLS_{hh}) using GeoSlam Horizon scanner. Moreover, we have used terrestrial laser scanning (TLS) using FARO Focus s70. With all mentioned devices, we have focused on individual tree detection and diameter at breast height measurements by cylinder-based algorithm across eight test sites with dimensions 25x25 m. Altogether, 301 trees were located on test sites, and 268 were considered for the analysis and comparisons (DBH > 7 cm). TLS provided the most accurate and reliable data. Across all test sites, we achieved the highest accuracy (rRMSE ranged from 3.7% to 6.4%) and tree detection rate (90.6–100%). When we have considered only trees with DBH higher than 20 cm, the tree detection rate was 100% across all test sites (altogether 159 trees). When the threshold of trees considered in the evaluation was changed to 10 cm and then to 20 cm (from 7 cm), the accuracy (rRMSE) and tree detection rate increased for all devices significantly. Results achieved (DBH > 7 cm) by iPad Pro were closest to TLS results. The rRMSE ranged across test sites from 8.6% to 12.9% and tree detection 64.5% to 87.5%. PLS_{hh} and MultiCam, the rRMSE ranged from 13.1% to 24.9% and 14% to 38.2%, respectively. The tree detection rate ranged from 55.6% to 75% and 57.1% to 71.9%, respectively. The time needed to conduct data collection on a test site was fastest using MultiCam (approx. 8 min) and slowest using TLS (approx. 40 min).

* Corresponding authors at: Faculty of Forestry and Wood Sciences, Czech University of Life Sciences Prague, Kamycká 129, 16500 Prague, Czech Republic (M. Mokroš).

E-mail addresses: mokros@fld.czu.cz (M. Mokroš), tomas.mikita@mendelu.cz (T. Mikita), singha@fld.czu.cz (A. Singh), tomastik@tuzvo.sk (J. Tomaštík), xchuda@is.tuzvo.sk (J. Chudá), p.wezyk@ur.krakow.pl (P. Wężyk), kuzelka@fld.czu.cz (K. Kuželka), surovy@fld.czu.cz (P. Surový), martin.klimanek@mendelu.cz (M. Klimánek), karolina.zieba@urk.edu.pl (K. Zięba-Kulawik), rogerio@unicentro.br (R. Bobrowski), xinlian.liang@whu.edu.cn (X. Liang).

https://doi.org/10.1016/j.jag.2021.102512
Received 10 June 2021; Received in revised form 10 August 2021; Accepted 19 August 2021
Available online 1 September 2021

1. Introduction

The development of new measurement techniques (e.g., laser scanning, or LIDAR) and the increasement of computational power of personal and mobile devices have in the last two decades changed the traditional inventory of forest properties and structures (Liang et al., 2016). New techniques provide new possibilities for users to take the forest to the laboratory and evaluate the needed characteristics in post-processing, e.g., in three-dimensional (3D) spaces. This procedure widens the possibilities to investigate forest conditions compared with traditional measures (tree height, diameter at breast height (DBH), trunk position).

3D data is useful in forest inventory and modelling applications, especially when combined with advanced visualisation techniques (Fabrika et al., 2018). However, the adoption of mentioned methods is limited by several constraints. Terrestrial laser scanners (TLS) are generally expensive and laborious in the field, although their spatial accuracy is very high (Liang et al., 2018a). The Structure-from-Motion (SfM) photogrammetry is easy to use from the user point of view, which relies on low-cost camera measurement equipment. The results are, however, highly dependent on the user's experience and the data-acquirement methodology that is complicated under conditions of unstructured environments, e.g. (Liang et al., 2015; Mokroš et al., 2018; Piermattei et al., 2019).

These limitations inspired efforts to bring the technologies able to produce 3D point clouds in a ready-to-use manner. One of the directions is the development and deployment of mobile laser scanners (MLS) (Čerňava et al., 2019; Forsman et al., 2016b; Kukko et al., 2012; Liang et al., 2014, 2018b) and hand-held personal laser scanners (PLS_{hh}) (Balenović et al., 2021). This approach overcomes the static nature of terrestrial laser scanning (TLS) and mitigates occlusion effects. MLS and PLS_{hh} use Simultaneous Localization and Mapping (SLAM) (Durrant-Whyte and Bailey, 2006) to merge trajectories. The SLAM determines the "pose" of the device (position and orientation in a local coordinate system) at a particular moment using recognized features and simultaneously generates a map of the surroundings. The method can be conducted in real-time, but the results can be often improved in post-processing.

The methods of MLS and PLS_{hh} eliminated some limitations of TLS. On the other hand, MLS and PLS_{hh} typically have lower spatial accuracy, and many studies reported mismatches between different trajectories (Čerňava et al., 2019; Liang et al., 2018b).

The next logical step to promote the wide use of 3D information in vast daily applications is to improve the sensor availability to average users. With this regard, the sensors using infrared light were adopted using two measurement principles: "structured light" and "time-of-flight (ToF)" (Sarbolandi et al., 2015), with the latter being more suitable also for outdoor measurements. Concepts of the 3D reconstruction using mentioned sensors were evaluated by Microsoft Kinect cameras (Hyyppä et al., 2018; McGlade et al., 2020; Wasenmüller and Stricker, 2017). In 2014, Google announced the "Project Tango", where the sensors were incorporated into mobile phones. The technology was based on three functionalities: depth perception (measuring of distances), motion tracking (using visual-inertial odometry) and area learning (recognition of already known features). The first two devices – a phone (codename Peanut) and a tablet (Yellowstone) were only available to developers. The first commercial device was the Lenovo Phab 2 Pro phablet, followed by the Asus Zenfone AR. The support for the technology was stopped in March 2018, most probably due to negligible success in the main area of interest – augmented and virtual reality. However, the 3D reconstruction capabilities were evaluated by researchers in many areas, including cultural heritage (Boboc et al., 2019; Schöps et al., 2015), environment monitoring (Chudý et al., 2018) and others. Despite the short lifespan, forestry applications were reported mainly aiming at diameters and positions of trees (Fan et al., 2018; Hyyppä et al., 2018; Tomaštík et al., 2017). Currently, modified versions of ToF sensors are included in smartphones and tablets. In 2020, Apple announced its latest iPad Pro and iPhone 12 Pro/Pro Max, which integrated such a sensor. Following these recent technical progresses, it can be foreseen that there will be more and more low-cost solutions coming into professional and consumer market in the near future. 3D information of the environment will be easier to be collected, but the applicability of such acquired 3D information is still unclear. In this study, we compared four solutions and their performance in the capturing 3D point clouds within a forest environment, i.e., a professional TLS, a state-of-the-art PLS_{hh}, a consumer-level mobile scanning using iPad Pro 2020 with a LiDAR sensor for the first time, and a self-developed multi-camera system for mobile photogrammetry (MultiCam). The idea of the multi-camera system is to provide a solution to compensate for the individual hand-held camera in order to achieve a successful mobile type of data acquisition. Among the four techniques, three sensors are based on active LiDAR sensors and one is based on passive sensors. All devices are compared with each other based on the tree detection rate, the accuracy of DBH measurements and the time needed for data acquisition.

2. Methodology

2.1. Test sites

The test sites are located in the middle of Slovakia within the Kremnica Mountains. Eight research plots with 25 × 25 m dimensions were established (Fig. 1).

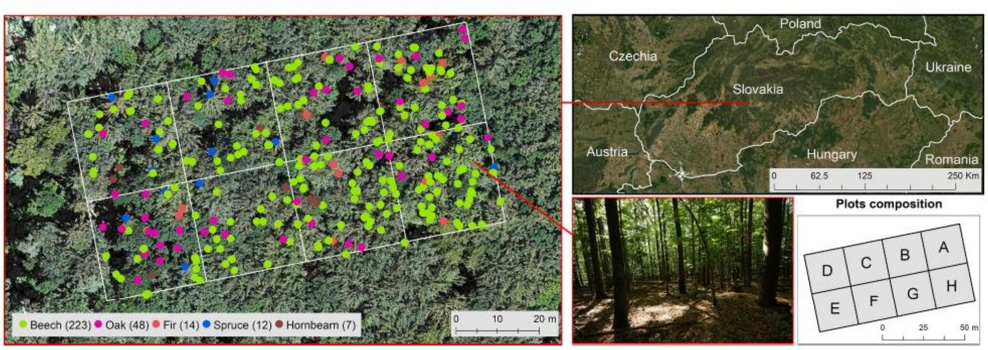

Fig. 1. The overview of all test sites with positions of individual trees (points – tree species based) and borders of research plots (white line) is on the left. On the top right is a position of plots within Slovakia. On the bottom right is a composition of test sites and a photograph from the research plot H.

Table 1
Range and mean of diameter at breast height across test sites with number of trees.

Plot	DBH range (cm)	DBH avg. (cm)	No. of trees	Density (trees/ha)
A	3.3–63.3	22.2	41	656
B	3.1–57.7	25.1	36	576
C	4.7–68.6	27.7	32	512
D	5.1–71.7	30.1	26	416
E	3.9–59.7	26.3	34	544
F	7.4–74.3	31.4	28	448
G	4.7–55.9	21.3	50	800
H	3.8–54.8	22.2	54	864

The number of trees varied from 26 to 54 across test sites (all trees considered) with dominant tree species European beech (*Fagus sylvatica* L.) and Norway spruce (*Picea abies* (L.) H. Karst.). In total, there are 301 trees and 268 trees have a diameter greater than 7 cm. The mean DBH varied from 21.3 cm to 31.4 cm across research plots (Table 1). The mean DBH of all trees was 25.0 cm.

2.2. Conventional in-situ measurements

Trees within each test site were measured by total station Topcon GPT3000M, and perimeters of trees were measured by measuring tape. Firstly, two orientation points and the first position of the total station, representing the first corner of the research plot were built up. The points were measured using the GNSS receiver Topcon Hiper SR combined with the total station Topcon 9000. The corners of the remaining research plots represent the corners of the grid with dimensions 25 × 25 m. They were calculated using coordinate increments of 25 m in the directions of the X and Y axes based on the first total station position, staked out by the total station, and permanently stabilised. The data set was collected with the aim to reach the highest allowed coordinate and elevation errors at the level of 0.02 m, using the corner points as a base for calculation of other consequential objects-representing points.

Afterwards, the position and perimeters of trees and the position of targets were measured for georeferencing purposes. All data were collected from one total station position in the middle of the plots, and two corner points were used as orientation points. The position for the machine was chosen so that all trees could be seen from one place (it was possible in most cases). The six targets oriented to the plot centre were evenly distributed in the plots, and their polar coordinates were measured in a non-prism operation mode. The polar coordinates of the trees at the height of 1.3 m were measured by length offset of the spatial polar method. According to the perimeter of trees, the lengths were adjusted by the radius of a particular individual during office processing. All polar coordinates were transferred to Cartesian coordinates after that.

2.3. Data acquisition and pre-processing

In the experiment, we used four devices: TLS, PLS_{hh}, Apple iPad Pro 2020 with LiDAR sensor (iPad), and a prototype of a multi-camera system (MultiCam). Two main distinguishing parameters are data acquisition approach, i.e., static (TLS) and mobile (PLS_{hh}, iPad, MultiCam), and the type of sensor used, i.e., active (TLS, PLS_{hh}, iPad) and passive (MultiCam).

We have approached data acquisition paths (Fig. 2) and pre-processing workflows differently based on the device properties and capabilities. However, for the same device, the workflow was the same across all research plots, and the processing to final tree positions and DBH estimation was also similar for all point clouds.

2.3.1. Terrestrial laser scanning

In the experiment, we used a Faro Focus s70 laser scanner (FARO Technologies, Inc., Florida, USA). It has a range from 0.5 to 70 m. The accuracy is ±2 mm on 10 m or ±3.5 mm on 25 m. We have used the resolution (point spacing) of 6.14 mm/10 m. One scan took 2 min and 24 s (2 kpt/sec). The advantages of the scanner, important for forestry use, are small dimensions (230 × 183 × 103 mm) and low weight (4.2 kg including battery). Since the scanner is a shift-based type of scanner, the scanning time is quite fast and at the same time with a high number of captured points.

A multi-scan approach was used to scan all research plots. Eight positions were placed on the border or near the border of the research plot and one in the centre of the research plot. The positions on the border were placed near the corners and near the middle of the plot side. The placement was based on the condition of each plot with regards to achieving the lowest occlusions (Fig. 2).

Plastic spheres were placed in the research plots for the purpose of the individual scan merging. Within each plot, twelve spheres were placed inside of the plot. With such a number of spheres and altogether nine scan positions, it was secured that more than four spheres were seen from each scanning position. Merging and georeferencing of the point clouds were done in Faro Scene software (ver. 2020.0.6) using the default workflow. We have used artificial black and white targets on tree trunks to georeference all merged point clouds to the System of the Unified Trigonometrical Cadastral Network (S-JTSK, EPSG:5514).

2.3.2. Hand-held personal laser scanning

The data acquisition by PLS_{hh} was performed using a GeoSLAM Horizon scanner (GeoSLAM Ltd., Nottingham, UK). It has a collection rate of 300,000 points per second, an accuracy of 1–3 cm and a range of 100 m. Before the scanning, it was necessary to place plastic spheres for

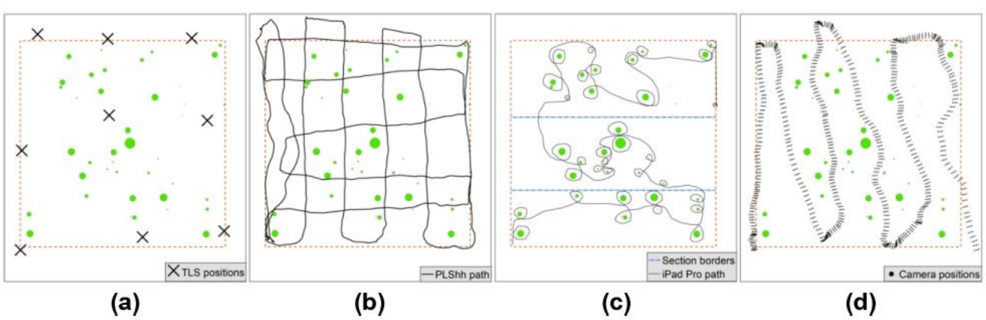

Fig. 2. Data acquisition positions (cross) and paths (black line) of all used devices on an example of plot A. Green circles represent tree positions, and their size is proportional to the diameter measured in the field. Paths of *a*, *b* and *d* are actual paths derived from devices. In the case of *c*, the path is illustration of the actual scanning path.

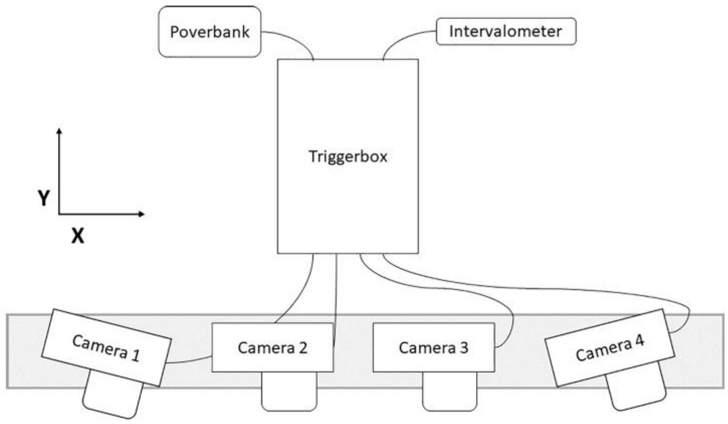

Fig. 3. The scheme of the multi-camera system. Cameras are connected directly to Triggerbox, which is powered by a powerbank and controlled by an intervalometer. Below are examples of images from each camera from plot A from the same position during the mobile imagery.

the subsequent georeferencing of the point cloud. It was not possible to use markers placed on trunks since they were not adequately visible due to the noise. The spheres were placed at the four corners of each plot and scanning always started in the upper right corner and proceeded along the lines at about 5 m intervals with a subsequent cross pass with a diagonal return to the starting point (Fig. 2b). This measurement method was chosen in order to obtain a higher density of points. The data acquisition in one plot, including the placement of reference spheres, did not exceed 10 min.

GeoSLAM Hub software (ver. 5.3.1) was used for post-processing of scanned data, and subsequently, point clouds from each surface were georeferenced into the JTSK system in GeoSLAM Draw software (ver. 3.1). During processing in GeoSLAM HUb, we used default parameters and workflow.

2.3.3. iPad pro scanning

The third device used for scanning the study sites was a 4th generation iPad Pro 2020 tablet (Apple Inc. San Francisco, USA). This is the generation that is equipped with an Apple LiDAR sensor able to scan the environment. Based on the information that Apple has not officially announced, the sensor is a direct time-of-flight custom-designed LiDAR scanner that also uses a camera and motion sensor to measure depth. The sensor is able to scan up to 5 m. We have used a 3d Scanner App (Laan Labs, New York, USA). The app also provides the possibility to colourise and export mesh and point clouds.

Since the range of the scanner is 5 m, we have used a different approach of data acquisition as with other mobile devices (PLS_{hh}, MultiCam). The plots were divided into three segments, and the path started in the first segment, and the operator walked around each tree in sequence. And when all trees were scanned, the path continued to the following segment (Fig. 2c). In the iPad measurement, the operator needed to carefully walk around trees and avoid rescanning already scanned trees. In cases where rescanning of already scanned trees was done, the reconstruction of such trees got worse. In some cases where trees were very near each other, it was necessary to scan them together.

During pre-processing of point clouds, we have found out that it was

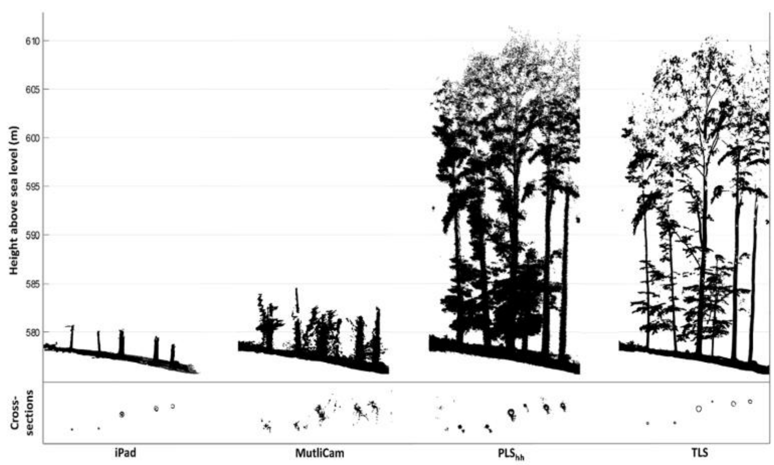

Fig. 4. Examples of point clouds from all devices in Plot B in the side view (top) and 5 cm cross-section at DBH height (below), i.e., 1.275–1.325 cm above the ground.

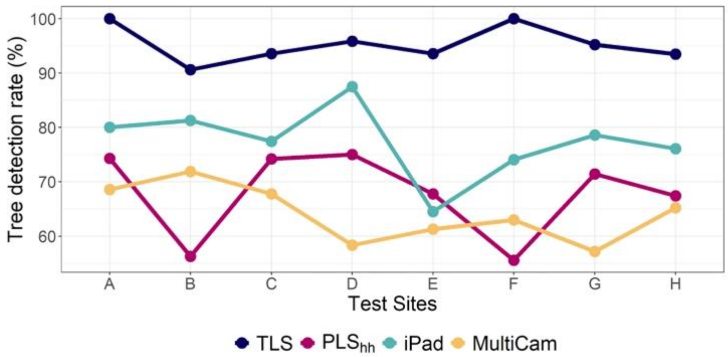

Fig. 5. Tree detection rate of all devices used across eights plots.

not possible to use markers that were placed on tree trunks for georeferencing. Due to this fact, resulting point clouds were aligned with point clouds from TLS in CloudCompare using Iterative Closest Point (ICP) algorithm. It was necessary to georeference point clouds to be able to compare them with reference data.

2.3.4. Multi-camera mobile photogrammetry

Data acquisition by mobile photogrammetry was done by the multi-camera prototype (MultiCam) constructed by authors. The MultiCam consists of four cameras placed on the aluminium profile. We have used Sony a6300 cameras with Sony 10–18 mm F4 OSS lens (Sony Corp., Tokyo, Japan). Two middle cameras were facing in the walking direction, and two cameras on edge have been shifted to the side (Fig. 3). The overlap of at least 60% on 3 m was ensured between edge and middle camera pairs. The overlap was checked before each plot imagery.

We have controlled the imagery capturing by TriggerBox (Esper Ltd., Nottingham, United Kingdom). This device is a multi-camera shutter controller which can control up to six cameras at once. The synchronisation of the shutter for all cameras is secured by very low delay (0.000002 s). The TriggerBox was powered by a powerbank (5,000 mAH), and the shutter was controlled by an intervalometer.

The whole MultiCam system weighs 4.1 kg. It consists of four cameras with lenses (2.5 kg), rig (0.9 kg), TriggerBox with cables (0.45 kg), intervalometer (0.12 kg) and powerbank (0.1 kg). The price is approximately 7,200 euros, where 6,800 euros is for cameras with lenses.

The image capturing was set to one image per second for each camera simultaneously. The path of data acquisition consists of six strips. The distance between strips was approximately 5 m. The MultiCam was facing in the walking direction. On turns, the walking speed was slowed down to ensure high overlap. The number of images ranged through plots from 1,616 to 1,916 (median = 1,850) with all four cameras considered. The number of positions per plot ranged from 404 to 479 (median = 462.5).

The camera settings were adjusted accordingly to the light conditions. Since the mobile approach for data acquisition was used in this experiment, the shutter speed was set to 1/320 s. The ISO was set to 3200 and aperture to 7.1.

Processing of images to georeferenced point clouds was done using Agisoft Metashape (Agisoft LLC, Saint Petersburg, Russia). Firstly, we calibrated the camera using a chessboard screen and the calibration module within the Agisoft Metashape. We have captured images from multiple angles following the calibration protocol from Agisoft documentation. The calibration file was then used within the alignment

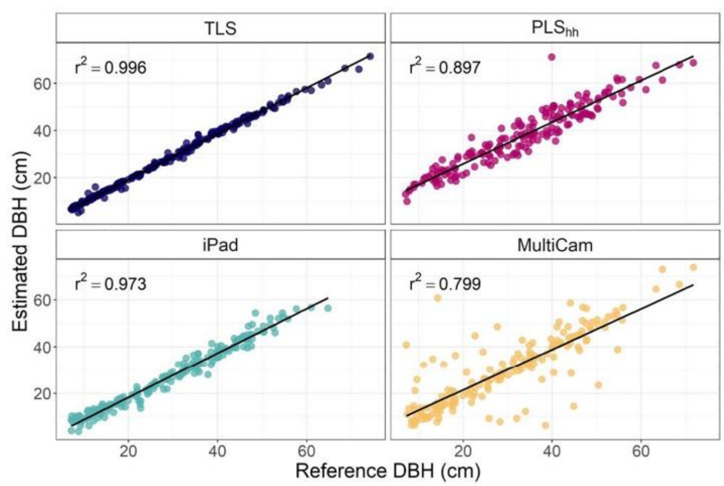

Fig. 6. Conventional and point cloud based methods for DBH measurement, according to each device used, with its regression line and r squared.

Table 2
Results of tree attribute estimation (when all trees across eight plots were considered), i.e., root mean square error and bias in both absolute and relative values, tree detection rate (TDR), false tree detection (FTD) for devices used across all eight plots. Then we report data acquisition time per plot, the weight of the devices with all necessary accessories and approximate price (sources: echosurveying.com and amazon.com).

	RMSE (cm)	rRMSE (%)	Bias (cm)	rBias (%)	TDR (%)	FTD (No.)	Time (min)	Weight (kg)	Approximate Price $
TLS	1.45	5.18	−0.98	3.48	95.15	12	40	6.2	20,970
PLS_{hh}	6.26	18.88	4.34	13.11	67.91	10	10	3.8	30,350
iPad	3.14	10.89	−2.12	7.35	77.24	0	15	0.5	799
MultiCam	6.98	22.86	−0.78	2.56	64.18	137	8	4.1	7,200

process. The images were aligned with "High quality", which is the original resolution of images. We have not used any preselection, which means each image was compared to each image in the dataset. After alignment, we manually searched for markers that were placed on trunks. Markers were used to georeference the tie point cloud to S-JTSK system. On each plot, at least four markers were found. Next step, the densification of tie points was performed with medium quality. Generated point clouds were exported for tree detection and DBH estimation.

The examples of point clouds with their cross-sections at 1.3 m are shown in Fig. 4. Differences in the point-cloud data quality can be clearly seen from the cross-section sub-figures, where the TLS data has the highest level of data accuracy, iPad also provide data with little noise, and MultiCam and PLS_{hh} contain clear noise.

2.4. Tree detection and DBH estimation

The point cloud data from stationary TLS and mobile PLS_{hh}, iPad and MultiCam were processed through the same processing chain as described in (Liang et al., 2018b).

The TLS, PLS_{hh} and MultiCam point clouds were sampled. The point closest to the centre of gravity within each 1 cm voxel was selected. The sampling process gives a comparable data set of the original point cloud in the sense of the point distribution, where the gravity is a unique point that the position vectors relative to this point sum to zero and the point closest to the gravity faithfully represents this unique point without introducing any additional measurement errors. The original point clouds from the iPad were used because of its low resolution.

The DTM was reconstructed using a morphological filter and linear interpolation. Stem points were identified through point-based analyses. Point distributions were studied within their immediate neighbourhood, where potential stem points have vertical planar structures. Tree stem models were built from the recognised stem points as a series of 3D cylinders representing the stem growth. The DBH and location of a stem were estimated from the cylinder element at the breast height (1.3 m above the ground).

2.5. Data evaluation

The tree positions and diameter estimation have been calculated for point clouds generated by each device for all eight plots. These estimated trees were matched with field data measured by total station and measuring tape. For each reference tree, a buffer with a 1 m radius was made to help to locate matches. The pairing was done manually in ArcGIS for desktop 10.7 (ESRI, California, USA) to ensure the correctness of matches.

When all pairs were identified, we calculated estimation errors. Errors were calculated by subtracting reference diameter with estimated diameter (1). To exclude gross error, we have deleted estimated DBH when the relative DBH error exceeded 100% of that particular tree (2).

$$DBH_{err} = DBH_{es} - DBH_r. \tag{1}$$

$$rDBH_{err} = (DBH_{es}\tilde{A}\cdot DBH_{err})*100. \tag{2}$$

where DBH_{err} is a calculated error of estimated DBH, DBH_{es} is a DBH estimated from point cloud, DBH_r is measured DBH in the field and $rDBH_{err}$ is relative error of estimated DBH.

Furthermore, bias, relative bias (rBias), root mean square error (RMSE), and relative RMSE (rRMSE) were calculated to compare the results between devices.

The tree detection rate was calculated based on correct matches between reference and estimated DBH. Falsely detected trees were also identified and reported.

One sample t-Test was used to statistically identify the significance of over- or underestimation of DBH by estimation. We have tested calculated errors of DBH estimation against zero.

A two-way analysis of variance (ANOVA) was used to identify the influence of the device and plot on the DBH estimation accuracy.

3. Results

3.1. Tree detection

The sum of trees with DBH higher than 7 cm is 268 across all test sites. The tree detection rate of all trees was as follows: 95.15% (TLS), 67.91% (PLS_{hh}), 77.24% (iPad), 64.18% (MultiCam).

TLS provided the highest tree detection rate overall. Within each plot, the detection rate ranged from 93.5% to 100%, where 100% tree detection rate was achieved on two plots. PLS_{hh} tree detection rate ranged from 55.6% to 74.3%, for iPad, it ranged from 64.5% to 87.5%, and for MultiCam, it ranged from 57.1% to 71.9% (Fig. 5, Table A1).

The highest amount of falsely detected trees was from MultiCam point clouds, through which 137 trees were falsely detected from an amount of 327 detected trees. The opposite was achieved by the iPad, where 0 trees were falsely detected across all plots. Then TLS had 12 and PLS_{hh} 10 falsely detected trees across all plots. The number of falsely detected trees for each plot and device is shown in the Table A2.

3.2. DBH estimation

The correlation between the reference and estimated DBH was highest when point cloud from TLS was used ($r^2 = 0.996$) and lowest for MultiCam ($r^2 = 0.799$) (Fig. 6). DBH estimated from iPad had also reached a high correlation similar to TLS ($r^2 = 0.973$).

The bias and relative bias for all considered trees measured from a point cloud of TLS, PLS_{hh}, iPad and MultiCam was −0.98 cm (3.48%), 4.34 cm (13.11%), −2.12 cm (7.35%) and −0.78 cm (2.56%) respectively (Table 2). The range across plots was −1.43 cm to −0.7 cm, 2.58 cm to 6.00 cm, −2.59 cm to −1.79 and −5.04 cm to 2.53 cm respectively (Tables A3 and A4).

The DBH estimated from TLS, iPad and MultiCam underestimated the conventional DBH measurements. For TLS and iPad, the underestimation was statistically significant. In the case of PLS_{hh}, the DBH is significantly overestimated (Fig. 7). The significance of over- and underestimation was tested by One-Sample t-Test.

When all trees from eight plots were used to calculate RMSE and rRMSE, the highest accuracy was achieved by TLS with RMSE 1.45 cm and rRSME 5.18%. The least accurate results were achieved by MultiCam, where RMSE was 6.98 cm, and rRMSE was 22.86% (Table 2). When results are grouped by plots, TLS achieved the most accurate results across all plots with RMSE ranging from 1 cm to 2 cm and rRMSE

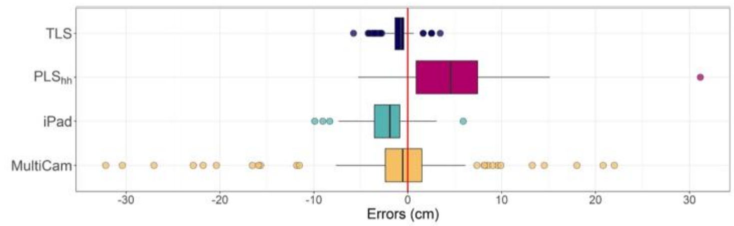

Fig. 7. Boxplots of absolute errors (cm), where boxplots correspond to the 25th and 75th percentiles and whiskers are 1.5 * interquartile range. The line inside the boxplots corresponds to the median. Dots represent outliers.

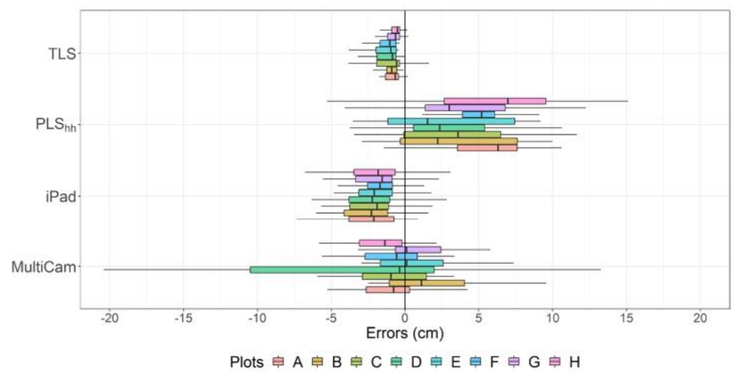

Fig. 8. Boxplots of absolute errors (cm). boxplots correspond to the 25th and 75th percentiles and whiskers are 1.5 * interquartile range. The line inside the boxplots corresponds to the median.

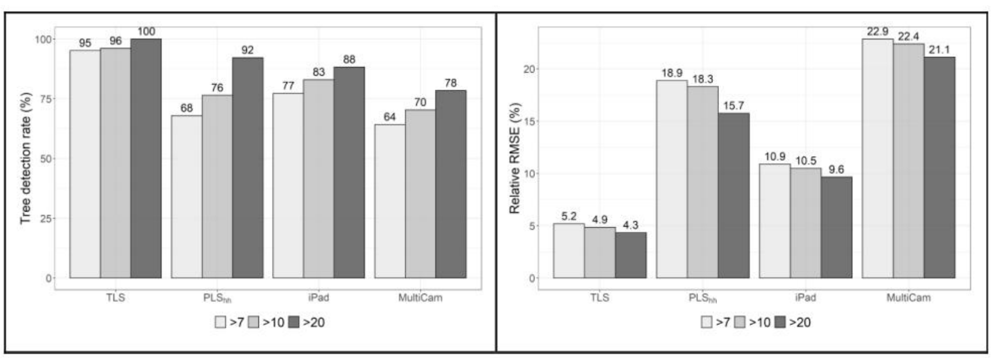

Fig. 9. The changes of tree detection rate (left) and rRMSE (right) for three DBH thresholds (7 cm, 10 cm and 20 cm) grouped by used devices.

from 3.7% to 6.4%. Regarding the least accurate results, the MultiCam has achieved it on six plots and PLS_{hh} on two plots (B and G). The range was 5.3 cm to 14.3 cm (18.8–38.2%) and 4.8 cm to 8.8 cm (13.1–24.9%), respectively. The iPad achieved RMSE 3.14 cm and rRMSE 10.89% when all trees were considered. The RMSE and rRMSE for all used devices for each plot are shown in Tables A5 and A6.

Two-way ANOVA was used to test the significant influence of devices, plots and their interaction on the accuracy of DBH estimation. The ANOVA indicates a significant impact of devices, plots and their interactions (Table A7). We have used the Tukey post hoc test to identify which devices, plots and interactions are significantly different from each other. When only devices were compared, only the difference between TLS and MultiCam was not statistically significant. When plots were compared, only the difference between Plot D and B was statistically significant. To compare interactions 496 pairs were made of those 154 were statistically significantly different from each other and 145 of them were pairs that contained PLS_{hh}. This difference can be clearly seen in Fig. 8. The remaining pairs that were significantly different were pairs of MultiCam plot B with all iPad plots.

3.3. DBH thresholds

Next, we have evaluated trees with DBH higher than 10 cm and 20 cm. The hypothesis is that the results for such trees are going to be more

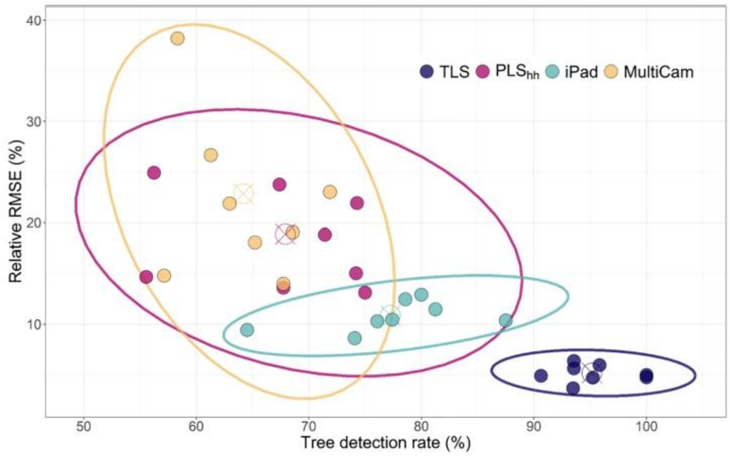

Fig. 10. Scatter plot visualising tree detection rate and rRMSE grouped by used devices. Each device has eight filled points (representing test sites) with one data ellipse and one crossed circle which represents an overall tree detection rate and rRMSE of trees with DBH larger than 7 cm.

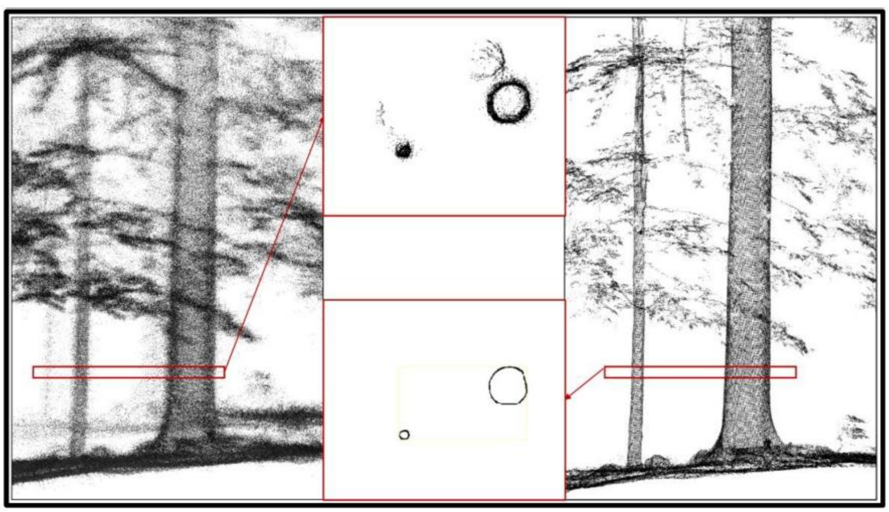

Fig. 11. The point clouds of two individual trees from PLS_{hh} (left) and TLS (right). A top view of 10 cm cross-sections at the breast height in both datasets is also illustrated in the middle.

accurate with a higher tree detection rate and the larger the tree size, the higher possibility is the correct detection/modelling. Across the plots, 301 trees were measured by conventional methods with all DBH sizes considered, 268 trees (89%) with DBH higher than 7 cm, 229 (76%) with >10 cm and 153 (51%) with >20 cm. The accuracy (rRMSE) and tree detection rate increased significantly and linearly for all devices when the threshold of DBH was changed to 10 cm and then to 20 cm (Fig. 9, Table A8).

4. Discussion

4.1. The overall evaluation on the extracted tree parameters

Results showed that DBH estimation from TLS point clouds is achieving the most accurate results together with the highest tree detection rate across all test sites and overall when compared to the other three mobile devices (Fig. 10). The reliable accuracy achieved by iPad Pro across all sites is showing a high potential for future applications, especially when other high-quality sensors and options of smart devices will be used. On the other hand, PLS_{hh} and MultiCam data have issues such as a high amount of noise and inaccurate alignments, results typically have lower accuracy.

The most visible advantage of TLS and PLS_{hh} is the long-range of the sensors. It is usually tens of meters and with scanners that we have used it was 70 m for TLS and 100 m for PLS_{hh}. Such range is sufficient for tree height measurements (Jurjević et al., 2020; Wang et al., 2019) or crown reconstruction. This is not feasible with iPad or MultiCam. The range of the iPad is 5 m. The MultiCam system is based on passive sensor (camera). The range is based on the field of view of the camera and only objects captured at least from two positions are going to be reconstructed. Furthermore, the far objects are going to be reconstructed with lower detail than those close to the camera, since the ground sample distance (GSD) will be bigger. The example of point clouds from all devices of plot A are shown in Video 1.

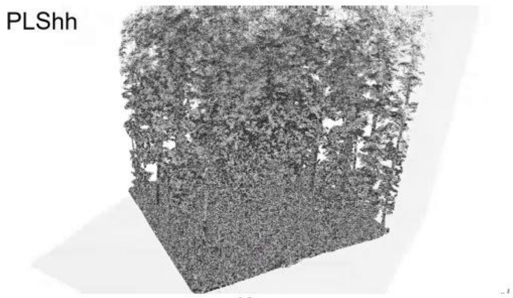

Video 1.

4.2. Hand-held personal laser scanning

Among published studies, the range of tree detection rate was 57–100% (Balenović et al., 2021). The highest rate (100%) tree detection rate for trees over 10 cm of DBH was reported by (Bauwens et al., 2016) over ten plots (331 trees) with different conditions. (Chen et al., 2019) achieved 90.9% tree detection rate for trees over 5 cm and with the same threshold (>5cm), authors (Gollob et al., 2020) achieved a tree detection rate higher than 95% within the majority of 20 plots. On the other hand, some authors achieved worse results. For example (Del Perugia et al., 2019) used three different data collection approaches, and with the one where the distance between strips was 15 m, the tree detection rate was 57%, but when the distance was decreased to 10 m, the tree detection rate was significantly higher (94%).

Based on these results, we assumed that the point cloud would be denser and the issue of occlusion would be significantly decreased if we would have use the distance between lines approximately 5 m and we would have also add perpendicular line paths. But our results rejected this hypothesis. The tree detection rate ranged from 56% to 75%. We assume that this approach brought a higher amount of data to be processed and aligned, which caused more geometric discrepancies. Within all plots, the trunks are not aligned precisely, and many trunks are misaligned themselves (Fig. 11). The problem of the forest environment is that there is an only small number of objects with clearly defined edges that could improve the alignment of the applied SLAM algorithm in the GeoSLAM. According to our results, the chosen trajectory with cross repetition tended to worsen rather than improve the SLAM results.

Although the PLS_{hh} method is promising in forestry, finding the optimal trajectory for data collection will require considerable effort. It is not possible to determine a single procedure for all forest types. Young forest stands with smaller DBH, and higher density will require different data collection than older stands with higher DBH.

When TLS was compared with PLS_{hh}, (Gollob et al., 2020) achieved higher tree detection by PLS_{hh}. This can be caused by the relatively low number of TLS scan positions (four with one in the centre). A similar comparison was done by (Ryding et al., 2015) where 54 trees were detected by TLS and 45 by PLS_{hh}. (Cabo et al., 2018) reported 100% agreement between TLS and PLS_{hh}, where both devices detected 271 trees across two plots.

Based on the review paper of (Balenović et al., 2021), the rRMSE of DBH estimation using PLS_{hh} varied from 3.5% (Hyyppä et al., 2020) to 23% (Ryding et al., 2015). The accuracy of DBH estimation achieved by us was from 13% to 25% and 18.9% overall. The accuracy increased significantly when the threshold of consideration was changed to 10 cm and 20 cm as an opposite of 7 cm. Overall it was changed to 18.3% and 15.7%, respectively. (Ryding et al., 2015) achieved 23% rRMSE when all trees were considered and 9% when only trees with DBH higher than 10 cm were considered. Furthermore, they also calculate rRMSE for trees smaller than 10 cm DBH and the rRMSE was 46%.

Our results also confirm the significant influence of DBH threshold of considered trees. The tree detection rate and accuracy of DBH estimation increased significantly when we have considered trees with DBH > 10 cm and then only those with >20 cm. This is clearly raising the important issue of where the threshold should be and how it will influence whole forest stand results.

4.3. Smart devices with ToF

The advantages of using smart devices such as smartphones or tablets is the easy manipulation (weight and size) and also familiarity with such devices within a majority of the population. Furthermore, in future, when additional sensors or functions of such devices are going to be explored and used for forestry applications, the employment will be even more reasonable. For example, the usage of GNSS data from smartphones for positioning within forest environment (Tomaštík et al., 2017). In recent years studies focused mainly on two paths. Firstly, the "Project Tango" where developers mainly focused on augmented reality applications. To be able to scan the environment, devices with infrared depth sensors were needed. For example, Lenovo Phab 2 Pro phablet. Authors (Fan et al., 2018; Hyyppä et al., 2018; Tomaštík et al., 2017) explored the application for the tree parameters estimation. The accuracy (rRMSE) achieved for DBH estimation within plots varied from 6.8% to 8.8% (Tomaštík et al., 2017) and from 2% to 11.1% (Fan et al., 2018). The results achieved within the presented study ranged from 8.6% to 12.6%. These results are similar and slightly worse than the previous reported studies. However, the main difference between the iPad Pro scanning and Google Tango approach is that Google Tango has implemented the SLAM algorithm with the "loop closure" detection, which improves the trajectory accuracy using the alignment of multiple-times scanned features. This algorithm is helping to localise the device without using a GNSS device or sensor.

The disadvantage when we have used the iPad to scan the plots was the removal of already scanned areas due to the lack of SLAM-like algorithm. We needed to always check whether we are far enough from already scanned trees to avoid rescanning them from faraway positions, which would lead to worse accuracy of such trees. Since the range is 5 m it was possible to avoid it in the majority of cases. But for more dense plots this can cause issues during scanning and will lead to worse accuracy. We believe that the implementation of the SLAM algorithm will help to eliminate such issues.

Besides Google Tango, Microsoft Kinect is another similar alternative. (McGlade et al., 2020) has conducted an experiment within an urban park with larger trees (mean DBH 73.4 cm). The data acquisition focused on individual trees, and it was static from a tripod with a different distance from the trunk (1–3 m). The RMSE ranged from 6.8 cm to 16.9 cm. What is approximately 9.2–23.0% of rRMSE (the average DBH was 73.4 cm).

4.4. Multi-camera photogrammetry

Few studies have been published which used more than one camera at once to conduct a photogrammetry image collection of forest stands. Moreover, we believe only (Forsman et al., 2016a) has dealt with more than two cameras at once. They used a camera rig with five cameras. Since the two cameras have been found to have insufficient optical stabilisation they were used just partially. Altogether 25 research plots with a 20 m radius were used. On these plots, images from the centre were taken from 12 positions. It was possible to sufficiently reconstruct point clouds on six plots for the DBH estimation and evaluation. The relative root mean square error varied from 12.4% to 60.5% within six plots. The range of the presented study using MultiCam is 14.8–38.2%. The study of (Forsman et al., 2016a) used a multi-camera rig, but the data acquisition was static and only from the centre of a plot by three cameras and partially with two other cameras.

In our experiment, we have used mobile photogrammetry. In the majority of published papers on the subject of using terrestrial photogrammetry for measuring DBH is a static approach prefered or the so-called stop-and-go method. With this approach, the operator is taking images only when it is not moving with the camera on a tripod or in hand. When mobile is compared to a stop-and-go (static) approach, the advantage is faster data acquisition. In Mokroš et al. (2018), the average time needed to conduct mobile photogrammetry was slightly above 13 min, and by the stop-and-go method, it was 31 min on average for the same plot (35 × 35 m).

On the other hand, the mobile photogrammetry is more prone to fail to align images and generate sufficient and accurate point clouds. The operator is continuously moving and taking images. It is essential to secure a sufficient overlap between images. From our experience, the trickiest part of such data acquisition is the turning points outside the plot where the operator needs to turn back to the plot and do another line strip. In these places, the alignment photogrammetry process is failing most. Our hypothesis was that using multiple cameras in a row will greatly help to keep the overlap during the walking but also on those turning points. This hypothesis seems correct. We have aligned all images on turning points or in other parts of imagery paths. We have not needed to repeat data acquisition.

The challenge of mobile photogrammetry is the camera settings. Since the operator is constantly moving during imagery, the shutter speed must be quite high to avoid blurry images. When the shutter speed is high in a fairly dark environment, as the dense forest during vegetation season is, the ISO and aperture must be set appropriately to achieve bright enough images. In our case, we have used 1/320 s shutter speed, 3200 ISO and 7.1 aperture. The ideal combination for such data acquisition should be explored. If we change the shutter speed to faster values, the ISO and aperture should be adjusted, but we do not have an answer yet which settings will bring results with less noise and with higher accuracy. Regarding the stop-and-go method, the shutter speed can be slower especially when a tripod is used. This is the main advantage of the static approach versus the mobile one.

Overall terrestrial photogrammetry can provide high accuracy of DBH measurements. The RMSE can achieve sub-centimetre accuracy. Especially in cases where a stop-and-go approach is used and only one tree at a time is photographed. In Mokroš et al. (2020), authors used such an approach, and the rRMSE has not exceeded 1% in all 40 trees, and they were able to measure the annual trunk increment of mature trees. When authors focus on multiple trees at plots using a single camera, the rRMSE can vary from 2% (Mikita et al., 2016) to 61% (Forsman et al., 2016a). Results are highly dependent on the data acquisition approach, camera and lens, camera settings, forest stand parameters and so on.

In the present study, we have achieved an rRMSE range 14–38%. We believe that the results could be improved. In future experiments, we will focus on the different setup of cameras on the rig, higher number of cameras, composition, or orientation. Furthermore, the influence of different camera settings should be tested.

5. Conclusion

We presented here a comparison of well-known terrestrial laser scanning (TLS), state-of-the-art hand-held personal laser scanning (PLS_{hh}), laser scanning based on iPad Pro (hand-held) and mobile photogrammetry with a self-constructed multi-camera system (MultiCam). The comparison was based on the performance within forest stands focusing on tree detection, DBH estimation and overall performance. Altogether, eight plots (25 × 25 m), with 301 trees (602 trees per ha), were established. Data acquisition of one plot lasted 40 min (TLS), 10 min (PLS_{hh}), 15 min (iPad) and 8 min (MultiCam). TLS achieved tree detection above 90% for all eight plots. None of the other used devices reached a 90% tree detection rate. The highest range among them was when iPad was used 64.5% 87.5%. The tree detection rate range of PLS_{hh} and MultiCam was 55.6–74.3% and 57.1–71.9%, respectively. Similar results were achieved when the accuracy of DBH estimation was compared. TLS had RMSE under 2 cm for all plots. None of the other used devices reached such accuracy. Nevertheless, iPad performed the closest results, 2.6–3.4 cm.

Each device provides certain benefits. The advantage of TLS and PLS_{hh} is the coverage of the upper parts of trees. Therefore, also tree height or crown parameters are possible to measure directly from point clouds. On the other hand, both devices are significantly more expensive than the iPad or MultiCam. Thus, if the goal is to measure DBH, these devices could be the suitable alternative. However, further experiments have to be done within forests with different levels of complexity. Furthermore, experiments focusing on achieving 100% tree detection rate on the plot, and in the case of MultiCam, the focus should be on decreasing point cloud noise. Only iPad Pro is a solution that provides point cloud right away in the field. This advantage is highly usable for forestry practice, where operators can have results right away in the field. On the other hand, the data acquisition must be done very carefully to avoid rescanning already scanned parts, which makes it less practical in the field, especially in more complex forests. Potentially it might be solved by SLAM algorithm implementation.

Overall, TLS provided the most accurate and reliable results. Nevertheless, the performance of iPad Pro with the LiDAR sensor had the DBH estimation accuracy and tree detection rate closest to the TLS results when PLS_{hh} and MultiCam are considered for comparison.

Funding

This work was supported by grant No. CZ.02.1.01/0.0/0.0/16_019/0000803 ("Advanced research supporting the forestry and wood-processing sector's adaptation to global change and the 4th industrial revolution") financed by OP RDE, by the Scientific Grant Agency of the Ministry of Education, Science, Research, and Sport of the Slovak Republic and the Slovak Academy of Sciences [grant number VEGA 1/0335/20] and by the Internal Grant Agency of the Faculty of Forestry and Wood Technology, Mendel University in Brno, Czech Republic, grant number LDF_TP_2019012 "Remote Sensing to Support the Sustainability of Forest Production Under the Condition of Ongoing Climate Change".

Declaration of Competing Interest

The authors declare that they have no known competing financial interests or personal relationships that could have appeared to influence the work reported in this paper.

Appendix A

Tables A1–A8.

Table A1
Tree detection rate (%) of all devices used for each plot are reported.

	A	B	C	D	E	F	G	H
TLS	100	90.6	93.5	95.8	93.5	100	95.2	93.5
PLS_{hh}	74.3	56.2	74.2	75	67.7	55.6	71.4	67.4
iPad	80	81.2	77.4	87.5	64.5	74.1	78.6	76.1
MultiCam	68.6	71.9	67.7	58.3	61.3	63	57.1	65.2

Table A2
Falsely detected trees (n) of all devices used for each plot are reported.

	A	B	C	D	E	F	G	H
TLS	2	3	2	3	1	0	1	0
PLS_{hh}	3	1	0	1	0	3	2	0
iPad	0	0	0	0	0	0	0	0
MultiCam	25	12	18	16	19	14	12	21

Table A3
BIAS (cm) of all devices used for each plot are reported.

	A	B	C	D	E	F	G	H
TLS	−0.92	−0.96	−0.95	−1.43	−1.14	−1.15	−0.86	−0.7
PLS_{hh}	5.55	4.59	3.5	2.82	2.58	4.85	3.97	6
iPad	−2.59	−2.6	−2.17	−1.79	−2.15	−1.8	−1.95	−1.87
MultiCam	−1.62	2.53	−1.33	−5.04	−1.65	−0.12	1.3	−1.78

Table A4
rBIAS (%) of all devices used for each plot are reported.

	A	B	C	D	E	F	G	H
TLS	3.67	3.37	3.19	4.32	3.85	3.67	3.44	2.67
PLS_{hh}	19.21	12.94	10.03	7.78	7.03	13.33	13.41	18.95
iPad	9.87	8.87	6.93	5.57	7.07	5.88	7.51	6.79
MultiCam	6.05	9.9	3.83	13.5	5.1	0.37	4.5	5.9

Table A5
RMSE (cm) of all devices used for each plot are reported.

	A	B	C	D	E	F	G	H
TLS	1.3	1.4	1.7	2	1.9	1.5	1.2	1
PLS_{hh}	6.3	8.8	5.2	4.8	5	5.3	5.6	7.5
iPad	3.4	3.4	3.3	3.3	2.9	2.6	3.2	2.8
MultiCam	5.1	5.9	4.9	14.3	8.6	7.1	4.3	5.4

Table A6
rRMSE (%) of all devices used for each plot are reported.

	A	B	C	D	E	F	G	H
TLS	5	4.9	5.6	6	6.4	4.7	4.7	3.7
PLS_{hh}	21.9	24.9	15	13.1	13.6	14.7	18.8	23.7
iPad	12.9	11.5	10.5	10.4	9.4	8.6	12.5	10.3
MultiCam	19.1	23	14	38.2	26.7	21.9	14.8	18.1

Table A7
Analysis of variance results.

	term	df	sumsq	meansq	statistic	p value
1	Device	3	0.470974	0.156991	99.34317	1.66E−54
2	Plot	7	0.024285	0.003469	2.195353	0.032723
3	Device:Plot	21	0.072798	0.003467	2.193635	0.001581
4	Residuals	784	1.238951	0.00158	NA	NA

Table A8
Absolute and relative root mean square error and tree detection rate for used devices across all eight plots for trees with DBH higher than 7 cm, 10 cm and 20 cm are reported.

	RMSE (cm)			rRMSE (%			TDR (%)		
	>7	>10	>20	>7	>10	>20	>7	>10	>20
TLS	1.45	1.51	1.67	5.18	4.86	4.33	95.15	96.07	100
PLS_{hh}	6.26	6.24	6.09	18.88	18.3	15.7	67.91	76.42	92.16
iPad	3.14	3.21	3.58	10.89	10.5	9.65	77.24	82.97	88.24
MultiCam	6.98	7.16	8.00	22.86	22.4	21.1	64.18	70.3	78.43

References

Balenović, I., Liang, X., Jurjević, L., Hyyppä, J., Seletković, A., Kukko, A., 2021. Hand-Held Personal Laser Scanning – Current Status and Perspectives for Forest Inventory Application. Croat. J. Eng. 19.

Bauwens, S., Bartholomeus, H., Calders, K., Lejeune, P., 2016. Forest Inventory with Terrestrial LiDAR: A Comparison of Static and Hand-Held Mobile Laser Scanning. Forests 7, 127. https://doi.org/10.3390/f7060127.

Boboc, R.G., Duguleanã, M., Voinea, G.-D., Postelnicu, C.-C., Popovici, D.-M., Carrozzino, M., 2019. Mobile Augmented Reality for Cultural Heritage: Following the Footsteps of Ovid among Different Locations in Europe. Sustainability 11, 1167. https://doi.org/10.3390/su11041167.

Cabo, C., Del Pozo, S., Rodríguez-Gonzálvez, P., Ordóñez, C., González-Aguilera, D., 2018. Comparing Terrestrial Laser Scanning (TLS) and Wearable Laser Scanning (WLS) for Individual Tree Modeling at Plot Level. Remote Sens. 10, 540. https://doi.org/10.3390/rs10040540.

Čerňava, J., Mokroš, M., Tuček, J., Antal, M., Slatkovská, Z., 2019. Processing Chain for Estimation of Tree Diameter from GNSS-IMU-Based Mobile Laser Scanning Data. Remote Sens. 11, 615. https://doi.org/10.3390/rs11060615.

Chen, S., Liu, H., Feng, Z., Shen, C., Chen, P., 2019. Applicability of personal laser scanning in forestry inventory. PLoS ONE 14, e0211392. https://doi.org/10.1371/journal.pone.0211392.

Chudý, F., Slámová, M., Tomaštík, J., Tunák, D., Kardoš, M., Saloň, Š., 2018. The application of civic technologies in a field survey of landslides. Land Degrad. Dev. 29, 1858–1870. https://doi.org/10.1002/ldr.2957.

Del Perugia, B., Giannetti, F., Chirici, G., Travaglini, D., 2019. Influence of Scan Density on the Estimation of Single-Tree Attributes by Hand-Held Mobile Laser Scanning. Forests 10, 277. https://doi.org/10.3390/f10030277.

Durrant-Whyte, H., Bailey, T., 2006. Simultaneous localization and mapping: part I. IEEE Rob. Autom. Mag. 13, 99–110. https://doi.org/10.1109/MRA.2006.1638022.

Fabrika, M., Valent, P., Scheer, Ľ., 2018. Thinning trainer based on forest-growth model, virtual reality and computer-aided virtual environment. Environ. Model. Softw. 100, 11–23. https://doi.org/10.1016/j.envsoft.2017.11.015.

Fan, Y., Feng, Z., Mannan, A., Khan, T.U., Shen, C., Saeed, S., 2018. Estimating Tree Position, Diameter at Breast Height, and Tree Height in Real-Time Using a Mobile Phone with RGB-D SLAM. Remote Sens. 10, 1845. https://doi.org/10.3390/rs10111845.

Forsman, M., Börlin, N., Holmgren, J., 2016a. Estimation of Tree Stem Attributes Using Terrestrial Photogrammetry with a Camera Rig. Forests 7, 61. https://doi.org/10.3390/f7030061.

Forsman, M., Holmgren, J., Olofsson, K., 2016b. Tree Stem Diameter Estimation from Mobile Laser Scanning Using Line-Wise Intensity-Based Clustering. Forests 7, 206. https://doi.org/10.3390/f7090206.

Gollob, C., Ritter, T., Nothdurft, A., 2020. Forest Inventory with Long Range and High-Speed Personal Laser Scanning (PLS) and Simultaneous Localization and Mapping (SLAM) Technology. Remote Sens. 12, 1509. https://doi.org/10.3390/rs12091509.

Hyyppä, E., Yu, X., Kaartinen, H., Hakala, T., Kukko, A., Vastaranta, M., Hyyppä, J., 2020. Comparison of Backpack, Handheld, Under-Canopy UAV, and Above-Canopy UAV Laser Scanning for Field Reference Data Collection in Boreal Forests. Remote Sens. 12, 3327. https://doi.org/10.3390/rs12203327.

Hyyppä, J., Virtanen, J.-P., Jaakkola, A., Yu, X., Hyyppä, H., Liang, X., 2018. Feasibility of Google Tango and Kinect for Crowdsourcing Forestry Information. Forests 9, 6. https://doi.org/10.3390/f9010006.

Jurjević, L., Liang, X., Gašparović, M., Balenović, I., 2020. Is field-measured tree height as reliable as believed – Part II, A comparison study of tree height estimates from conventional field measurement and low-cost close-range remote sensing in a deciduous forest. ISPRS J. Photogramm. Remote Sens. 169, 227–241. https://doi.org/10.1016/j.isprsjprs.2020.09.014.

Kukko, A., Kaartinen, H., Hyyppä, J., Chen, Y., 2012. Multiplatform Mobile Laser Scanning: Usability and Performance. Sensors 12, 11712–11733. https://doi.org/10.3390/s120911712.

Liang, X., Hyyppä, J., Kaartinen, H., Lehtomäki, M., Pyörälä, J., Pfeifer, N., Holopainen, M., Brolly, G., Francesco, P., Hackenberg, J., Huang, H., Jo, H.-W., Katoh, M., Liu, L., Mokroš, M., Morel, J., Olofsson, K., Poveda-Lopez, J., Trochta, J., Wang, D., Wang, J., Xi, Z., Yang, B., Zheng, G., Kankare, V., Luoma, V., Yu, X., Chen, L., Vastaranta, M., Saarinen, N., Wang, Y., 2018a. International benchmarking of terrestrial laser scanning approaches for forest inventories. ISPRS J. Photogramm. Remote Sens. 144, 137–179. https://doi.org/10.1016/j.isprsjprs.2018.06.021.

Liang, X., Hyyppä, J., Kukko, A., Kaartinen, H., Jaakkola, A., Yu, X., 2014. The Use of a Mobile Laser Scanning System for Mapping Large Forest Plots. IEEE Geosci. Remote Sens. Lett. 11, 1504–1508. https://doi.org/10.1109/LGRS.2013.2297418.

Liang, X., Kankare, V., Hyyppä, J., Wang, Y., Kukko, A., Haggrén, H., Yu, X., Kaartinen, H., Jaakkola, A., Guan, F., Holopainen, M., Vastaranta, M., 2016. Terrestrial laser scanning in forest inventories. ISPRS J. Photogramm. Remote Sens. 115, 63–77. https://doi.org/10.1016/j.isprsjprs.2016.01.006.

Liang, X., Kukko, A., Hyyppä, J., Lehtomäki, M., Pyörälä, J., Yu, X., Kaartinen, H., Jaakkola, A., Wang, Y., 2018b. In-situ measurements from mobile platforms: An emerging approach to address the old challenges associated with forest inventories. ISPRS J. Photogramm. Remote Sens. 143, 97–107. https://doi.org/10.1016/j.isprsjprs.2018.04.019.

Liang, X., Wang, Y., Jaakkola, A., Kukko, A., Kaartinen, H., Hyyppä, J., Honkavaara, E., Liu, J., 2015. Forest Data Collection Using Terrestrial Image-Based Point Clouds From a Handheld Camera Compared to Terrestrial and Personal Laser Scanning. IEEE Trans. Geosci. Remote Sens. 53, 5117–5132. https://doi.org/10.1109/TGRS.2015.2417316.

McGlade, J., Wallace, L., Hally, B., White, A., Reinke, K., Jones, S., 2020. An early exploration of the use of the Microsoft Azure Kinect for estimation of urban tree Diameter at Breast Height. Remote Sens. Lett. 11, 963–972. https://doi.org/10.1080/2150704X.2020.1802528.

Mikita, T., Janata, P., Surový, P., 2016. Forest Stand Inventory Based on Combined Aerial and Terrestrial Close-Range Photogrammetry. Forests 7, 165. https://doi.org/10.3390/f7080165.

Mokroš, M., Liang, X., Surový, P., Valent, P., Čerňava, J., Chudý, F., Tunák, D., Saloň, Š., Merganič, J., 2018. Evaluation of Close-Range Photogrammetry Image Collection Methods for Estimating Tree Diameters. ISPRS Int. J. Geo-Inf. 7, 93. https://doi.org/10.3390/ijgi7030093.

Mokroš, M., Výbošťok, J., Grznárová, A., Bošela, M., Šebeň, V., Merganič, J., 2020. Non-destructive monitoring of annual trunk increments by terrestrial structure from motion photogrammetry. PLoS ONE 15, e0230082. https://doi.org/10.1371/journal.pone.0230082.

Piermattei, L., Karel, W., Wang, D., Wieser, M., Mokroš, M., Surový, P., Koreň, M., Tomaštík, J., Pfeifer, N., Hollaus, M., 2019. Terrestrial Structure from Motion Photogrammetry for Deriving Forest Inventory Data. Remote Sens. 11, 950. https://doi.org/10.3390/rs11080950.

Ryding, J., Williams, E., Smith, M.J., Eichhorn, M.P., 2015. Assessing Handheld Mobile Laser Scanners for Forest Surveys. Remote Sens. 7, 1095–1111. https://doi.org/10.3390/rs70101095.

Sarbolandi, H., Lefloch, D., Kolb, A., 2015. Kinect range sensing: Structured-light versus Time-of-Flight Kinect. Comput. Vis. Image Underst. 139, 1–20. https://doi.org/10.1016/j.cviu.2015.05.006.

Schöps, T., Sattler, T., Häne, C., Pollefeys, M., 2015. 3D Modeling on the Go: Interactive 3D Reconstruction of Large-Scale Scenes on Mobile Devices. In: 2015 International Conference on 3D Vision. Presented at the 2015 International Conference on 3D Vision, pp. 291–299. https://doi.org/10.1109/3DV.2015.40.

Tomaštík, J., Saloň, Š., Tunák, D., Chudý, F., Kardoš, M., 2017. Tango in forests – An initial experience of the use of the new Google technology in connection with forest inventory tasks. Comput. Electron. Agric. 141, 109–117. https://doi.org/10.1016/j.compag.2017.07.015.

Wang, Y., Lehtomäki, M., Liang, X., Pyörälä, J., Kukko, A., Jaakkola, A., Liu, J., Feng, Z., Chen, R., Hyyppä, J., 2019. Is field-measured tree height as reliable as believed – A comparison study of tree height estimates from field measurement, airborne laser scanning and terrestrial laser scanning in a boreal forest. ISPRS J. Photogramm. Remote Sens. 147, 132–145. https://doi.org/10.1016/j.isprsjprs.2018.11.008.

Wasenmüller, O., Stricker, D., 2017. Comparison of Kinect V1 and V2 Depth Images in Terms of Accuracy and Precision. In: Chen, C.-S., Lu, J., Ma, K.-K. (Eds.), Computer Vision – ACCV 2016 Workshops, Lecture Notes in Computer Science. Springer International Publishing, Cham, pp. 34–45. https://doi.org/10.1007/978-3-319-54427-4_3.

References

Balenović, I., Liang, X., Jurjević, L., Hyyppä, J., Seletković, A., Kukko, A., 2021. Hand-Held Personal Laser Scanning – Current Status and Perspectives for Forest Inventory Application. Croat. J. Eng. 19.

Bauwens, S., Bartholomeus, H., Calders, K., Lejeune, P., 2016. Forest Inventory with Terrestrial LiDAR: A Comparison of Static and Hand-Held Mobile Laser Scanning. Forests 7, 127. https://doi.org/10.3390/f7060127.

Boboc, R.G., Duguleană, M., Voinea, G.-D., Postelnicu, C.-C., Popovici, D.-M., Carrozzino, M., 2019. Mobile Augmented Reality for Cultural Heritage: Following the Footsteps of Ovid among Different Locations in Europe. Sustainability 11, 1167. https://doi.org/10.3390/su11041167.

Cabo, C., Del Pozo, S., Rodríguez-Gonzálvez, P., Ordóñez, C., González-Aguilera, D., 2018. Comparing Terrestrial Laser Scanning (TLS) and Wearable Laser Scanning (WLS) for Individual Tree Modeling at Plot Level. Remote Sens. 10, 540. https://doi.org/10.3390/rs10040540.

Čerňava, J., Mokroš, M., Tuček, J., Antal, M., Slatkovská, Z., 2019. Processing Chain for Estimation of Tree Diameter from GNSS-IMU-Based Mobile Laser Scanning Data. Remote Sens. 11, 615. https://doi.org/10.3390/rs11060615.

Chen, S., Liu, H., Feng, Z., Shen, C., Chen, P., 2019. Applicability of personal laser scanning in forestry inventory. PLoS ONE 14, e0211392. https://doi.org/10.1371/journal.pone.0211392.

Chudý, F., Slámová, M., Tomaštík, J., Tunák, D., Kardoš, M., Saloň, Š., 2018. The application of civic technologies in a field survey of landslides. Land Degrad. Dev. 29, 1858–1870. https://doi.org/10.1002/ldr.2957.

Del Perugia, B., Giannetti, F., Chirici, G., Travaglini, D., 2019. Influence of Scan Density on the Estimation of Single-Tree Attributes by Hand-Held Mobile Laser Scanning. Forests 10, 277. https://doi.org/10.3390/f10030277.

Durrant-Whyte, H., Bailey, T., 2006. Simultaneous localization and mapping: part I. IEEE Rob. Autom. Mag. 13, 99–110. https://doi.org/10.1109/MRA.2006.1638022.

Fabrika, M., Valent, P., Scheer, Ľ., 2018. Thinning trainer based on forest-growth model, virtual reality and computer-aided virtual environment. Environ. Model. Softw. 100, 11–23. https://doi.org/10.1016/j.envsoft.2017.11.015.

Fan, Y., Feng, Z., Mannan, A., Khan, T.U., Shen, C., Saeed, S., 2018. Estimating Tree Position, Diameter at Breast Height, and Tree Height in Real-Time Using a Mobile Phone with RGB-D SLAM. Remote Sens. 10, 1845. https://doi.org/10.3390/rs10111845.

Forsman, M., Börlin, N., Holmgren, J., 2016a. Estimation of Tree Stem Attributes Using Terrestrial Photogrammetry with a Camera Rig. Forests 7, 61. https://doi.org/10.3390/f7030061.

Forsman, M., Holmgren, J., Olofsson, K., 2016b. Tree Stem Diameter Estimation from Mobile Laser Scanning Using Line-Wise Intensity-Based Clustering. Forests 7, 206. https://doi.org/10.3390/f7090206.

Gollob, C., Ritter, T., Nothdurft, A., 2020. Forest Inventory with Long Range and High-Speed Personal Laser Scanning (PLS) and Simultaneous Localization and Mapping (SLAM) Technology. Remote Sens. 12, 1509. https://doi.org/10.3390/rs12091509.

Hyyppä, E., Yu, X., Kaartinen, H., Hakala, T., Kukko, A., Vastaranta, M., Hyyppä, J., 2020. Comparison of Backpack, Handheld, Under-Canopy UAV, and Above-Canopy UAV Laser Scanning for Field Reference Data Collection in Boreal Forests. Remote Sens. 12, 3327. https://doi.org/10.3390/rs12203327.

Hyyppä, J., Virtanen, J.-P., Jaakkola, A., Yu, X., Hyyppä, H., Liang, X., 2018. Feasibility of Google Tango and Kinect for Crowdsourcing Forestry Information. Forests 9, 6. https://doi.org/10.3390/f9010006.

Jurjević, L., Liang, X., Gašparović, M., Balenović, I., 2020. Is field-measured tree height as reliable as believed – Part II, A comparison study of tree height estimates from conventional field measurement and low-cost close-range remote sensing in a deciduous forest. ISPRS J. Photogramm. Remote Sens. 169, 227–241. https://doi.org/10.1016/j.isprsjprs.2020.09.014.

Kukko, A., Kaartinen, H., Hyyppä, J., Chen, Y., 2012. Multiplatform Mobile Laser Scanning: Usability and Performance. Sensors 12, 11712–11733. https://doi.org/10.3390/s120911712.

Liang, X., Hyyppä, J., Kaartinen, H., Lehtomäki, M., Pyörälä, J., Pfeifer, N., Holopainen, M., Brolly, G., Francesco, P., Hackenberg, J., Huang, H., Jo, H.-W., Katoh, M., Liu, L., Mokroš, M., Morel, J., Olofsson, K., Poveda-Lopez, J., Trochta, J., Wang, D., Wang, J., Xi, Z., Yang, B., Zheng, G., Kankare, V., Luoma, V., Yu, X., Chen, L., Vastaranta, M., Saarinen, N., Wang, Y., 2018a. International benchmarking of terrestrial laser scanning approaches for forest inventories. ISPRS J. Photogramm. Remote Sens. 144, 137–179. https://doi.org/10.1016/j.isprsjprs.2018.06.021.

Liang, X., Hyyppä, J., Kukko, A., Kaartinen, H., Jaakkola, A., Yu, X., 2014. The Use of a Mobile Laser Scanning System for Mapping Large Forest Plots. IEEE Geosci. Remote Sens. Lett. 11, 1504–1508. https://doi.org/10.1109/LGRS.2013.2297418.

Liang, X., Kankare, V., Hyyppä, J., Wang, Y., Kukko, A., Haggrén, H., Yu, X., Kaartinen, H., Jaakkola, A., Guan, F., Holopainen, M., Vastaranta, M., 2016. Terrestrial laser scanning in forest inventories. ISPRS J. Photogramm. Remote Sens. 115, 63–77. https://doi.org/10.1016/j.isprsjprs.2016.01.006.

Liang, X., Kukko, A., Hyyppä, J., Lehtomäki, M., Pyörälä, J., Yu, X., Kaartinen, H., Jaakkola, A., Wang, Y., 2018b. In-situ measurements from mobile platforms: An emerging approach to address the old challenges associated with forest inventories. ISPRS J. Photogramm. Remote Sens. 143, 97–107. https://doi.org/10.1016/j.isprsjprs.2018.04.019.

Liang, X., Wang, Y., Jaakkola, A., Kukko, A., Kaartinen, H., Hyyppä, J., Honkavaara, E., Liu, J., 2015. Forest Data Collection Using Terrestrial Image-Based Point Clouds From a Handheld Camera Compared to Terrestrial and Personal Laser Scanning. IEEE Trans. Geosci. Remote Sens. 53, 5117–5132. https://doi.org/10.1109/TGRS.2015.2417316.

McGlade, J., Wallace, L., Hally, B., White, A., Reinke, K., Jones, S., 2020. An early exploration of the use of the Microsoft Azure Kinect for estimation of urban tree Diameter at Breast Height. Remote Sens. Lett. 11, 963–972. https://doi.org/10.1080/2150704X.2020.1802528.

Mikita, T., Janata, P., Surový, P., 2016. Forest Stand Inventory Based on Combined Aerial and Terrestrial Close-Range Photogrammetry. Forests 7, 165. https://doi.org/10.3390/f7080165.

Mokroš, M., Liang, X., Surový, P., Valent, P., Čerňava, J., Chudý, F., Tunák, D., Saloň, Š., Merganič, J., 2018. Evaluation of Close-Range Photogrammetry Image Collection Methods for Estimating Tree Diameters. ISPRS Int. J. Geo-Inf. 7, 93. https://doi.org/10.3390/ijgi7030093.

Mokroš, M., Výbošťok, J., Grznárová, A., Bošela, M., Šebeň, V., Merganič, J., 2020. Non-destructive monitoring of annual trunk increments by terrestrial structure from motion photogrammetry. PLoS ONE 15, e0230082. https://doi.org/10.1371/journal.pone.0230082.

Piermattei, L., Karel, W., Wang, D., Wieser, M., Mokroš, M., Surový, P., Koreň, M., Tomaštík, J., Pfeifer, N., Hollaus, M., 2019. Terrestrial Structure from Motion Photogrammetry for Deriving Forest Inventory Data. Remote Sens. 11, 950. https://doi.org/10.3390/rs11080950.

Ryding, J., Williams, E., Smith, M.J., Eichhorn, M.P., 2015. Assessing Handheld Mobile Laser Scanners for Forest Surveys. Remote Sens. 7, 1095–1111. https://doi.org/10.3390/rs70101095.

Sarbolandi, H., Lefloch, D., Kolb, A., 2015. Kinect range sensing: Structured-light versus Time-of-Flight Kinect. Comput. Vis. Image Underst. 139, 1–20. https://doi.org/10.1016/j.cviu.2015.05.006.

Schöps, T., Sattler, T., Häne, C., Pollefeys, M., 2015. 3D Modeling on the Go: Interactive 3D Reconstruction of Large-Scale Scenes on Mobile Devices. In: 2015 International Conference on 3D Vision. Presented at the 2015 International Conference on 3D Vision, pp. 291–299. https://doi.org/10.1109/3DV.2015.40.

Tomaštík, J., Saloň, Š., Tunák, D., Chudý, F., Kardoš, M., 2017. Tango in forests – An initial experience of the use of the new Google technology in connection with forest inventory tasks. Comput. Electron. Agric. 141, 109–117. https://doi.org/10.1016/j.compag.2017.07.015.

Wang, Y., Lehtomäki, M., Liang, X., Pyörälä, J., Kukko, A., Jaakkola, A., Liu, J., Feng, Z., Chen, R., Hyyppä, J., 2019. Is field-measured tree height as reliable as believed – A comparison study of tree height estimates from field measurement, airborne laser scanning and terrestrial laser scanning in a boreal forest. ISPRS J. Photogramm. Remote Sens. 147, 132–145. https://doi.org/10.1016/j.isprsjprs.2018.11.008.

Wasenmüller, O., Stricker, D., 2017. Comparison of Kinect V1 and V2 Depth Images in Terms of Accuracy and Precision. In: Chen, C.-S., Lu, J., Ma, K.-K. (Eds.), Computer Vision – ACCV 2016 Workshops, Lecture Notes in Computer Science. Springer International Publishing, Cham, pp. 34–45. https://doi.org/10.1007/978-3-319-54427-4_3.

4.2 Benchmarking of algorithms for point cloud processing

4.2.1 An approach for tree volume estimation using RANSAC and RHT algorithms from TLS dataset

published as: Singh, A., Kushwaha, S. K. P., Nandy, S., & Padalia, H. (2022). An approach for tree volume estimation using RANSAC and RHT algorithms from TLS dataset. Applied Geomatics, 14(4), 785-794.

Extended summary:

The basic tree attributes (DBH and tree height) are the key to the advanced tree attributes (stem volume and above-ground biomass). The conceptual methodology and detailed results are mentioned in papers III and VI. In paper III, DBH and tree height were estimated using TLS point cloud with randomized hough transformation (RHT) and random sample consensus (RANSAC) algorithms.

Tree parameter extraction using RHT

This method involves a coordinate transformation from a Cartesian to a polar coordinate system and further the parametric description of objects. In the first step, DBH subsets of each tree cloud were projected to a horizontal plane, and a possible center of the circle was located for every point of the point cloud. The frequent center will be selected as a resulting center. The implementation of the RHT algorithm was done in 3D Forest software. RHT detects the circle on the tree PCD at 1.3 m and 0.65 above the lowest point of the tree PCD. The tree position allocation was done by the intersection of two vectors from two circles with the DTM surface of the tree PCD. The DBH was estimated based on the sub-section of tree PCD from 1.25 to 1.35 m.

Tree height was also calculated in 3D Forest software by allocating the lowest point of the tree cloud at the base of a tree. Tree height was calculated as the z-coordinate difference between the highest and lowest (tree base) of the tree PCD.

Tree parameter extraction using RANSAC

This method encompasses two phases. The first phase is the hypothesis phase. In this phase, the minimal sampling set (MSS) of points is formed using all the input points to create a specific mathematical shape that satisfies some shape parameter. This phase would help to measure a tree DBH and height proportionally. The second phase deals with the testing of these MSS. These sampling points were tested against all the dataset points. The points resembling the MSS points form a new set of points known as a consensus set (CS).

The second step helped in the removal of outliers from the dataset. The algorithm is run multiple times to filter out all the outliers from MSS and get a probable threshold. The inliers were then selected in a cylinder shape, as shown in Figure 20.

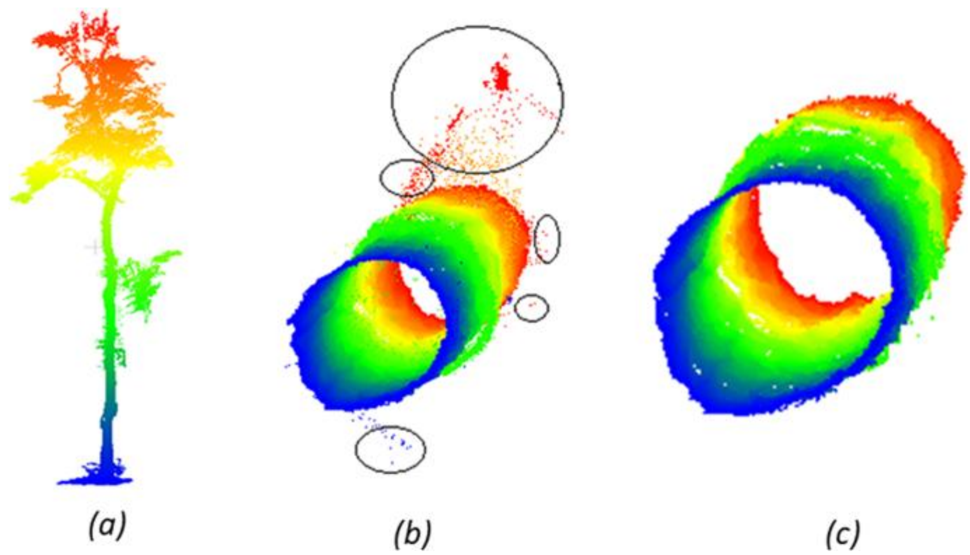

Figure 20: Visualization of (a) extracted tree point cloud, (b) presence of noise encircled with a black circle, (c) filtered point cloud of tree stem at 1.34 m.

Relation between tree parameters retrieved using RHT and field-measurements

The tree parameters, such as DBH and tree height, were retrieved separately using RHT and field measurement. The correlation R^2 between DBH obtained using RHT and field-measured values is 0.99, and 0.93 is obtained with tree height, which is mentioned in Figure 21. The R^2 value obtained for heights calculated using both methods are 0.93, as shown in Figure 21.

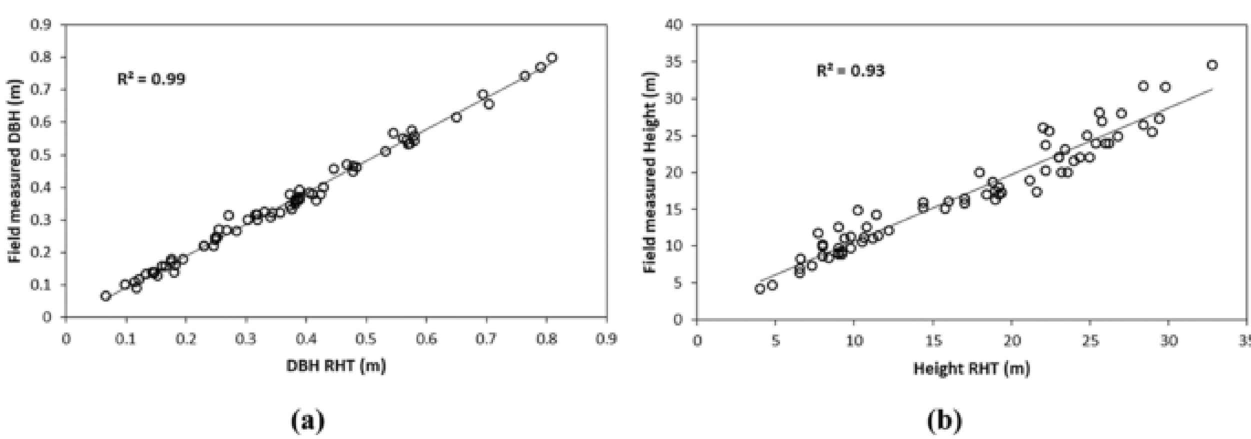

Figure 21: Correlation between (a) DBH observed using RHT and field-measured DBH and (b) height estimated using RHT and field-measured height.

Relation between tree parameters retrieved using RANSAC and field measurements

The correlation value between heights calculated using RANSAC and the field-based method is obtained as 0.80 shown in Figure 22. whereas for DBH, it is 0.98, as depicted in Figure 22. a. So, it can be anticipated that DBH is more correlated with the field-based DBH than tree height.

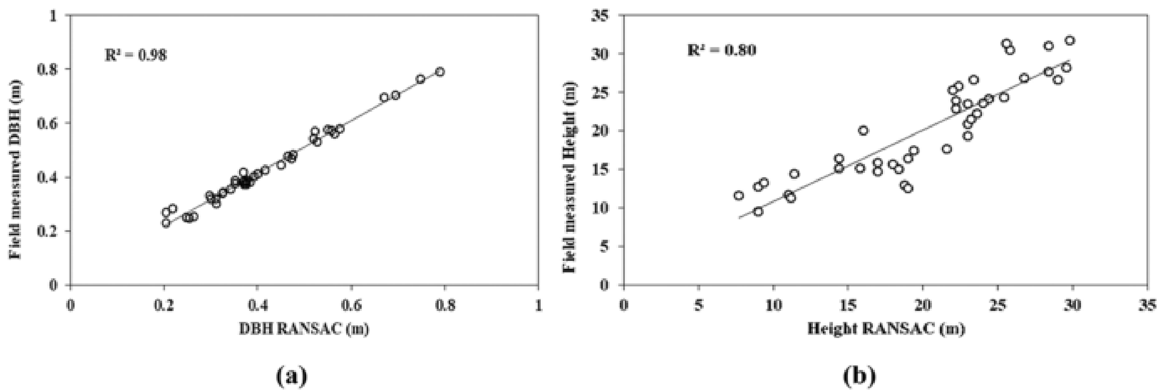

Figure 22: Correlation between (a) DBH calculated using RANSAC and field-measured DBH and (b) height estimated using RHT and field-measured height.

The significance of the radius of the tree circumference was used to establish a relation between radius and stem volume. The radius for all the trees was calculated and statistically analyzed. The R^2 value obtained for radius and field-based stem volume is 0.84, which shows a very significant relation between stem volume and radius; the relation is depicted in Figure 23.

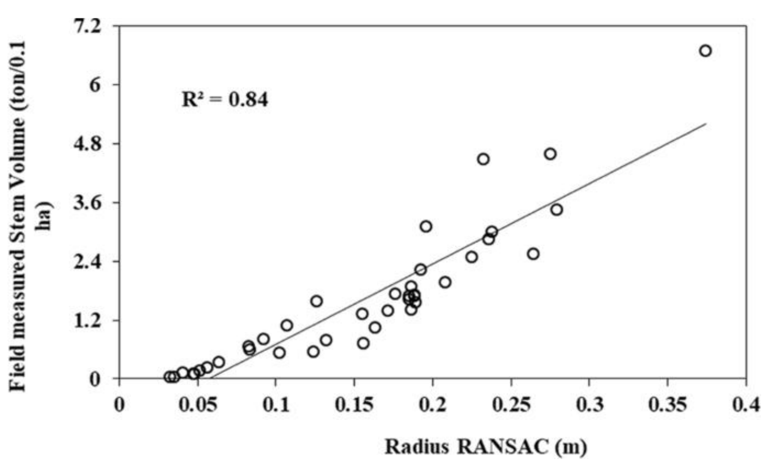

Figure 23: Relation between radius calculated using RANSAC and stem Volume calculated using the Forest Survey of India (FSI) equation

The correlation value obtained between the field estimated and RANSAC-based stem volume is 0.95. The correlation plot is shown in Figure 24. This represents the potential of RANSAC to calculate the stem volume by merely using the radius and height of the tree. In FSI volumetric equations, the stem volume is highly dependent on the species of the tree. In contrast, in RANSAC the calculation of stem volume was mainly done with the tree structural parameters (radius of the stem and tree height).

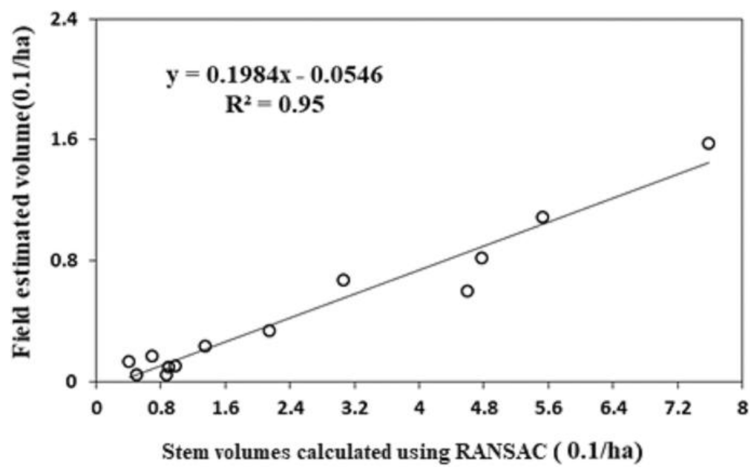

Figure 24: Relation between RANSAC and field estimated volume

Secondly, the stem volume was estimated using DBH, and height was estimated with the RHT algorithm in 3D Forest software. A relation between stem volumes was estimated using field-based volumetric equations and RHT. The statistical analysis found that the R^2 is 0.99, representing the high correlation between the stem volume estimated using RHT and the field measured; hence, RHT can be directly used for estimating stem volume. The correlation plot is depicted in Figure 25.

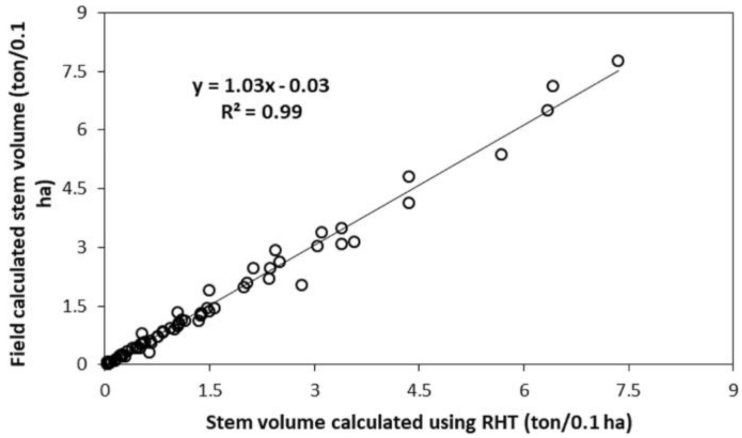

Figure 25: Correlation plot between stem volume calculated using RHT and field estimated volume

4.2.2 A review of point cloud processing software solutions in forest applications

published as: Murtiyoso, A., Cabo, C., Singh, A., Obaya, D. P., Cherlet, W., Stoddart, J., Fol, C. R., Beloiu Schwenke, M., Rehush, N., Stereńczak, K., Calders, K., Griess, V. C., & Mokroš, M. (2024). A Review of Software Solutions to Process Ground-based Point Clouds in Forest Applications. Current Forestry Reports. https://doi.org/10.1007/s40725-024-00228-2

Extended summary:

3D point clouds have provided forest practitioners and scientists with a new way of surveying timber and ecological resources and conducting previously impossible research. As a result, more and more scientific groups are intensively developing methods and technologies to automate the surveying of ground plots and the determination of stand characteristics using point clouds.
However, there is a lack of standardization and dynamic comparison focusing on end users, such as foresters, ecologists, scientists, and similar. There is a need for a joint initiative that will manage the new findings and based on them, make standards for the above-mentioned end users.

In paper VII, a compiled list of available algorithms that deal with the processing of forest point clouds was tested and implemented based on certain criteria. From this variety of algorithms available, it might be challenging for users to decide which one to choose to fulfill their goals to the best. Within the framework of 3DForEcoTech COST Action, a comprehensive database was compiled to collect information about existing forest point cloud processing algorithms in one place. The database currently includes 24 algorithms with special emphasis on point clouds obtained by close-range techniques and ground-based platforms. Of the 24 solutions identified, 20 were open-source, 2 were free software, and 2 were commercial. For each of the algorithms identified in our database, metadata was collected while installation and test runs were conducted to assess their applicability for forestry. From these tests, technical guides on installation and general use were written and will be included in the web platform. The database was also published as a web-based platform, in which users may consult it easily using a query system. In this way, the database may serve the community as a single source of information to select a specific software/algorithm that works for their requirements.

Conclusion:

A comparative analysis of RHT and RANSAC algorithms is done for the estimation of DBH and tree height. The results showed that DBH and tree height estimated suing RHT is more correlated with the field measured values. Thereafter, stem volume estimation was also done using RHT and RANSAC and evaluated with the field measured value. The results showed that the estimated and observed values of stem volumes are highly correlated and therefore can be used for the estimation of stem volume by surpassing the volumetric equations prosed by Forest Survey of India.

Thereafter, in subsection 4.2.2 a thorough review was done on point cloud processing software solutions in forest applications. Installation and testing of all the enlisted algorithms compiled using the currently and thoroughly used algorithms or software solutions was done. A database including guidelines on usage and protocol was created and published on the website of 3DForEcotech project.

Applied Geomatics
https://doi.org/10.1007/s12518-022-00471-x

ORIGINAL PAPER

An approach for tree volume estimation using RANSAC and RHT algorithms from TLS dataset

Arunima Singh[1,2] · S. K. P. Kushwaha[3] · Subrata Nandy[1] · Hitendra Padalia[1]

Received: 18 April 2022 / Accepted: 7 October 2022

Abstract

Forest structure plays a crucial role in maintaining the ecosystem balance. All the biogeochemical cycles need trees for the successful execution of the processes. Nowadays, one of the most critical concerns is the accurate and precise assessment of forest biomass. The biomass assessment can be done by knowing the canopy metrics, stem volume, and specific wood gravity. This research used a terrestrial laser scanner (TLS) to retrieve tree parameters, providing point cloud data (PCD). The parameters derived from PCD are diameter at breast height (DBH) and tree height using randomized Hough transformation (RHT). With these tree parameters, the stem volume of the tree was calculated and correlated with the Forest Survey of India (FSI) equation. The radius, DBH, tree height, and stem volume were also obtained using the Random Sample Consensus (RANSAC) algorithm. The volume calculated using the RANSAC algorithm is statistically analyzed with the volume calculated with the FSI equations available for specific tree species. The R^2 value obtained for the volume calculated by the RANSAC and FSI equations is 0.95. In contrast, the correlation value obtained for the volume calculated by RHT and FSI equations is 0.99. Therefore, it shows that both algorithms are highly correlated and can be used as an alternative method for stem volume calculation, which will be less time-consuming and more accurate as well as precise. This method tries to explain the alternative method to calculate tree stem volume without using the species-specific FSI equations, which may sometimes produce biases and uncertainty in calculating stem volume and biomass.

Keywords Forest · Terrestrial laser scanner (TLS) · Random Sample Consensus (RANSAC) · Randomized Hough transformation (RHT) · Diameter at breast height (DBH)

Introduction

Forests are the natural entity that is important for sustaining life on the earth. It releases an ample amount of oxygen and absorbs carbon dioxide. The maintenance and regulation of changes occurring frequently need to be monitored because these are one of the most sensitive parts of the earth. Remote sensing brings much potential in this context. The abrupt changes in biomass of the forests can be monitored using remote sensing. It also helps to collect information from the core areas of very dense forests which is inaccessible to humans. Remote sensing helps us to monitor some of the crucial and critical parts of the forest and gives us a comparative analysis of the area for the preceding years. Traditionally, destructive techniques were used for biomass assessment. Later, these methods were discarded due to environmental concerns and time taking procedures. Modern technology leads us toward the non-destructive methodologies that can be implemented for assessing forest biomass.

✉ Arunima Singh
singharunima92@gmail.com

S. K. P. Kushwaha
s.k.p.kushwaha92@gmail.com

Subrata Nandy
subrato.nandy@gmail.com

Hitendra Padalia
hitendra@iirs.gov.in

1 Forestry and Ecology Department, Indian Institute of Remote Sensing (IIRS), Dehradun 248001, Uttarakhand, India

2 Faculty of Forestry and Wood Sciences, Czech University of Life Sciences, Prague 16500, Czech Republic

3 Geomatics Group, Department of Civil Engineering, Indian Institute of Technology, Roorkee 247667, Uttarakhand, India

Published online: 15 October 2022

A terrestrial laser scanner (TLS) is a ground-based instrument used nowadays for validation purposes and as a non-destructive instrument in forest inventory. The parameters such as diameter at breast height (DBH) and tree height were retrieved using this instrument data and regressed with the field-measured values using a measuring tape and a range-finder. The results show a perfect correlation between the TLS measured, and field-measured values of the parameters of the tree (Liang et al. 2016). The application of a TLS is in a wide range of disciplines (Newnham et al. 2015). Further inventory application that has been done using a TLS to retrieve DBH and height found that the DBH was more correlated with the biomass than height when compared with the field-measured values. Besides that, a TLS shows promising results in the inventory of heterogeneous urban forests (Moskal et al. 2012). The extended biomass allometric equation was developed for the mangrove trees using a TLS (Olagoke 2015). The volume estimation was done using a 3-D point cloud–based technique, in which the stem was divided into small cylindrical sections. The diameter of these cylindrical sections was used to calculate volume (Rudiger Hildebrandt 2012).

SimpleTree software, which encompasses improved cylindrical radii and has an optimized approach to correct the user-given parameters automatically, was developed using TLS point cloud data (PCD) (Hackenberg et al. 2015). Two-scale classification methods can also be explored, followed by the clustering and direction growing algorithm developed for dense forests to identify the tree stems and other fine structures (Shaoba Xia et al. 2015). Detecting single stems of variable diameters is still challenging, and the study has conveyed a fruitful methodology. The conceptual development of the cylindrical structure of the tree was stored as hierarchical tree-like data having previous and forehead point relations (Hackenberg et al. 2014). A geometrical model-fitting strategy was developed using the RANSAC algorithm for tree detection and delineation for LiDAR PCD (Tittmann et al. 2011). The stem reconstruction technique was developed using PCD of TLS, a self-adaptive cylinder growing method (Wang et al. 2016). For the enhanced forest monitoring and management, the canopy metrics have been retrieved using the PCD of the TLS. Once the canopy metrics are known, the volume and biomass can be assessed with higher accuracy (Lim et al. 2013). The tree stem diameter and height were retrieved using randomized Hough transformation (RHT) and RANSAC algorithms (Olofsson et al. 2014). The RANSAC algorithm was also used to form primitive structures of PCD obtained by the TLS.

The primitive structures could be cylinders, cones, squares, rectangles, etc. Models such as computer-aided design (CAD) were used to automatically represent shape proxies (Schnabel et al. 2007). The research has been performed to segment trees into leaf, branch, and stem using the region growing technique and principle component analysis (PCA) (Koma et al. 2018). The TLS can also be used for the quantification of post-fire effects by deriving 18 metrics temporally (Gupta et al. 2015). The crown variables were derived using an airborne laser scanner (ALS) and a TLS, and the parameters used were individual tree height, crown base height, crown area, and crown volume, and showed that ALS and TLS combined can give better results (Jung et al. 2011). One more essential parameter is leaf area index (LAI), the technique used to convert 3D PCD into 2D raster images like hemispherical photographs to estimate LAI (Zheng et al. 2013). It is also possible to find leaf orientation from TLS data using the total least square fitting approach (Zheng and Moskal 2012a, b).

TLS was very much exploited for the assessment of above ground biomass (AGB); the technique used was quantitative structure models (QSM) and AGB was calculated using species-specific wood density equations (Tanago et al. 2018). Urban forestry is also a concept for environmental regulation; a TLS is used to create tree maps along with mobile laser scanners (MLSs) and ALS (Holopainen et al. 2013). The stem diameter and volume were derived by incorporating circle fitting and scan mode (Pueschel et al. 2013). A circular point cloud slicing technique was evolved to study the spatial variation of point density in radial and azimuth directions (Zheng and Moskal 2012a, b). Maximum likelihood (MLE) was used for better estimation of canopy profile, the direction of leaf angle, and LAI (Zhao et al. 2015). Different techniques and methodologies were used to explore PCD acquired using different platforms. Hence, a TLS can be used for different purposes for the quantitative and qualitative assessment of trees. The hypothesis of this research is to investigate the high potential of RHT and RANSAC for the estimation of stem volume. Also, identification of tree parameters such as DBH, radius, and tree height correlation with the stem volume is highly significant.

The main aim of this research is to utilize the already established technique for tree volume estimation to reinstate the classical tree harvesting technique to modern non-destructive methods. So, RHT and RANSAC are used for this purpose. The objective is to find the best algorithm for stem volume calculation and statistically analyze its importance for retrieving tree attribute information using TLS without knowing the species of the tree.

Study area and dataset

The study area used in this research is Barkot Forest, and the dataset used is PCD of TLS and field-measured data.

Study area

The Barkot Forest is located between the latitude of 30°03′52″ to 30°10′43″ N and longitude of 78°09′49″ to 78°17′09″ E. The forest is present along the Dehradun-Rishikesh road, Uttarakhand, India. The altitude ranges from 340 to 560 m above mean sea level (MSL). The total area of the forest is 84.96 km^2. The forest type is moist deciduous and dominated by the *Shorea robusta* (Sal) species; the understory vegetation is dominated by *Mallotus philippensis* (Rohini). The rivers present in the study area are Song and Ganga, and the nearby towns are Doiwala and Rishikesh. Forest terrain is flat and undulating; the study area is at the foot of the Himalayas and surrounded by the lesser Himalayan Mountains in the north and the Shivalik range in the south. With the increase in the depth of the soil, the consistency becomes non-sticky friable to sticky firm; the lower horizon of the soil profile is moist, firm, compact, and comparatively hard. The location of the study area is shown in Fig. 1.

TLS specification

In this research, a TLS is a ground-based static LiDAR system that produces dense 3D information about the trees in the forest plot. Riegl VZ 400 TLS was used for extensive scanning of the 13 plots. This instrument is of class 1 laser class. The measurement range varies between 1.5 and 600 m. The instrument has a laser pulse reception rate of 100 kHz, and the wavelength used for scanning is near-infrared (NIR; 1050 nm). The accuracy and precision are ± 5 mm and ± 3 mm, respectively. The horizontal scan angle range is up to 360°, and the vertical scan range is 100° (+ 60°/ − 40°). The scanning mechanism is based on a rotating multifaceted mirror. The scanner rotating head scans top to bottom in the vertical scan and anti-clockwise in the horizontal scan. The maximum angle resolution is 0.0005° (108 arcsec). More specification details are shown in Table 1.

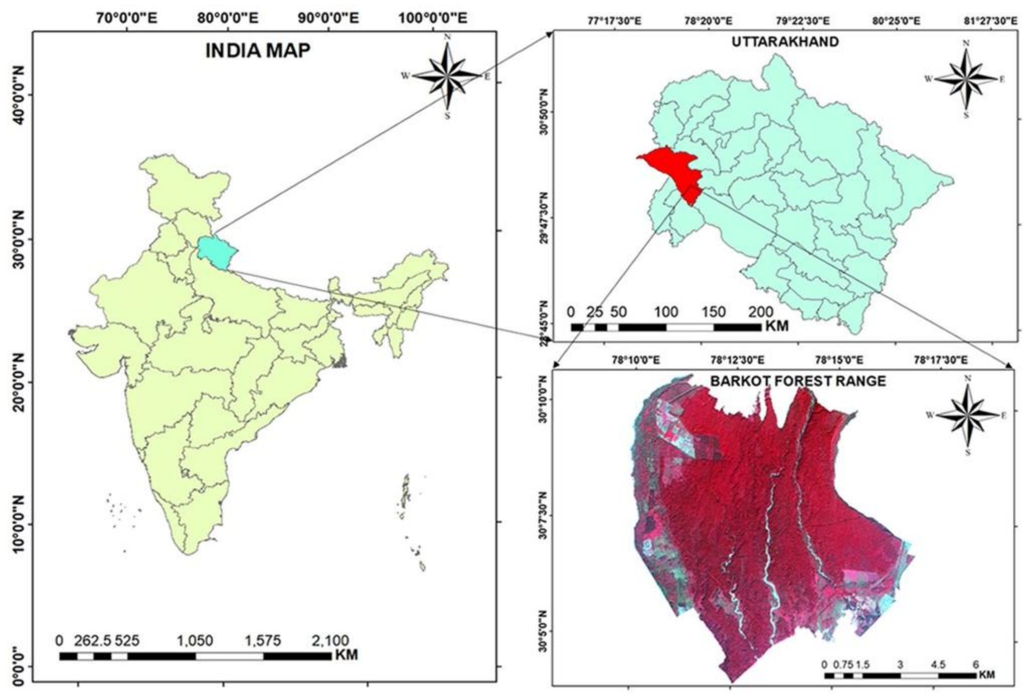

Fig. 1 Study area

Table 1 TLS instrument specification

Parameter	Description	
Laser class	Class 1	
Scanner performance	Vertical scan	Horizontal scan
Scan angle range	Total 100° (+60°/− 40°)	Max. 360°
Scan speed	3 lines/s to 120 lines/s	0°/s to 60°/s
Scanning mechanism	Rotating multifaceted mirror	Rotating head
Angular step width *Δθ (vertical)* *Δφ (horizontal)*	$0.0024° \leq \Delta\theta \leq 0.288°$ between consecutive laser shoots	$0.024° \leq \Delta\varphi \leq 0.5°$ between consecutive scan lines
Angle resolution	0.0005° (1.8 arcsec)	0.0005° (1.8 arcsec)
Inclination sensor	Integrated for vertical position	Scanner setup
Compass	Optional for vertical scanner setup position	
Accuracy	5 mm	
Precision	3 mm	
Effective measurement rate (meas/sec)	42,000 (long range mode)–122,000 (high speed mode)	
Maximum measurement range	600 m	
Minimum measurement range	1.5 m	
Laser beam divergence	0.35 mrad	
Laser pulse reception rate (PRR)	100 kHz	
Laser wavelength	Near-infrared (1050 mm)	

Methodology

Field data collection

Total 13 plots of 25 m × 25 m were established in the Barkot Forest using the traditional forest inventory method. The sampling of the plots was done using the stratified random sampling method. The tree structure measurements considered were tree height and DBH; the tree height was measured using a hypsometer and DBH was taken using a measuring tape. The database was prepared for each tree in the 13 plots according to the specific species of the trees. Later, the stem volume and total tree biomass were calculated using the National Forest Inventory (NFI) volumetric equations.

TLS data acquisition

The data acquisition is performed using a TLS, and four scans were performed in each plot, one at the center of the plot and three at the sides. The multiple scans were done to minimize the tree occlusion and get maximum point cloud density. The TLS Riegl VZ-400 works up to the range of 600 m. The horizontal angle taken was 0° to 360°, and vertical angle scan was set at 30° to 130°, and angular resolution opted was 0.03°. Before the start of the scanning process, the retro-reflectors were placed well-distributed and kept constant throughout the scanning of the plot. Tagging of each tree in the plot was priorly done. So, a total of 13 plots of 25 m × 25 m were scanned and processed. The positioning of the TLS and the data acquisition scheme are shown in Fig. 2.

Fig. 2 TLS scanning scheme

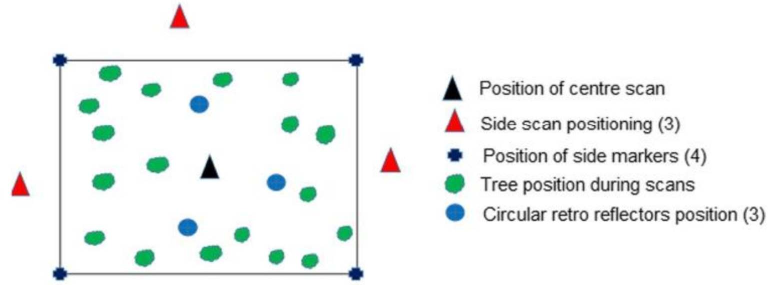

Registration of scans

The registration of scans was done to bring all the scans to a common coordinate system because all the scans were in a different local coordinate system The PCD registration was done in the RiSCAN pro software. The co-registration was done by considering the key points and four common features in between two scan positions using the Iterative Closest Point (ICP) algorithm. One of the scans was fixed, and the other scans were co-registered with reference to the fixed scan. For the registration, a minimum of three tie points were required. After the co-registration of scans, the merged PCD for each plot were prepared. To remove the unwanted points (outliers) in the PCD, noise filtering was done in CloudCompare software for all the 13 plots. A glimpse of scanned plot and location of the reflector used while scanning is shown in Fig. 3.

Extraction of a plot and single trees

Extraction of plots from the merged point cloud data was done with the reference of reflectors placed at the four corners of a plot, so that segmentation of a plot would be easier. After extracting the plot, individual trees were identified and segmented out from the plot. The extraction of a single tree out of a plot was also performed in the Cloud Compare software and is shown in Fig. 4.

Estimation of tree parameters using the RHT method

This method involves a coordinate transformation from a Cartesian to a polar coordinate system and further the parametric description of objects. In the first step, DBH subsets of each tree cloud were projected to a horizontal plane, and a possible center of the circle was located for every point of the point cloud. The frequent center will be selected as a resulting center (Xu and Oja 2009). The implementation of the RHT algorithm was done in 3D Forest software. RHT

Fig. 3 Location of retro-reflector (red dot) in the plot scan

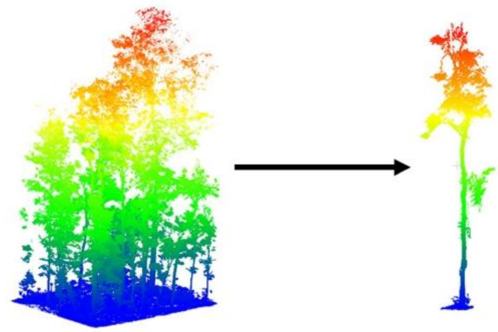

Fig. 4 Showing the extracted plot and tree

detects the circle on tree PCD at 1.3 m and 0.65 above the lowest point of the tree PCD. The tree position allocation was done by intersection of two vectors from two circles with the DTM surface of tree PCD. The DBH was estimated based on the sub-section of tree PCD from 1.25 to 1.35 m.

Parametrically, the circle is described as:

$$r^2 = (x - a)^2 + (y - b)^2$$

The coordinates x and y can be written as:

$$x = a - r * \cos(\alpha)$$

$$y = b - r * \cos(\alpha)$$

where

r = radius

(a, b) = coordinates of the center

(x, y) = coordinates of a point on the circle

α = angle

The DBH of the tree stem was calculated using the RHT algorithm and then, the stem volume of the tree was calculated using the following equations

$$\boldsymbol{V = \pi r^2 H}$$

where r is the radius of the tree stem in meters (m). H is the height of the tree in meters (m), and V represents the stem volume.

Tree height estimation

Tree height was also calculated in 3D Forest software by allocating the lowest point of the tree cloud at the base of a tree. Tree height was calculated as the z coordinate difference between the highest and lowest (tree base) of the tree PCD. The display of height is in meters as a vertical line touching the highest point of the cloud. Similarly,

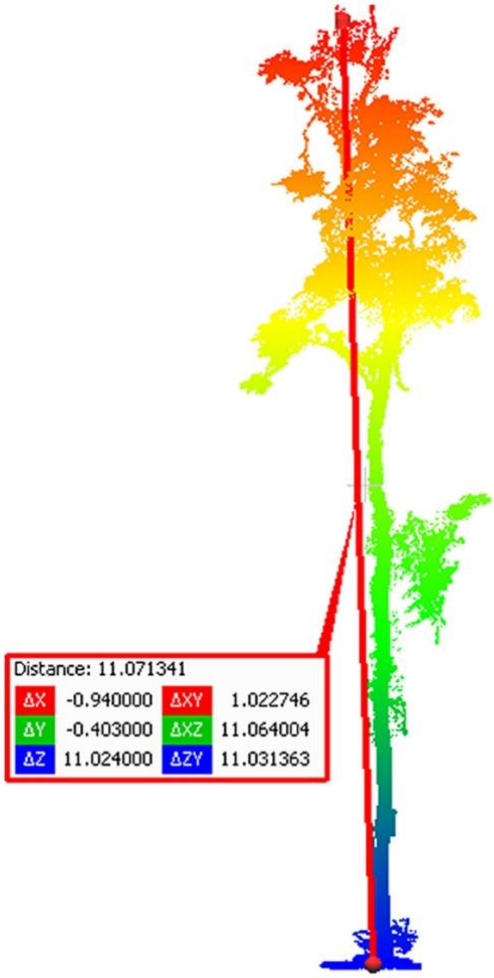

Fig. 5 Height of a single tree (m)

height estimation was done for all the trees in the plots. The height of a single tree is shown in Fig. 5.

Tree parameter retrieval using the RANSAC algorithm

RANSAC is based on a random sampling of observed data, and it uses a voting scheme to find the optimal fitting results based on inliers and outliers in the provided data.

This method encompasses two phases. The first phase is the hypothesis phase. In this phase, the minimal sampling set (MSS) of points is formed using all the input points to create a specific mathematical shape that satisfies some shape parameter. This phase would help to measure a tree DBH and height proportionally. The second phase deals with the testing of these MSS. These sampling points were tested against all the dataset points. The points resembling the MSS points form a net set of points known as a consensus set (CS) (Tran et al. 2015). The second step helped in the removal of outliers from the dataset. The algorithm is run multiple times to filter out all the outliers from MSS and get a probable threshold. The inliers were then selected in a cylinder shape, as shown in Fig. 6c.

Parameters of RANSAC for cylinder primitive structure

The parameters are used to define a cylindrical primitive structure. The stem was considered the cylinder, and all the measurements were done using these parameters:

1) ***D*:** Dataset having inliers and outliers, which were further characterized and removed using the RANSAC algorithm.
2) **MSS:** Also known as minimal sample set of points. These are formed using random mathematical shape parameters out of all the points entered as *D* and finally gave a model with definite shape parameters.
3) ***k*:** It defines the number of points required for the MSS.
4) **Theta:** Parameters obtained from the MSS points were height, radius, center, etc.
5) **CS:** The consensus set of points with less than the threshold error.
6) ***δ*:** This is the error threshold, which is responsible for whether the point belongs to the model or not.

Considering all these parameters, the algorithm decided on the geometrical shape. After removing all the errors above the error threshold limit, the surface points were decided for a mathematical shape. Here, the shape formed was the cylinder. The parameters required for making a cylinder were radius and height.

The radius of the tree stems was obtained from the RANSAC algorithm by using the following equation:

$$\boldsymbol{d} = 2\boldsymbol{r}$$

where d is the DBH of the tree stem point cloud in meters. The volume of the stems was obtained using the volume equation of the cylinder.

$$\boldsymbol{V} = \boldsymbol{\pi r}^2\boldsymbol{H}$$

where r is the radius of the tree stem in meters (m). H is the height of the tree in meters (m). The tree stem volumes (V) were calculated using two algorithms, i.e., RANSAC and

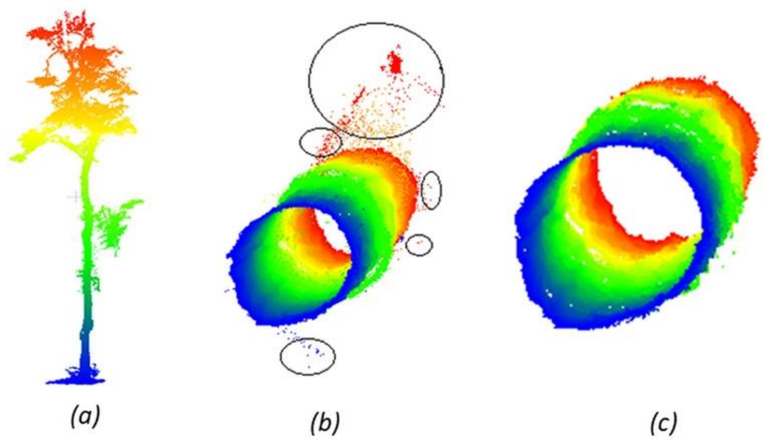

Fig. 6 **a** Tree point cloud. **b** Black encircled area is noise, which is filtered. **c** Filtered point cloud of tree stem at 1.34 m

RHT. The correlation between the volumes was calculated with the tree volume calculated using FSI-based species-specific equations. The overall methodology followed during this research is depicted in Fig. 7.

Results and discussion

Co-registration of scans

The co-registration of individual scans is performed in RiScan PRO software for all the 13 plots. The center and scan position 1 for plot 1 were registered with an error of 0.03. The center scan and scan position 2 were registered with an error of 0.017. The error value of 0.029 is obtained for the center and scan position 3. The detailed scan pair information for plot 1 with its RMSE value is mentioned in Table 2 as a reference.

Relation between tree parameters retrieved using RHT and field-based measurement

The tree parameters such as DBH and tree height were retrieved using RHT and field measurement separately.

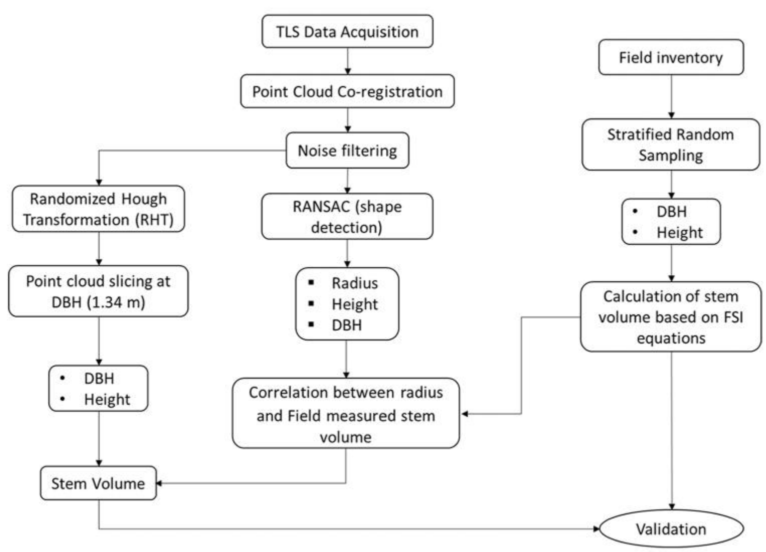

Fig. 7 Workflow

Table 2 RMSE values of different scan pairs during co-registration

SCAN pair	RMSE
Center and scan position 1	0.03
Center and scan position 2	0.017
Center and scan position 3	0.029

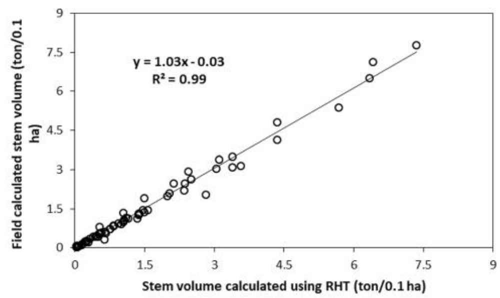

Fig. 9 Correlation plot between stem volumes calculated using RHT and field-based method

The correlation value R^2 between DBH obtained using RHT and field-measured values is 0.99, and 0.93 is obtained with tree height, which is mentioned in Fig. 8. It shows a strong relationship between the values obtained using RHT and field measurement, which is shown in Fig. 8a. Heights are also calculated using the RHT algorithm and field-based measurement separately. The R^2 value obtained for heights calculated using both methods is 0.93 as shown in Fig. 8b. The DBH calculated using RHT is based on the concept that the DBH subset is projected to the tree cloud to find the center of the cloud (Xu and Oja 2009).

Relation between stem volumes calculated using the field-based method and RHT

Stem volumes of trees were calculated for 13 plots using the RHT algorithm. A relation between stem volumes calculated using field-based volumetric equation and RHT was estimated. The statistical analysis was done and found that the R^2 is 0.99, representing the high correlation between the stem volume calculated using RHT and the field measured; hence, RHT can be directly used for estimating stem volume. The correlation plot is depicted in Fig. 9.

Relation between tree parameters retrieved using RANSAC and field-based measurement

RANSAC is based on the concept of random sample consensus. The PCD of the tree stem was organized into outliers and inliers; the points are aligned based on the axis of the primitive structure, which is considered a cylinder here. The points that fit best in the structure are chosen, and others are discarded (Tran et al. 2015). Tree parameters such as tree height, DBH, and radius were calculated again using an algorithm known as RANSAC. The correlation value between heights calculated using RANSAC and the field-based method is obtained as 0.80 which is shown in Fig. 10b, whereas, for DBH, it is 0.98, depicted in Fig. 10a. So, it can be anticipated that DBH is more correlated with the field-based DBH than tree height. The significance of the radius of the tree circumference was used to establish a relation between radius and stem volume. The radius for all the trees was calculated and statistically analyzed. The R^2 value obtained for radius and field-based stem volume is 0.84, which shows a very significant relation between stem volume and radius; the relation is depicted in Fig. 11.

Relation between stem volume calculated using field-based method and RANSAC

The stem volumes for all the trees in 13 plots were calculated using the RANSAC algorithm based on the statistical analysis with the tree parameters such as radius, DBH, and tree height. The correlation value obtained between field estimated and RANSAC-based stem

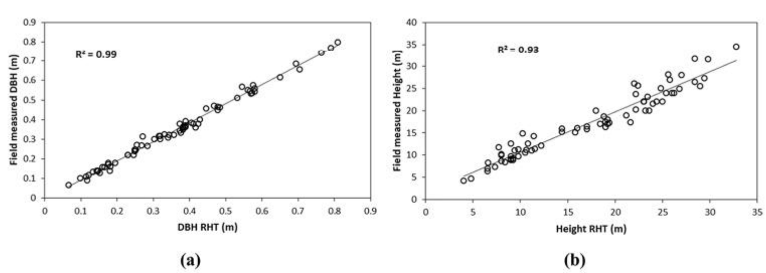

Fig. 8 Correlation between **a** DBH observed using RHT and field, and **b** height estimated using RHT and field

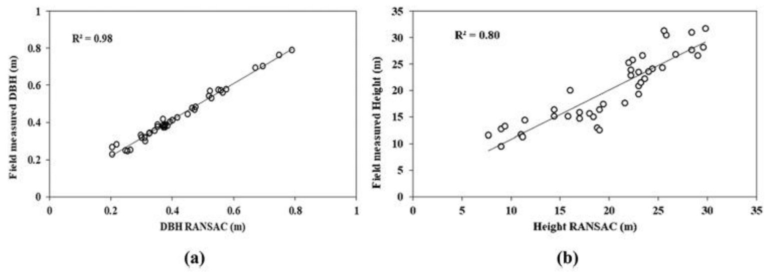

Fig. 10 Correlation between **a** DBH observed using RANSAC and field-based measurement, and **b** height estimated using RHT and field-based measurement

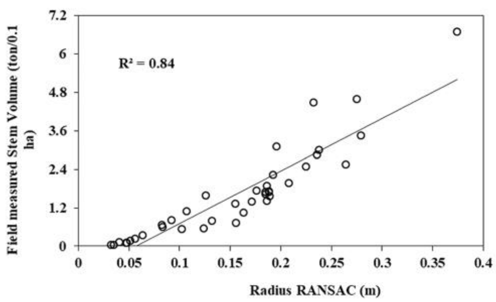

Fig. 11 Relation between radius calculated using RANSAC and stem volume calculated using the FSI equation

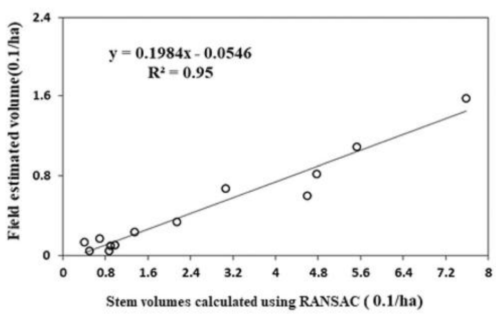

Fig. 12 Relation between RANSAC-calculated volume and field-estimated volume

volume is 0.95. The correlation plot is shown in Fig. 12. This represents the potential of RANSAC to calculate the stem volume by merely using the radius and height of the tree. In FSI volumetric equations, the stem volume if highly dependent on the species of the tree, whereas in RANSAC the calculation of stem volume was mainly done with the tree structural parameters (radius of the stem and tree height).

Conclusions and recommendations

Conclusions

The research is based on the hypothesis that the stem volume calculated strongly correlates with the independent variables such as DBH, radius, and height. The high correlation between the tree parameters and stem volume proves the hypothesis correct. Also, there is high potential in the algorithm such as RHT and RANSAC to calculate stem volume. This is proved that the assumption was correct and found a strong correlation between all the variables taken into account, such as DBH, tree height, stem volume, and radius, using two algorithms and a field-based method. Apart from this, the second objective was the calculation of stem volumes for all the trees in different plots using these two algorithms and found that the correlation is promising for the volumes calculated using the RHT, RANSAC algorithm, and FSI volumetric equations. This research attempted to form an alternative method for the calculation of stem volume without using FSI volumetric equations. The intention is to remove the biases obtained due to species-specific volumetric equations. The alternative method used is the RANSAC and RHT algorithms for stem volume calculation and was found to be highly correlated with the values obtained using field-based volumetric equation calculation. So, this can be a reliable method for calculating stem volume without knowing the species of the trees.

Recommendations and future scope

The future scope of this research is to establish more relations with other tree parameters and stem volume. The volumetric equation could be improved using other parameters such as canopy cover, crown projection area, and LAI. The tree parameter retrieval needs to be 100% assured to minimize the uncertainty in the biomass calculation. This can be done with the further development of the volumetric equations, which will be fully automatized and free from any restrictions and solely based on the structure of the tree.

There is another possibility in this research to extend with the experimentation of different combinations of scan positions in the plot. The tree parameter estimation can be widely varied with different scan positions which also depend on the number of tree detection in the plot. Also, apart from RHT and RANSAC, other algorithms such as treeseg, rTLS (R software package), and Forest Structural Complexity Tool (FSCT) algorithm should also be compared to see the accuracy in the tree parameter retrieval for the estimation of stem volume.

Acknowledgements This research was supported by the Indian Institute of Remote Sensing (IIRS)/ISRO, Dehradun, Uttarakhand, India. We would like to thank Dr. Prakash Chauhan, Director of IIRS, for his continuous support and motivation. We thank the Forestry and Ecology Department for providing infrastructure and hardware support.

Declarations

Conflict of interest The authors declare no competing interests.

References

De Tanago JG, Lau A, Bartholomeus H, Herold M, Avitabile V, Raumonen P, Calders K (2018) Estimation of above- ground biomass of large tropical trees with terrestrial LiDAR. Methods Ecol Evol 9(2):223–234. https://doi.org/10.1111/2041-210X.12904

Gupta V, Reinke KJ, Jones SD, Wallace L, Holden L (2015) Assessing metrics for estimating fire induced change in the forest understorey structure using terrestrial laser scanning. Remote Sens 7(6):8180–8201. https://doi.org/10.3390/rs70608180

Hackenberg J, Morhart C, Sheppard J, Spiecker H, Disney M (2014) Highly accurate tree models derived from terrestrial laser scan data: a method description. Forests 5(5):1069–1105. https://doi.org/10.3390/f5051069

Hackenberg J, Spiecker H, Calders K, Disney M, Raumonen P (2015) SimpleTree—an efficient open-source tool to build tree models from TLS clouds. Forests 6(11):4245–4294

Holopainen M, Kankare V, Vastaranta M, Liang X, Lin Y, Vaaja M, Alho P (2013) Urban Forestry & Urban Greening Tree mapping using airborne, terrestrial and mobile laser scanning – a case study in a heterogeneous urban forest. Urban For Urban Green 12(4):546–553. https://doi.org/10.1016/j.ufug.2013.06.002

Jung S, Kwak D, Park T, Lee W, Yoo S (2011) Estimating crown variables of individual trees using airborne. Remote Sens 3(11):2346–2363. https://doi.org/10.3390/rs3112346

Koma Z, Rutzinger M, Bremer M (2018) Automated segmentation of leaves from deciduous trees in terrestrial laser scanning point clouds. IEEE Geoscience and Remote Sensing Letters 15(9):1456–1460

Liang X, Kankare V, Hyyppä J, Wang Y, Kukko A, Haggrén H et al (2016) Terrestrial laser scanning in forest inventories. ISPRS J Photogramm Remote Sens 115:63–77

Lim K, Treitz P, Wulder M, St-onge B, Flood M (2013) LiDAR remote sensing of forest structure. Prog Phys Geogr: Earth Environ 1(2003):88–106. https://doi.org/10.1191/0309133303pp360ra

Moskal LM, Zheng G, Sensing R, Cooperative PF, Resources F (2012) Retrieving forest inventory variables with terrestrial laser scanning (TLS) in urban heterogeneous forest. Remote Sens 4(1):1–20. https://doi.org/10.3390/rs4010001

Newnham GJ, Armston JD, Calders K, Disney MI, Lovell JL, Schaaf CB, Danson FM (2015) Terrestrial laser scanning for plot-scale forest measurement. Curr For Rep 1(4):239–251. https://doi.org/10.1007/s40725-015-0025-5

Olagoke CP (2015) Extended biomass allometric equations for large mangrove trees from terrestrial LiDAR data. Trees 30(3):935–947. https://doi.org/10.1007/s00468-015-1334-9

Olofsson K, Holmgren J, Olsson H (2014) Tree stem and height measurements using terrestrial laser scanning and the RANSAC algorithm. Remote Sens 6(5):4323–4344. https://doi.org/10.3390/rs6054323

Pueschel P, Newnham G, Rock G, Udelhoven T, Werner W, Hill J (2013) ISPRS Journal of Photogrammetry and Remote Sensing The influence of scan mode and circle fitting on tree stem detection, stem diameter and volume extraction from terrestrial laser scans. ISPRS J Photogramm Remote Sens 77:44–56. https://doi.org/10.1016/j.isprsjprs.2012.12.001

Rudiger Hildebrandt AI (2012) From points to numbers : a database-driven approach to convert terrestrial LiDAR point clouds to tree volumes. Eur J Forest Res 131(6):1857–1867. https://doi.org/10.1007/s10342-012-0638-1

Schnabel R, Wahl R, Klein R (2007) Efficient RANSAC for point-cloud shape detection. Comput Graphics Forum 26(2):214–226

Tittmann P, Shafii S, Hartsough B, Hamann B (2011) Tree detection and delineation from LiDAR point clouds using RANSAC. Proceedings of SilviLaser 1–23

Tran T, Cao V, Laurendeau D (2015) Computers & graphics extraction of cylinders and estimation of their parameters from point clouds. Comput Graph 46:345–357. https://doi.org/10.1016/j.cag.2014.09.027

Wang D, Hollaus M, Puttonen E, Pfeifer N (2016) Fast and robust stem reconstruction in complex environments using terrestrial laser scanning. Int Arch Photogramm Remote Sens Spatial Inf Sci XLI-B3, 411–417. 10.5194/isprs-archives-XLI-B3-411-2016

Xia S, Wang C, Pan F, Xi X, H Z, H L (2015) Detecting stems in dense and homogeneous forest using single-scan TLS. Forests6(11):3923–3945.https://doi.org/10.3390/f6103923

Xu L, Oja E (2009) Randomized hough transform. In Encyclopedia of Artificial Intelligence (pp. 1343–1350). IGI Global

Zhao K, García M, Liu S, Guo Q, Chen G, Zhang X, Meng X (2015) Agricultural and forest meteorology terrestrial LiDAR remote sensing of forests : maximum likelihood estimates of canopy profile, leaf area index, and leaf angle distribution. Agric for Meteorol 209–210:100–113. https://doi.org/10.1016/j.agrformet.2015.03.008

Zheng G, Moskal LM (2012a) International Journal of Applied Earth Observation and Geoinformation Spatial variability of terrestrial laser scanning based leaf area index. Int J Appl Earth Obs Geoinf 19:226–237. https://doi.org/10.1016/j.jag.2012.05.002

Zheng G, Moskal LM (2012b) Leaf orientation retrieval from terrestrial laser scanning (TLS) data. IEEE Trans Geosci Remote Sens 50(2):3970–3979. https://doi.org/10.1109/TGRS.2012.2188533

Zheng G, Moskal LM, Kim S (2013) Retrieval of effective leaf area index in heterogeneous forests with terrestrial laser scanning. IEEE Trans Geosci Remote Sens 51(2):777–786. https://doi.org/10.1109/TGRS.2012.2205003

Current Forestry Reports
https://doi.org/10.1007/s40725-024-00228-2

REMOTE SENSING (J SUAREZ, SECTION EDITOR)

A Review of Software Solutions to Process Ground-based Point Clouds in Forest Applications

Arnadi Murtiyoso[1] · Carlos Cabo[2] · Arunima Singh[3] · Dimas Pereira Obaya[4] · Wout Cherlet[5] · Jaz Stoddart[6] · Cyprien Raymi Fol[1] · Mirela Beloiu Schwenke[1] · Nataliia Rehush[7] · Krzysztof Stereńczak[8,9] · Kim Calders[5] · Verena Christiane Griess[1] · Martin Mokroš[3,10,11]

Accepted: 5 August 2024

Abstract

Purpose of Review In recent years, the use of 3D point clouds in silviculture and forest ecology has seen a large increase in interest. With the development of novel 3D capture technologies, such as laser scanning, an increasing number of algorithms have been developed in parallel to process 3D point cloud data into more tangible results for forestry applications. From this variety of available algorithms, it can be challenging for users to decide which to apply to fulfil their goals best. Here, we present an extensive overview of point cloud acquisition and processing tools as well as their outputs for precision forestry. We then provide a comprehensive database of 24 algorithms for processing forest point clouds obtained using close-range techniques, specifically ground-based platforms.

Recent Findings Of the 24 solutions identified, 20 are open-source, two are free software, and the remaining two are commercial products. The compiled database of solutions, along with the corresponding technical guides on installation and general use, is accessible on a web-based platform as part of the COST Action 3DForEcoTech. The database may serve the community as a single source of information to select a specific software/algorithm that works for their requirements.

Summary We conclude that the development of various algorithms for processing point clouds offers powerful tools that can considerably impact forest inventories in the future, although we note the necessity of creating a standardisation paradigm.

Keywords Forest · Ground-based · Point Cloud · Review · Software · Web Platform

Introduction

Forests are complex terrestrial ecosystems that are dynamic in time and space. They are home to 80% of the terrestrial biodiversity of the planet [1]. Since time immemorial, people have benefited from the numerous functions of the forest in the form of goods and services provided by forest ecosystems, such as the provision of timber, clean water and air, protection against natural hazards, and many others. However, forests in Central Europe have not always been treated with the same care as they are today, and the complexity and interdependence of their functions have only recently become valued. By the late 14th century, Central Europe's forests were severely damaged by over-exploitation, resulting in a timber shortage. This shortage led to the first attempts at planned reforestation, and the subsequent genesis of the fields of forestry and forest sciences [2]. By the late 18th century, the principle of sustainability was developed, advocating the creation and conservation of forests and the use of wood in a stable and sustained manner [3]. Ensuring sustainability required an intimate knowledge of the current condition and extent of forests, as well as their development; this need formed the foundation for the field of forest inventory [4]. Forest inventory is defined as the systematic collection of data and forest information for their assessment or analysis. Basic information collected in forest inventories includes species, diameter at breast height, height, age, defects, and site quality. Such detailed inventories are still carried out today both at the national and local level. However, they are labour intensive and require trained personnel, making them very costly. In the 20th century, new and more efficient methods using 3D mapping

Extended author information available on the last page of the article

Published online: 17 August 2024

technology have been developed, but their application has focused mainly on assessing timber volumes and the potential for timber harvesting.

With an increasing population and growing resource demands, managing forests only for the provision of timber is no longer sufficient. In combination with rising labour costs and declining timber prices, there is now a clear need for more affordable yet detailed solutions. Additionally, the major impact of climate change is leading to initiatives such as climate-smart forestry [5]. The emphasis is on creating resilient forest ecosystems where timber is no longer the main product. That being said, such a forestry approach will lead to even more demanding forest management and inventory work.

The development of 3D capture technology has triggered a revolution in the way forest resources are surveyed. Airborne Laser Scanning (ALS), for example, has made it possible to map extensive areas of forests and even whole countries [6–8]. The quantification of point cloud in terms of different types of statistics has facilitated the development of statistical models that make it possible to predict many biometric features of trees and to characterise forest areas continuously (wall-to-wall maps) [9].

High-altitude aerial methods, such as ALS and photogrammetry, provide a large-scale forest perspective but with sparse detail. On the other hand, Terrestrial Laser Scanning (TLS), Mobile Laser Scanning (MLS), and close-range photogrammetry technologies, deployed in either a ground-based or a close-range aerial manner via Unmanned Aerial Vehicles (UAVs), provide a small-scale but very detailed perspective on forests [10]. This makes ground-based methods able to map the shape and dimension of individual trees more precisely than aerial methods and to obtain information about the forest understorey and regeneration [11–14].

These 3D mapping technologies may therefore be considered an alternative to traditional forest measurements and are often used in forestry and forest ecology studies, with a trend towards more use of laser scanning [15]. In the last two decades, many studies have demonstrated the high accuracy of direct measurements of forest parameters when using TLS technology [16, 17]. However, its practical application remains a challenge due to the variety of devices, the limitations imposed by the cost of implementing these technologies, and, most importantly, the lack of user know-how and lack of standards regarding data collection and processing. Furthermore, depending on the scale level of the inventory (national, local, or anything in between), different 3D technologies may be considered. As no standard currently exists on the levels of scale and detail, it may be difficult for users to determine which sensor to use in which circumstances. In many cases, there is also a need to develop algorithms for detecting and determining target characteristics of forest ecosystems, due to the highly fragmented processing solutions. However, the intensification of scientific work and technological developments in recent years suggest that these technologies will see considerable use in the near future.

Three-dimensional point clouds have provided forest practitioners and scientists with a completely new way of assessing and monitoring forest resources and services, and of conducting research that was previously impossible. As a result, more and more scientific groups and practitioners are intensively developing, often in parallel, methods and technologies to automate the surveying of ground plots and the determination of stand characteristics using point clouds. Here, again, there is a lack of standardisation and dynamic comparison with a focus on end users, such as foresters, ecologists and scientists. There is therefore a need for a joint initiative to manage the new findings and make standards for the above-mentioned end users.

In this paper we describe the results of one such initiative, conducted within the context of the 3DForEcoTech COST Action. In this initiative, our objectives were: (1) to compile a list of available ready-to-use processing solutions to derive forest characteristics from ground-based point clouds based on criteria such as availability, focus and relevance, and (2) to introduce a web platform with information about the identified processing solutions, their availability, technical guides on installation and general use, and benchmark results. Based on responses to a questionnaire distributed within the vast network created by the COST Action, we identified a total of 24 solutions.

In this review, we formulate three main aims: (1) to explain the use of point clouds in forestry; (2) to summarise forest point cloud processing and various approaches used by the different algorithms; and (3) to describe the 24 solutions compiled in the COST action survey. We also provide an overview of the potentials and limitations of the compiled solutions, for use by practitioners and researchers who would like to process point clouds for forestry applications. The remaining sections of this paper are organised as follows. In Sect. 2 we explain the use of point clouds in forestry. In Sect. 3 we describe a literature study on the state of the art in forest point cloud processing and the different approaches used by the different algorithms. In Sect. 4 we describe the 24 compiled solutions and discuss some of the main observations. We finish with concluding remarks in Sect. 5.

Point Clouds for Forest Applications

Common Point Cloud Acquisition Techniques

A point cloud describes a collection of points known in a cartesian tridimensional system and together forming a 3D object [18]. As such, a point cloud is by nature a geometric entity. Early conceptions of a point cloud already existed in traditional land surveying [19]. However, the generation of dense point clouds -- as the term is commonly understood today -- only started with the advent of lidar [20]. Lidar, or laser scanning, is today one of the techniques most commonly implemented in generating point clouds of real-world objects [16, 21, 22*]. As an active range-based sensor, a lidar device emits laser waves and records the distance between an object and the origin, along with sweeping angles, thus computing discrete 3D coordinates which form the backbone of a point cloud. A distinction is generally made between aerial and ground-based lidar [23, 24]. Aerial lidar, or ALS, may be distinguished according to its platform, with UAV [25] being pertinent within the context of close-range sensing. TLS and MLS are the most prominent examples of ground-based lidar [18]. The term "lidar" refers to the technology used, but is most commonly associated with and sometimes even considered interchangeable with ALS, while TLS and MLS are sometimes referred to as simply "laser scanning" [26]**. For ground-based forest mapping, TLS may be considered as the reference, due to the high quality of the data that may be achieved using this technique [16, 27, 28].

The other major alternative to lidar is photogrammetry. Photogrammetry is a much older technology, dating back to the first use of aerial photography [29]. Unlike lidar, it involves a passive image-based sensor which captures electromagnetic waves reflected by the surveyed object. Photogrammetry originally relied on empirical principles, and later on mathematical ones, to infer 3D coordinates from 2D images [30]. It was not until the last few decades that it managed to rival lidar in the generation of dense point clouds, thanks to new developments in the field of computer vision. Automated image orientation was developed in parallel with Structure from Motion (SfM) methods [31], while Multi-View Stereo (MVS) and dense matching principles [32, 33] truly boosted photogrammetry's popularity. Recent developments also saw an increasing interest in learning-based MVS [34] and novel 3D rendering methods, such as Neural Radiance Fields (NeRF) [35] and 3D Gaussian splatting [36]. Similar to its lidar counterpart, photogrammetry may be implemented both from an aerial and from a terrestrial perspective. Aerial photogrammetry traditionally involves the acquisition of nadir images from an aerial platform, which includes drones. However, oblique views are also common, especially in close-range photogrammetry [37]. Terrestrial close-range photogrammetry is especially known to be able to deliver high-precision results with a relatively low initial investment [38, 39]. However, it is not applied often in a forestry setting, mainly due to its difficult set-up in a forest environment. Indeed, traditional pinhole photogrammetry relies on multiple overlapping images taken in a convergent network, something which is difficult to achieve in a heterogeneous and uneven environment [40].

In recent years, novel sensors have been developed with a focus on portability and low cost, at the expense of precision. This philosophy of sensor development generally tries to fill the gap between very high precision, expensive solutions and low cost, generally lower quality ones. An interesting example can be seen in the development of MLS, which combines lidar technology with Simultaneous Localisation and Mapping (SLAM) methods. MLS has recently seen many applications in forestry, thanks to its portability [16, 41]. While its precision is generally lower than stationary TLS, in many cases it is high enough for mapping forest attributes. The same reasoning has also pushed the use of low-cost sensors in forestry, for example, depth cameras [42], spherical and fish-eye photogrammetry [40, 43], and the novel Solid-State Lidar (SSL) [44]. Figure 1 summarises the different categories of close-range point cloud generation techniques. In this paper, we focus on solutions for processing ground-based point clouds.

In terms of visualisation, the increasing availability of affordable online platforms for processing large 3D point clouds has facilitated the integration of point cloud data with cutting-edge visualisation technologies, such as Virtual Reality (VR) [45]. A major challenge in 3D rendering is related to memory requirements. To overcome this issue, many methods involve converting point clouds into meshes to optimise memory usage and ensure smooth visualisation [46, 47].

Data Types and Formats

The 3D representation of an object may take several forms, with the point cloud being one of the most common and the simplest in structure: point clouds are at their geometric base simple lists of coordinates. Other forms of 3D representations, like meshes, as well as volumetric and parametric models, are also commonly used, depending on the requirements. 3D meshes often consist of triangles, whose vertices are extracted from the point cloud. Volumetric and parametric 3D models can use simple geometric primitives and are also commonly used in information systems, e.g. Building Information Models (BIM), or Quantitative Structure Models (QSM). Despite their geometric simplicity, point clouds can be stored in various formats: binary files,

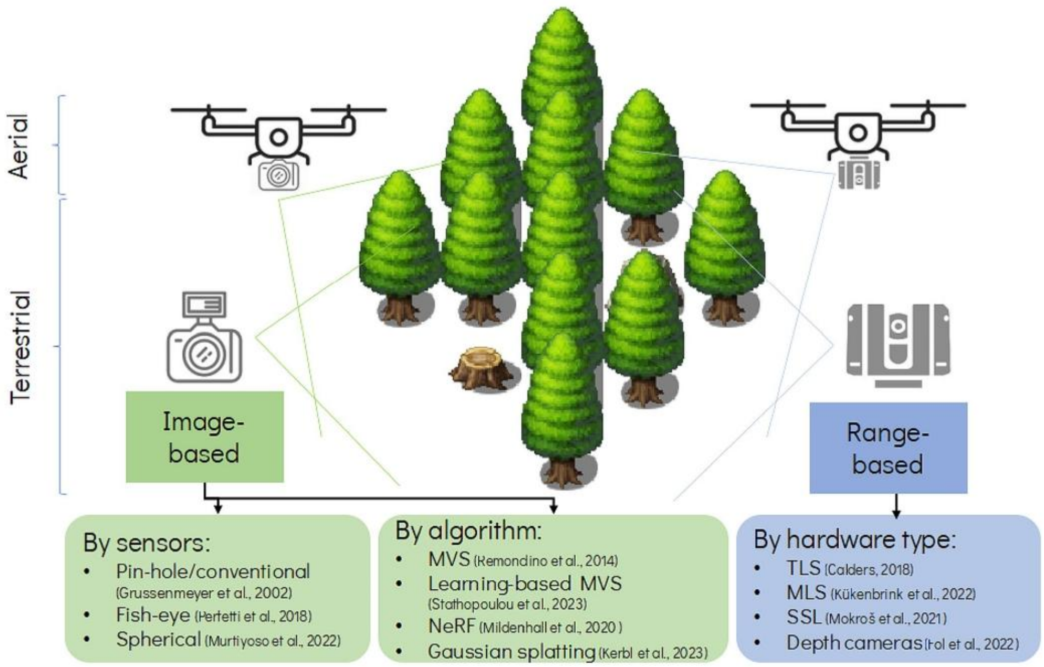

Fig. 1 The different close-range point cloud acquisition techniques available for forest mapping, categorised according to the type of data acquired and then further divided into sub-categories according to the sensor and algorithm (for image-based techniques) and hardware type (for range-based techniques)

Table 1 Features of some of the most common 3D formats available for 3D point cloud data

Format	Data type	Binary/ASCII	Compression	Custom fields
LAS	Point cloud	Binary	Optional with LAZ extension	Yes
PLY	Point cloud, mesh	Both	No	Yes
PCD	Point cloud	Both	Optional	Yes
OBJ	Point cloud, mesh	ASCII	No	No
TXT	Point cloud, volumetric model	ASCII	No	Yes

which are usually fast to read/write and allow compact storage; and text files, which are more inefficient but simpler to use and adapt. Point clouds can also be stored in a structured or an unstructured manner. Unstructured point clouds are simply lists of coordinates and attributes that can be conceptually pictured as a data table with as many rows as points and as many columns as dimensions and attributes. All the points in an unstructured point cloud must be in the same coordinate system. Conversely, structured point clouds have a more complex arrangement: they store the data as they were gathered in the field, together with all the additional information needed to generate a coherent point cloud with a unified coordinate system. Structured point clouds are frequently generated in ground-based laser scanning (specifically in TLS) and with depth-cameras but are not so common in ALS and photogrammetry.

Table 1 lists some of the most common point cloud formats on the market. Additionally, some formats support mesh and volumetric model representations on top of the point cloud. LAS is a binary and unstructured format that is used as a general exchange file format. It was initially designed for ALS point clouds, but due to its simplicity it is now used for any point cloud type. Most software for processing point cloud data includes reading and writing capabilities for this format. LAZ is a very common variant of LAS that allows data compression (both with or without information loss). Text files are also frequently used for point cloud storage and exchange. In most cases, data are stored in ASCII code and in an unstructured manner, with one point per line in the text file and the coordinates and attributes separated with commas, spaces or tabulated spaces. However, although there are some predefined text-file formats for point clouds, there is no clear standard for extended use, not even for the inclusion of metadata and/or headings.

Regarding structured point clouds, almost every manufacturer of ground-based laser scanners has developed their own format. These formats may be used for point cloud registration, denoising, colouring, and initial shape detections. However, in most cases, especially in forestry, these formats are only used for pre-processing the point clouds before transforming them into other exchange formats, such as LAS/LAZ or text files. E57 is another popular manufacturer-agnostic structured point cloud file format with read/write support in many software solutions and algorithms. This format is often encountered with TLS in the fields of engineering, heritage and architecture, but it is not yet popular in forestry. Very few software solutions related to forestry allow the use of this format.

Examples of Point Cloud Applications in Silviculture and Forest Ecology

Point cloud data obtained through laser scanning or similar technologies that generate 3D representations have numerous applications in silviculture and forest ecology. Furthermore, 3D data become increasingly important within the monitoring context of Essential Climate Variables (ECV) and Essential Biodiversity Variables (EBV) [48, 49]. Some examples of point cloud applications are:

1. Forest and tree attribute inventory: Point cloud data can be used to estimate conventional to complex forest attributes, such as tree height, Diameter at Breast Height (DBH), canopy cover, leaf area distribution, stem volume and Above Ground Biomass (AGB) [17, 50**, 51]. This information is crucial for forest management and monitoring purposes. For example, lidar data, combined with allometric models, can be used to estimate above ground carbon stocks in forests [52]. This information may be used to assess the carbon sequestration potential and to evaluate the effectiveness of climate change mitigation strategies.
2. Tree species classification: By analysing the structural characteristics of point cloud data, such as point density and canopy shape, we can apply machine learning algorithms to retrieve information at the individual tree level, e.g. using semantic and instance segmentation of point clouds [53].
3. Forest structure analysis: Point cloud data enable the quantification of forest structural parameters like canopy height profiles, vertical vegetation layers, and canopy gap distribution [54, 55]. By using lidar data, we can also provide valuable information on the need fire modelling, estimate forest canopy fuel parameters, map fire risk, and evaluate the effectiveness of fire management strategies [56].
4. Forest regeneration monitoring: Point cloud data can help assess the success of forest regeneration efforts by quantifying sapling density, height and spatial distribution within a forested area [57, 58]. These data aid in the evaluation of forest recovery after disturbances such as logging and fire.
5. Forest visualisation: Recent advancements in 3D scanning technologies and the increasing availability of affordable online platforms for processing large 3D point clouds have facilitated the integration of point cloud data with cutting-edge visualisation technologies, such as VR [45]. These applications can play a crucial role in supporting forest management practices and have the potential to contribute to the education of future foresters [59].

State of the Art of Processing Algorithms

Point Cloud Processing Pipeline in Forestry

A main goal of the pipeline of point cloud processing for forestry is to derive or directly measure information about essential parameters of the forest on an individual tree basis from captured point clouds. We consider measurements of tree dimensions, such as DBH, tree height, volume and selected crown parameters, essential parameters for forestry and precision forestry. The post-acquisition pipeline can be divided into general pre-processing and thematic (forest-specific) processing. The pipeline is specific for each of the processing solutions that are included in this paper, first because there are various goals of these solutions and second because the developers took different paths, for example in the selection of the programming language.

As the first step, general pre-processing is normally done within the dedicated software of the scanning device, depending on the acquisition method. For example, manufacturers of laser scanners (whether terrestrial or mobile) provide robust software solutions focusing on pre-processing and many additional post-processing options. This usually covers the registration of multiple scan positions for TLS or the application of SLAM post-processing for MLS data, in order to register the point cloud accurately. Another important process is the georeferencing, filtering and classification of the point clouds. These solutions are however commercial in nature and is thus unavailable for users who do not possess a specific license. In the case of photogrammetry, the 2D images are processed into 3D point clouds. This task is fully handled by photogrammetric software. Some of the more popular options include Agisoft Metshape (Agisoft LCC, Saint Petersburg, Russia) and Pix4D (Pix4D S.A., Prilly, Switzerland) [60], both of which are also commercial solutions. The pre-processing of photogrammetric point clouds is more computationally demanding than that for lidar point clouds [61], but it generally has the major advantage of lower cost.

In general, these methods or even tool-specific software packages provided by manufacturers do not have tools for individual tree measurements. They therefore constitute a first step in the pipeline, whose aim is to prepare the point cloud for further processing more specifically targeting individual tree measurements. In this regard, the thematic processing of the pipeline has the goal of measuring the parameters of individual trees. The method with which this is done varies based on the software or algorithm used. It usually starts with the segmentation or classification of the point cloud. This can be approached with different levels of complexity. For example, the FSCT pipeline [62] starts with semantic segmentation, where the point cloud is segmented into four categories using deep learning. On the other hand, simpler approaches that do not use deep learning first focus on the classification of terrain points. For example, Dendrocloud [63] divides the 3D point cloud by raster projection with a specified cell size, where the minimum z-value is searched and assigned to that particular cell. 3DForest [64] on the other hand, uses a voxelisation of the point cloud, where the minimal z-value is iteratively searched through neighbouring voxels. Based on these points, digital terrain is created, which is then used as a normalised surface from which cross-sections are generated.

The most important parameter to measure is DBH, as evidenced by the overwhelming availability across the processing solutions from the compiled list described in the following sections. In most solutions this is done on spatially grouped cross sections, often using either circle fitting or cylinder fitting with the help of the Random Sample Consensus (RANSAC) algorithm. In this regard, individual tree detection is a prominent functionality which would enable the solutions to compute the DBH as well as other tree parameters such as diameter at multiple heights, tree height, and stem volume.

Notions of Levels of Detail and Scene Scale

Different scenes may require different types of sensors and various kinds of processing strategies, depending on the scale of the scene and the requirements of the application. While a systematic formal definition of levels of detail in the general use of 3D data, particularly in urban environments, was presented in e.g., the CityGML paradigm [65], similar attempts for formal but specific forestry definitions are lacking in the literature. One such attempt was presented in [66], summarised in Fig. 2. [67*] also presented an interesting approach to categorise 3D data generation techniques based on the complexity and size of the scene; this approach

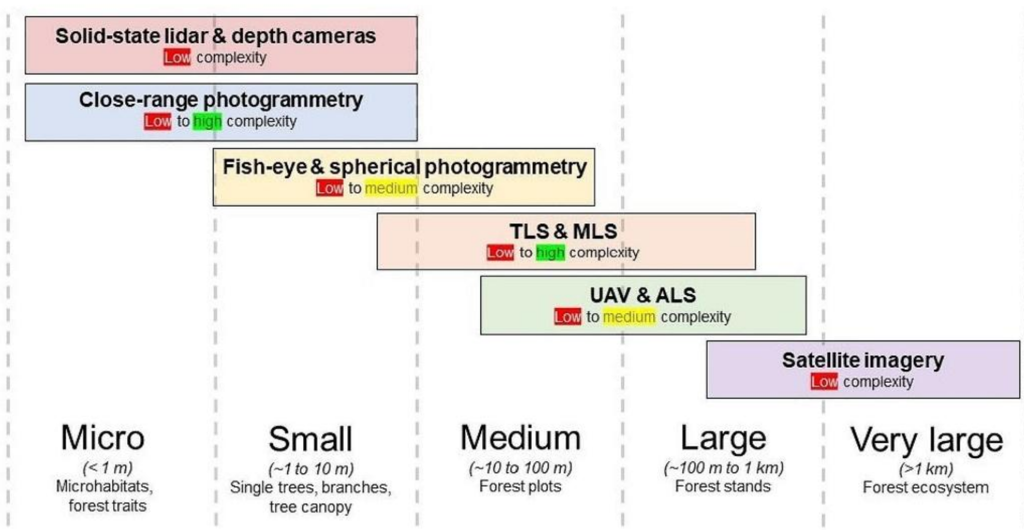

Fig. 2 Categorisation of the different levels of detail in 3D forests based on their spatial scales and how several 3D reconstruction techniques can address the requirements of these scale levels*Adapted from* [66]

influenced the creation of Fig. 2, in which the levels of detail are divided according to the spatial scale.

In general, definitions of scales and levels of detail exist in discussion of forests. While these definitions are not directly analogous to similar ones used in urban settings, it is possible to propose a sufficiently descriptive categorisation example, at least for the purposes of this paper. This notion of level of detail in forest point clouds is by no means authoritative, in part because the definitions of forest scale levels may also be subject to different interpretations. As can be seen in Fig. 2, five scale levels have been identified, ranging from very small objects (e.g. microhabitats) to large scenes. Figure 2 likewise proposed a categorisation of several 3D techniques in responding to the needs of each scale level.

Figure 2 refers to five scale levels, namely micro, small, medium, large, and very large. These levels were identified based on a purely spatial data point of view; this means that the levels' definitions refer to both the area of the forest to be covered by the 3D mapping and the expected geometric accuracy of the point cloud. In this context, note that the measurement of tree parameters such as DBH, tree height, or tree position are sensor-agnostic in nature since they are computed as derivatives of the point cloud as the main result of 3D sensors. However, the precision and accuracy of those parameters will be highly related to the quality of the point cloud and therefore choice of sensor; hence the proposal suggested by Fig. 2 to help future new users of the technology decide which sensor is best suited to their needs.

Nevertheless, an important notion in the discussion of levels of detail is the relationship between the expected quality (be it in terms of point cloud resolution, precision or accuracy) and the most appropriate technology to attain it. This in turn influences the way processing algorithms are developed. It is worth noting that in Fig. 2 both TLS and MLS represent a "middle-ground" compromise between details and scale. This explains their popularity in forest applications, as highlighted by the identified processing algorithms. Figure 2 does not, however, take into account other factors, such as occlusion in the forest.

Heuristic vs. Machine Learning Methods

Point cloud processing algorithms can be roughly split into two groups: heuristic and machine learning algorithms. Heuristic algorithms represent a set of logical rules that guide the user step by step toward the target result. In point cloud processing routines, heuristic approaches usually operate on the fitting of geometric primitives (lines, circles and cylinders), the calculation of statistics/features per area unit (e.g. cells) or space unit (e.g. voxels), and feature thresholding. Due to their logical and understandable nature (hence the term "knowledge-based"), heuristic approaches often serve as a starting approach for extracting target information from a point cloud. They are especially suitable when the amount of data is limited [68]. Today, in the forest domain, heuristic approaches dominate point cloud processing routines and are often used to extract a wide range of forest characteristics, e.g. the identification of individual trees and tree stems [69–71], DBH and tree height [72–75], forest structure characteristics [76], and Leaf-Area Index (LAI) [77–79].

A prominent example of the great success of a heuristic approach to point cloud processing is the QSM, which comprise a set of rules to reconstruct tree architecture using cylinder-based models [80, 81]. These models are widely used to derive the total volume and AGB of the tree, as well as its components [82–84]. However, heuristic algorithms may suffer from generality issues (intra- and extra-technological transferability/scalability). When they are applied to new data, some processing steps in heuristic algorithms might need adjustments (e.g. reconsidering thresholds and adding or removing processing steps), contributing an empirical aspect to the point cloud processing.

In contrast to heuristic algorithms, Machine Learning (ML) is generally used to extract forest characteristics that do not follow a clear geometric pattern and are hardly describable using a set of logical rules. ML implies supervised or unsupervised learning on a variable space, which is usually compiled using engineered features or real measurements (e.g. XYZ coordinates, spectral response). This approach previously operated on classic machine learning algorithms (e.g. Random Forest, Support Vector Machine, and XGBoost) and a set of engineered features to identify tree species [85–87] or to separate leaves from wood [88–90]. Today, however, Deep Learning (DL) is gaining attention from forest researchers. In other domains, DL has achieved state-of-the-art performance (sometimes even outperforming humans) in classification, segmentation and object detection tasks for both image and point cloud data. Forest researchers have begun to explore its potential for individual tree segmentation [91–93], tree species identification [94–96], and semantic point cloud segmentation [28, 97, 98]. However, the forest domain is generally a user of existing DL solutions rather than a developer of new ones. Thus, it tends to be a few steps behind the current state-of-the-art. It also suffers from a lack of large and representative public datasets to develop and calibrate DL models and fairly benchmark them against other solutions [99].

Within the context of the algorithms identified in this paper, most use a heuristic-based approach to generate the output. However, both ML and DL have been used in several algorithms in varying levels. Indeed, ML is not always used directly (e.g. for semantic or instance segmentation) but may be used to support the heuristic process, for example in performing individual tree segmentation, before referring to heuristic methods to generate the output parameters.

Identified State-of-the-Art Algorithms

Methodology

The process of compiling the algorithm list for terrestrial point cloud processing software solutions was conducted through a series of structured activities under the 3DForEcoTech Cost Action project. These activities were widely publicised within the 3DForEcoTech community and its extended networks, and they involved various channels and platforms accessible to participants. This effort resulted in an initial list of 65 available software solutions, which was subsequently refined to 24, based on criteria such as availability, focus and relevance. The creation of the initial list involved comprehensive activities conducted within Working Group 3 (WG3) of the COST Action 3DForEcoTech, including the distribution of an online questionnaire and multiple COST Action meetings.

The aim of the questionnaire was to gather preliminary information about algorithm implementations for point cloud processing in forestry, focusing on ground-based point clouds, tree/forest metrics, and publicly available solutions, regardless of their being free, open-source or even commercial. It was distributed to all 450 participants of 3DForEcoTech, representing over 50 countries. Participants were encouraged to share the questionnaire within their professional networks. Additionally, members of 3DForEcoTech convened meetings to complement the questionnaire results by identifying additional software solutions that may not have been considered in the questionnaire.

Following the collection of questionnaire responses and additional research from WG3 meetings, the initial software list comprising 65 solutions was compiled. This list underwent iterative review processes, facilitated by three Short Term Scientific Missions (STSM), each involving a different researcher. STSMs are funded scientific collaborations within the framework of COST Actions. The review process ensured: (i) compliance with the initial questionnaire requirements for participant submissions, (ii) functionality verification of the online-available versions of the software, (ii) evaluation of the software's capability to process simple point clouds, (iii) assessment of the software documentation, and (iv) specificity for terrestrial point cloud processing. Additionally, technical guides on installation and running instructions, along with relevant supplementary information, were compiled for each software solution.

To create a comprehensive database and overview of terrestrial point cloud processing software solutions, data were gathered from publicly available documentation provided by the authors/distributors of the implementations. Insights obtained during STSMs were also incorporated into the database. This resource compiles essential information for each software solution, including inputs, outputs, processes, and scope of use, and is intended to serve a valuable reference for understanding the functionalities and applicability of each implementation within the context of terrestrial point cloud processing in forest environments. Table 2 contains all the categories and items assessed in the list and database, including their basic information, availability, suitable inputs (point cloud technologies and file formats), scope of the application, and outputs.

Table 2 Categories of the identified algorithms according to the sensor, input, scale and output criteria

Information and availability	Availability		Free software
			Non-commercial
			Commercial
	Licence		
	Implementation		Package/library
			Plugin
			Standalone
	Download site		
	Documentation site		
	Contact (owner/author/distributor)		
	Notable obstacles and/or requirements		
Input point cloud technology	Laser scanning	Terrestrial	Single scan
			Multiscan
		Mobile	
	Terrestrial photogrammetry		
Input format files	.LAS/.LAZ		
	Other file formats		
	Allows batch processing		
Scale of applicability	Entire plots		
	Single trees		
Pre-processing (including subproduct outputs)	Data fusion of different point clouds		
	Digital terrain model (DTM)		
	Height normalisation (over the DTM)		
	Voxelisation		
Output parameters	Per tree	Diameter at breast height (DBH)	
		Individual tree detection and location	
		Diameters along the stem	
		Total tree height (TH)	
		Trunk/stem volume	
		Crown parameters (diameter, volume, etc.)	
		Segmentation of the stems	
		Quantitative structure model (QSM)	
	Per plot	Lead-wood classification	
		Percolation/empty space	
		Leaf-area index (LAI)	
		Total leaf area	

Identified Software Implementations

Each of the identified software was tested with different configuration environments. The software was mainly tested based on three important requirements, i.e. the ease and requirements of implementation, the main functionality of the software, and the possibility of errors occurring during the installation procedure. Table 3 presents the names of the identified solutions and a few important metadata, including their associated licences. The table also shows that the majority of the solutions are either open-source (20) or free (2), with another 2 available as commercial software. In most cases a relevant scientific publication was identified from the literature, although some contain explanations on the algorithmic background while others focus on its applications. Most of the open-source software solutions are hosted by the git platform www.github.com. Notably, the use of the R language is prevalent, although Python is a close second.

Table 4 presents the characteristics of the identified solutions in more detail. In general, of the 24 solutions identified in this paper, all are able to process TLS data. While several solutions do not support SfM and MLS data, most of them are generally sensor-agnostic. LAS is the most prevalent point cloud format, while batch processing is not a common feature. However, it should be noted that most of the identified solutions are in the form of source code. Batch processing is therefore theoretically possible, if not directly available. Note that within Table 4, several cells had either a "probably yes" (PY) or "probably no" (PN). This implies that according to our tests the concerned solution includes respectively availability or non-availability of the criteria mentioned in the column, sometimes in an indirect manner. However, we relegated it to "probably" due to the absence of a formal indication of such capability or lack thereof in the software's official documentation.

It is also interesting to note that while most solutions provide basic tree parameters, such as DBH (up to 75%) and tree height (up to 54%), a few are highly specialised. For example, Crossing3DForest was designed solely to create QSM models and TLS2trees for stem segmentation. None of the identified software and algorithms provide a feature to compute total leaf area. Figure 3 summarises the findings graphically.

Table 3 General information and availability of the 24 identified algorithms. Green cells denote open-source, yellow free software, and blue commercial solutions

	Name	License	Link	Relevant publication
R package	Allometric	(1)	https://allometric.org/	[100]
	Crossing3DForest	(2)	https://gitlab.com/Puletti/crossing3dforest	[101]
	CspStandSegmentation	(2)	https://github.com/JulFrey/CspStandSegmentation	N/A
	FORTLS	(2)	https://github.com/Molina-Valero/FORTLS	[102]
	ITSMe	(2)	https://github.com/lmterryn/ITSMe	[86]
	rTLS	(2)	https://github.com/Antguz/rTLS	[103]
	rTLSDeep	(2)	https://github.com/carlos-alberto-silva/rTLsDeep	[104]
	TreeLS	(2)	https://github.com/cran/TreeLS	[73]
	VoxR	(2)	https://github.com/Blecigne/VoxR	[105]
C#	Forest-taxator	N/A	https://github.com/maciej-malaszek/forest-taxator	[106]
Matlab	LeWoS	(1)	https://github.com/dwang520/LeWoS	[90]
	Point_Cloud_Tools	(3)	https://github.com/tuomasyr/Point-Cloud-Tools	[107]
	TreeQSM	(2)	https://github.com/InverseTampere/TreeQSM	[108]
Python	FSCT	(2)	https://github.com/SKrisanski/FSCT	[62]
	OPALS	N/A	https://opals.geo.tuwien.ac.at/	[109]
	TLS2trees	(2)	https://github.com/philwilkes/TLS2trees	[91]
	TLSeparation	(1)	https://github.com/TLSeparation/source	N/A
	treetool	(2)	https://github.com/porteratzo/TreeTool	[110]
Standalone	3DFIN	(2)	https://github.com/3DFin/3DFin	[75]
	3DForest	(2)	https://www.3dforest.eu/	[64]
	Computree	(4)	https://computree.onf.fr/	[111]
	dendrocloud	N/A	https://gis.tuzvo.sk/dendrocloud/	[63]
	AID-FOREST	N/A	https://dielmo.com/	[112]
	LiDAR 360	N/A	https://www.greenvalleyintl.com//LiDAR360	N/A

Licences: (1) MIT; (2) GPL-3; (3) CC BY 4.0; (4) GPL/LGPL

Table 4 Table of the identified software solutions and algorithms, with the availability of features indicated in the columns. "Y" denotes availability and "N" non-availability. "PY" denotes "probably yes" while "PN" signifies "probably no"

	Point cloud technology				Input format			Scale		Pre-processing			Output parameters												
Software	TLS single scan	TLS multiscan (single file)	Mobile LS	SfM point clouds	.LAS / .LAZ	Other	Batch processing	Plot level	Tree level	Voxelisation	DTM	Height normalisation	Data fusion	DBH	Individual tree detection	Diameters along stem	Tree height	Trunk volume	Crown parameters	Stem segmentation	Leaf-wood classification	QSM	Percolation/ empty space	LAI	Total leaf area
allometric	Y	Y	Y	Y	Y	N	N	Y	N	N	N	N	N	Y	N	Y	N	Y	N	N	N	N	N	N	N
Crossing3DForest	Y	Y	Y	Y	Y	Y	N	Y	N	Y	N	N	N	N	N	N	N	N	N	N	N	N	Y	N	N
CspStandSegmentation	Y	Y	Y	Y	Y	Y	N	Y	Y	Y	N	N	N	N	Y	N	N	N	N	N	N	N	N	N	N
FORTLS	Y	Y	Y	N	Y	N	N	Y	Y	N	N	Y	N	Y	Y	N	N	N	N	N	N	N	N	N	N
ITSMe	Y	Y	Y	Y	Y	Y	N	N	Y	N	N	N	N	Y	N	Y	Y	Y	Y	N	N	N	N	N	N
rTLS	Y	Y	Y	Y	N	Y	N	Y	Y	Y	N	N	N	Y	N	N	Y	Y	Y	N	N	N	Y	Y	N
rTLSDeep	Y	Y	Y	Y	Y	N	N	N	Y	N	N	N	N	N	N	N	N	N	N	N	Y	N	N	N	N
TreeLS	Y	Y	Y	PY	Y	Y	N	Y	Y	Y	N	Y	N	Y	Y	N	Y	N	N	Y	N	N	N	N	N
VoxR	Y	Y	Y	Y	PY	Y	N	N	Y	Y	N	N	N	Y	N	N	Y	N	Y	N	N	N	N	N	N
Forest-taxator	Y	Y	Y	Y	Y	N	N	Y	N	N	Y	N	N	Y	N	Y	N	N	N	N	N	N	N	N	N
LeWoS	Y	Y	Y	Y	Y	Y	N	Y	Y	N	N	N	N	N	N	N	N	N	N	N	Y	N	N	N	N
Point_Cloud_Tools	Y	Y	Y	Y	Y	Y	N	Y	Y	N	N	N	N	Y	Y	Y	Y	Y	Y	Y	Y	N	N	N	N
TreeQSM	Y	Y	PN	PN	Y	N	N	N	Y	N	N	N	N	Y	N	Y	Y	Y	Y	Y	N	Y	N	N	N
FSCT	Y	Y	Y	Y	Y	N	Y	Y	N	N	Y	Y	N	Y	Y	Y	Y	Y	N	Y	N	N	N	N	N
OPALS	Y	Y	Y	Y	Y	Y	Y	Y	Y	Y	Y	Y	N	Y	Y	Y	Y	N	N	N	N	N	N	N	N
TLS2trees	Y	Y	Y	Y	N	Y	N	Y	N	N	N	N	N	N	N	N	N	N	N	Y	N	N	N	N	N
TLSeparation	Y	Y	Y	Y	Y	Y	N	N	Y	Y	N	N	N	N	N	N	N	N	N	Y	Y	N	N	N	N
treetool	Y	Y	Y	Y	Y	N	Y	Y	N	N	Y	N	N	Y	Y	Y	N	N	N	N	N	N	N	N	N
3DFIN	Y	Y	Y	Y	Y	N	N	Y	Y	Y	N	N	N	Y	Y	Y	Y	N	N	N	N	N	N	N	N
3DForest	Y	Y	Y	Y	N	Y	N	Y	Y	Y	N	N	N	Y	Y	Y	Y	N	Y	N	N	Y	N	N	N
Computree	Y	Y	Y	Y	Y	Y	N	Y	Y	Y	Y	Y	Y	Y	Y	Y	Y	Y	Y	N	N	Y	N	N	N
dendrocloud	Y	Y	Y	Y	Y	Y	N	Y	Y	N	Y	N	Y	Y	Y	Y	N	N	N	N	N	N	N	N	N
AID-FOREST	Y	Y	Y	Y	Y	N	N	Y	Y	N	Y	Y	N	Y	Y	Y	Y	Y	N	N	N	N	N	N	N
LiDAR 360	Y	Y	N	N	Y	Y	N	Y	Y	Y	Y	Y	Y	Y	Y	Y	Y	N	Y	N	N	N	Y	Y	N
Percentage of "Yes"	100%	100%	92%	83%	83%	63%	13%	79%	75%	46%	33%	29%	13%	75%	54%	58%	54%	33%	33%	25%	17%	13%	13%	8%	0%

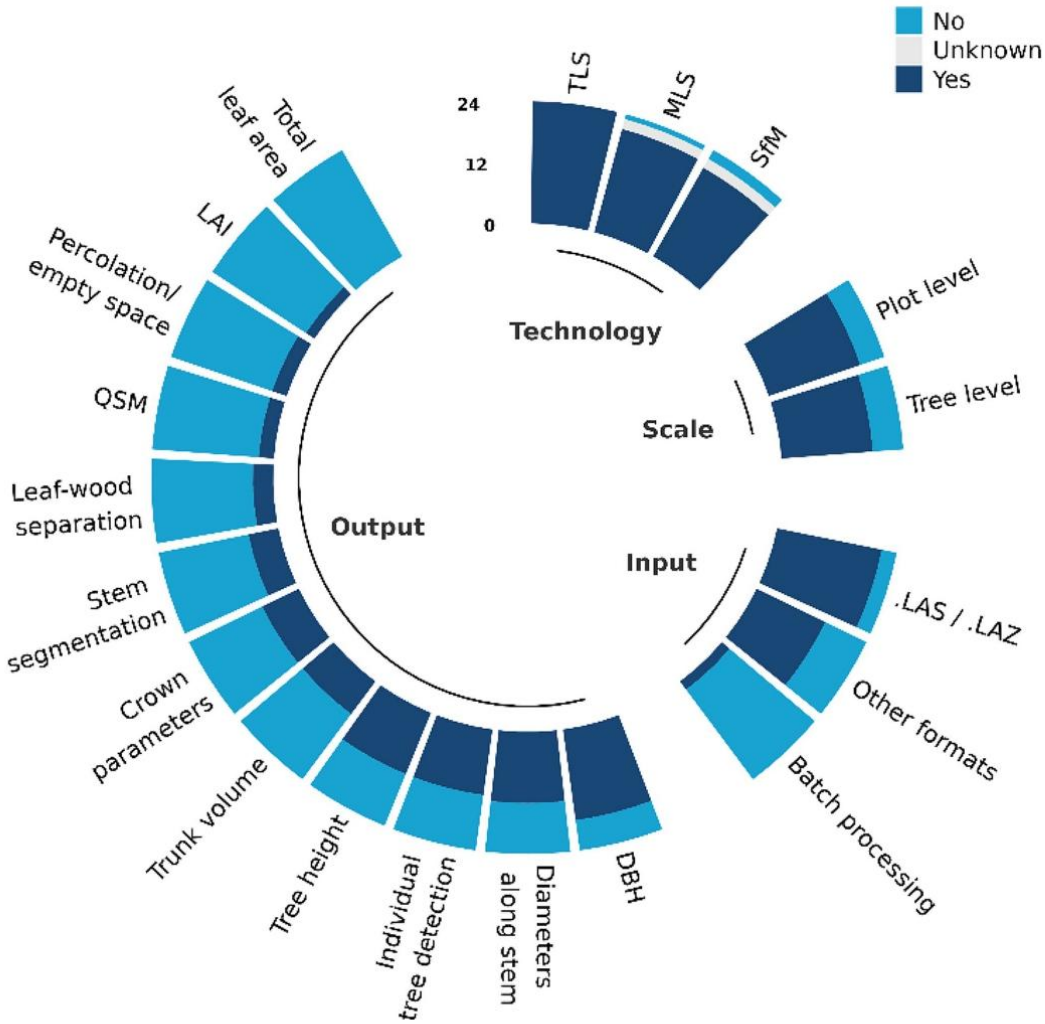

Fig. 3 Polar plot showing the distribution of the identified solutions, classified into the pre-determined categories

Online Dissemination Platform

Based on the identified software list and successful testing, an online platform was created for the end users. The information in Table 4 is reflected in the platform and should help users in choosing which solution suits their needs best and meets the required accuracy. As a preliminary system, the platform contains information from Table 4 in the form of a web application. The selection criteria in the platform are based on the categories defined in Table 2 and information from the columns of Table 4 was thereafter fed into it. In this way, the web-based platform may serve the community as a single source of information to select a specific software or algorithm that works for their requirements. Furthermore, the online nature of the platform means that it will evolve in time with regular updates of new algorithms and features. In order to further improve the information presented in the database especially regarding technical capabilities, a benchmark was also performed on the solutions. This benchmarking was performed during a hackathon organised by 3DForEcoTech in September 2023, and its results will be described in a future publication.

The platform is currently hosted within the 3DForEcoTech website (https://3dforecotech.eu/database/ last accessed 24 April 2024), where users may perform queries based on the available categories (represented as columns in Table 4). From the results of this query request, users may then choose a specific algorithm and click on it to see more information on a dedicated page for each algorithm. A conceptual drawing of how the online platform works is given in Fig. 4, and a concrete example of its implementation, taken directly from the website, is showcased in Fig. 5. This information page contains a description of the algorithm, as well as links to the respective codes and/or implementation. Furthermore, for each algorithm identified in the database, metadata were collected during installation and test runs, to assess its applicability for forestry. From these tests, technical guides on installation and general use were written and included in the web platform. These user guides are provided along with installation steps, basic computational configuration requirements, contact details of the author of the tool, and information on how to deal with possible errors in specific computational configurations.

Comparisons and Discussions

In this review, we leveraged the unique opportunity presented by a community of 450 researchers and practitioners from 50 countries dedicated to and/or interested in the application of close-range technologies for characterising forest environments, along with their extensive networks. We believe there is a pressing need to establish a standardised dynamic database of processing solutions that are dedicated to ground-based point clouds and forest measurements. In this paper we present one option to fulfil this need. It has already been established in many studies that 3D point clouds are well suited to measure individual tree parameters with high levels of detail and accuracy that can even exceed the conventional approaches (e.g. [15, 16]). Furthermore, it is important to note that this technology provides an option to measure on a level of detail that was not possible before. This in turn helps to address questions that previously could only be answered on a theoretical basis. However, these technologies are not yet commonly used by the wider community or relevant stakeholders, such as foresters, forest ecologists and scientists outside the remote sensing field [66].

By conducting a questionnaire and creating a database of processing solutions, we aimed to show what solutions are available and ready to use. More importantly, in this review we hoped to identify what has already been solved properly within the available solutions, thereby aiding the community in avoiding doing work on the same solution in the future. On the other hand, we also aimed to identify gaps in the state of the art to highlight areas where future developers should focus.

Observed Trends

In the discourse surrounding this review, it became evident that the landscape of ground-based point cloud processing in forest environments is primarily oriented towards automating precision forest inventory at the plot level. This involves the meticulous measurement of individual trees, encompassing parameters such as tree location, DBH and tree height. Such an approach closely mirrors the methodology employed in traditional forest inventories, thus establishing a familiar framework for practitioners transitioning into the realm of point cloud analysis. However, despite the prevalence of these automated inventory solutions, there remains a notable gap in the exploitation of the full potential offered by

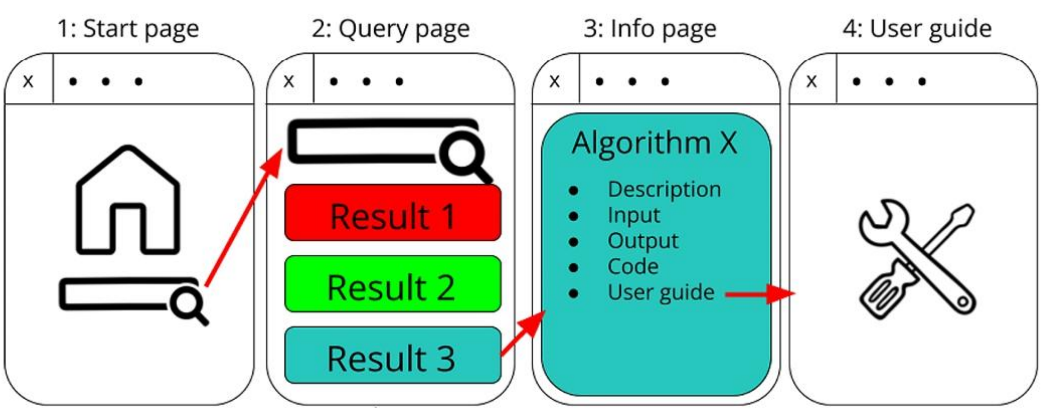

Fig. 4 Conceptual representation of how the online platform presents Table 4 as a queriable database

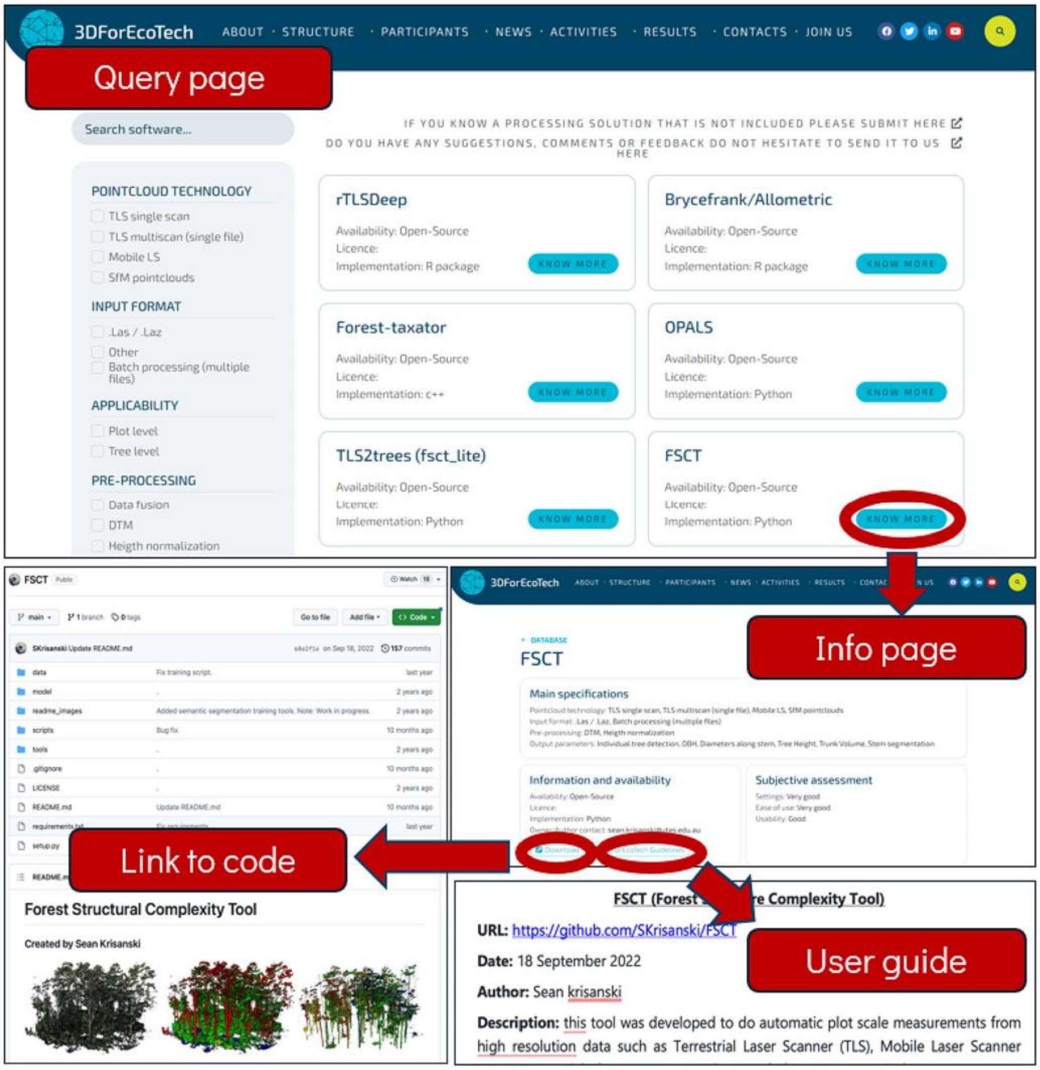

Fig. 5 A concrete example of how the online query works. In this example, FSCT was queried by the user. The platform provides a description of the software solution and a link to the user guide

ground-based point clouds. While certain software solutions delve into more complex metrics and analyses, the broader utilisation of these datasets has yet to be fully realised. Ground-based point clouds, by their very nature, offer a spatially explicit and three-dimensional representation of forest structure. This wealth of data holds considerable promise for enabling measurements and estimations that surpass the capabilities of conventional methods, including traditional inventories reliant on manual tree-by-tree measurements, aerial lidar surveys, and other forms of remote sensing. It is imperative to recognise that ground-based point clouds possess unique attributes that distinguish them from other data sources. Unlike traditional inventories, which are often limited by the labour-intensive nature of tree-by-tree assessments, point clouds offer a comprehensive and continuous dataset that captures the intricacies of forest ecosystems in unprecedented detail. Furthermore, their three-dimensional nature facilitates advanced analyses, such as volumetric assessments, canopy characterisation, and habitat mapping, which have the potential to revolutionise our understanding of forest dynamics and biodiversity.

In addition, advancements in Artificial Intelligence (AI) methods applied to point clouds are beginning to usher in algorithms for quantifying and mapping complex variables. However, as emphasised throughout this work, publicly available implementations remain scarce. In the specific case of utilising novel DL methods, additional challenges arise from creating publicly available implementations, including those stemming from the complexity of configuring and executing processes with specific hardware requirements, such as the utilisation and management of GPU-based systems, along with the need for extensive training data and long processing times to ensure functionality. These complexities underscore the ongoing need for further research and development to overcome barriers to widespread adoption, to facilitate user-friendly operability, and to maximise the potential of AI-driven approaches in ground-based point cloud processing.

In light of these considerations, while existing ground-based point cloud processing software solutions have made large strides in automating forest inventory processes, there exists a compelling opportunity to further innovate and expand the scope of analysis. By leveraging the spatially explicit and multidimensional nature of point cloud data, researchers and practitioners can unlock new avenues for ecological research, conservation planning, and sustainable forest management. As such, future developments in this field should aim to harness the full potential of ground-based point clouds, driving forward advancements in forest science and management.

Identified Gaps

This study represents a unique opportunity to gain a comprehensive overview of existing implementations of algorithms aimed at automating forest mensuration, inventory and mapping. Although algorithms can be identified through systematic paper searches, compiling a complete repertoire of available software would require alternative means, which are not always straightforward -- especially for non-specialists. Thus, we encourage researchers to share, along with scientific publications, their point-cloud processing solutions implemented in a way that is as user-friendly as possible. This will foster other researchers to not repeat, but build on existing solutions and develop them further. It is also worth noting that most of the identified algorithms and software are usually focused on a particular problem related to the developer's needs. Indeed, the solutions are generally good enough in terms of their main functionality but may falter when repurposed for other needs. While this is a logical outcome of the software development process (i.e. to solve a particular problem), there is a growing need for fully automated software which includes all the pre-processing and post-processing steps. The same incoherence can also be seen by the fact that most solutions work with different set-ups in terms of input file format and type (whether plot level or individual tree level). None of the identified software solutions has flexibility for the point cloud input data and file formats, making them quite rigid. Further challenges are also associated with the configuration and implementation of each software solution, due to the specific computational requirements. Furthermore, this ad hoc approach to software development has also hindered the full exploitation of 3D data. As such, in real world applications a 3D mapping mission is often times still accompanied by in situ measurements (albeit reduced), which in some cases may increase the cost, complexity, and required expertise of the mission. This is naturally contrary to the promise of 3D remote sensing technologies of performing simpler measurements.

On the other hand, having several processing solutions that target the same output (e.g. DBH) is natural and welcomed, since different algorithms can be used to derive it and different datasets can be applied while developing the solution. However, a reasonable and fair comparison of the performance of such solutions is highly needed. From this perspective, it is crucial to establish *publicly available benchmark datasets* that comprise multi-sensor and multi-platform point clouds and accurate reference measurements of forest attributes from various forest ecosystems, optimally from all over the world. Furthermore, such datasets would be crucial for solution development, since they would foster the development of robust, sensor-agnostic and bias-free approaches. The use of a standard dataset for benchmarking purposes is already common practice in other domains, such as computer vision [113, 114] and 3D architecture [115].

Role of a Dynamic and Online Database

The web platform/online database established as a product of this survey is a step in the direction of knowledge consolidation in one place and a groundbreaking opportunity to provide the scientific community with a curated list of algorithms, supplemented by additional metadata. This resource will enable users to select the most suitable software for their needs, circumstances and output data, while simultaneously empowering software creators to avoid reinventing the wheel. By doing so, they can allocate their time and resources more efficiently, ultimately advancing the field of terrestrial point cloud processing and enhancing its accessibility and utility within the scientific community.

The compilation of the list and the database involved meticulous review and analysis of available documentation, as well as direct interaction with the software solutions during the STSMs. By consolidating this information, the database provides a comprehensive reference for researchers, practitioners and stakeholders interested in ground-based point cloud processing. It facilitates informed decision-making and enables comparison among different software solutions based on their capabilities and suitability for specific applications within forestry and related fields.

Conclusions and Outlook

In this paper, we described a review of state of the art point cloud processing for ground-based forest applications, and we presented a list of the available algorithms and software solutions. The aim of the list's compilation was to collect the scattered information in one place, which we accomplished via the creation of an online searchable database. The paper thus also summarises the state of 3D technology in forestry. We then categorised the compiled list of 24 solutions. Most of the identified solutions are open-source or free, with an observed trend towards the general use of TLS technology. This is evidenced by the fact that while many of the solutions are sensor-agnostic, all of them take TLS data as their default input. Furthermore, a few tree parameters predominate as the computed output, in particular DBH. This may be interpreted as the high demand for such values in forestry applications and, by extension, the ever growing interest in using 3D technologies for forest applications. It is, however, an important caveat that variables such as DBH and tree height are some of the basic tree parameters; it is therefore only natural that solutions would aim to provide them, regardless of the general state of the use of 3D technology in forestry.

On the other hand, the development of software solutions is steadily progressing. Developers are creating software solutions based on the most recent challenges for point cloud processing that they encountered in their work as their principal functionality. However, there is increasing demand for software solutions which can not only carry out a single specific function but also help to assess basic forest inventory parameters with appropriate accuracy. Also, there should be a better solution for the computational requirement of the specific software or tools. To grow user groups and facilitate the use of existing tools by various user types, not just highly trained professionals, developers should focus on the user-friendliness and ease of application of their tools.

In the near future, a benchmarking of the identified solutions will be carried out to assess their geometric quality. This benchmarking is intended to provide future users of the web platform not only semantic information and metadata on the solutions, but also tangible values that determine the applicability of each solution according to the users' needs. A standardisation of this nature is also envisaged for other aspects of ground-based 3D forest mapping, e.g. sensors and protocols, within the context of the 3DForEcoTech COST Action.

Acknowledgements This article is based upon work from COST Action 3DForEcoTech CA20118, supported by COST (European Cooperation in Science and Technology). W. Cherlet and K. Calders were funded by the European Union (ERC-2021-STG grant agreement no. 101039795). Views and opinions expressed are, however, those of the authors only and do not necessarily reflect those of the European Union or the European Research Council Executive Agency. Neither the European Union nor the granting authority can be held responsible for them. M. Beloiu Schwenke was funded by the Swiss National Science Foundation (grant no. IZCOZ0_213355). C. Cabo received funding from the UK NERC (NE/T001194/1), from the Spanish Ministry of Universities and NextGenerationEU (MU21-UP2021-030), and the Spanish Knowledge Generation project (PID2021-126790NB-I00). The authors would also like to thank Melissa Dawes for professional language editing.

Author Contributions AM: Conceptualization, Methodology, Validation, Writing-original draft, Writing-review & editing, Supervision. CC: Conceptualization, Methodology, Writing-original draft, Data curation, Formal analysis, investigation, Supervision. AS: Data curation, Formal analysis, Investigation, Writing-original draft. DPO: Formal analysis, Investigation, Writing-original draft. WC: Formal analysis, Investigation, Writing-original draft. JS: Formal analysis, Investigation, Writing-original draft. CRF: Formal analysis, Investigation, Writing-original draft. MBS: Formal analysis, Investigation, Writing-original draft. NR: Formal analysis, Investigation, Writing-original draft. KS: Formal analysis, Investigation, Writing-original draft. KC: Formal analysis, Investigation, Supervision, Writing-original draft. VCG: Resources, Validation, Writing-original draft. MM: Conceptualization, Project administration, Resources, Supervision, Writing-original draft. All authors reviewed the manuscript.

Funding Open access funding provided by Swiss Federal Institute of Technology Zurich

Data Availability No datasets were generated or analysed during the current study.

Declarations

Competing Interests The authors declare no competing interests.

References

1. IPBES. (2019) Summary for policymakers of the global assessment report on biodiversity and ecosystem services of the intergovernmental science-policy platform on biodiversity and ecosystem services. Bonn, Germany.
2. Hasel K, Schwartz E. Forstgeschichte – Ein Grundriss für Studium Und Praxis. Remagen: Verlag Dr. Kessel; 2002.
3. von Carlowitz HC. Sylvicultura Oeconomica. Leipzig: Braun; 1713.
4. Hartig GL. Anweisung Zur Taxation Der Forste, Oder Zur Bestimmung Des Holzertrags Der Wälder. Darmstadt: Stahl; 1795.
5. Bowditch E, Santopuoli G, Binder F, et al. What is Climate-Smart Forestry? A definition from a multinational collaborative process focused on mountain regions of Europe. Ecosyst Serv. 2020;43:101113.
6. Nelson R, Krabill W, Tonelli J. Estimating forest biomass and volume using airborne laser data. Remote Sens Environ. 1988;24:247–67.
7. Næsset E. Predicting forest stand characteristics with airborne scanning laser using a practical two-stage procedure and field data. Remote Sens Environ. 2002;80:88–99.
8. McRoberts RE, Andersen H-E, Næsset E. Using Airborne laser scanning data to support forest sample surveys. Forestry applications of Airborne Laser scanning: concepts and Case studies. Dordrecht: Springer Netherlands; 2014. pp. 269–92.
9. White JC, Wulder MA, Varhola A, Vastaranta M, Coops NC, Cook BD, Pitt D, Woods M. A best practices guide for generating forest inventory attributes from airborne laser scanning data using an area-based approach. Forestry Chron. 2013;89:722–3.
10. Bartholomeus H, Calders K, Whiteside T, Terryn L, Krishna Moorthy SM, Levick SR, Bartolo R, Verbeeck H. Evaluating data inter-operability of multiple UAV–LiDAR systems for measuring the 3D structure of Savanna Woodland. Remote Sens (Basel). 2022;14:5992.
11. Campbell MJ, Dennison PE, Hudak AT, Parham LM, Butler BW. Quantifying understory vegetation density using small-footprint airborne lidar. Remote Sens Environ. 2018;215:330–42.
12. Disney M. Terrestrial LiDAR: a three-dimensional revolution in how we look at trees. New Phytol. 2019;222:1736–41.
13. Liu L, Pang Y, Li Z, Si L, Liao S. Combining Airborne and Terrestrial laser scanning technologies to measure Forest Understorey volume. Forests. 2017;8:111.
14. Korpela I, Hovi A, Morsdorf F. Understory trees in airborne LiDAR data — selective mapping due to transmission losses and echo-triggering mechanisms. Remote Sens Environ. 2012;119:92–104.
15. Calders K, Adams J, Armston J, et al. Terrestrial laser scanning in forest ecology: expanding the horizon. Remote Sens Environ. 2020;251:112102.
16. Kükenbrink D, Marty M, Bösch R, Ginzler C. Benchmarking laser scanning and terrestrial photogrammetry to extract forest inventory parameters in a complex temperate forest. Int J Appl Earth Obs Geoinf. 2022;113:102999.
17. Calders K, Verbeeck H, Burt A, Origo N, Nightingale J, Malhi Y, Wilkes P, Raumonen P, Bunce RGH, Disney M. Laser scanning reveals potential underestimation of biomass carbon in temperate forest. Ecol Solutions Evid. 2022. https://doi.org/10.1002/2688-8319.12197.
18. Murtiyoso A, Grussenmeyer P. Virtual disassembling of historical edifices: experiments and assessments of an automatic approach for classifying multi-scalar point clouds into architectural elements. Sens (Switzerland). 2020;20:2161.
19. Grussenmeyer P, Landes T, Voegtle T, Ringle K. Comparison methods of terrestrial laser scanning, photogrammetry and tachometry data for recording of cultural heritage buildings. Int Archives Photogrammetry Remote Sens Spat Inform Sci. 2008;XXXVI:213–8.
20. Elseberg J, Borrmann D, Nüchter A. One billion points in the cloud – an octree for efficient processing of 3D laser scans. ISPRS J Photogrammetry Remote Sens. 2013;76:76–88.
21. Macher H, Landes T, Grussenmeyer P. From Point clouds to Building Information models: 3D semi-automatic Reconstruction of indoors of existing buildings. Appl Sci. 2017;7:1–30.
22. Mallet C, Bretar F. Full-waveform topographic lidar: state-of-the-art. ISPRS J Photogrammetry Remote Sens. 2009;64:1–16. This paper is a very useful starting point to understand the use of lidar for topographic purposes.
23. Wehr A, Lohr U. Airborne laser scanning—an introduction and overview. ISPRS J Photogrammetry Remote Sens. 1999;54:68–82.
24. van Genderen JL. Airborne and terrestrial laser scanning. Int J Digit Earth. 2011;4:183–4.
25. Colomina I, Molina P. Unmanned aerial systems for photogrammetry and remote sensing: a review. ISPRS J Photogrammetry Remote Sens. 2014;92:79–97.
26. Granshaw SI. Photogrammetric terminology: fourth edition. Photogramm Rec. 2020;35:143–288. This publication is an important ISPRS document that describes the various terms used in modern photogrammetry and remote sensing. The current paper follows both the definitions and spellings recommended in this reference.
27. Calders K, Origo N, Burt A, Disney M, Nightingale J, Raumonen P, Åkerblom M, Malhi Y, Lewis P. Realistic forest stand Reconstruction from Terrestrial LiDAR for Radiative transfer modelling. Remote Sens (Basel). 2018;10:933.
28. Rehush N, Abegg M, Waser LT, Brändli U-B. Identifying tree-related microhabitats in TLS point clouds using machine learning. Remote Sens (Basel). 2018;10:1735.
29. Wolf P, DeWitt B, Wilkinson B. Elements of photogrammetry with applications in GIS. 4th ed. McGraw-Hill Education; 2014.
30. Grussenmeyer P, Al Khalil O. Solutions for exterior orientation in photogrammetry: a review. Photogram Rec. 2002;17:615–34.
31. Wu C, Agarwal S, Curless B, Seitz SM. (2011) Multicore bundle adjustment. Proceedings of the IEEE Computer Society Conference on Computer Vision and Pattern Recognition 3057–3064.
32. Furukawa Y, Ponce J. Accurate, dense, and robust multi-view stereopsis. IEEE Trans Pattern Anal Mach Intell. 2009;32:1362–76.
33. Hirschmüller H. (2011) Semi-Global Matching Motivation, Developments and Applications. In: Photogrammetric Week. pp 173–184.
34. Stathopoulou EK, Remondino F. A survey on conventional and learning-based methods for multi-view stereo. Photogramm Rec. 2023. https://doi.org/10.1111/phor.12456.
35. Mildenhall B, Srinivasan PP, Tancik M, Barron JT, Ramamoorthi R, Ng R. (2020) NeRF: representing scenes as neural Radiance fields for View Synthesis. Lecture Notes in Computer Science (including subseries Lecture Notes in Artificial Intelligence and Lecture Notes in Bioinformatics) 12346 LNCS:405–21.
36. Kerbl B, Kopanas G, Leimkühler T, Drettakis G. (2023) 3D Gaussian Splatting for Real-Time Radiance Field Rendering. ACM Trans Graph 42.
37. Rupnik E, Nex F, Remondino F. (2014) Oblique multi-camera systems-orientation and dense matching issues. International

Archives of the Photogrammetry, Remote Sensing and Spatial Information Sciences, 2014;40:107–14.
38. Börlin N, Murtiyoso A, Grussenmeyer P, Menna F, Nocerino E. Flexible photogrammetric computations using Modular Bundle Adjustment: the Chain Rule and the collinearity equations. Photogramm Eng Remote Sens. 2019;85:361–8.
39. Nocerino E, Menna F, Remondino F, Saleri R. Accuracy and block deformation analysis in automatic UAV and terrestrial photogrammetry - lesson learnt. ISPRS Annals Photogrammetry Remote Sens Spat Inform Sci. 2013;II–5/W1:2–6.
40. Murtiyoso A, Hristova H, Rehush N, Griess VC. (2022) Low-cost mapping of forest under-storey vegetation using spherical photogrammetry. The International Archives of the Photogrammetry, Remote Sensing and Spatial Information Sciences XLVIII-2/W1-2022:185–190.
41. Cabo C, Del Pozo S, Rodríguez-Gonzálvez P, Ordóñez C, González-Aguilera D. Comparing terrestrial laser scanning (TLS) and wearable laser scanning (WLS) for individual tree modeling at plot level. Remote Sens (Basel). 2018. https://doi.org/10.3390/rs10040540.
42. Fol CR, Murtiyoso A, Griess VC. (2022) Evaluation of Azure Kinect Derived Point clouds to determine the Presence of microhabitats on single trees based on the Swiss standard parameters. International Archives of the Photogrammetry, Remote Sensing and Spatial Information Sciences. XLIII-B2-2022: 989–994.
43. Perfetti L, Polari C, Fassi F, Troisi S, Baiocchi V, Del Pizzo S, Giannone F, Barazzetti L, Previtali M, Roncoroni F. (2018) Fisheye Photogrammetry to Survey Narrow Spaces in Architecture and a Hypogea Environment. Latest Developments in Reality-Based 3D Surveying and Modelling 3–28.
44. Mokroš M, Mikita T, Singh A, et al. Novel low-cost mobile mapping systems for forest inventories as terrestrial laser scanning alternatives. Int J Appl Earth Obs Geoinf. 2021;104:102512.
45. Garrido D, Rodrigues R, Sousa AA, Jacob J, Silva DC. (2021) Point Cloud Interaction and Manipulation in Virtual Reality. 2021 5th International Conference on Artificial Intelligence and Virtual Reality (AIVR) 15–20.
46. Poux F, Valembois Q, Mattes C, Kobbelt L, Billen R. Initial user-centered design of a virtual reality Heritage System: applications for Digital Tourism. Remote Sens (Basel). 2020;12:2583.
47. Kharroubi A, Hajji R, Billen R, Poux F. (2019) Classification and integration of massive 3D points clouds in a virtual reality (VR) environment. The International Archives of the Photogrammetry, Remote Sensing and Spatial Information Sciences XLII-2/W17:165–71.
48. Calders K, Brede B, Newnham G, et al. StrucNet: a global network for automated vegetation structure monitoring. Remote Sens Ecol Conserv. 2023. https://doi.org/10.1002/rse2.333.
49. Valbuena R, O'Connor B, Zellweger F, et al. Standardizing ecosystem morphological traits from 3D information sources. Trends Ecol Evol. 2020;35:656–67.
50. Liang X, Hyyppä J, Kaartinen H, et al. International benchmarking of terrestrial laser scanning approaches for forest inventories. ISPRS J Photogrammetry Remote Sens. 2018;144:137–79. This publication presents a very important topic where the use of TLS for forestry is meticulously investigated and benchmarked.
51. Yusup A, Halik U, Keyimu M, Aishan T, Abliz A, Dilixiati B, Wei J. Trunk volume estimation of irregular shaped Populus Euphratica riparian forest using TLS point cloud data and multivariate prediction models. Ecosyst. 2023;10:100082.
52. Asner GP, Mascaro J. Mapping tropical forest carbon: calibrating plot estimates to a simple LiDAR metric. Remote Sens Environ. 2014;140:614–24.
53. Weiser H, Schäfer J, Winiwarter L, Krašovec N, Fassnacht FE, Höfle B. Individual tree point clouds and tree measurements from multi-platform laser scanning in German forests. Earth Syst Sci Data. 2022;14:2989–3012.
54. Vepakomma U, St-Onge B, Kneeshaw D. Spatially explicit characterization of boreal forest gap dynamics using multi-temporal lidar data. Remote Sens Environ. 2008;112:2326–40.
55. Suwardhi D, Fauzan KN, Harto AB, Soeksmantono B, Virtriana R, Murtiyoso A. 3D modeling of individual trees from LiDAR and Photogrammetric Point clouds by Explicit Parametric representations for Green Open Space (GOS) Management. ISPRS Int J Geoinf. 2022;11:174.
56. González-Olabarria J-R, Rodríguez F, Fernández-Landa A, Mola-Yudego B. Mapping fire risk in the Model Forest of Urbión (Spain) based on airborne LiDAR measurements. Ecol Manage. 2012;282:149–56.
57. Brolly G, Király G, Czimber K. Mapping Forest Regeneration from Terrestrial Laser scans. Acta Silvatica et Lignaria Hungarica. 2013;9:135–46.
58. Heinzel J, Ginzler C. A single-Tree Processing Framework using terrestrial laser scanning data for detecting Forest Regeneration. Remote Sens (Basel). 2019;11:60.
59. Wallgrün JO, Huang J, Zhao J, Brede B, Lau A, Klippel A. (2021) Embodied digital twins of forest environments. UC Santa Barbara GIScience 2021 Short Paper Proceedings. https://doi.org/10.25436/E2059Z
60. Kingsland K. Comparative analysis of digital photogrammetry software for cultural heritage. Digit Appl Archaeol Cult Herit. 2020;18:e00157.
61. Piermattei L, Karel W, Wang D, Wieser M, Mokroš M, Surový P, Koreň M, Tomaštík J, Pfeifer N, Hollaus M. (2019) Terrestrial Structure from Motion Photogrammetry for Deriving Forest Inventory Data. Remote Sens (Basel). https://doi.org/10.3390/rs11080950
62. Krisanski S, Taskhiri MS, Gonzalez Aracil S, Herries D, Muneri A, Gurung MB, Montgomery J, Turner P. (2021) Forest Structural Complexity Tool—An Open source, fully-automated Tool for Measuring Forest Point clouds. Remote Sens (Basel). https://doi.org/10.3390/rs13224677
63. Koreň M, Hunčaga M, Chudá J, Mokroš M, Surový P. The influence of Cross-section thickness on diameter at breast height estimation from Point Cloud. ISPRS Int J Geoinf. 2020. https://doi.org/10.3390/ijgi9090495.
64. Krucek M, Kral K, Cushman KC, Missarov A, Kellner JR. Supervised segmentation of ultra-high-density drone lidar for large-area mapping of individual trees. Remote Sens (Basel). 2020;12:3260.
65. Nys GA, Poux F, Billen R. City JSON building generation from airborne LiDAR 3D point clouds. ISPRS Int J Geoinf. 2020. https://doi.org/10.3390/ijgi9090521.
66. Murtiyoso A, Holm S, Riihimäki H, Krucher A, Griess H, Griess VC, Schweier J. Virtual forests: a review on emerging questions in the use and application of 3D data in forestry. Int J for Eng. 2023;35:29–42.
67. * Remondino F, Barazzetti L, Nex F, Scaioni M, Sarazzi D. (2011) UAV photogrammetry for mapping and 3D modeling - current status and future perspectives. The International archives of the photogrammetry, remote sensing and spatial Information sciences XXXVIII:25–31. This publication is an important resource not only as regards to the use of UAV, but also the choice of sensor.
68. Murtiyoso A, Grussenmeyer P. (2019) Automatic Heritage Building Point Cloud Segmentation and Classification Using Geometrical Rules. In: International Archives of the Photogrammetry, Remote Sensing and Spatial Information Sciences. pp 821–827.
69. Heinzel J, Huber MO. Tree stem diameter estimation from volumetric TLS Image Data. Remote Sens (Basel). 2017;9:614.
70. Zhang W, Wan P, Wang T, Cai S, Chen Y, Jin X, Yan G. A Novel Approach for the detection of standing Tree stems from plot-level terrestrial laser scanning data. Remote Sens (Basel). 2019;11:211.

71. Burt A, Disney M, Calders K. Extracting individual trees from lidar point clouds using treeseg. Methods Ecol Evol. 2019;10:438–45.
72. Olofsson K, Holmgren J, Olsson H. Tree stem and height measurements using Terrestrial Laser scanning and the RANSAC Algorithm. Remote Sens (Basel). 2014;6:4323–44.
73. de Conto T, Olofsson K, Görgens EB, Rodriguez LCE, Almeida G. Performance of stem denoising and stem modelling algorithms on single tree point clouds from terrestrial laser scanning. Comput Electron Agric. 2017;143:165–76.
74. Trochta J, Krůček M, Vrška T, Král K. 3D forest: an application for descriptions of three-dimensional forest structures using terrestrial LiDAR. PLoS ONE. 2017;12:e0176871.
75. Cabo C, Ordóñez C, López-Sánchez CA, Armesto J. Automatic dendrometry: Tree detection, tree height and diameter estimation using terrestrial laser scanning. Int J Appl Earth Obs Geoinf. 2018;69:164–74.
76. Atkins JW, Bohrer G, Fahey RT, Hardiman BS, Morin TH, Stovall AEL, Zimmerman N, Gough CM. Quantifying vegetation and canopy structural complexity from terrestrial LiDAR data using the forestr r package. Methods Ecol Evol. 2018;9:2057–66.
77. Béland M, Baldocchi DD, Widlowski J-L, Fournier RA, Verstraete MM. On seeing the wood from the leaves and the role of Voxel size in determining leaf area distribution of forests with terrestrial LiDAR. Agric Meteorol. 2014;184:82–97.
78. Béland M, Widlowski J-L, Fournier RA, Côté J-F, Verstraete MM. Estimating leaf area distribution in savanna trees from terrestrial LiDAR measurements. Agric Meteorol. 2011;151:1252–66.
79. Li Y, Guo Q, Su Y, Tao S, Zhao K, Xu G. Retrieving the gap fraction, element clumping index, and leaf area index of individual trees using single-scan data from a terrestrial laser scanner. ISPRS J Photogrammetry Remote Sens. 2017;130:308–16.
80. Raumonen P, Kaasalainen M, Åkerblom M, Kaasalainen S, Kaartinen H, Vastaranta M, Holopainen M, Disney M, Lewis P. Fast Automatic Precision Tree models from Terrestrial laser scanner data. Remote Sens (Basel). 2013;5:491–520.
81. Hackenberg J, Spiecker H, Calders K, Disney M, Raumonen P. SimpleTree —An efficient Open Source Tool to Build Tree models from TLS clouds. Forests. 2015;6:4245–94.
82. Calders K, Newnham G, Burt A, et al. Nondestructive estimates of above-ground biomass using terrestrial laser scanning. Methods Ecol Evol. 2015;6:198–208.
83. Brede B, Calders K, Lau A, Raumonen P, Bartholomeus HM, Herold M, Kooistra L. Non-destructive tree volume estimation through quantitative structure modelling: comparing UAV laser scanning with terrestrial LIDAR. Remote Sens Environ. 2019;233:111355.
84. Bornand A, Rehush N, Morsdorf F, Thürig E, Abegg M. Individual tree volume estimation with terrestrial laser scanning: evaluating reconstructive and allometric approaches. Agric Meteorol. 2023;341:109654.
85. Akerblom M, Raumonen P, Mäkipää R, Kaasalainen M. Automatic tree species recognition with quantitative structure models. Remote Sens Environ. 2017;191:1–12.
86. Terryn L, Calders K, Disney M, Origo N, Malhi Y, Newnham G, Raumonen P, Å, kerblom M, Verbeeck H. (2020) Tree species classification using structural features derived from terrestrial laser scanning. ISPRS Journal of Photogrammetry and Remote Sensing 168:170–181.
87. Hakula A, Ruoppa L, Lehtomäki M, et al. Individual tree segmentation and species classification using high-density close-range multispectral laser scanning data. ISPRS Open J Photogrammetry Remote Sens. 2023;9:100039.
88. Ma L, Zheng G, Eitel JUH, Magney TS, Moskal LM. Determining woody-to-total area ratio using terrestrial laser scanning (TLS). Agric Meteorol. 2016;228–229:217–28.
89. Krishna Moorthy SM, Calders K, Vicari MB, Verbeeck H. Improved supervised Learning-Based Approach for Leaf and Wood classification from LiDAR Point clouds of forests. IEEE Trans Geosci Remote Sens. 2020;58:3057–70.
90. Wang D, Momo Takoudjou S, Casella E. LeWoS: a universal leaf-wood classification method to facilitate the 3D modelling of large tropical trees using terrestrial LiDAR. Methods Ecol Evol. 2020;11:376–89.
91. Wilkes P, Disney M, Armston J, et al. TLS2trees: a scalable tree segmentation pipeline for TLS data. Methods Ecol Evol. 2023;14:3083–99.
92. Wielgosz M, Puliti S, Wilkes P, Astrup R. Point2Tree(P2T)—Framework for Parameter tuning of Semantic and Instance Segmentation used with mobile laser scanning data in Coniferous Forest. Remote Sens (Basel). 2023;15:3737.
93. Xiang B, Peters T, Kontogianni T, Vetterli F, Puliti S, Astrup R, Schindler K. (2023) Towards accurate instance segmentation in large-scale Lidar point clouds. ISPRS annals of the photogrammetry, remote sensing and spatial Information sciences X-1-W1-2023:605–12.
94. Xi Z, Hopkinson C, Rood SB, Peddle DR. See the forest and the trees: effective machine and deep learning algorithms for wood filtering and tree species classification from terrestrial laser scanning. ISPRS J Photogrammetry Remote Sens. 2020;168:1–16.
95. Seidel D, Annighöfer P, Thielman A, Seifert QE, Thauer J-H, Glatthorn J, Ehbrecht M, Kneib T, Ammer C. Predicting Tree species from 3D laser scanning point clouds using deep learning. Front Plant Sci. 2021. https://doi.org/10.3389/fpls.2021.635440.
96. Allen MJ, Grieve SWD, Owen HJF, Lines ER. Tree species classification from complex laser scanning data in Mediterranean forests using deep learning. Methods Ecol Evol. 2023;14:1657–67.
97. Krishna Moorthy SM, Bao Y, Calders K, Schnitzer SA, Verbeeck H. Semi-automatic extraction of liana stems from terrestrial LiDAR point clouds of tropical rainforests. ISPRS J Photogrammetry Remote Sens. 2019;154:114–26.
98. Krisanski S, Taskhiri MS, Gonzalez Aracil S, Herries D, Turner P. Sensor Agnostic Semantic Segmentation of structurally diverse and Complex Forest Point clouds using deep learning. Remote Sens (Basel). 2021;13:1413.
99. Lines ER, Allen M, Cabo C, Calders K, Debus A, Grieve SWD, Miltiadou M, Noach A, Owen HJF, Puliti S. (2022) AI applications in forest monitoring need remote sensing benchmark datasets. ArXiv. https://doi.org/10.48550/arXiv.2212.09937
100. Frank B, Mauro F, Allensworth E. (2024) allometric: Structured Allometric Models for Trees.
101. Puletti N, Castronuovo R, Ferrara C. (2023) crossing3dforest: an R package for evaluating empty space structure in forest ecosystems. bioRxiv. https://doi.org/10.1101/2023.02.01.526548
102. Molina-Valero JA, Martínez-Calvo A, Ginzo Villamayor MJ, Novo Pérez MA, Álvarez-González JG, Montes F, Pérez-Cruzado C. Operationalizing the use of TLS in forest inventories: the R package FORTLS. Environ Model Softw. 2022;150:105337.
103. Antonio Guzmán QJ, Hernandez R, Sanchez-Azofeifa A. (2021) rTLS: Tools to Process Point Clouds Derived from Terrestrial Laser Scanning.
104. Klauberg C, Vogel J, Dalagnol R, Ferreira MP, Hamamura C, Broadbent E, Silva CA. (2023) Post-hurricane damage severity classification at the individual Tree Level using Terrestrial Laser scanning and Deep Learning. Remote Sens (Basel). https://doi.org/10.3390/rs15041165
105. Lecigne B, Delagrange S, Messier C. Exploring trees in three dimensions: VoxR, a novel voxel-based R package dedicated to analysing the complex arrangement of tree crowns. Ann Bot. 2017;121:589–601.

106. Małaszek M, Zembrzuski A, Gajowniczek K. (2022) ForestTaxator: a tool for detection and approximation of cross-sectional area of trees in a cloud of 3D points. Mach Graphics Vis 31.
107. Yrttimaa T. (2021) Automatic Point Cloud Processing Tools to Characterize Trees. https://doi.org/10.5281/zenodo.5779288
108. Disney MI, Boni Vicari M, Burt A, Calders K, Lewis SL, Raumonen P, Wilkes P. Weighing trees with lasers: advances, challenges and opportunities. Interface Focus. 2018;8:20170048.
109. Pfeifer N, Mandlburger G, Otepka J, Karel W. OPALS – a framework for Airborne Laser scanning data analysis. Comput Environ Urban Syst. 2014;45:125–36.
110. Liang X, Litkey P, Hyyppa J, Kaartinen H, Vastaranta M, Holopainen M. Automatic stem mapping using single-scan terrestrial laser scanning. IEEE Trans Geosci Remote Sens. 2011;50:661–70.
111. Computree Core Team. (2024) Computree platform.
112. Lopez Serrano FR, Rubio E, García Morote FA, et al. Artificial intelligence-based software (AID-FOREST) for tree detection: a new framework for fast and accurate forest inventorying using LiDAR point clouds. Int J Appl Earth Obs Geoinf. 2022;113:103014.
113. Knapitsch A, Park J, Zhou Q-Y, Koltun V. Tanks and temples: Benchmarking large-scale scene reconstruction. ACM Trans Graphics (ToG). 2017;36:1–13.
114. Hackel T, Savinov N, Ladicky L, Wegner JD, Schindler K, Pollefeys M. (2017) SEMANTIC3D.NET: a new large-scale point cloud classification benchmark. ISPRS annals of the photogrammetry, remote sensing and spatial Information sciences IV-1-W1:91–8.
115. Matrone F, Lingua A, Pierdicca R, Malinverni ES, Paolanti M, Grilli E, Remondino F, Murtiyoso A, Landes T. (2020) A benchmark for large-scale heritage point cloud semantic segmentation. The International Archives of the Photogrammetry, Remote Sensing and Spatial Information Sciences 43:1419–1426.

Authors and Affiliations

Arnadi Murtiyoso[1] · Carlos Cabo[2] · Arunima Singh[3] · Dimas Pereira Obaya[4] · Wout Cherlet[5] · Jaz Stoddart[6] · Cyprien Raymi Fol[1] · Mirela Beloiu Schwenke[1] · Nataliia Rehush[7] · Krzysztof Stereńczak[8,9] · Kim Calders[5] · Verena Christiane Griess[1] · Martin Mokroš[3,10,11]

✉ Arnadi Murtiyoso
arnadi.murtiyoso@usys.ethz.ch

Carlos Cabo
carloscabo@uniovi.es

Arunima Singh
singha@fld.czu.cz

Dimas Pereira Obaya
dpero@unileon.es

Wout Cherlet
wout.cherlet@ugent.be

Jaz Stoddart
j.stoddart@kew.org

Cyprien Raymi Fol
cyprien.fol@usys.ethz.ch

Mirela Beloiu Schwenke
mirela.beloiu@usys.ethz.ch

Nataliia Rehush
nataliia.rehush@wsl.ch

Krzysztof Stereńczak
k.sterenczak@ibles.waw.pl

Kim Calders
kim.calders@ugent.be

Verena Christiane Griess
verena.griess@usys.ethz.ch

Martin Mokroš
m.mokros@ucl.ac.uk

1 Forest Resources Management, Institute of Terrestrial Ecosystems, Department of Environmental Systems Science, ETH Zurich, Zurich, Switzerland

2 Department of Mining Exploitation and Prospecting, University of Oviedo, Campus de Mieres, Mieres, Spain

3 Faculty of Forestry and Wood Sciences, Czech University of Life Sciences, Prague, Czech Republic

4 Grupo de Investigación en Geomática e Ingeniería Cartográfica (GEOINCA), University of León, León, Spain

5 Q-ForestLab, Department of Environment, Ghent University, Ghent, Belgium

6 Jodrell Laboratory, Royal Botanic Gardens, Kew, UK

7 Swiss National Forest Inventory, Swiss Federal Institute for Forest, Snow and Landscape Research WSL, Birmensdorf, Switzerland

8 Department of Geomatics, Forest Research Institute, Raszyn, Poland

9 IDEAS NCBR Sp. z o.o, Warsaw, Poland

10 Department of Geography, University College London, London, UK

11 Technical University in Zvolen, Zvolen, Slovakia

4.3 **Estimation of occlusion in canopy top points using TLS**

4.3.1 Qualitative Analysis of Tree Canopy Top Points Extraction from Different Terrestrial Laser Scanner Combinations in Forest Plots.

published as: Kushwaha, S. K. P., Singh, A., Jain, K., Vybostok, J., & Mokros, M. (2023). Qualitative Analysis of Tree Canopy Top Points Extraction from Different Terrestrial Laser Scanner Combinations in Forest Plots. ISPRS International Journal of Geo-Information, 12(6), 250.

Extended summary:

The effect of occlusion and quantitative analysis of the tree canopy top points was shown in paper **V**. Eight plots were considered 25 x 25 m, of which four plots were of medium density and the other four with high density, see Table 6. Six TLS scan combinations were made from nine scan positions for each plot, such as Center Scans (CS), Four Corners Scans (FCS), Four Corners with Centre Scans (FCwCS), Four Sides Centre Scans (FSCS), Four Sides Centre with Centre Scans (FSCwCS).

Table 6: Shows the number of trees in each subplot for both the TLS plots.

Plot TLS_Plot1		Plot TLS_Plot2	
Subplots	**Number of Trees**	**Subplots**	**Number of Trees**
TLS_1a	49	TLS_2a	102
TLS_1b	45	TLS_2b	72
TLS_1c	32	TLS_2c	78
TLS_1d	33	TLS_2d	76

After merging point clouds obtained from each TLS scan position, noise filtering was done, as the noise can give false results during canopy top points extraction. Different grid sizes were tested, and canopy top points were extracted at a 10 cm grid size. If the grid size is less than 10cm, the number of points being extracted is quite dense in numbers; similarly, if the grid size is more than 10 cm, the number of points being extracted is very few, which would not have served our purpose of extracting canopy top point at each tree stem position. Canopy top points at each tree stem position were manually extracted from all the TLS combinations from the canopy top layer points. The results show that the most significant combination of scans was FSCwCS with respect to ANS.

The rRMSE obtained for plots TLS_Plot1 and TLS_Plot2 ranged from 0.14 % to 2.48 % and 0.096 % to 1.22 %, respectively.

Conclusion:

An experiment was done to estimate and analyze the presence of occlusion in canopy top points. A methodology was developed to qualitatively analysis the canopy top points extracted from different combinations of TLS scan positions. Overall, six scan combinations were made and compared with all nine scan (ANS) combination. The results showed that the FSCwCS scan combination was most significant to ANS and the canopy top points extracted from the FSCwCS was close to ANS combination. The CS combination had the highest number of points with the relative height deviation greater than 10 m as the coverage of the TLS radially decreased towards the corners and edges of the plots.

International Journal of
Geo-Information

MDPI

Article

Qualitative Analysis of Tree Canopy Top Points Extraction from Different Terrestrial Laser Scanner Combinations in Forest Plots

Sunni Kanta Prasad Kushwaha [1,2,*], Arunima Singh [3], Kamal Jain [1], Jozef Vybostok [2] and Martin Mokros [2,3]

[1] Geomatics Group, Department of Civil Engineering, Indian Institute of Technology, Roorkee 247667, Uttarakhand, India
[2] Faculty of Forestry, Technical University in Zvolen, 96001 Zvolen, Slovakia
[3] Faculty of Forestry and Wood Sciences, Czech University of Life Sciences, 16500 Prague, Czech Republic
* Correspondence: s.k.p.kushwaha92@gmail.com

Abstract: In forestry research, for forest inventories or other applications which require accurate 3D information on the forest structure, a Terrestrial Laser Scanner (TLS) is an efficient tool for vegetation structure estimation. Light Detection and Ranging (LiDAR) can even provide high-resolution information in tree canopies due to its high penetration capability. Depending on the forest plot size, tree density, and structure, multiple TLS scans are acquired to cover the forest plot in all directions to avoid any voids in the dataset that are generated. However, while increasing the number of scans, we often tend to increase the data redundancy as we keep acquiring data for the same region from multiple scan positions. In this research, an extensive qualitative analysis was carried out to examine the capability and efficiency of TLS to generate canopy top points in six different scanning combinations. A total of nine scans were acquired for each forest plot, and from these nine scans, we made six different combinations to evaluate the 3D vegetation structure derived from each scan combination, such as Center Scans (CS), Four Corners Scans (FCS), Four Corners with Center Scans (FCwCS), Four Sides Center Scans (FSCS), Four Sides Center with Center Scans (FSCwCS), and All Nine Scans (ANS). We considered eight forest plots with dimensions of 25 m × 25 m, of which four plots were of medium tree density, and the other four had a high tree density. The forest plots are located in central Slovakia; European beech was the dominant tree species with a mixture of European oak, Silver fir, Norway spruce, and European hornbeam. Altogether, 487 trees were considered for this research. The quantification of tree canopy top points obtained from a TLS point cloud is very crucial as the point cloud is used to derive the Digital Surface Model (DSM) and Canopy Height Model (CHM). We also performed a statistical evaluation by calculating the differences in the canopy top points between ANS and the five other combinations and found that the most significantly different combination was FSCwCS respective to ANS. The Root Mean Squared Error (RMSE) of the deviations in tree canopy top points obtained for plots TLS_Plot1 and TLS_Plot2 ranged from 0.89 m to 14.98 m and 0.61 m to 7.78 m, respectively. The relative Root Mean Squared Error (rRMSE) obtained for plots TLS_Plot1 and TLS_Plot2 ranged from 0.15% to 2.48% and 0.096% to 1.22%, respectively.

Keywords: forest; TLS; scan combinations; top canopy points; vegetation structure

Citation: Kushwaha, S.K.P.; Singh, A.; Jain, K.; Vybostok, J.; Mokros, M. Qualitative Analysis of Tree Canopy Top Points Extraction from Different Terrestrial Laser Scanner Combinations in Forest Plots. *ISPRS Int. J. Geo-Inf.* **2023**, *12*, 250. https://doi.org/10.3390/ijgi12060250

Academic Editor: Wolfgang Kainz

Received: 24 March 2023
Revised: 9 June 2023
Accepted: 15 June 2023
Published: 19 June 2023

1. Introduction

Forest inventories are essential to understanding tree structure dynamics. To understand the productivity of the forest, a biomass assessment is required, which is dependent on the Diameter at Breast Height (DBH) and tree height information. Forest ecosystems play a crucial role in maintaining the natural balance since biogeochemical cycles are also dependable on the healthy vegetation structure. Due to these reasons, accurate and precise assessment of forest biomass has become a critical concern. Quantification of forest biomass by calculating the forest volume is one of the important factors for estimating accurate forest biomass for the maintenance of the global carbon cycle [1]. Therefore, the estimation of individual tree parameters is of utmost importance; the total structural information of the tree also accounts for the canopy. Thus, out of the whole structure of the tree, the accurate assessment of the total canopy cover allows us to understand the physiological behaviors of a tree to the whole forest ecosystem [2].

Canopy cover is a very crucial indicator in forest monitoring and management applications. Canopy cover is not only important for the measurement of trees, but it can also predict wildfire. Ladder fuels can bridge the gap between the surface and canopy of the tree and can be responsible for more severe canopy fires [3]. Treetop points can be referred to as the highest point of a particular tree, whereas canopy top points are the top points obtained throughout the entire canopy region. Imagine it as all the points that would come into contact first if a large blanket was laid from above the forest point cloud. These canopy top points contribute to the generation of the Digital Surface Model (DSM) and Canopy Height Model (CHM). However, in this research, only a few of the canopy top points are considered for evaluation, i.e., canopy top points present at each tree location. Tree canopy point extraction using a Terrestrial Laser Scanner (TLS) has always been difficult because of sparse points and higher noise at the treetop during the scans, which can be due to dense canopies, occlusions, larger tree heights, etc.

When the forest structures are complex with high tree densities, it is quite challenging and time-consuming to acquire accurate tree attributes [4]. There is also a margin of error while calculating tree heights through manual measurements in the field as there are foliage occlusions which makes it difficult to identify the treetop or canopy top points at a particular location. The rapid modelling of vegetation structures with accurate 3D geometrical information has been gaining a lot of demand in recent years, especially when field measurements are very expensive or nearly impossible. This has spurred the development of the latest technologies. The extraction of forestry parameters (such as DBH and tree height) is also possible using a multi-platform Light Detection and Ranging (LiDAR) system [5]. A TLS is a ground-based static LIDAR portable system. TLS has already shown promising results in acquiring forest metrics, including individual tree parameters [6] with millimeter-level details [7]. It is also used for capturing the branch-level information of trees in the forest plots and the local physiological state of the structure [8]. TLS has shown potential in assessing the canopy fuel properties in terms of canopy cover, canopy height, fuel strata gap, etc. [9]. TLS not only provides insights into the tree canopy but also helps to understand the vegetation's structural complexity and its relationship with biodiversity. The 3D information has also been utilized to explore other models and measurements of trees. To this end, the fundamentals of forest ecological theories have also been tested by the Radiative Transfer (RT) model approach, which is used to analyze the radiation mechanism in plants for photosynthesis, responses to stress, and partitioning in energy consumption [10,11]. TLS is used to derive unbiased and nondestructive estimates of the tree structure and volume and can, therefore, be used to address key uncertainties in forest Above Ground Biomass (AGB) estimates [12]. A comparative analysis was also performed using TLS and traditional forest inventory methods, including pixel and pipe methods [13], to evaluate the best and most automated method for tree parameter extraction.

TLS has also been used for tropical forest structure estimation [14]. Since tropical forests are the most complicated structure and comprise a large portion of underexplored forest ecosystems, the relative vegetation profile was generated using a TLS point cloud. It is also essential to assess the type of structural differences between the various types of tropical forests [15]. TLS can also help to understand the correlation and cause of Basal Stem Rot (BSR) and its effects on the oil palm plantation and its canopy architecture [16]. To correctly estimate tree attributes, a 3D Quantitative Structure Model (QSM) is very useful for measuring DBH and tree height and estimating AGB [17,18].

In forests, it is always thought that a greater number of TLS scans are required to obtain more detailed information on the vegetation structure. However, this may not be efficient in all cases. As the number of scans increases, it also increases the redundancy in the dataset, overall data size, and acquisition and processing time of the TLS scans. Therefore, it is very important to evaluate the TLS approach in different forests and with different constraints. A study was also carried out to analyze the influence of scan resolution, scanner parameters, pulse duration, and scan speed on the tree stem diameter and volume extraction using phase-shift FARO Photon 120 TLS data [19]. The influence of TLS visibility in forest plots for tree metrics also has an important contribution. The efficiency and effectiveness of 40 TLS scanning positions were tested, and the results showed that distributing TLS scanning positions evenly within the forest plot produced good results. Setting similar distances between each scanning position and edges of the plots produced an accurate overall visibility of the forest stand [20]. Another study was conducted to test how different scanner positions and plot sizes affect tree detection and diameter measurements for forest inventories data collection, which was tested for circular plots with a radius of 20 m [21].

In our previous research [22], we analyzed the efficiency of all six different scanning combinations for the ground coverage and quality of the Digital Terrain Model (DTM) produced in different forest plots. It was observed that the Four Sides Center with Center Scans (FSCwCS) combination was the most suitable scan combination to generate a DTM similar to that of the All Nine Scans (ANS) combination. This research motivated us to analyze the effect and efficiency of the TLS combinations at canopy surface points in forest plots to determine if the FSCwCS combination is also suitable for canopy top points extraction with respect to the ANS combination.

An extensive qualitative analysis was conducted for eight forest plots, of which four plots had medium tree densities, and the other four had high tree densities. The main objective of this research was to extract the tree canopy points in all six TLS scanning combinations considered and to evaluate their performances in the canopy cover region. Qualitative analysis of the efficiency of the TLS in canopy penetration and generation of vegetation structure was evaluated above each tree stem position in all of the eight plots considered in this research. CHM and DSM are derived from the point cloud dataset, and if there are noise and occlusions in the point cloud dataset, it will affect the quality of the DSM or CHM. Therefore, we have focused on the technical aspect of the raw point cloud dataset itself and evaluated the TLS efficiency in canopy top points in different combinations.

2. Materials and Methods

2.1. Study Area

The forest plots considered for this research are located in central Slovakia within the Kremnica Mountains. Multiple tree species are present in the study area region. The dominant tree species is European beech (*Fagus sylvatica*) with a mixture of European oak (*Quercus robur*), Silver fir (*Abies alba*), Norway spruce (*Picea abies*) and European hornbeam (*Carpinus betulus*). The location information for both study areas (TLS_Plot1 and TLS_Plot2) is depicted in Figure 1.

For the experiment, we established eight research plots spread within two forest stands with two levels of densities; four subplots had a medium tree density (TLS_Plot1), and four subplots had a high tree density (TLS_Plot2) (Figure 1). The number of trees in the medium-density subplots varied from 32 to 49 trees, and in the high-density subplots, from 72 to 102 trees per plot (Table 1). The forest plots were considered with 25 m × 25 m dimensions.

Table 1. Number of trees in each of the four subplots for both research plots TLS_Plot1 and TLS_Plot2.

TLS_Plot1		TLS_Plot2	
Subplots	**Number of Trees**	**Subplots**	**Number of Trees**
TLS_1a	49	TLS_2a	102
TLS_1b	45	TLS_2b	72
TLS_1c	32	TLS_2c	78
TLS_1d	33	TLS_2d	76

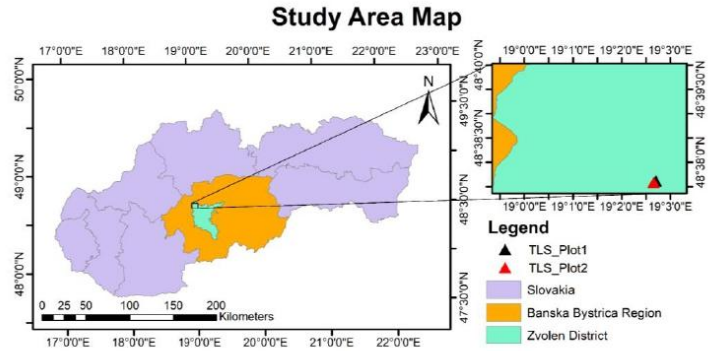

Figure 1. Study area map depicting the location of TLS_Plot1 and TLS_Plot2.

2.2. Data Acquisition and Pre-Processing

The forest plots were established through a geodetic survey using the Global Navigation Satellite System (GNSS) receiver Topocon Hiper SR combined with the total station Topocon 900. A total of nine TLS scans were performed in each of the eight forest plots using the Faro Focus s70 laser scanner (FARO Technologies, Inc., Lake Mary, FL, USA). Eight positions were evenly placed on the border of the plots, and one was placed in the plot's center. We used plastic spheres on reference sticks for co-registering the individual TLS scan point clouds. These spheres were evenly spread around and inside the plots to ensure that at least four of them would be seen from each TLS scan position. We used a TLS resolution (point spacing) of 6.14 mm/10 m. Each scan took 2 min and 24 s (2 kpt/s).

All the raw TLS scans were imported into Faroscene software for pre-processing. Reflectors (plastic spheres) were detected automatically, and false reflectors were manually deleted. These detected reflectors from each scan position were used to merge the point clouds obtained from each scan position. Six checkerboards were placed at the center of the plot so that the checkerboards were visible from the center TLS scan position. These checkerboards were automatically detected and used for georeferencing the point clouds.

From all the scan positions, a total of six possible combinations were considered for the data analysis, which is briefly presented in the following section.

2.2.1. CS Combination

In this combination, only one scan position was considered, which was positioned at the center of the forest plot. As the scan was in the center, the TLS could collect the data in one complete sphere of influence. The sphere of influence is the imaginary region in which the TLS is capable of generating a point cloud (Figure 2).

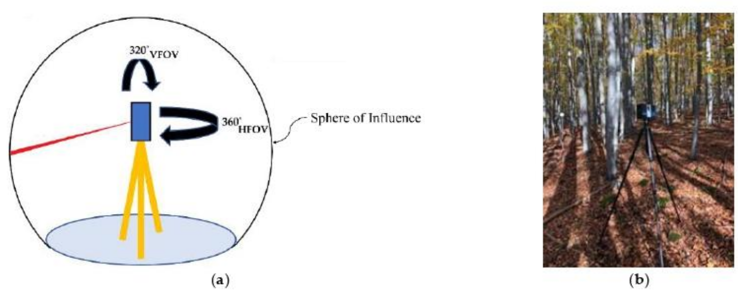

Figure 2. (**a**) Diagram of a TLS with its 360° Horizontal Field of View (HFOV) and 320° Vertical Field of View (VFOV), and the region of data generation is its sphere of influence. (**b**) Image of the TLS instrument in one of the forest plots.

2.2.2. FCS Combination

In this combination, four scan positions were considered, which were positioned at the four corners of the forest plot. The TLS scans were placed at the corners so that the scans could cover only 90° HFOV of the plot from each corner position, generating a point cloud in a quarter sphere of influence. Thus, all four scans at the corners could only contribute to one sphere of influence for the dataset when combined together.

2.2.3. FCwCS Combination

In this combination, five scan positions were considered. Four scans were placed at the four corners and one at the center of the forest plot. As the scans were placed at the corner and center, they could cumulatively contribute to two spheres of influence for the dataset. Four corners scans contribute to one sphere of influence, and the center scan contributes to one sphere of influence.

2.2.4. FSCS Combination

In this combination, four scan positions were considered. Which were placed at the center of all four sides. As each scan could cover only a 180° HFOV of the plot, they contributed to a half sphere of influence for the dataset. Therefore, a total of two spheres of influence for the dataset could be created in this combination.

2.2.5. FSCwCS Combination

In this combination, five scan positions were considered. Four scans from the center of each side and one at the center of the forest plot. Each side center scan contribute half of a sphere of influence, and the center scan contributes one complete sphere of influence. Therefore, a total of three spheres of influence for the dataset could be created with this combination.

2.2.6. ANS Combination

In this combination, nine scan positions were considered. Four scans were placed at the four corners, four other scans at the four side centers, and one at the center of the forest plot. The corner scans contribute to a quarter sphere of influence, the side center scans contribute half a sphere of influence, and the center scan contributes a complete sphere of influence. A total of four spheres of influence for the dataset could be created with this combination.

The theoretical representation of the patterns and positions of the TLS combinations followed for the data acquisition and processing are depicted in Figure 3; However, these behaved differently because of the standing trees in the forest plots. Hypothetically speaking, based on the theoretical maps from Figure 3, the combination FSCwCS should produce the most similar canopy top points to those of the ANS combination even with 4 fewer scan positions, as was observed for terrain points [22]. Further evaluation is needed to support or reject this hypothesis.

As the ANS scan combination had the highest number of scans and sphere of influence, the ANS scan combination was used as the reference dataset, which the other scan combination dataset was evaluated against. For visualization, the ANS scan combination point cloud datasets obtained for plots TLS_1a and TLS_2a are shown in Figure 4a,b, respectively.

2.3. Research Methodology

Six different TLS scan combination datasets were generated for each forest plot. Then, the canopy top points were extracted in each TLS scan combination, and a few canopy top points at the local grid of each tree stem position were clipped using the clipping tool in Cloudcompare [23]. Here, a local grid represents an imaginary region bounding the tree stem above which the canopy top points were extracted (Figure 6).

Multiple top points were extracted within the local grid for each combination. The highest point among these multiple points was considered the canopy top point for that particular combination at that local grid of that particular tree stem. These points were used for further analysis. Using the canopy top points extracted in the ANS scan combination as a reference, relative height differences with the canopy top points extracted in the other five scan combinations were calculated. The spatial analysis of relative height deviation was performed, and the results are shown in Figures 9 and 11. The research methodology followed throughout this research is represented as a workflow in Figure 5.

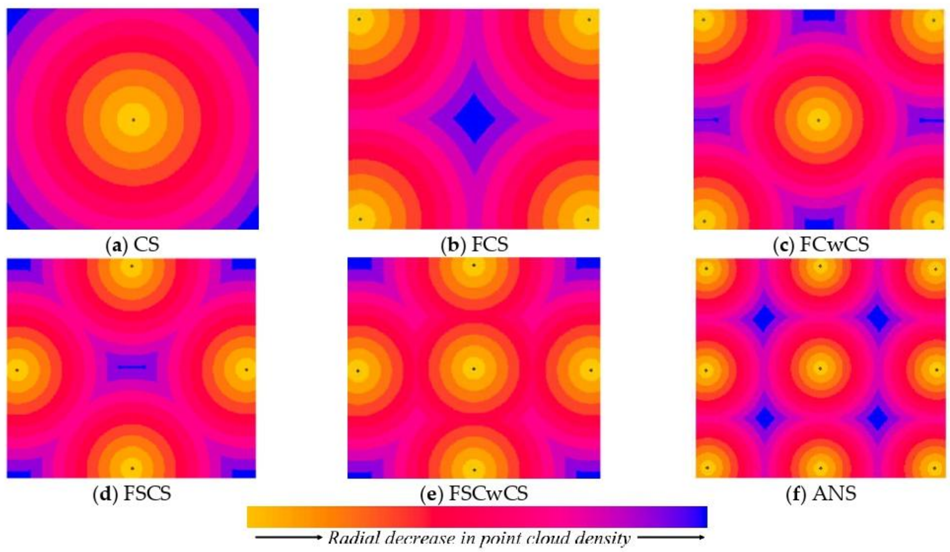

Figure 3. Theoretical representation of TLS scan positions and their spheres of influence in all six scan combination patterns. (**a**) Center Scans (CS), (**b**) Four Corners Scans (FCS), (**c**) Four Corners with Center Scans (FCwCS), (**d**) Four Sides Center Scans (FSCS), (**e**) Four Sides Center with Center Scans (FSCwCS), and (**f**) All Nine Scans (ANS)—The ANS combination was used as a reference.

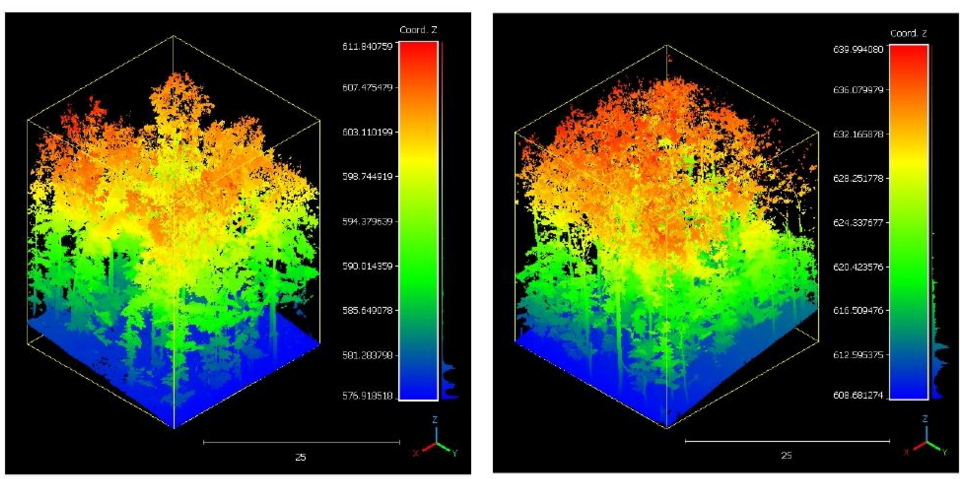

(**a**) (**b**)

Figure 4. ANS scan combination point cloud datasets for plots (**a**) TLS_1a and (**b**) TLS_2a.

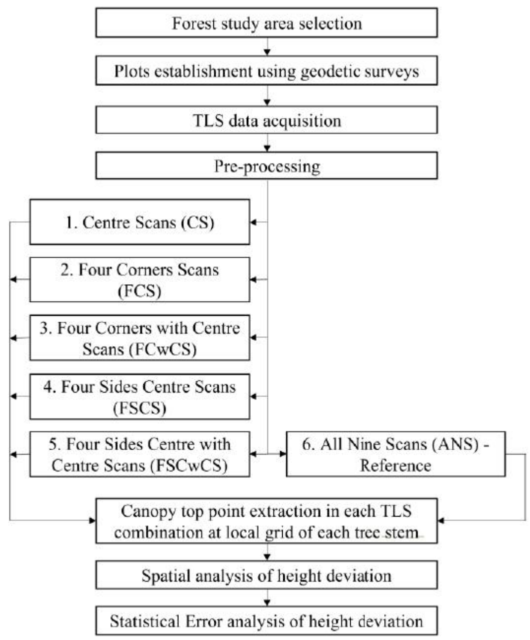

Figure 5. Research methodology.

2.3.1. Canopy Top Points Extraction at Each Stem Local Grid Positions

The canopy top points were extracted in all the scan combinations for all eight forest plots in Dendrocloud [24]. The extract surface tool in the Dendrocloud software Version 1.53 was used to extract all the canopy surface points from the point cloud datasets with a grid size of 10 cm. The tool basically extracts the highest points within a cuboid region on the grid size mentioned as the canopy top point. The overall point cloud datasets are represented in the larger cuboid, and the canopy points extracted in a local cuboid region are shown in a smaller cuboid (base shown in blue) in Figure 6.

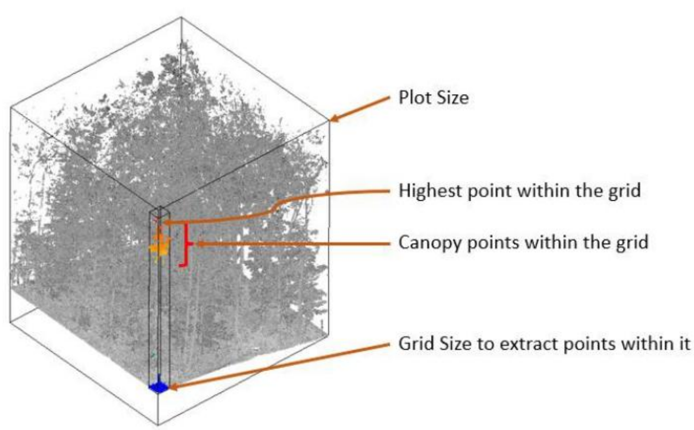

Figure 6. Diagram showing the grid size with respect to to the plot size in which the highest points were extracted to identify canopy top points in each TLS scan combination.

The canopy top points extracted from all the TLS scan combinations are shown for TLS_1a and TLS_2a in Figure 7a,b, respectively.

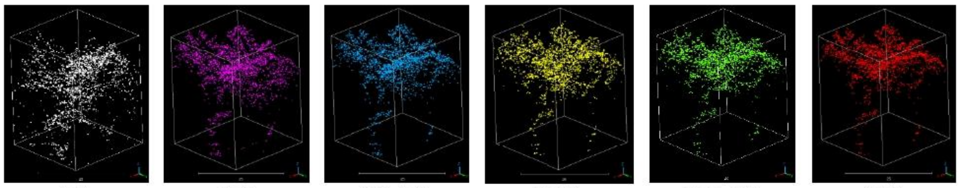

CS FCS FCwCS FSCS FSCwCS ANS

(**a**) TLS_1a

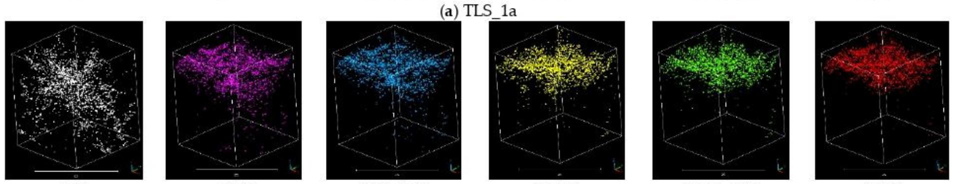

CS FCS FCwCS FSCS FSCwCS ANS

(**b**) TLS_2a

Figure 7. Canopy top points obtained in each TLS scan combination for forest plots (**a**) TLS_1a, (**b**) TLS_2a.

All the canopy top points obtained from all six combinations were opened together along with tree stems, and the point clouds were manually clipped to obtain the highest canopy point at that tree stem position. Then, the highest point in each canopy top point cloud at that tree stem position was used to represent the canopy top point at that tree stem position from all six TLS combinations (Figure 8). The canopy top points extracted at each stem grid position were used for spatial analysis of the variations in the heights between all the TLS scan combinations.

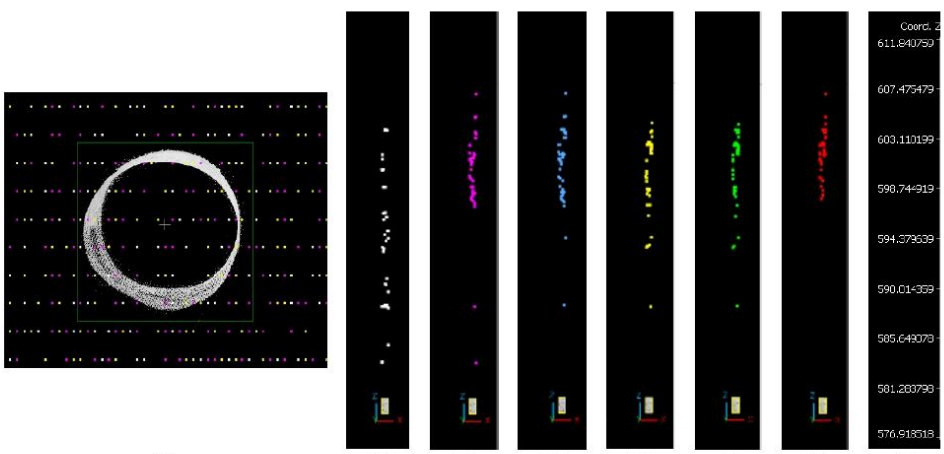

(**a**) (**b**) (**c**) (**d**) (**e**) (**f**) (**g**) (**h**)

Figure 8. (**a**) Image representing canopy top points from all six combinations and a tree stem within a local grid (shown as a green bounding box) in which the canopy top points were extracted corresponding to the tree stem (top view). Canopy top points extracted above the tree stem for (**b**) CS shown in white, (**c**) FCS shown in pink, (**d**) FCwCS shown in blue, (**e**) FSCS shown in yellow, (**f**) FSCwCS shown in green, (**g**) ANS shown in red (front view), and (**h**) scale bar for points shown in (**b**–**g**).

2.3.2. Data Evaluation

The point cloud data collected using TLS were divided into 6 TLS scan combinations for the plots in TLS_Plot1 and TLS_Plot2. Afterward, the relative elevation deviation between the canopy top points was calculated for each combination in the plots with respect to the ANS combination. Using all the combinations, we calculated the errors to evaluate the data.

The Root Mean Squared Error (RMSE), Mean Absolute Error (MAE), and relative Root Mean Squared Error (rRMSE) were calculated to compare the results obtained from the different combinations in the plots as shown in Equations (1)–(3), respectively.

$$\mathrm{RMSE} = \sqrt{\frac{1}{N}\sum_{i=1}^{N}\left(Y_i - \hat{Y}\right)^2} \quad (1)$$

$$\mathrm{MAE} = \frac{1}{N}\sum_{i=1}^{N}\left|Y_i - \hat{Y}\right| \quad (2)$$

$$\mathrm{rRMSE} = \frac{\sqrt{\frac{1}{N}\sum_{i=1}^{N}\left(Y_i - \hat{Y}\right)^2}}{\frac{1}{N}\sum_{i=1}^{N} Y_i} \times 100 \quad (3)$$

where,

Y_i is the actual observation (m),
$\hat{Y}$ is the estimated observation (m), and
N is the total number of observations.

To measure the statistical significance of all the combinations in terms of relative elevation deviation between the canopy top points and plot combinations, a two-way Analysis of Variance (ANOVA) was used. To identify the statistical significance of the difference between combinations, plots, and the relative elevation deviation between the canopy top points, Tukey post hoc tests were performed. The statistical analysis was conducted in R software.

3. Results

Spatial analysis and canopy top height differences for forest plot TLS_1a are presented in Section 3.1, forest plot TLS_2a is presented in Section 3.2, and forest plots TLS_1b, 1c 1d, 2b, 2c, and 2d are presented in Appendix A section.

3.1. Spatial Analysis for Forest Plot TLS_1a

After the canopy top points extraction at each stem grid position in the forest plots for all the scan combinations, further analysis was conducted to observe the elevation deviation between the canopy top points in all the scan combinations with respect to the ANS scan combination at each tree stem position. The elevation deviations were spatially plotted to see the observations with reference to the spatial distribution along the plot. The plotting was based on the relative height deviation in meters; from 0 m to 1 m, 1 m to 2 m, 2 m to 5 m, 5 m to 10 m, and greater than 10 m are shown in dark green, light green, blue, light pink, and red colors, respectively. The maximum number of canopy points with an elevation difference of less than 1 m was generated with the FSCwCS combination, whereas the maximum canopy height difference of more than 10 m was observed in the CS combination. The spatial height deviations for plot TLS_1a are shown in Figure 9.

Canopy Top Height Differences for Forest Plot TLS_1a

The deviations in the relative spatial height difference between canopy top points in CS, FCS, FCwCS, FSCS, and FSCwCS with respect to the ANS scan combination for each tree in TLS_1a is shown as a graph in Figure 10.

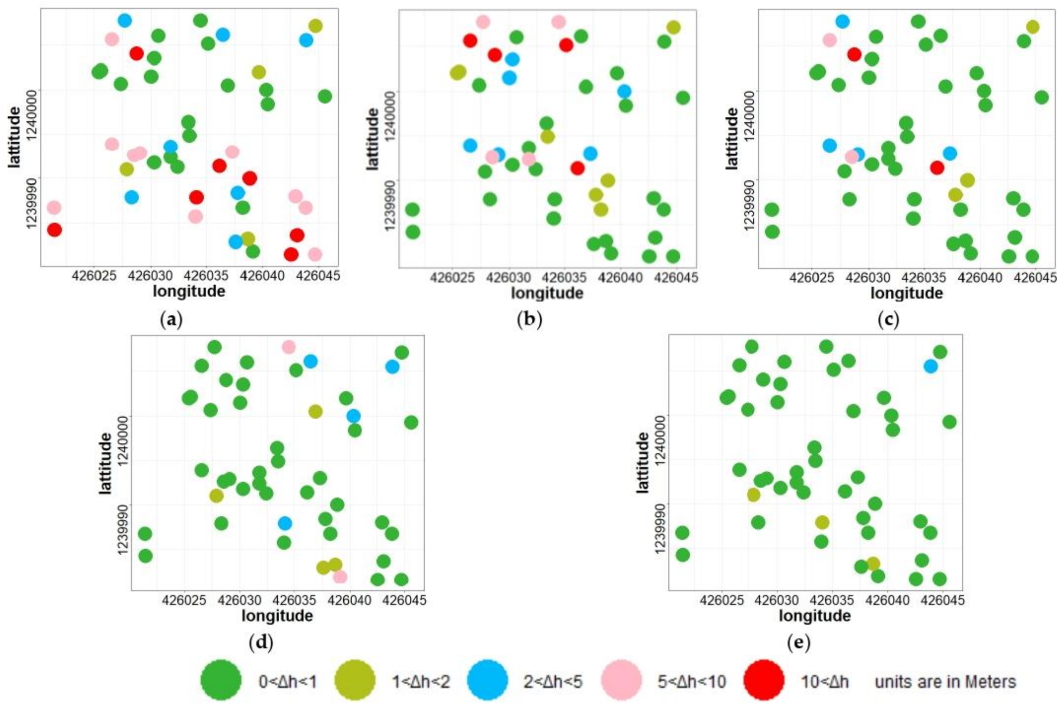

Figure 9. The spatial height differences between canopy top points obtained at each tree stem position in each of the TLS scan combinations for forest plot TLS_1a with respect to ANS scan combination. (**a**) Δh CS and ANS, (**b**) Δh FCS and ANS, (**c**) Δh FCwCS and ANS, (**d**) Δh FSCS and ANS, and (**e**) Δh FSCwCS and ANS.

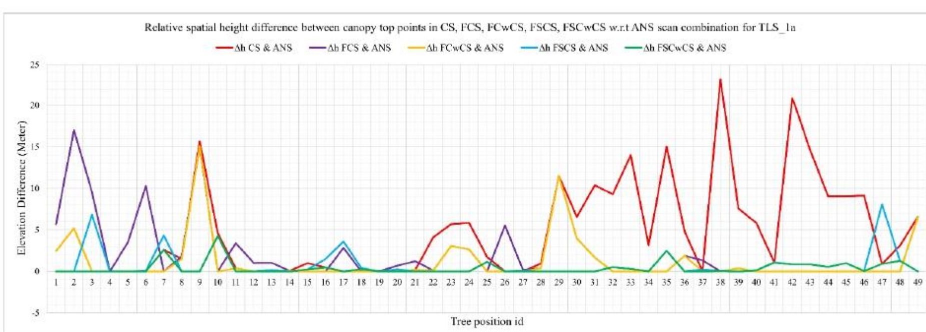

Figure 10. Graph showing relative spatial height differences between canopy top points in CS, FCS, FCwCS, FSCS, and FSCwCS with respect to ANS scan combination for each tree in TLS_1a.

3.2. Spatial Analysis for Forest Plot TLS_2a

The spatial height difference between canopy top points obtained from each of the TLS scan combinations for forest plot TLS_2a with respect to the ANS scan combination at each tree stems position is shown in Figure 11. The maximum number of canopy points with an elevation difference of less than 1 m was generated with the FSCwCS combination, whereas the maximum number of canopy points with an elevation difference of more than 10 m was observed in the CS combination.

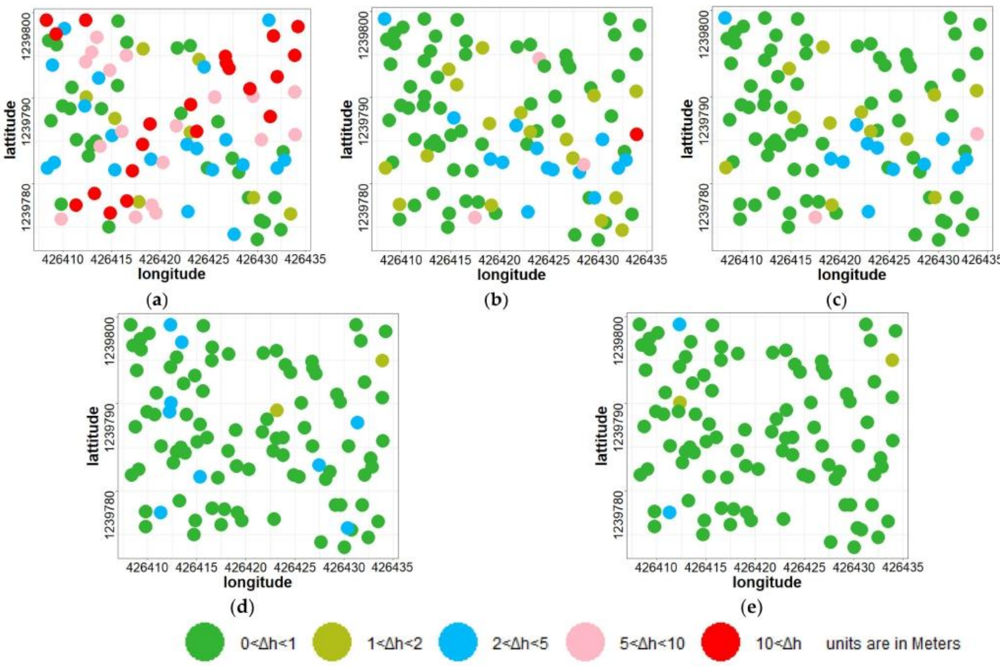

Figure 11. The spatial height differences between canopy top points obtained at each tree stem position from each of the TLS scan combinations for forest plot TLS_2a with respect to ANS scan combination. (**a**) Δh CS and ANS, (**b**) Δh FCS and ANS, (**c**) Δh FCwCS and ANS, (**d**) Δh FSCS and ANS, and (**e**) Δh FSCwCS and ANS.

Spatial Canopy Top Height Differences for Forest Plot TLS_2a

The relative spatial height difference between canopy top points in CS, FCS, FCwCS, FSCS, and FSCwCS with respect to the ANS scan combination for each tree in TLS_2a is shown as a graph in Figure 12.

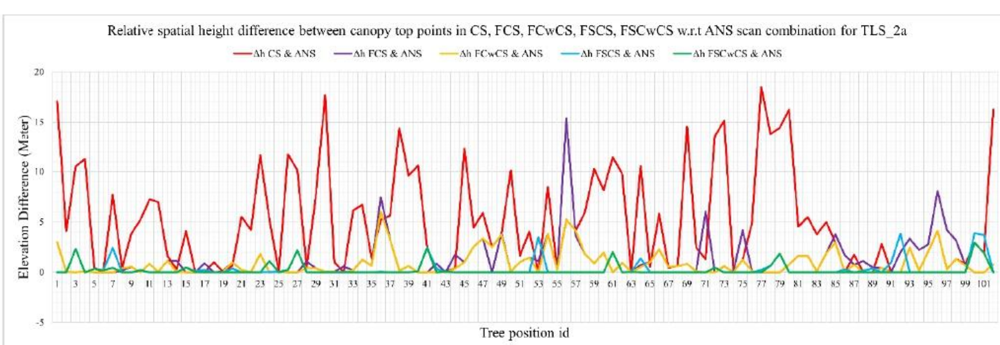

Figure 12. Graph showing relative spatial height differences between canopy top points in CS, FCS, FCwCS, FSCS, and FSCwCS with respect to ANS scan combination for TLS_2a.

3.3. Qualitative Statistical Analysis for the Relative Canopy Heights

The relative elevation deviation between the canopy top points was calculated for each combination in the plots with respect to the ANS results in all the plots. Using the observation and analysis results obtained in the previous sections, the rRMSE was calculated. Statistical analysis was performed on the results obtained from the values computed from rRMSE. The rRMSE value obtained for TLS_Plot1 ranged from 0.15% to 2.48%. Overall, the combination of Z.FSCwCS and Z.ANS in TLS_1a showed the best results for the elevation deviation of the canopy points of trees in the respective plot.

The statistical error observed for TLS_Plot2 was analyzed. The scan combinations that came with the lowest error in the elevation difference of canopy points are Z.FSCwCS and Z.ANS for all the plots. The rRMSE values ranged between 0.096% and 1.22%. Overall, the TLS_2c plot with the combination of FSCwCS and ANS had the lowest error in the elevation differences of canopy points in all the trees among all the plots.

The rRMSE values obtained from all the relative canopy heights at each tree stem position from CS, FCS, FCwCS, FSCS, and FSCwCS with respect to the ANS scan combination for TLS_Plot1 and TLS_Plot2 are shown in Figure 13a,b.

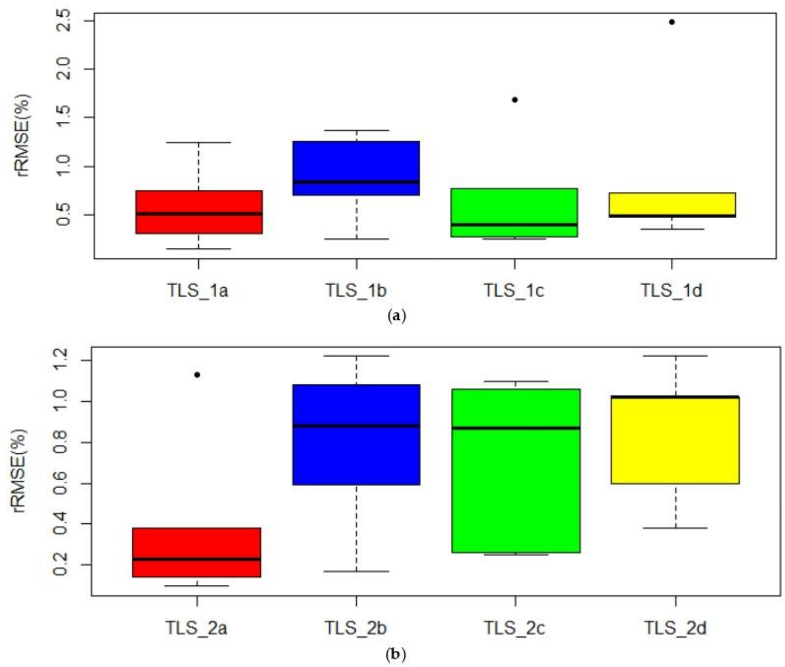

Figure 13. Graph plots showing rRMSE for (**a**) TLS_Plot1 and (**b**) TLS_Plot2.

Two-way ANOVA was performed considering different scan position combinations as one group and plots as another group to analyze the significant difference and impact on the relative elevation deviation of all combinations between the canopy top points among all the plots. It was performed to see whether there was any significant difference between the groups and within the group.

Hence, the relative elevation deviation of all combinations between the canopy top points among all the plots was significant at all tree stem positions. The scan combinations and their interactions with the plots were significantly impacting the relative elevation deviation of canopy top points. The ANOVA is shown in Table A1. Later, we performed a Tukey post hoc test to support ANOVA because we found a significant difference between the two groups (combinations and plots). So, due to the significant difference between these groups, the change in combinations of scan positions in the plot significantly affected the difference in the elevation of canopy points. Moreover, plots and combinations were significantly different from each other. When only combinations were compared, the Z.FCwCS-Z.ANS, Z.FSCwCS-Z.ANS, Z.FSCS-Z.FCS, and Z.FSCwCS-Z.FCwCS were not significant. When the Canopy Top Points Layer (CTPL) obtained from all plots was compared, CTPL_1c-CTPL_1b, CTP L_1d-CTPL_1c, and CTPL_2c-CTPL_2b were insignificant. To compare interactions, 1125 pairs were generated, out of which 732 pairs were significantly different from each other. The differences are depicted in Tables A2 and A3.

4. Discussions

4.1. Noise Removal above the Canopy Regions

After merging the point clouds obtained from each TLS scan position, noise filtering is an important step, as noise can produce false results during canopy top points extraction. We have manually removed the noise as best as possible in this research using prior experience in point cloud data processing. However, we would like to present the situation of the points obtained at the canopy and above the canopy layer. Some points are too far from the canopy, which can easily be segmented out as noise, which is shown as sure noise points within red boundaries in Figure 14. Some points were close to the canopy and very sparsely dispersed. In this case, it is quite challenging to determine whether they are noise; they are shown as unsure noise points within violet boundaries in Figure 14. Since we are evaluating the canopy top points, it was critically important to segment out noise precisely. This was performed by observing the point cloud in different views and at small chunk levels to determine if a point is a noise.

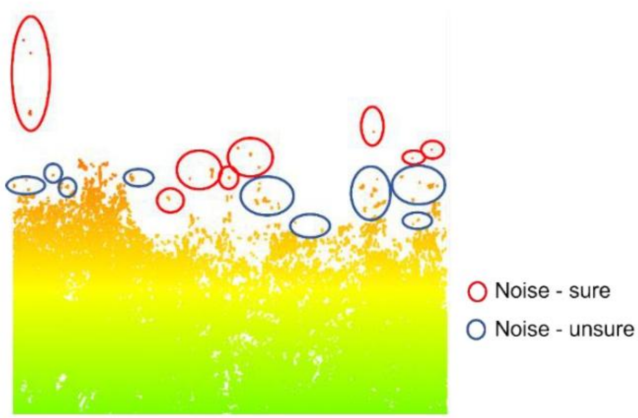

Figure 14. Shows a close-up front view of the forest point cloud at the canopy level, which shows sure noise points in red boundaries and unsure noise points in violet boundaries.

4.2. Selection of Grid Size for Canopy Top Points Extraction in Dendrocloud

The canopy top points can be extracted at different grid sizes in Dendrocloud software. We have tried different grid sizes, and we came to a conclusion to extract the canopy top points using a 10cm grid size. If the grid size was more than 10 cm, the number of points being extracted was quite dense; similarly, if the grid size was less than 10 cm, the number of points being extracted was too low, which would not have served our purpose of extracting canopy top point at each tree stem position.

4.3. Highest Point Extraction at Each Tree Stem Position

The canopy top points at each tree stem position were manually extracted from all the TLS combinations from the canopy top layer points obtained from the process mentioned in Section 4.2. As the axis of the trees was not perpendicular for all the trees, there were some trees whose trunks were in between two plots which was a critical situation to consider; for example, there were some trees whose trunks were in one plot and the top in a different plot and there were also fallen trees whose branches were perpendicular which were falsely identified as individual trees, etc. With all these constraints under consideration, analyzing all eight plots and with six combinations was quite time-consuming. However, the accuracy of these extracted points was critical for the relative spatial analysis of the canopy top points at each tree stem position.

4.4. Effect of Number of Scans and Position of Scans on the Point Cloud Generation

In research carried out by Trochta J. et al., they found that the number of trees detected in a forest plot depended on the number of scanners and the close proximity of the trees to the scanner position. They tested tree detection in four scenarios with one scan, two scans, three scans, and four scans in different forest sites with different terrain undulations [25].Wan. P et al. conducted similar research to evaluate the efficiency of tree detection using TLS. However, they only used single scans in forests with three levels of densities and concluded that a single scan is only reliable for small forest plots that are less than 10 m in size [26].

In our research, we observed that the CS combination had the highest number of points with a relative height deviation greater than 10 m as the coverage of the TLS radially decreased towards the corners and edges of the plots. The combination of FSCwCS produced the least difference in canopy top points compared to the ANS combination, which we had predicted based on our previous work.

5. Conclusions

In this paper, we presented the statistical evaluation of the generation of point clouds at the top of the tree canopies in eight forest plots with varying tree densities using different TLS scan combinations. Different TLS scan positions have a varying penetration depth of the LiDAR beam through the dense canopy regions due to tree occlusions and various other factors. This aspect was evaluated with respect to the ANS scan combination, which was considered a reference scan combination for this research. The results in Sections 3.1–3.3 and Appendix A show that the Four Sides Center with Center Scans (FSCwCS) combination is quite efficient in producing canopy top points above the tree stem positions, similar to the ANS scan combination, which consists of nine TLS scanning positions. The deviation of the canopy top points was the lowest in the FSCwCS combination. Hence, the authors recommend that if the forest plots are around 25 m $\times$ 25 m in size, the FSCwCS combination can be considered for the optimum generation of canopy top surface points without increasing the time, number of scans, or size of the data.

In the future, we would like to test the quality of the DSM or CHM produced using different TLS scan combinations, as this research was based on point cloud-based analysis at the top points of the canopy at the location of each tree. It would be interesting to see the variation in the DSM or CHM surface at each pixel, including canopy top points, points above branches, and surface points in non-canopy regions.

Author Contributions: Conceptualization, Sunni Kanta Prasad Kushwaha and Arunima Singh; Methodology, Sunni Kanta Prasad Kushwaha and Arunima Singh; Software, Sunni Kanta Prasad Kushwaha; Validation, Sunni Kanta Prasad Kushwaha and Arunima Singh.; Formal analysis, Sunni Kanta Prasad Kushwaha; Investigation, Sunni Kanta Prasad Kushwaha and Martin Mokros; Resources, Martin Mokros and Kamal Jain; Data curation, Sunni Kanta Prasad Kushwaha and Martin Mokros; Writing—original draft preparation, Sunni Kanta Prasad Kushwaha, Arunima Singh and Martin Mokros; Writing—review and editing, Sunni Kanta Prasad Kushwaha, Arunima Singh, Jozef Vybostok and Martin Mokros; Visualization, Sunni Kanta Prasad Kushwaha; Supervision, Martin

Mokros and Kamal Jain; Project administration, Martin Mokros; Funding acquisition, Jozef Vybostok and Martin Mokros. All authors have read and agreed to the published version of the manuscript.

Funding: This work was supported by grant No. CZ.02.1.01/0.0/0.0/16_019/0000803 ("Advanced research supporting the forestry and wood-processing sector's adaptation to global change and the 4th industrial revolution") financed by OP RDE, by the Scientific Grant Agency of the Ministry of Education, Science, Research, and Sport of the Slovak Republic and the Slovak Academy of Sciences [grant number VEGA 1/0335/20] and by the Slovak Research and Development Agency through Grant Nos. APVV-18-0305 and APVV-20-0391. The APC was funded by grant number VEGA 1/0335/20.

Data Availability Statement: Not applicable.

Acknowledgments: The authors would like to thank the anonymous reviewers for their thoughtful comments and suggestions on the original manuscript.

Conflicts of Interest: The authors declare no conflict of interest.

Appendix A.

Appendix A.1. Statistical Errors Obtained for Plots TLS_Plot1 and TLS_Plot2

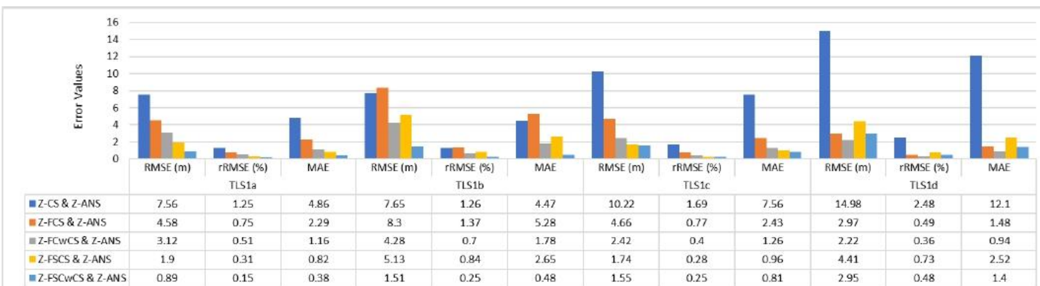

	TLS1a			TLS1b			TLS1c			TLS1d		
	RMSE (m)	rRMSE (%)	MAE	RMSE (m)	rRMSE (%)	MAE	RMSE (m)	rRMSE (%)	MAE	RMSE (m)	rRMSE (%)	MAE
Z-CS & Z-ANS	7.56	1.25	4.86	7.65	1.26	4.47	10.22	1.69	7.56	14.98	2.48	12.1
Z-FCS & Z-ANS	4.58	0.75	2.29	8.3	1.37	5.28	4.66	0.77	2.43	2.97	0.49	1.48
Z-FCwCS & Z-ANS	3.12	0.51	1.16	4.28	0.7	1.78	2.42	0.4	1.26	2.22	0.36	0.94
Z-FSCS & Z-ANS	1.9	0.31	0.82	5.13	0.84	2.65	1.74	0.28	0.96	4.41	0.73	2.52
Z-FSCwCS & Z-ANS	0.89	0.15	0.38	1.51	0.25	0.48	1.55	0.25	0.81	2.95	0.48	1.4

(**a**)

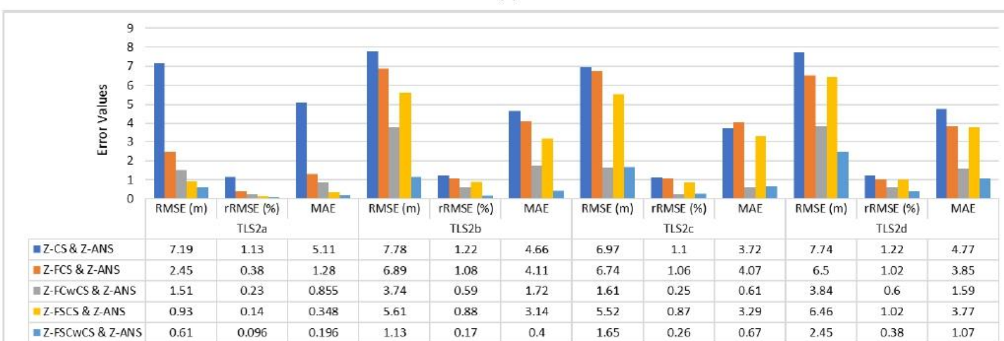

	TLS2a			TLS2b			TLS2c			TLS2d		
	RMSE (m)	rRMSE (%)	MAE	RMSE (m)	rRMSE (%)	MAE	RMSE (m)	rRMSE (%)	MAE	RMSE (m)	rRMSE (%)	MAE
Z-CS & Z-ANS	7.19	1.13	5.11	7.78	1.22	4.66	6.97	1.1	3.72	7.74	1.22	4.77
Z-FCS & Z-ANS	2.45	0.38	1.28	6.89	1.08	4.11	6.74	1.06	4.07	6.5	1.02	3.85
Z-FCwCS & Z-ANS	1.51	0.23	0.855	3.74	0.59	1.72	1.61	0.25	0.61	3.84	0.6	1.59
Z-FSCS & Z-ANS	0.93	0.14	0.348	5.61	0.88	3.14	5.52	0.87	3.29	6.46	1.02	3.77
Z-FSCwCS & Z-ANS	0.61	0.096	0.196	1.13	0.17	0.4	1.65	0.26	0.67	2.45	0.38	1.07

(**b**)

Figure A1. Graphs plots showing RMSE, MAE, and MSE for (**a**) TLS_Plot1, (**b**) TLS_Plot2.

Appendix A.2. Spatial Analysis for Forest Plot TLS_1b

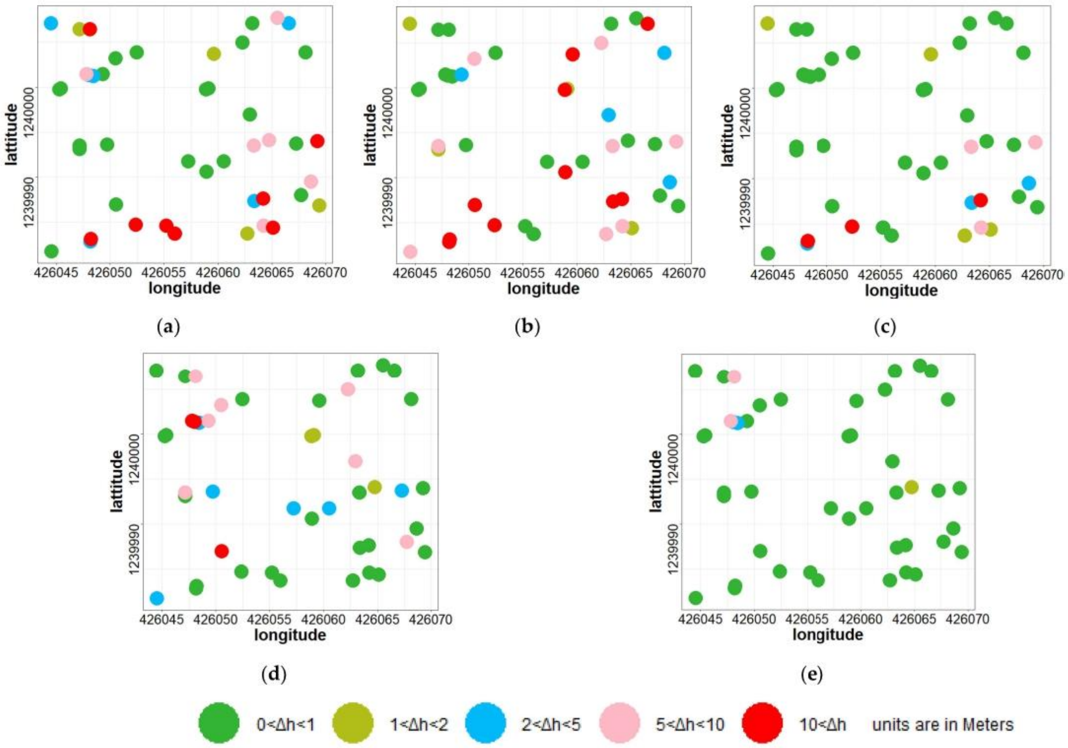

Figure A2. The spatial height differences between canopy top points obtained at each tree stem position in each of the TLS scan combinations for forest plot TLS_1b with respect to ANS scan combination. (**a**) Δh CS and ANS; (**b**) Δh FCS and ANS; (**c**) Δh FCwCS and ANS; (**d**) Δh FSCS and ANS; (**e**) Δh FSCwCS and ANS.

Spatial Canopy Top Height Differences for Forest Plot TLS_1b

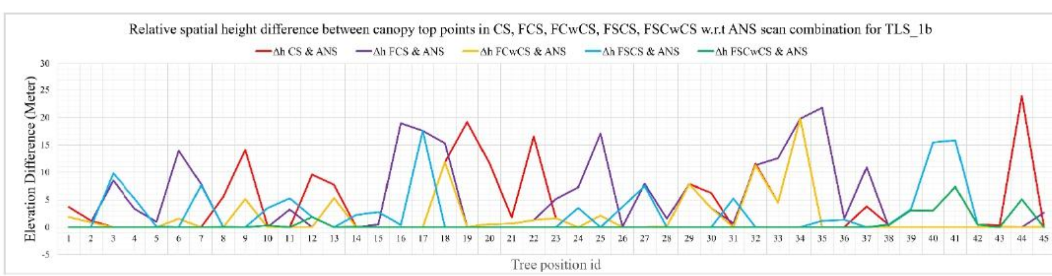

Figure A3. Graph showing relative spatial height differences between canopy top points in CS, FCS, FCwCS, FSCS, and FSCwCS with respect to ANS scan combination for TLS_1b.

Appendix A.3. Spatial Analysis for Forest Plot TLS_1c

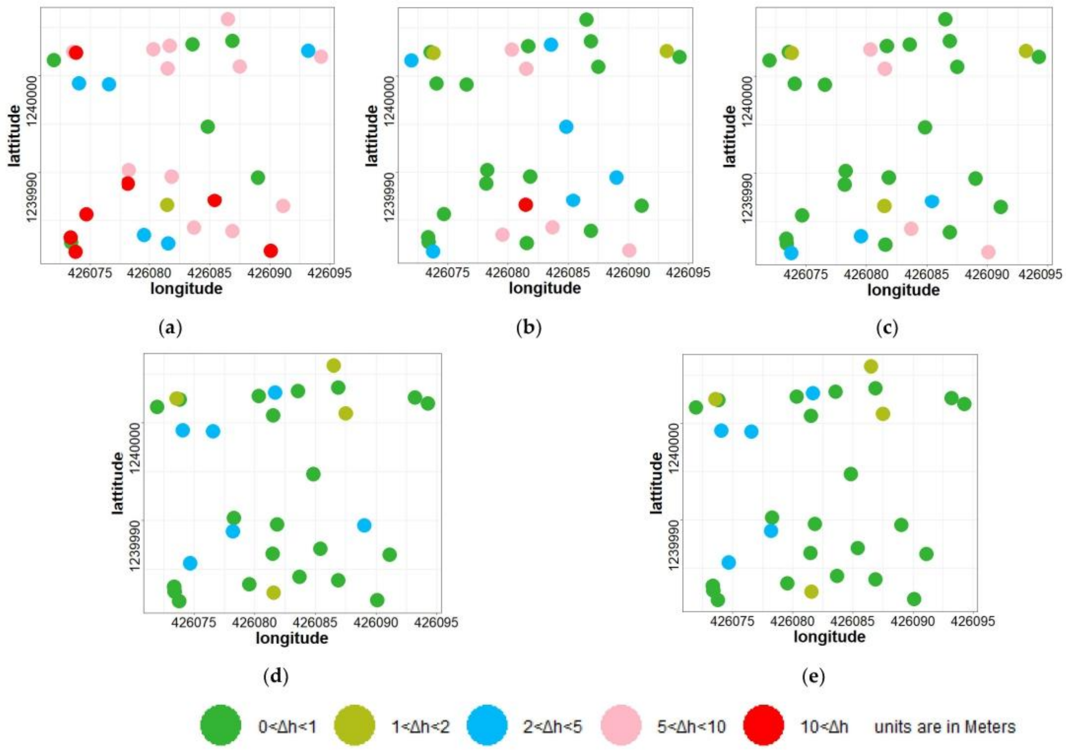

Figure A4. The spatial height differences between canopy top points obtained at each tree stem position in each of the TLS scan combinations for forest plot TLS_1c with respect to ANS scan combination. (**a**) Δh CS and ANS, (**b**) Δh FCS and ANS, (**c**) Δh FCwCS and ANS, (**d**) Δh FSCS and ANS, and (**e**) Δh FSCwCS and ANS.

Spatial Canopy Top Height Differences for Forest Plot TLS_1c

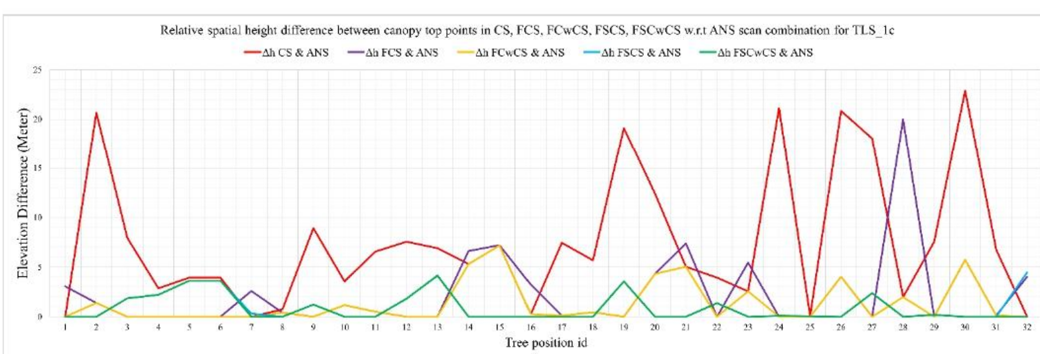

Figure A5. Graph showing relative spatial height differences between canopy top points in CS, FCS, FCwCS, FSCS, and FSCwCS with respect to ANS scan combination for TLS_1c.

Appendix A.4. Spatial Analysis for Forest Plot TLS_1d

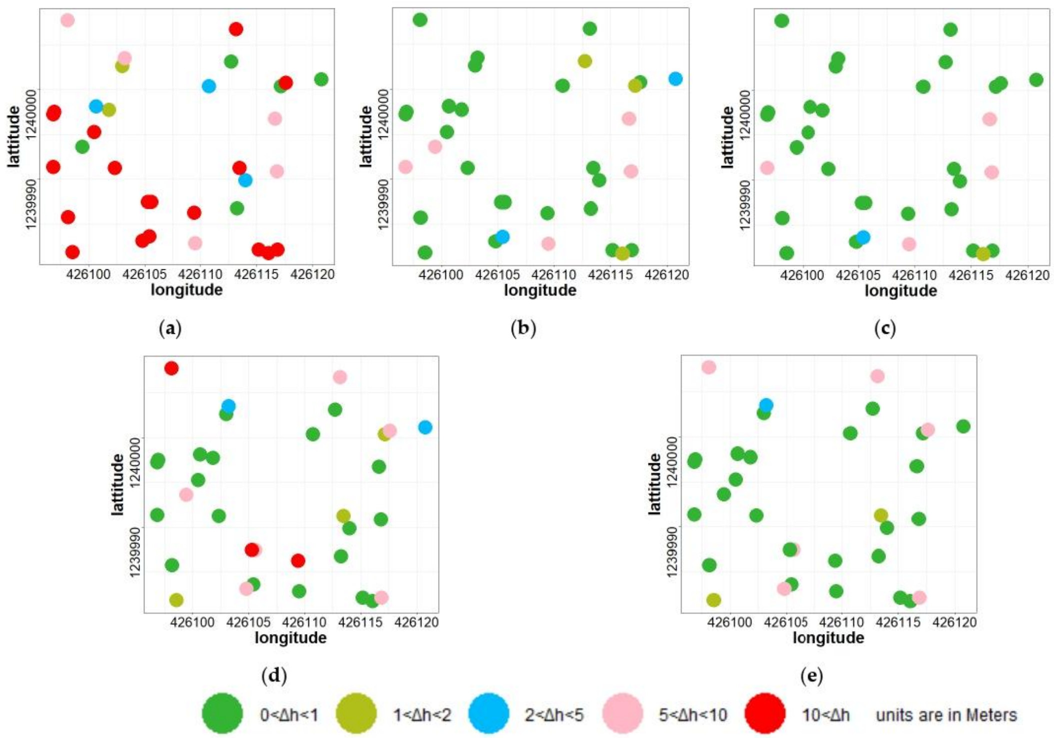

Figure A6. The spatial height differences between canopy top points obtained at each tree stem position in each of the TLS scan combinations for forest plot TLS_1d with respect to ANS scan combination. (**a**) Δh CS and ANS, (**b**) Δh FCS and ANS, (**c**) Δh FCwCS and ANS, (**d**) Δh FSCS and ANS, and (**e**) Δh FSCwCS and ANS.

Spatial Canopy Top Height Differences for Forest Plot TLS_1d

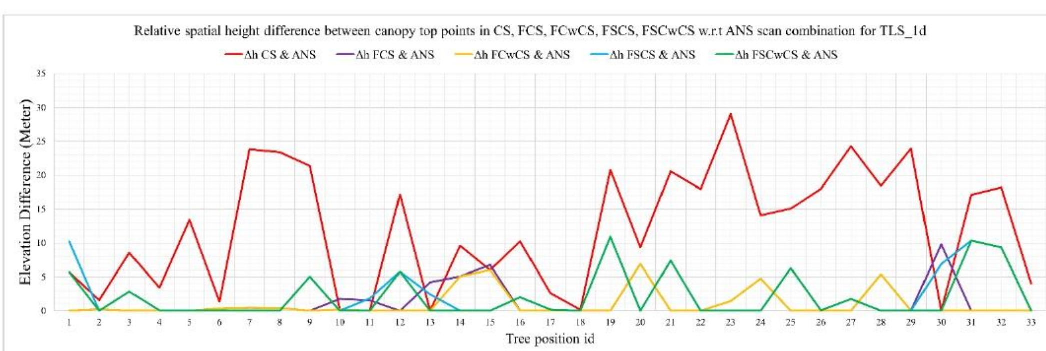

Figure A7. Graph showing relative spatial height differences between canopy top points in CS, FCS, FCwCS, FSCS, and FSCwCS with respect to ANS scan combination for TLS_1d.

Appendix A.5. Spatial Analysis for Forest Plot TLS_2b

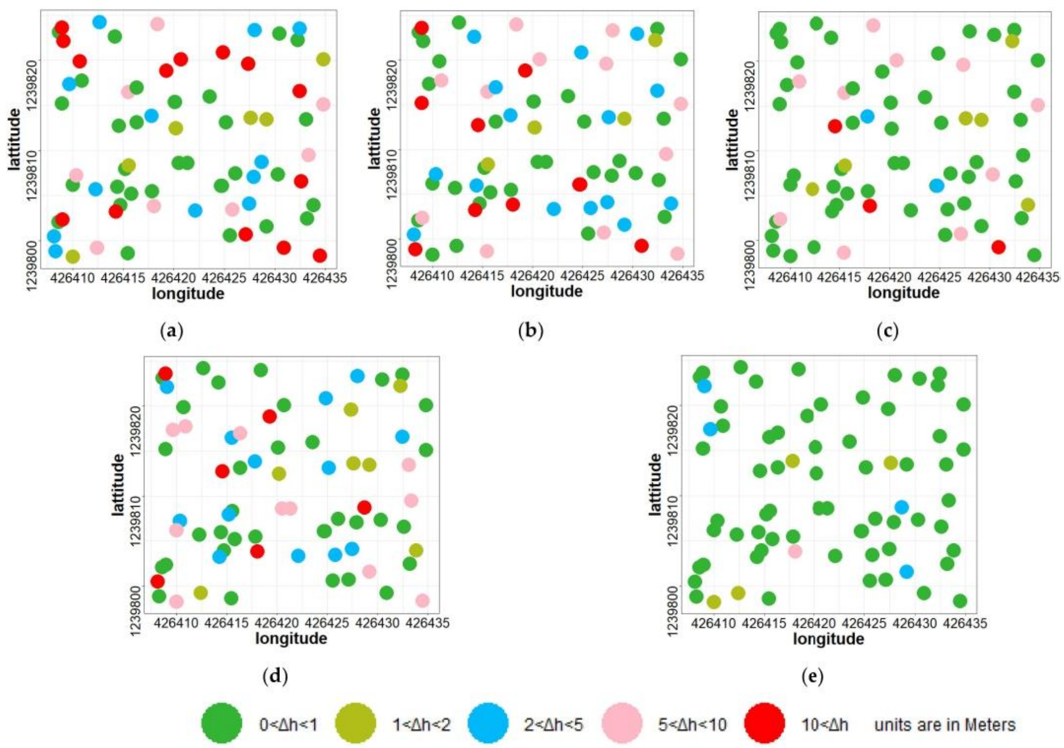

Figure A8. The spatial height differences between canopy top points obtained at each tree stem position in each of the TLS scan combinations for forest plot TLS_2b with respect to ANS scan combination. (**a**) Δh CS and ANS, (**b**) Δh FCS and ANS, (**c**) Δh FCwCS and ANS, (**d**) Δh FSCS and ANS, and (**e**) Δh FSCwCS and ANS.

Spatial Canopy Top Height Differences for Forest Plot TLS_2b

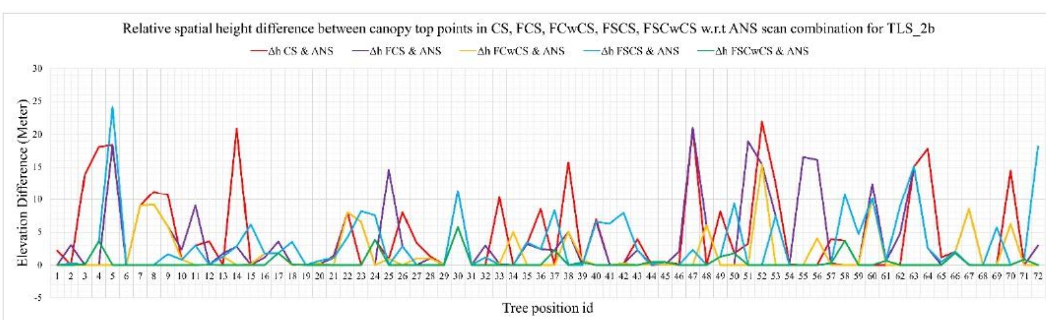

Figure A9. Graph showing relative spatial height differences between canopy top points in CS, FCS, FCwCS, FSCS, and FSCwCS with respect to ANS scan combination for TLS_2b.

Appendix A.6. Spatial Analysis for Forest Plot TLS_2c

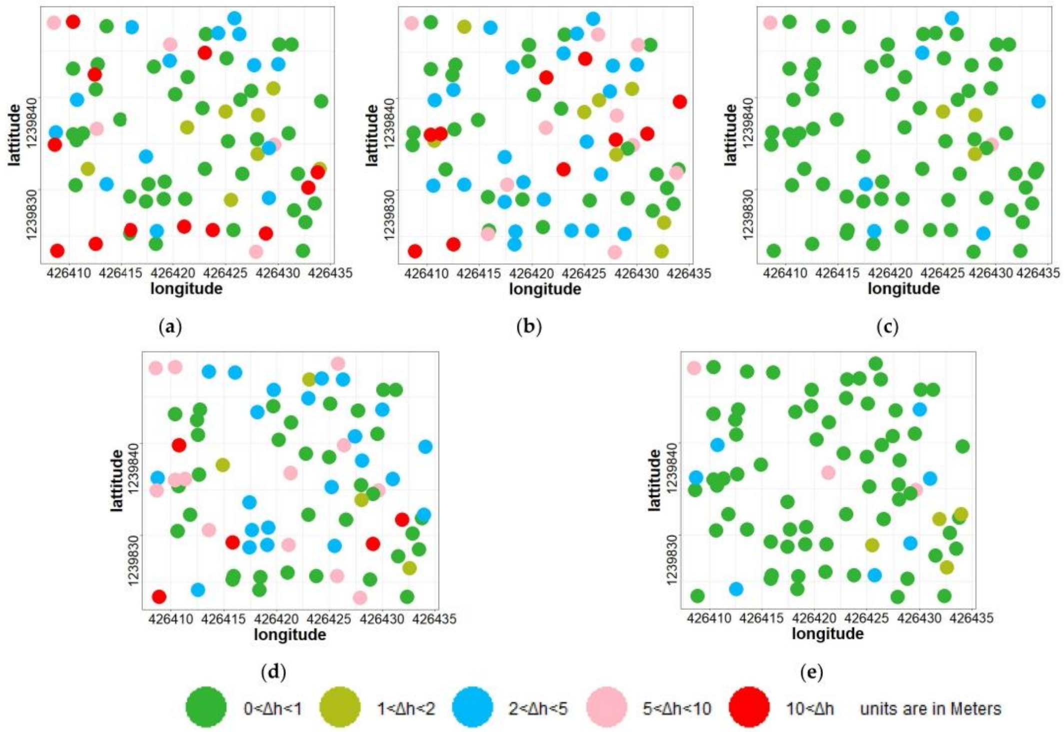

Figure A10. The spatial height differences between canopy top points obtained at each tree stem position in each of the TLS scan combinations for forest plot TLS_2c with respect to ANS scan combination. (**a**) Δh CS and ANS, (**b**) Δh FCS and ANS, (**c**) Δh FCwCS and ANS, (**d**) Δh FSCS and ANS, and (**e**) Δh FSCwCS and ANS.

Spatial Canopy Top Height Differences for Forest Plot TLS_2c

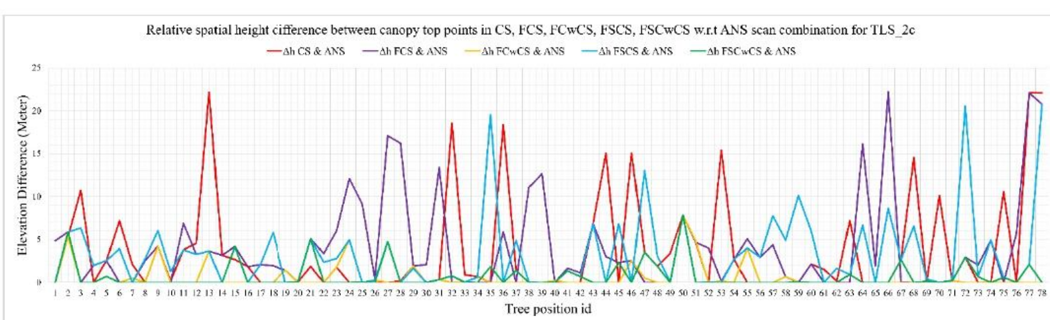

Figure A11. Graph showing relative spatial height differences between canopy top points in CS, FCS, FCwCS, FSCS, and FSCwCS with respect to ANS scan combination for TLS_2c.

Appendix A.7. Spatial Analysis for Forest Plot TLS_2d

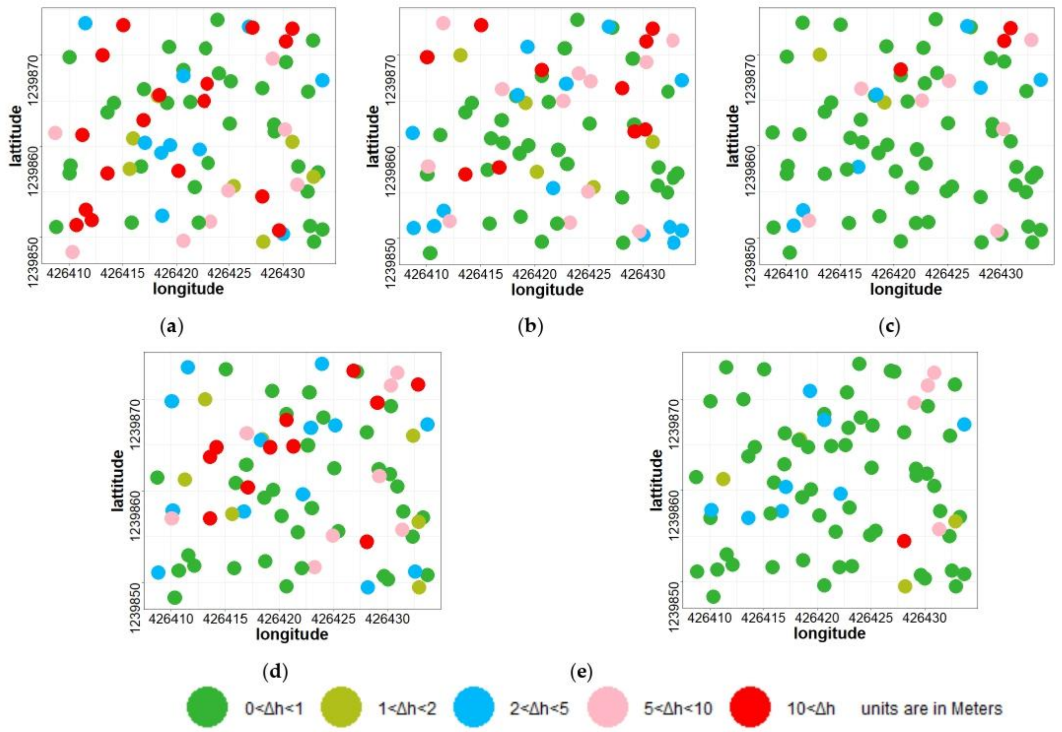

Figure A12. The spatial height differences between canopy top points obtained at each tree stem position in each of the TLS scan combinations for forest plot TLS_2d with respect to ANS scan combination. (**a**) Δh CS and ANS, (**b**) Δh FCS and ANS, (**c**) Δh FCwCS and ANS, (**d**) Δh FSCS and ANS, and (**e**) Δh FSCwCS and ANS.

Spatial Canopy Top Height Differences for Forest Plot TLS_2d

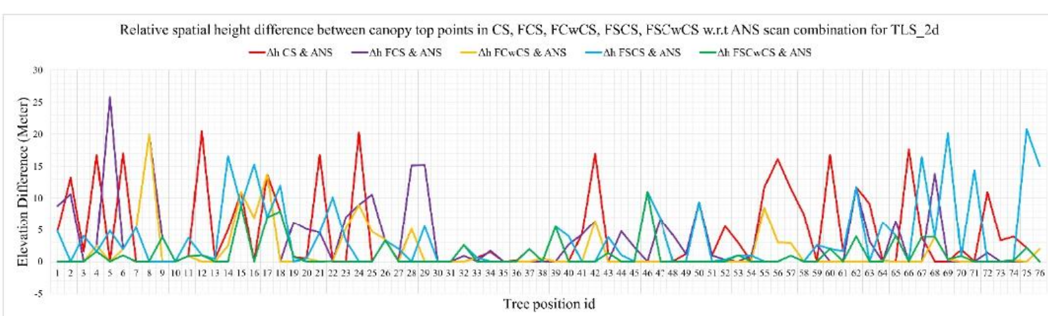

Figure A13. Graph showing relative spatial height differences between canopy top points in CS, FCS, FCwCS, FSCS, and FSCwCS with respect to ANS scan combination for TLS_2d.

Table A1. Analysis of variance results.

S.no.	Terms	Df	Sum Sq	Mean Sq	F Value	Pr (>F)
1	Combination	5	9171	1834	67.015	$<2 \times 10^{-16}$ ***
2	Plot	7	577,370	82,481	3013.445	$<2 \times 10^{-16}$ ***
3	Combination: Plot	35	3057	87	3.191	1.04×10^{-9} ***
4	Residuals	2874	78,665	27	NA	NA

Signif. codes: 0 '***'; 0.001 '**'; 0.01 '*'; 0.05 '.'; 0.1 ' ' 1.

Table A2. Tukey post hoc test results for multiple comparisons of means of combinations.

Terms	Combination. Diff	Combination. Lwr	Combination. Upr	Combination.P.Adj
Z.CS-Z.ANS	5.321615678	−6.277687548	−4.365543809	0
Z.FCS-Z.ANS	−3.110681938	−4.066753807	−2.154610069	0
Z.FCwCS-Z.ANS	−1.21057849	−2.166650359	−0.25450662	0.004199711
Z.FSCS-Z.ANS	−2.217747268	−3.173819137	−1.261675399	0
Z.FSCwCS-Z.ANS	−0.609996896	−1.566068765	0.346074973	0.453265265
Z.FCS-Z.CS	2.21093374	1.254861871	3.167005609	0
Z.FCwCS-Z.CS	4.111037189	3.15496532	5.067109058	0
Z.FSCS-Z.CS	3.10386841	2.147796541	4.059940279	0
Z.FSCwCS-Z.CS	4.711618783	3.755546913	5.667690652	0
Z.FCwCS-Z.FCS	1.900103449	0.94403158	2.856175318	2.37×10^{-7}
Z.FSCS-Z.FCS	0.89293467	−0.063137199	1.849006539	0.083054818
Z.FSCwCS-Z.FCS	2.500685043	1.544613173	3.456756912	0
Z.FSCS-Z.FCwCS	−1.007168779	−1.963240648	−0.05109691	0.032108868
Z.FSCwCS-Z.FCwCS	0.600581594	−0.355490275	1.556653463	0.471492715
Z.FSCwCS-Z.FSCS	1.607750372	0.651678503	2.563822241	2.52×10^{-5}

Table A3. Tukey post hoc test results for multiple comparisons of means by the plot.

Terms	Plot. Diff	Plot. Lwr	Plot. Upr	Plot.P.Adj
CTPL_1b-CTPL_1a	−1.24421	−2.58179	0.093376	0.090111
CTPL_1c-CTPL_1a	−1.50771	−2.98012	−0.03529	0.040289
CTPL_1d-CTPL_1a	−3.27041	−4.72927	−1.81156	0
CTPL_2a-CTPL_1a	30.49071	29.36467	31.61674	0
CTPL_2b-CTPL_1a	27.91473	26.71499	29.11448	0
CTPL_2c-CTPL_1a	28.32723	27.14632	29.50814	0
CTPL_2d-CTPL_1a	26.54387	25.35698	27.73076	0
CTPL_1c-CTPL_1b	−0.2635	−1.76155	1.234545	0.999483
CTPL_1d-CTPL_1b	−2.02621	−3.51093	−0.54148	0.000935
CTPL_2a-CTPL_1b	31.73491	30.57557	32.89426	0

Table A3. *Cont.*

Terms	Plot. Diff	Plot. Lwr	Plot. Upr	Plot.P.Adj
CTPL_2b-CTPL_1b	29.15894	27.92787	30.39001	0
CTPL_2c-CTPL_1b	29.57144	28.35872	30.78416	0
CTPL_2d-CTPL_1b	27.78808	26.56953	29.00662	0
CTPL_1d-CTPL_1c	−1.7627	−3.36996	−0.15545	0.020074
CTPL_2a-CTPL_1c	31.99841	30.6858	33.31103	0
CTPL_2b-CTPL_1c	29.42244	28.04607	30.79882	0
CTPL_2c-CTPL_1c	29.83494	28.47495	31.19493	0
CTPL_2d-CTPL_1c	28.05158	26.68639	29.41676	0
CTPL_2a-CTPL_1d	33.76112	32.46373	35.05851	0
CTPL_2b-CTPL_1d	31.18515	29.82329	32.54701	0
CTPL_2c-CTPL_1d	31.59764	30.25235	32.94294	0
CTPL_2d-CTPL_1d	29.81428	28.46373	31.16483	0
CTPL_2b-CTPL_2a	−2.57597	−3.57314	−1.5788	0
CTPL_2c-CTPL_2a	−2.16347	−3.1379	−1.18905	0
CTPL_2d-CTPL_2a	−3.94684	−4.9285	−2.96517	0
CTPL_2c-CTPL_2b	0.412498	−0.64625	1.471247	0.937254
CTPL_2d-CTPL_2b	−1.37087	−2.43628	−0.30545	0.002467
CTPL_2d-CTPL_2c	−1.78336	−2.82752	−0.7392	6.54×10^{-6}

References

1. Singh, A.; Kushwaha, S.K.P.; Nandy, S.; Padalia, H. An approach for tree volume estimation using RANSAC and RHT algorithms from TLS dataset. *Appl. Geomat.* **2022**, *14*, 785–794. [CrossRef]
2. Yu, H.; Yang, W.; Xia, G.S.; Liu, G. A color-texture-structure descriptor for high-resolution satellite image classification. *Remote Sens.* **2016**, *8*, 259. [CrossRef]
3. Forbes, B.; Reilly, S.; Clark, M.; Ferrell, R.; Kelly, A.; Krause, P.; Matley, C.; O'Neil, M.; Villasenor, M.; Disney, M.; et al. Comparing Remote Sensing and Field-Based Approaches to Estimate Ladder Fuels and Predict Wildfire Burn Severity. *Front. For. Glob. Chang.* **2022**, *5*, 818713. [CrossRef]
4. Calders, K.; Adams, J.; Armston, J.; Bartholomeus, H.; Bauwens, S.; Bentley, L.P.; Chave, J.; Danson, F.M.; Demol, M.; Disney, M.; et al. Terrestrial laser scanning in forest ecology: Expanding the horizon. *Remote Sens. Environ.* **2020**, *251*, 112102. [CrossRef]
5. Chen, J.; Chen, Y.; Liu, Z. Extraction of Forestry Parameters Based on Multi-Platform LiDAR. *IEEE Access* **2022**, *10*, 21077–21094. [CrossRef]
6. Cabo, C.; Ordóñez, C.; López-Sánchez, C.A.; Armesto, J. Automatic dendrometry: Tree detection, tree height and diameter estimation using terrestrial laser scanning. *Int. J. Appl. Earth Obs. Geoinf.* **2018**, *69*, 164–174. [CrossRef]
7. Kankare, V.; Puttonen, E.; Holopainen, M.; Hyyppä, J. The effect of TLS point cloud sampling on tree detection and diameter measurement accuracy. *Remote Sens. Lett.* **2016**, *7*, 495–502. [CrossRef]
8. Åkerblom, M.; Kaitaniemi, P. Terrestrial laser scanning: A new standard of forest measuring and modelling? *Ann. Bot.* **2021**, *128*, 653–662. [CrossRef]
9. García, M.; Danson, F.M.; Riaño, D.; Chuvieco, E.; Ramirez, F.A.; Bandugula, V. Terrestrial laser scanning to estimate plot-level forest canopy fuel properties. *Int. J. Appl. Earth Obs. Geoinf.* **2011**, *13*, 636–645. [CrossRef]
10. Disney, M. Terrestrial LiDAR: A three-dimensional revolution in how we look at trees. *New Phytol.* **2019**, *222*, 1736–1741. [CrossRef]
11. Walter, J.A.; Stovall, A.E.L.; Atkins, J.W. Vegetation structural complexity and biodiversity in the Great Smoky Mountains. *Ecosphere* **2021**, *12*, e03390. [CrossRef]
12. Wilkes, P.; Lau, A.; Disney, M.; Calders, K.; Burt, A.; Gonzalez de Tanago, J.; Bartholomeus, H.; Brede, B.; Herold, M. Data acquisition considerations for Terrestrial Laser Scanning of forest plots. *Remote Sens. Environ.* **2017**, *196*, 140–153. [CrossRef]

13. Wezyk, P.; Koziol, K.; Glista, M.; Pierzchalski, M. Terrestrial laser scanning versus traditional forest inventory first results from the polish forests. In Proceedings of the ISPRS Workshop on Laser Scanning 2007 and SilviLaser 2007, Espoo, Finland, 12–14 September 2007; Volume 36, pp. 424–429.
14. Palace, M.; Sullivan, F.B.; Ducey, M.; Herrick, C. Estimating Tropical Forest Structure Using a Terrestrial Lidar. *PLoS ONE* **2016**, *11*, e0154115. [CrossRef] [PubMed]
15. Decuyper, M.; Mulatu, K.A.; Brede, B.; Calders, K.; Armston, J.; Rozendaal, D.M.A.; Mora, B.; Clevers, J.G.P.W.; Kooistra, L.; Herold, M.; et al. Assessing the structural differences between tropical forest types using Terrestrial Laser Scanning. *For. Ecol. Manag.* **2018**, *429*, 327–335. [CrossRef]
16. Azuan, N.H.; Khairunniza-Bejo, S.; Abdullah, A.F.; Kassim, M.S.M.; Ahmad, D. Analysis of Changes in Oil Palm Canopy Architecture from Basal Stem Rot Using Terrestrial Laser Scanner. *Plant Dis.* **2019**, *103*, 3218–3225. [CrossRef] [PubMed]
17. Muumbe, T.P.; Tagwireyi, P.; Mafuratidze, P.; Hussin, Y.; van Leeuwen, L. Estimating above-ground biomass of individual trees with terrestrial laser scanner and 3D quantitative structure modelling. *South. For.* **2021**, *83*, 56–68. [CrossRef]
18. Seidel, D.; Fleck, S.; Leuschner, C.; Hammett, T. Review of ground-based methods to measure the distribution of biomass in forest canopies. *Ann. For. Sci.* **2011**, *68*, 225–244. [CrossRef]
19. Pueschel, P. The influence of scanner parameters on the extraction of tree metrics from FARO Photon 120 terrestrial laser scans. *ISPRS J. Photogramm. Remote Sens.* **2013**, *78*, 58–68. [CrossRef]
20. Abegg, M.; Kükenbrink, D.; Zell, J.; Schaepman, M.E.; Morsdorf, F. Terrestrial laser scanning for forest inventories-tree diameter distribution and scanner location impact on occlusion. *Forests* **2017**, *8*, 184. [CrossRef]
21. Gollob, C.; Ritter, T.; Wassermann, C.; Nothdurft, A. Influence of scanner position and plot size on the accuracy of tree detection and diameter estimation using terrestrial laser scanning on forest inventory plots. *Remote Sens.* **2019**, *11*, 1602. [CrossRef]
22. Kushwaha, S.K.P.; Singh, A.; Jain, K.; Mokros, M. Optimum Number and Positions of Terrestrial Laser Scanner To Derive Dtm At Forest Plot Level. *Int. Arch. Photogramm. Remote Sens. Spat. Inf. Sci.-ISPRS Arch.* **2022**, *43*, 457–462. [CrossRef]
23. CloudCompare. [GPL Software] Vrsion 2.12.4. 2022. Available online: https://www.danielgm.net/cc/release/ (accessed on 24 February 2023).
24. Koren, M. Dendrocloud Version 1.53. Available online: https://gis.tuzvo.sk/dendrocloud/download.aspx (accessed on 24 February 2023).
25. Trochta, J.; Král, K.; Janík, D.; Adam, D. Arrangement of terrestrial laser scanner positions for area-wide stem mapping of natural forests. *Can. J. For. Res.* **2013**, *43*, 355–363. [CrossRef]
26. Wan, P.; Wang, T.; Zhang, W.; Liang, X.; Skidmore, A.K.; Yan, G. Quantification of occlusions influencing the tree stem curve retrieving from single-scan terrestrial laser scanning data. *For. Ecosyst.* **2019**, *6*, 43. [CrossRef]

4.4 **LiDAR data fusion and future perspectives in forestry**

4.4.1 Aboveground Forest Biomass Estimation by the Integration of TLS and ALOS PALSAR Data Using Machine Learning

published as: Singh, A., Kushwaha, S. K. P., Nandy, S., Padalia, H., Ghosh, S., Srivastava, A., & Kumari, N. (2023). Aboveground forest biomass estimation by the integration of TLS and ALOS PALSAR data using machine learning. Remote Sensing, 15(4), 1143.

Extended summary:

In this paper, estimation of above ground forest biomass was done by the integration of TLS and ALOS PALSAR L-band datasets. A total of 13 plots were established and scanned with TLS. 23 parameters were retrieved using TLS and ALOS data for the integration at the LiDAR footprint. TLS was used to extract diameter at breast height (DBH) and tree height. The parameters derived from ALOS PALSAR L-band data are Gray-Level Co-Occurrence Matrix (GLCM) texture measures, Yamaguchi decomposition components, polarimetric parameters, and backscatter values of HH and HV band intensity.

The integration was performed using two machine learning approaches, Random Forest (RF) and Artificial Neural Network (ANN). The spatial distribution and uncertainty analysis was done and mapped using ALOS PALSAR data, shown in Figure 26.

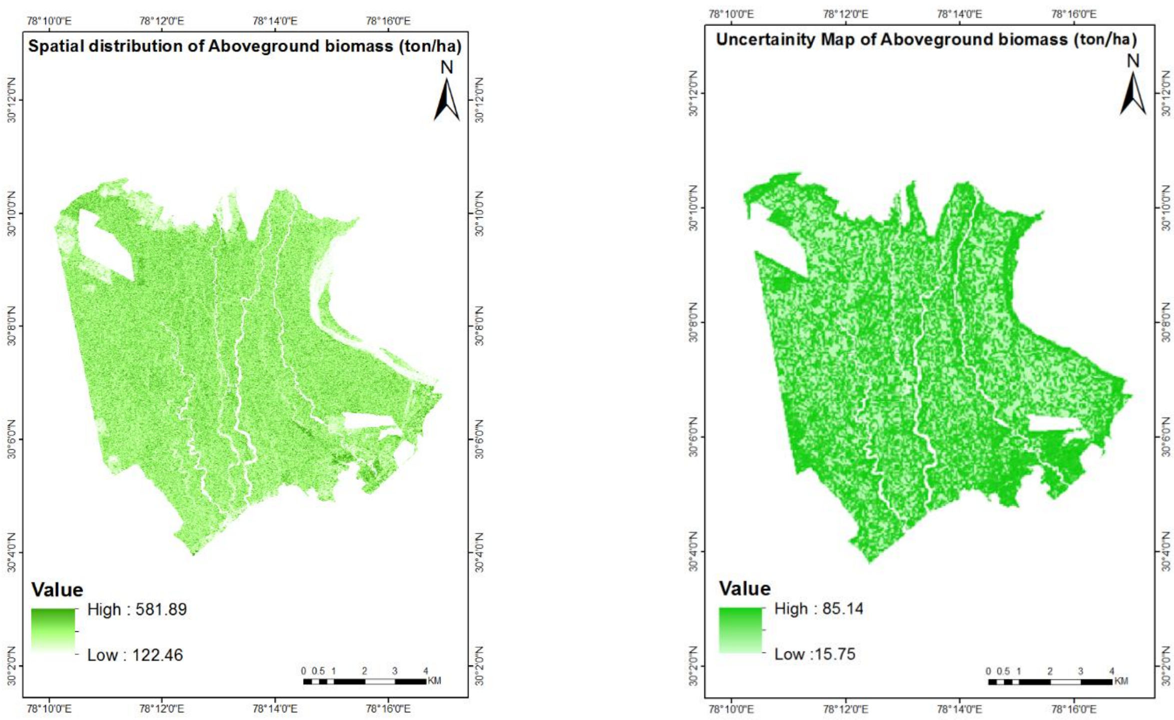

(a) (b)

Figure 26: Visualization of (a) Spatial distribution of AGB(ton/ha). (b) Uncertainty of AGB (ton/ha)

The variable used for the spatial distribution encompasses ALOS PALSAR GLCM textural variables, polarimetric, and TLS-derived parameters. The predicted biomass range was between 122.46 to 581.89 ton ha-1. The uncertainty of AGB distribution was determined using bootstrap resampling and the Monte Carlo approach. The range of uncertainty obtained was 15.75 to 85.14 ton ha-1.

The statistical measures for RF were found to be promising as compared to ANN for AGB estimation. The R^2 value obtained for the RF is 0.94 with an RMSE of 59.72 ton ha^{-1} for the predicted biomass value; RMSE% is 15.92, and RMSECV is 0.15. The R^2 value for ANN is 0.77 with an RMSE of 98.46 ton ha^{-1}, the RMSE% is obtained as 26.0, and the RMSECV is 0.26. RF performed better to estimate the biomass which ranges from 122.46 to 581.89 ton ha^{-1} with the uncertainty of 15.75 to 85.14 ton ha^{-1}, depicted in Table 7. The more detailed conceptual framework and results are shown in paper IV.

Table 7: Statistical evaluation of the models

Model	R^2	RMSE	RMSE%	$RMSE_{CV}$
RF	0.94	59.72	15.97	0.15
ANN	0.77	98.46	26.32	0.23

4.4.2 LiDAR Data Fusion to Improve Forest Attribute Estimates: A Review

published as Balestra, M., Marselis, S., Sankey, T. T., Cabo, C., Liang, X., Mokroš, M., ... & Hollaus, M. (2024). LiDAR Data Fusion to Improve Forest Attribute Estimates: A Review. Current Forestry Reports, 1-17.

Extended summary:

A thorough review of the LiDAR data fusion with other datasets, including hyperspectral, multispectral, and radar, is done with a panel of experts and reported important information, main challenges, and future scope. A structured review of the state-of-the-art studies on LiDAR data and fusion with other datasets was done to determine the study's main challenges and future directions. The questions addressed in this review are mentioned below:

1. What are the trends in LiDAR data fusion in the last decade?
2. What are the main motivations and applications of LiDAR data fusion?
3. What are the main methods used to perform data fusion?
4. What are the main gains of LiDAR data fusion?

The Preferred Reporting Items for Systematic Reviews and Meta-Analyses (PRISMA) approach was used to answer these questions. The keywords used for the search in the Web of Sciences database: are **LiDAR AND fus* (Topic) and forest* OR tree OR canop* (Topic) and structure OR height OR inventory (Topic)**. The publications used were with the status of ‘article’ or ‘review article’ with the date range of January 2014 to May 2023. A total of 664 papers were found on the Web of Science mentioned in Figure 27. Out of these, only 407 papers were considered based on the review criteria (2014-2023, English, article, or review). The papers were thoroughly studied by the reviewers for the selection of best-fitted papers based on the criteria (1) all the papers that were not addressing some aspects of forest or trees or related to forestry applications were eliminated, (2) the inclusion of LiDAR data in the fusion. The focus was also on the term used for data fusion, whether it should be data fusion, integration, or combination.

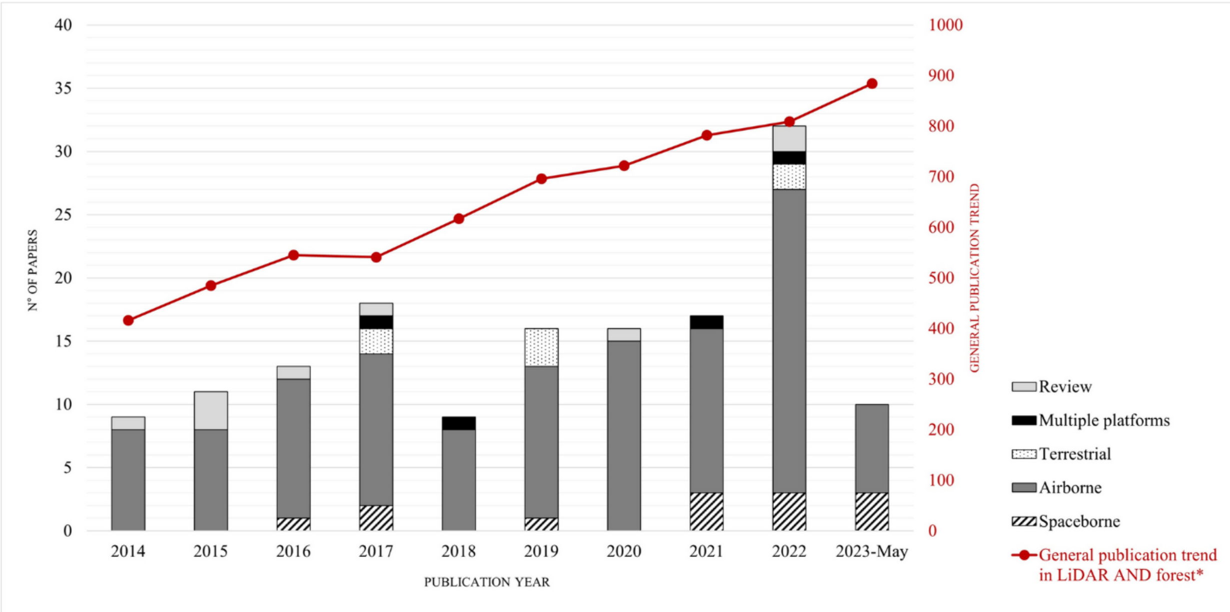

Figure 27: Number of publications on LiDAR data fusion and general publication trend in LiDAR in forestry applications over the last decade. The shade bars refer to the various LiDAR platforms. Multiple platforms indicate that LiDAR data from two (or more) different platforms was fused. Note that 2023 only includes papers published until May.

Extraction of Information from Literature

A coding scheme was developed to organize the information from 151 papers which is shown in Figure 28 to make the review process more understandable and comprehensive. Five main categories were considered in this coding scheme: general information, geographic location, survey area, data characteristics, and survey goals. In the general information category, the most pertinent information was considered for the later analysis of the papers. In geographic locations, different continents and countries were included. The survey area consisted of the scale of the study (global or local), and forest stands. Information on the platform and the LiDAR sensor name was used in data characteristics. Also, the datasets fused with the LiDAR data. The survey goals included the information on the application, the motivation for the fusion, and the outputs achieved with the fusion process.

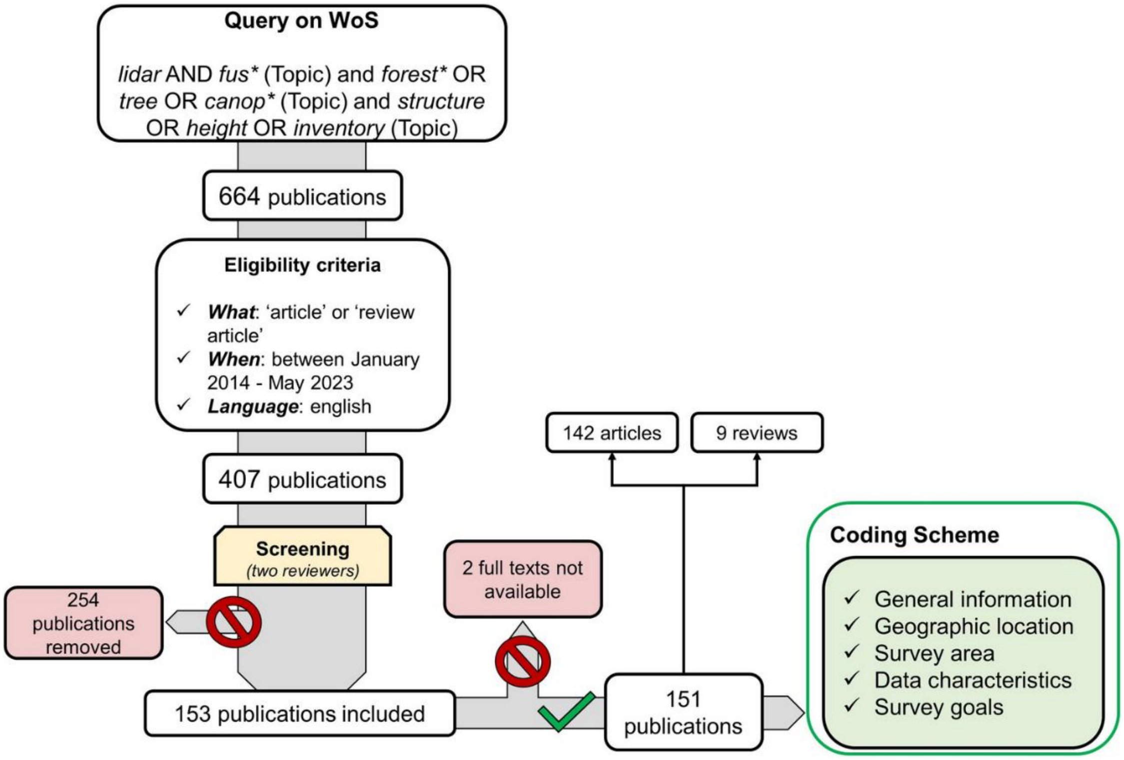

Figure 28: Framework of structural literature review and coding scheme

The review concluded that there is an uprising trend in the application of data fusion with both UAVs and airborne platforms in forestry observations. There is a potential to improve forestry observations with multi-sensors LiDAR data fusion in a great variety of applications. The term 'data fusion' should be considered to avoid confusion among commonly used terms such as 'data integration' and 'data combinations'. There are, furthermore, challenges in data fusion at the computational level, costs, processing times, data quality, and expertise in the application domain. Therefore, practitioners must carefully weigh the potential benefits of LiDAR data fusion in relation to the actual need for such benefits and the accompanying cost. A more detailed methodological framework and analysis can be found in the paper I.

Conclusion:

An experimental design and analysis are proposed in subsection 4.4.1. This subsection focused on the above-ground forest biomass estimation using TLS and ALOS PALSAR data using machine learning. RF and ANN were used for the prediction of AGB, and it was found that RF is more efficient and accurate for the prediction of AGB. Later, the AGB predicted values were correlated with the field-estimated AGB values, and the correlation was found to be high for RF. Then prediction of AGB was done with RF. The predicted AGB value (581.89 ton ha^{-1}) was highly correlated and close to the field referenced AGB values which is 685 ton ha^{-1}. This shows the potential of fusion of LiDAR with SAR data to combat the biomass saturation issues in highly matured forest areas.

Moreover, in subsection 4.4.2, a review of LiDAR data fusion was done to improve the forest attribute estimates. The major focus of the review was the appropriate use of words such as ‘data combination’, ‘data fusion’, ‘data integration’. Also, the challenges involved in the data fusion at computational level, costs, processing time, data quality, and expertise in the application domain was also focused.

remote sensing

MDPI

Article

Aboveground Forest Biomass Estimation by the Integration of TLS and ALOS PALSAR Data Using Machine Learning

Arunima Singh [1,2,*], Sunni Kanta Prasad Kushwaha [3], Subrata Nandy [2], Hitendra Padalia [2], Surajit Ghosh [4], Ankur Srivastava [5] and Nikul Kumari [5]

1 Faculty of Forestry and Wood Sciences, Czech University of Life Sciences, Kamýcká 129, Praha 6–Suchdol, 16500 Prague, Czech Republic
2 Forestry and Ecology Department, Indian Institute of Remote Sensing, Dehradun 248001, India
3 Geomatics Group, Indian Institute of Technology, Roorkee 247667, India
4 International Water Management Institute, 127 Sunil Mawatha, Battaramulla, Colombo 10120, Sri Lanka
5 Faculty of Science, University of Technology Sydney (UTS), 745 Harris St, Ultimo, NSW 2007, Australia
* Correspondence: singha@fld.czu.cz

Abstract: Forest inventory parameters play an important role in understanding various biophysical processes of forest ecosystems. The present study aims at integrating Terrestrial Laser Scanner (TLS) and ALOS PALSAR L-band Synthetic Aperture Radar (SAR) data to assess Aboveground Biomass (AGB) in the Barkot Forest Range, Uttarakhand, India. The integration was performed to overcome the AGB saturation issue in ALOS PALSAR L-band SAR data for the high biomass density forest of the study area using 13 plots. Various parameters, namely, Gray-Level Co-Occurrence Matrix (GLCM) texture measures, Yamaguchi decomposition components, polarimetric parameters, and backscatter values of HH and HV band intensity, were derived from the ALOS SAR data. However, TLS was used to obtain the diameter at breast height (dbh) and tree height for the sample plots. A total of 23 parameters was retrieved using TLS and SAR data for integration with the LiDAR footprint. The integration was performed using Random Forest (RF) and Artificial Neural Network (ANN). The statistical measures for RF were found to be promising compared with ANN for AGB estimation. The R^2 value obtained for the RF was 0.94, with an RMSE of 59.72 ton ha^{-1} for the predicted biomass value. The RMSE% was 15.92, while the $RMSE_{CV}$ was 0.15. The R^2 value for ANN was 0.77, with an RMSE of 98.46 ton ha^{-1}. The RMSE% was 26.0, while the $RMSE_{CV}$ was 0.26. RF performed better in estimating the biomass, which ranged from 122.46 to 581.89 ton ha^{-1}, while uncertainty ranged from 15.75 to 85.14 ton ha^{-1}. The integration of SAR and LiDAR data using machine learning shows great potential in overcoming AGB saturation of SAR data.

Keywords: aboveground biomass; Terrestrial Laser Scanner; Light Detection and Ranging; ALOS PALSAR; Random Forest; Artificial Neural Network

check for updates

Citation: Singh, A.; Kushwaha, S.K.P.; Nandy, S.; Padalia, H.; Ghosh, S.; Srivastava, A.; Kumari, N. Aboveground Forest Biomass Estimation by the Integration of TLS and ALOS PALSAR Data Using Machine Learning. *Remote Sens.* **2023**, *15*, 1143. https://doi.org/10.3390/rs15041143

Academic Editors: Houbing Song, Weipeng Jing, Huaiqing Zhang, Hua Sun, Qiaolin Ye and Fu Xu

Received: 20 December 2022
Revised: 1 February 2023
Accepted: 6 February 2023
Published: 20 February 2023

1. Introduction

Forest productivity estimation is important for forest management and ecosystem services monitoring [1]. Destructive sampling techniques are restricted due to labor intensiveness, tedious work, and unsuitability to inaccessible terrain. The emerging techniques of remote sensing are progressively superseding traditional methods. Dataset products from Terrestrial Laser Scanners (TLSs), Airborne Laser Scanning (ALS), Unmanned Aerial Vehicles (UAVs), and other space-borne (GEDI, ICESat-2) platforms, in combination with various machine learning algorithms, have become the preferred options for assessing and mapping aboveground biomasses (AGB) [2,3]. Machine learning algorithms, such as Random Forest (RF) and Artificial Neural Network (ANN) have been used to improve the saturation of biomass value ranges caused by data restrictions [4,5]. The primary aim is to reduce uncertainty in biomass assessment using remote sensing.

Data fusion and integration can play a crucial role in mitigating the uncertainty of biomass [6,7]. Used together, Synthetic Aperture Radar (SAR) and Light Detection and Ranging (LiDAR) overcome the saturation of biomass, with the specific bands of SAR data reducing result biases [8]. Previously, biomass was estimated based on empirical models using PolInsar and PolSAR techniques, which sometimes produced uncertainty of the biomass [9,10]. Subsequently, the use of LiDAR became ubiquitous; however, the occlusion of trees in a plot can occur due to different sets of scanning positions when using ground-based static LiDAR systems [11]. Thus, the resultant uncertainty is also reflected in the results. The detection of trees in forests also depends on the type and density of the forest as well as the scanning positions of the TLS [12].

The estimation of Aboveground Forest Carbon Stocks (AFCS) is always challenging in tropical regions due to structural complexity and high species diversity. ALOS PALSAR texture information resolves AFCS estimation issues in tropical regions [13]. Previously, empirical modeling, such as Extended Water Cloud Models (EWCMs) and Water Cloud Models (WCMs), showed the best correlation among forest parameters and HV backscatter values as well as volume scattering values [14]. The integration of different platform datasets yields promising results as well as complex information. Allometric modeling and biomass calibration and validation can be done using TLS and SAR data [15].

The aim of this study is to investigate other tree attributes derived with TLS and ALOS PALSAR and examine tree attribute correlations with biomass using machine learning. The objective is to overcome biomass saturation over high-density forests using RF and ANN. RF has been used for the estimation of biomass using airborne LiDAR data in moderately dense forests, taking into consideration the correlation between canopy cover and biomass [16–18]. Furthermore, other vegetation indices, such as NDVI, have been explored and exhausted to find the best possible correlation and prediction of biomass. Moreover, machine learning algorithms, such as RF and ANN, have been used to predict biomass using different combinations of tree metrics [19,20].

2. Materials and Methods

2.1. Study Area

The study area selected for this research was the Barkot Forest Range of Dehradun Forest division, Uttarakhand, India. It lies at a latitude of 30°03′52′′ to 30°10′43′′N and a longitude of 78°09′49′′ to 78°17′09′′E. The altitude ranges from 340 m to 560 m above Mean Sea Level (MSL). The study area is in the foothills of the Himalayas and is surrounded by the lesser Himalayas to the north and the Shivalik range to the south. The total area of the forest is 84.96 km^2. The forest type is tropical, moist, deciduous. It is dominated by *Shorea robusta* (Sal), with co-associated tree species such as *Mallotus philippensis* (Rohini). The topography of the study area varies from plain to undulating. As the depth of the soil increases, the consistency changes from non-sticky and friable to sticky and firm. A lower horizon of the soil profile is sticky, firm, compact, and comparatively hard [21,22]. The study area is shown in Figure 1.

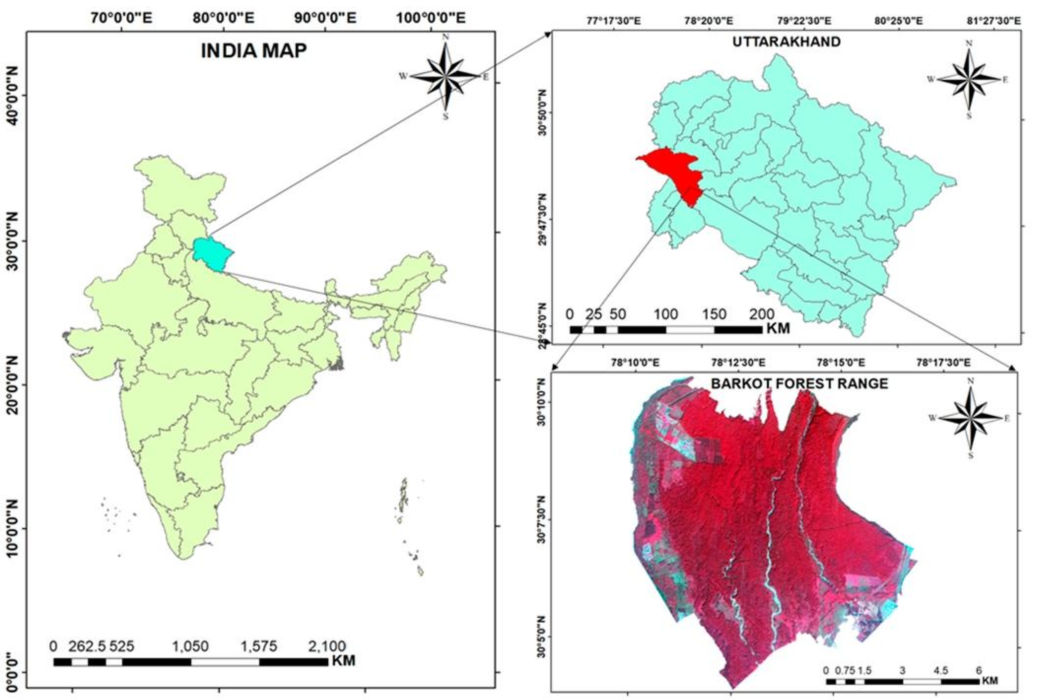

Figure 1. Study area [23].

2.2. Above-Ground Biomass Inventory

Tree inventory data were collected by demarcating 13 plots of 31.5 m $\times$ 31.5 m. The instruments used for the field data collection were measuring tape, rangefinders, and handheld GPSs. Field sampling was done at the LiDAR footprint using a stratified random sampling method. The sampling locations are shown in Figure 2. Tree parameters, such as dbh and tree height, were measured and the geo-location of each tree was recorded. The *CBH* (Circumference at Breast Height) was converted to *dbh* using the equation:

$$dbh = \frac{CBH}{\pi} \tag{1}$$

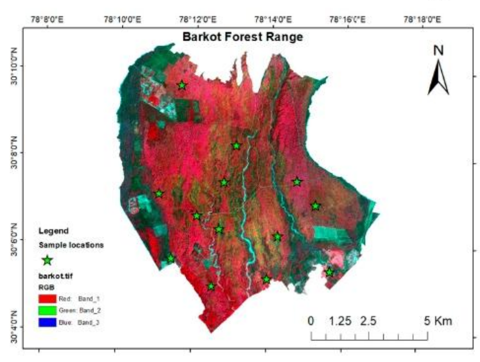

Figure 2. Sampling location of the field data collection.

The aboveground biomass was calculated using national species-specific volumetric equations. The tree volume was calculated for all the trees in the plot and then used to calculate biomass using the following equation:

$$Biomass = V * S * 1.59 \quad (2)$$

where V is stem volume, S is specific wood gravity, and 1.59 is biomass expansion factor. The biomass was calculated and regressed with the field estimated biomass for all the trees [24].

2.3. Terrestrial Lidar Data Acquisition and Processing

The point cloud of trees was generated using a terrestrial static LiDAR system (TLS Riegl VZ-400), which works in the range of 1.5 m to 600 m. The horizontal and vertical angles considered were 0° to 360° and 30° to 130°, respectively. The angular resolution selected for the data acquisition was 0.03°. The TLS data processing was conducted using RiSCAN Pro software 2.0. The TLS data were acquired using the scheme shown in Figure 3a. A total of four scans was completed, of which three were side scans and one was a center scan. Multiple scans were conducted to minimize the occlusion effect in the plots due to variability in the position and density of trees. Tags and retro-reflectors were used to identify the trees when segmenting out the plot and individual trees, as shown in Figure 3b.

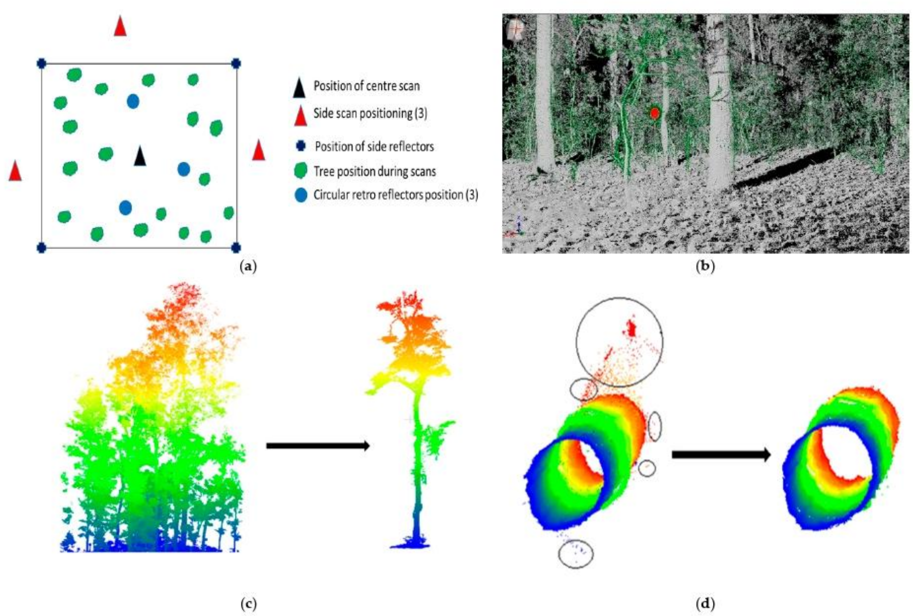

Figure 3. Representation of (**a**) scheme of the plot scanned with TLS and retro-reflectors; (**b**) scanned plot with the location of reflectors (red dot); (**c**) extracted plot and single tree; and (**d**) trunk of the tree with noise, and after the application of a noise filter [23].

For alignment between any two scans, a minimum of three common tie points was required. Figure 2 shows the scanned plot and the location of the reflectors. Iron rods were placed at the four corners of the plot as a reference to make extraction of the plot from the merged point cloud data easier. After extracting the plots, individual trees were identified and segmented out from the plots, as shown in Figure 3c. Thereafter, noise filtering was conducted to remove outliers from the dataset, as represented in Figure 3d.

Retrieval of Tree Parameters Using RANSAC Algorithm

The Random Sample Consensus (RANSAC) shape detection algorithm was used to estimate the dbh and height of the trees in the plot [25]. The following parameters were used for this purpose:

(1) D: Dataset with inliers and outliers, which were later characterized and removed using the RANSAC algorithm.
(2) MSS (Minimal Sample Set) of points: These were formed using random mathematical shape parameters out of all the points entered as D, finally yielding a model with definite shape parameters.
(3) k: The points which are required for the MSS.
(4) Theta: Parameters obtained from the MSS points, such as height, radius, center, etc.
(5) CS: The consensus set of points with an error less than the threshold error.
(6) δ: The error threshold, which is responsible for the points that belong to the model or not.

To obtain the dbh and height of the tree, the tree point clouds were fitted into a cylinder primitive [24]. A cylinder is defined by its height, axis, and radius. The points obtained from the MSS were used to form the CS of points. The cylinder was fitted to ensure no outlier points. The diameter of trees was calculated by the radius, using the following equation:

$$d = 2r \tag{3}$$

where "r" is the radius and "d" is the diameter of the tree.

The height of the tree was calculated by setting the lowest point of the tree cloud. After allocating the tree base position, the XY position was defined by computing the median coordinates of all the points that lay above the lowest tree point cloud to a user-defined height. The z-coordinate was defined using the points that lay closest to the XY position of the terrain.

2.4. ALOS PALSAR Data Processing

The PALSAR sensor was launched using the Japan Aerospace Agency (JAXA) and an onboard ALOS-1 (Advanced Land Observation Satellite) in 2006. This active microwave sensor has L-band technology and can acquire an image in both Fine Beam Single (FBS) and Fine Beam Dual (FBD) modes. The range resolution is between 0° and 60°. The image used in this study was acquired in April 2018 in quad-polarization (HH + HV + VH + VV). The SAR data was mutilooked to obtain a pixel resolution of 18.42 m.

The pre-processing of the data was conducted, including slant range to ground range conversion and generation of amplitude image using imagery (Q) and real (I) components of the image in Equation (4). This was further used in the power image generation in Equation (5). Speckle filtering was required to improve the visualization of the image, although this was at the expense of losing some pixel information. The filter used was the Boxcar filter. Another step was multilooking to obtain a square pixel. The final step was linear to backscatter image conversion, as shown in Equation (6).

$$Amplitude = \sqrt[2]{(I)^2 + (Q)^2} \tag{4}$$

$$Power = (Amp)^2 \tag{5}$$

$$\sigma^0{}_{i,j} = \frac{DN_{i,j}}{K}\left(\frac{1}{G(\theta_{i,j})^2}\right)\left(\frac{R_{(i,j)}}{R_{(ref)}}\right)^4 sin(\alpha_{i,j}) \tag{6}$$

where, the pixel intensity of the power image at the ith image line and the jth image column was $DN_{i,j} = I^2 + Q^2$. K, keeping absolute calibration constant. $\sigma^0{}_{i,j}$, Sigma nought at image line and the column "i, j" [26]. $G(\theta_{i,j})$, two-way antenna gain at the distributed target look angle corresponding to the pixel at image line and the column "i, j", as shown in Equation (7).

$$G(\theta_{i,j}) = 4\pi \frac{s}{\lambda^2} \tag{7}$$

where, $\theta_{i,j}$ is the look angle corresponding to the pixel at the image line and the column "i, j". $R_{(i,j)}$ is the slant range distance to the pixel at the image line and the column "i, j". $R_{(ref)}$ is the reference slant range distance (800 km for all beams and modes). $\alpha_{i,j}$ is the incidence angle at the pixel of the ith row and the jth column. The backscatter cross-section measures the object's reflective strength, which is known as sigma (σ). This cross-section is then represented in the logarithmic scale, i.e., a decibel (dB). The backscatter intensity can be observed in the linear to decibel conversion of the image [27], as shown in Equation (8).

$$dB = log10\ \sigma 0i, j\ (linear) \tag{8}$$

Decomposition of Scattering Components

The decomposition of the image was done using the Yamaguchi decomposition algorithm. Initially, the 2 × 2 scattering matrix was generated, while the coherency matrix was generated by multiplying the scattering matrix to lexicographic basis scattering vectors with its transpose [28]. The scattering matrix is depicted as follows:

$$\left[E_H^S\ E_V^S\right] = [S_{HH}\ S_{HV}\ S_{VH}\ S_{VV}]\left[E_H^I\ E_V^I\right] \tag{9}$$

The lexicographic basis scattering vector is represented as follows:

$$K_L = \left[S_{HH}\ \sqrt{2}S_{HV}\ S_{VV}\right] \tag{10}$$

The Pauli format of the scattering vector is represented as follows:

$$K_P = \frac{1}{\sqrt{2}}\ [S_{HH} + S_{VV}\ S_{HH} - S_{VV}\ 2S_{HH}] \tag{11}$$

The Yamaguchi equation is represented as follows:

$$\langle[T]\rangle = f_s\langle[T]\rangle_{surface} + f_d\langle[T]\rangle_{double-bounce} + f_v\langle[T]\rangle_{volume} + f_c\langle[T]\rangle_{helix} \tag{12}$$

where, $\langle[T]\rangle$ is the coherency matrix, $\langle[T]\rangle_{surface}$, $\langle[T]\rangle_{double\text{-}bounce}$, $\langle[T]\rangle_{volume}$, $\langle[T]\rangle_{helix}$, are the coherency matrices for surface, double-bounce, volume, and helix scattering, respectively. The f_s, f_d, f_v, f_c are their respective expansion coefficients. The volume scattering is modeled using the canopy of the tree, which includes the branches and the leaves. The modeled equation can be shown as follows:

$$\langle[T]\rangle_{volume} = \frac{1}{4}[2\,0\,0\,0\,1\,0\,0\,0\,1] \tag{13}$$

The surface scattering component was obtained for backscattered energy emerging from the ground only, as shown in the matrix below:

$$\langle[T]\rangle_{surface} = \left[1\ \beta^*\ 0\ \beta\ |\beta|^2\ 0\,0\,0\,0\right] \tag{14}$$

where β, is equal to $\frac{R_h - R_v}{R_h + R_v}$, R_h is the horizontal polarization and R_v is the vertical polarization coefficient of Fresnel's reflection. The double-bounce scattering was obtained from the scattering from the tree trunk and the surface of the ground.

$$\langle[T]\rangle_{double-bounce} = \left[|\alpha|^2\ \alpha\ 0\ \alpha^*\ 1\,0\,0\,0\,0\right] \tag{15}$$

where $\alpha = \frac{S_{HH}+S_{VV}}{S_{HH}-S_{VV}}$ and $|\alpha| < 1$. Finally, the helix scattering component was also considered, derived from the helical scatter.

$$\langle [T] \rangle_{helix} = \frac{1}{2}[0\ 0\ 0\ 0\ 1\ \pm j\ 0\ \pm j\ 1] \quad (16)$$

The polarimetric parameters used were Biomass Index (BMI), Canopy Structure Index (CSI), Volume Scattering Index (VSI), Radar Vegetation Index (RVI), cross-pol HH/VV ratio, cross-pol VV/VH ratio, and co-pol HH/VV ratio. The GLCM textural parameters were also used for the regression analysis of the biomass [29].

2.5. Prediction of AGB Using RF and ANN

The RF and neural net package were used in this study. RF was used to generate training and testing data using multiple decision trees. The model was trained using training datasets, while the prediction was made using testing datasets. RF and ANN were implemented in R software. Two input parameters were required, namely, ntree, the bootstrap samples used for creating several decision trees, and mtry, the number of variables provided for each tree for random sampling. The neural net was developed with several neurons, and these neurons were trained using the dataset provided. The hidden layer helped to learn the nodes from the previous layer and neurons to assign weights. The workflow is depicted in Figure 4.

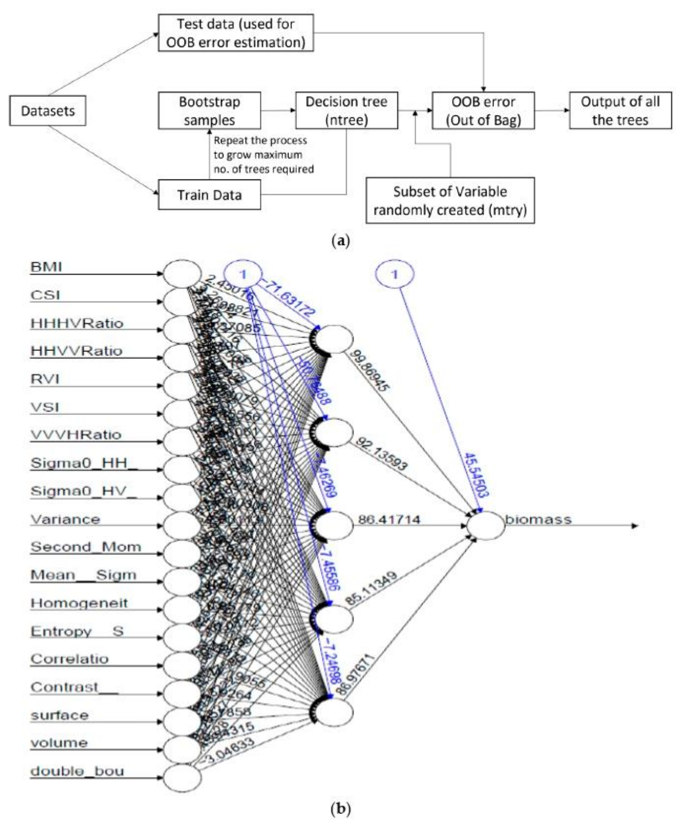

Figure 4. Workflow of (**a**) RF approach and (**b**) ANN approach for biomass prediction.

2.6. Mapping Spatial Distribution of AGB

The spatial distribution of AGB was based on the integration of TLS and ALOS PALSAR L-band data regression outputs using RF and ANN. The detailed workflow is depicted in Figure 5.

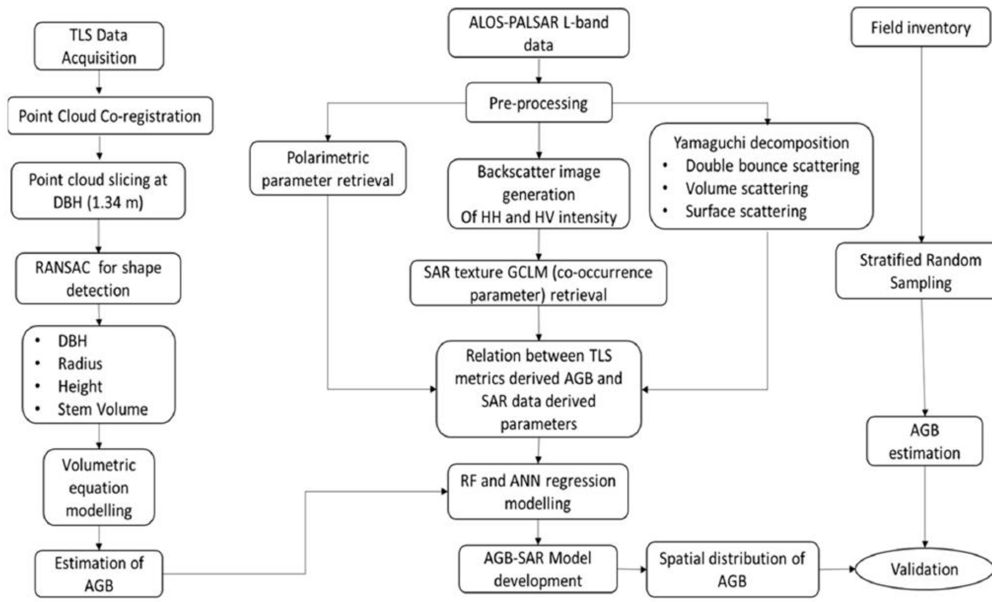

Figure 5. Methodology flowchart.

3. Results

3.1. Co-Registration of Scans

The 13 plots were scanned using TLS at four different scan positions, namely, center and three side scans. The scans were co-registered using the center scan fixed, while the remaining three scans were registered to the center scan. The RMSE obtained for the center to scan positions 1, 2, and 3 was 0.03, 0.017, and 0.029, respectively, for a single plot. The scan position pattern is depicted in Figure 3a.

3.2. TLS-Derived Parameters and Regression Analysis

Parameters such as dbh, dbh^2, and the height of the trees were retrieved using TLS point cloud. The correlation was established between field-estimated biomass and the TLS-derived parameters. As can be seen in Figure 6, the R^2 value obtained between height and biomass was 0.63; the logarithmic relation between height and biomass was also performed to improve the R^2 value to 0.88. The R^2 value obtained for dbh and biomass was 0.96. This value was enhanced by transforming the value of dbh. The transformation of dbh to dbh^2 changes the relation between dbh and biomass, with an R^2 value of 0.98.

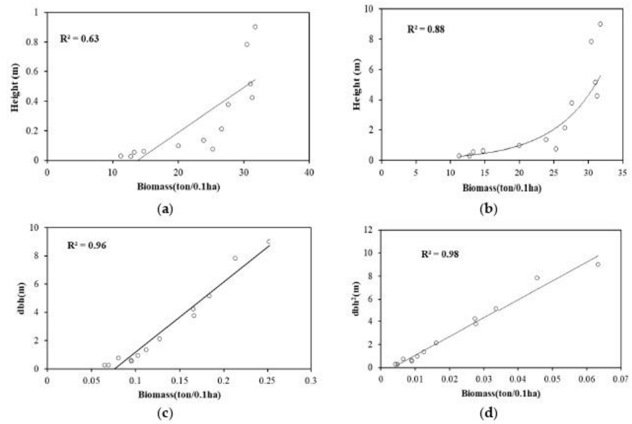

Figure 6. Correlation plots between TLS-derived parameters and biomass. (**a**) Correlation between height and biomass; (**b**) log-transformed correlation between height and biomass; (**c**) correlation between dbh and biomass; and (**d**) correlation between dbh^2 and biomass.

3.3. ALOS PALSAR L-Band Parameter Retrieval

3.3.1. Yamaguchi Decomposition

The correlation analysis was conducted using all three decomposition components of Yamaguchi, derived from ALOS PALSAR L-band data. It was observed that the R^2 value between double-bounce and biomass was 0.55, while the correlation value obtained for the surface scattering and biomass was 0.05. The R^2 value obtained for the volume scattering and biomass was 0.20. Therefore, a better correlation between the double-bounce and biomass can be inferred from the observed data. This seems to correlate with the field data given that the data was acquired in April, which is a leaf off-season in the study area. Thus, the backscatter was mostly from the woody portion of the trees, whereas less backscatter was observed from the canopy of the trees. The decomposition map is shown in Figure 7.

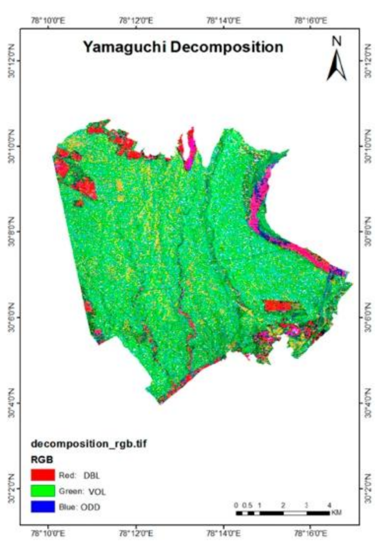

Figure 7. Yamaguchi decomposition of ALOS PALSAR L-band data.

3.3.2. Regression Analysis with Polarimetric Parameters

The polarimetric parameters used in this study were CSI, RANSAC shape detection, VSI, BMI, cross-pol HH/HV ratio, co-pol HH/VV ratio, cross-pol VV/VH ratio and, RVI. The R^2 value obtained for the CSI and biomass was 0.85, which showed a higher correlation between the canopy and the biomass. The ecosystem comprises more vertical and woody structures. The correlation R^2 obtained between VSI and biomass was 0.49, which clearly showed that the thickness of the canopy was less; hence, VSI is less significant in the biomass assessment [30]. The R^2 value obtained for BMI and biomass was 0.58 and 0.59 for RVI and biomass. This emphasizes the greater significance of RVI over BMI.

3.3.3. Regression Analysis with Backscatter and Textural Parameters

The biomass correlation was carried out using 7 textural variables, namely, mean, entropy, correlation, homogeneity, second moment (ASM), contrast, and variance. The backscatter values for HH and HV intensity were also considered. The regression analysis showed both a negative and a positive correlation. This is because in the modeling, both positive and negative correlations were useful in regulating the significance of the independent variables over the dependent variables. As can be seen in Figure 8, the positive R^2 value was obtained with entropy and variance. The R^2 value for the entropy was 0.21. The R^2 value obtained for the variance and biomass was 0.52. The degree of randomness and variability of the area was more relevant, whereas the negative R^2 value obtained was for ASM and mean. Therefore, textural parameters such as ASM, entropy, variance, and mean were significant in predicting the biomass of a natural forest.

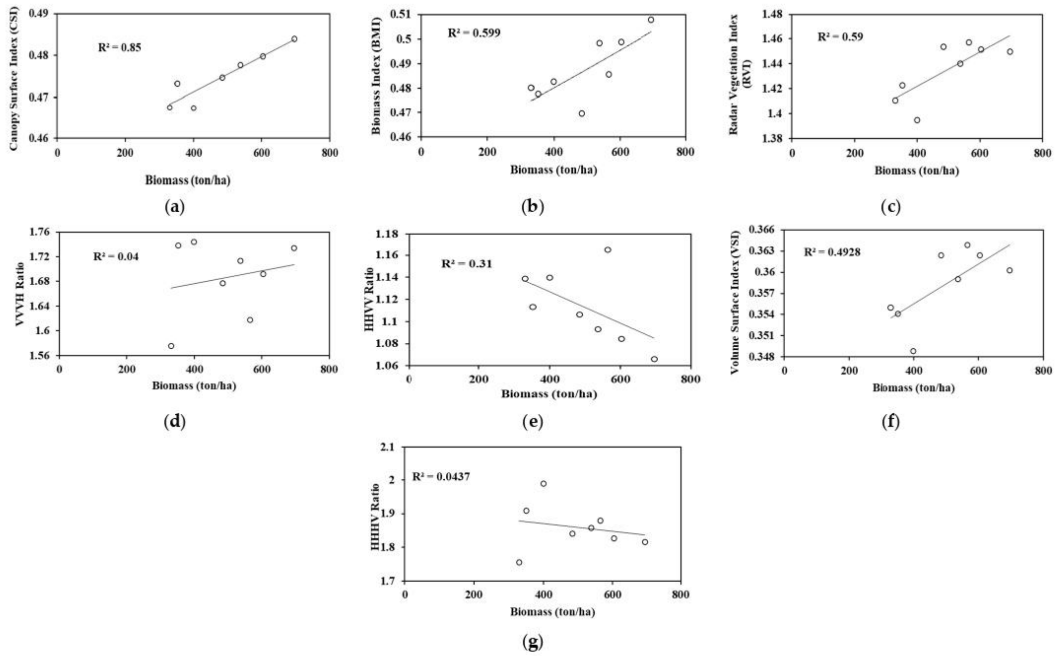

Figure 8. (**a**–**g**) Correlation between different SAR variables and the field-measured biomass.

The relation between the backscatter values for HH and HV intensity and the biomass showed that the R^2 value obtained for HH intensity and biomass was 0.40, while 0.49 was obtained for HV intensity. Log transformation was then conducted to enhance the correlation between the variables HH and HV intensity with the biomass. Thus, the R^2 value increased to 0.67 and 0.77 for HH and HV intensity with the biomass, respectively.

3.3.4. Regression between ALOS PALSAR L-Band and TLS-Derived Variables

The double-bounce and volume scattering were regressed with the height obtained using point cloud. The double-bounce scattering component was found to be more significant. As can be seen in Figure 9, the relation was not linear. The regression between height and volume scattering was log-transformed to better fit with an R^2 value of 0.40, while the double-bounce and height were transformed to a higher order to obtain a better correlation with the R^2 value of 0.53.

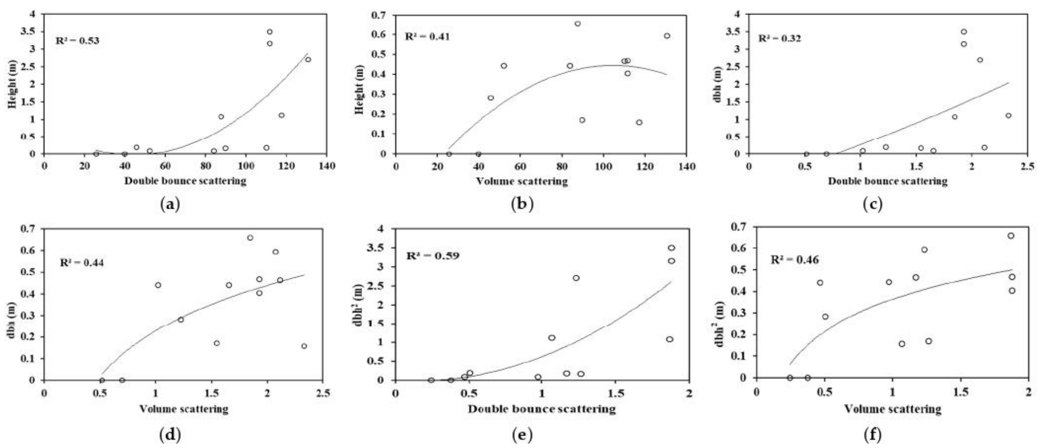

Figure 9. (**a**–**f**) Correlation plots of the ALOS PALSAR and TLS-derived variables.

The double-bounce scattering component showed a correlation of 0.32 with dbh, which was a high-order relation, while dbh and volume scattering were log-transformed, yielding an R^2 value of 0.44. A linear relation was found between dbh^2, double-bounce, and the volume-scattering components. The correlation value was enhanced to 0.59 with the high-order polynomial relation for dbh^2 and double-bounce, while the dbh^2 and volume scattering were log transformed to show some relation, yielding an R^2 value of 0.46. Here, the double-bounce showed a better correlation with dbh^2.

3.3.5. Integration of Outputs of ALOS PALSAR and TLS

RF Regression Approach

Based on the correlation values of the 19 variables, the RF regression approach was used to integrate the TLS and SAR parameters. The % IncMSE showed the mean square error in the absence of any independent variables, while the IncNodePurity defined the purity of nodes at ntree in the presence of any important variables, as shown in Figure 10a.

In Figure 10c, the range of error is shown as per the number of trees. As the number of trees increased, the error of the graph decreased. Training datasets and RMSE were used to optimize the parameter (ntree, mtry) values and found values that were used for the best prediction of the dependent variable (AGB). In Figure 10d, the prediction and observed biomass values were plotted based on the best RMSE and R^2 values, which were 38.95 and 0.94, respectively. Parameters such as ntree and mtry were optimized repeatedly to obtain the best results and reduce errors.

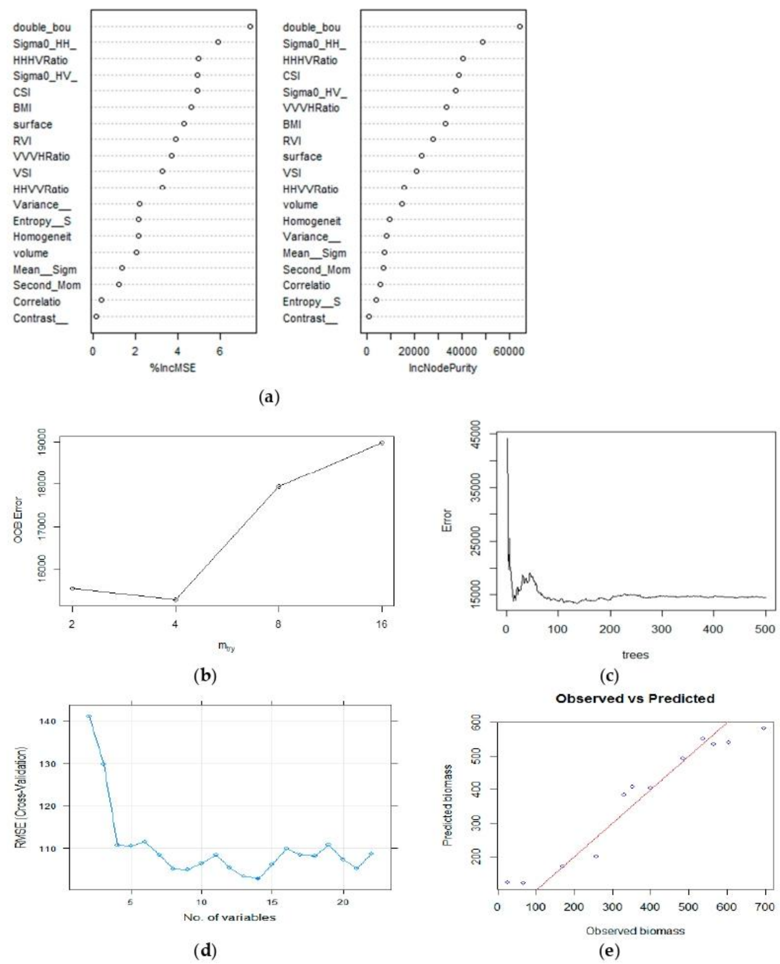

Figure 10. Visualization of (**a**) % IncMSE and IncNodePurity of the variables used to train the model; (**b**) out-of-bag (OOB) error while training the data; (**c**) estimated error based on different no. of trees, (**d**) error and RMSE of the number of variables and trees in the RF model; and (**e**) scatterplot for the observed and predicted biomass value (ton/ha).

A graph between the RMSE and the number of variables was plotted to obtain the cross-validation of the number of variables taken for the estimation of the dependent variable. The forest error rate was calculated using Out-of-Bag (OOB) error analysis. OOB error was calculated for four mtry values. The mtry value for which OOB fewer errors were found was 4, while the highest probability of error was found for mtry 16. Using this method, each tree was tested on 1/3rd of the number of observations and not used in building the tree, indicating that the high strength of the tree showed a lower error. The maximum error obtained for mtry was 16 due to the high correlation between trees. The lowest error was obtained for mtry 4 due to the lesser correlation between the trees.

ANN Regression Approach

ANN were trained and tested with 23 independent variables. The variables were divided based on the number of weights assigned to each variable. The hidden layers were optimized to obtain a better R^2 and RMSE. The negative weight assigned to any variable indicated the least contribution of that variable. The predicted and observed values of biomass are shown in Figure 11. The R^2 value obtained for the ANN was 0.77. The number of hidden layers was fitted to ensure maximum accuracy for the prediction. Several hidden layers were tried to ensure minimum RMSE and maximum accuracy for the model. Figure 3 shows the different number of hidden layers and their accuracy at each level. Based on the R^2 and RMSE of the model, an analysis was conducted and spatial distribution of biomass was carried out. The R^2 value for RF was 0.94, the RMSE was 59.72 ton ha^{-1}, and the percentage RMSE was 15.97. The R^2 value of ANN was 0.77, with an RMSE of 98.46 ton ha^{-1} and a percentage RMSE of 26.32, as shown in Table 1. Based on this analysis, the RF was found to be the best model for predicting biomass.

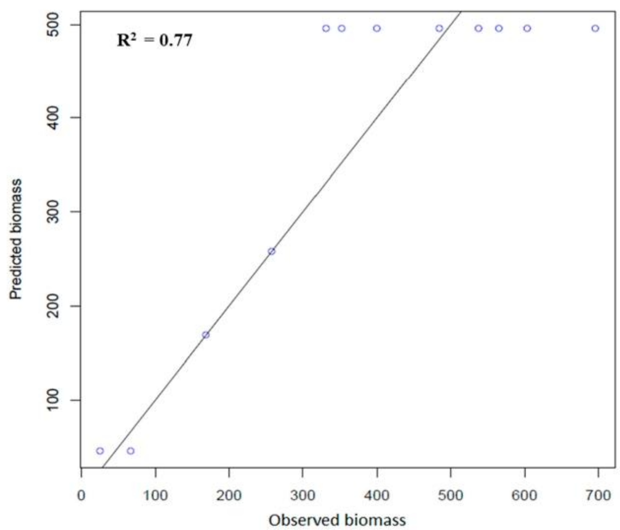

Figure 11. Scatterplot of the predicted Vs observed biomass (ton/ha) based on the ANN model.

Table 1. Statistical parameters for the models.

Sr. No.	Model	R^2	RMSE (ton ha^{-1})	RMSE%	$RMSE_{CV}$
1	**RF**	0.94	59.72	15.97	0.15
2	**ANN**	0.77	98.46	26.32	0.23

Spatial Distribution and Uncertainty of Biomass

The spatial distribution of biomass was conducted with RF predictions over the region of the Barkot Forest Range. The variable used for the spatial distribution encompassed the ALOS PALSAR GLCM textural variables as well as the polarimetric and TLS-derived parameters. The predicted biomass range was between 122.46 and 581.89 ton ha^{-1}.

The uncertainty distribution of AGB over the Barkot Forest Range was conducted using the bootstrap resampling method and the Monte Carlo approach. The uncertainty ranged from 15.75 to 85.14 ton ha^{-1}. The percentage of uncertainty obtained was 20.54%. The uncertainty map of the AGB and biomass spatial distribution is shown in Figure 12.

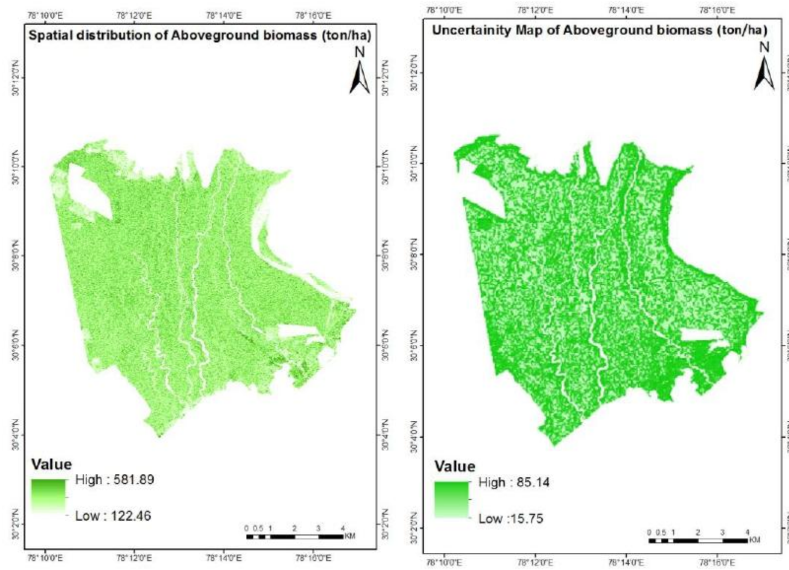

(**a**) (**b**)

Figure 12. Visualization of the (**a**) spatial distribution of AGB (t/ha) and (**b**) uncertainty of AGB (t/ha).

4. Discussion

In this study, we used terrestrial LiDAR (TLS) and ALOS PALSAR L-band derived variables to address the biomass saturation problem in forest regions. This method can be applied mainly in temperate forest zones, but can also be used in other forest-type regions. The RF and ANN model training was carried out using the calibration data. Previous research has shown that biomass value improvisation can be achieved by integrating different datasets or parameters derived from satellite data [19].

It has been shown that machine learning algorithms such as RF and ANN can estimate AGB with considerable accuracy. Overall, the RF showed promising accuracy when integrated with different RS (Remote Sensing) datasets over linear regression modeling [31].

The use of integrated data has shown great promise in reducing the underestimation of forest biomass values. Using a single RS dataset to predict biomass can result in considerable uncertainty [32]. SAR data can be used to estimate biomass, but there is a problem with the saturation of specific bands as forest density increases [33]. It has been observed that LiDAR data are more reliable in estimating biomass because they maintain the precision and accuracy of the predicted biomass. These data have yielded promising results, with an R^2 value of 0.98 and an RMSE of 0.08 Mg [34]. The collective information obtained from both SAR and LiDAR is key in overcoming the biomass saturation problem in SAR when using machine learning. This is because several machine learning algorithms have already been proven to yield the best results in estimating forest biomass.

The ALOS PALSAR-derived variables showed an important correlation with biomass. The GLCM texture variables showed a potential correlation with biomass, improving the area's biomass prediction values. In one study, it was shown that textural information yields good correlation with biomass, improving the AGB estimation [35]. ALOS PALSAR polarimetric parameters and Yamaguchi decomposition parameters, such as surface scattering, double-bounce, and volume scattering, were used to establish a correlation with the biomass. The results revealed that the CSI, RVI, and BMI showed a potentially high correlation with biomass [36].

The uncertainty prediction was also performed for the RF model since the quantification of uncertainty was required to prove the model's performance. The uncertainty in the spatially distributed AGB indicated that the pattern of forest distribution plays a crucial role in modeling biomass. Moreover, the uncertainty value was lower in the high-density areas of the forest and higher in the low-density areas because of the low correlation of biomass with tree attributes derived using ALOS.

5. Conclusions

In the current research, biomass was predicted using both ALOS PALSAR L-band and TLS-derived parameters in the study area of the Barkot Forest Range. Biomass was calculated using TLS-derived parameters. Correlations were also examined between biomass and various SAR parameters, such as texture (GCLM co-occurrence), backscattered values, polarimetric ratios, other SAR indices, and parameters derived using TLS. Thus, the two models, RF and ANN, were trained with field data. Then, the integration of the above-mentioned parameters or indices was conducted using two machine learning algorithms, RF and ANN. The best fit model obtained for the prediction of biomass was RF, with an R^2 value of 0.94 and an RMSE of 15.9%. In contrast, the R^2 obtained for ANN was 0.77, with an RMSE of 26.3%. It has been concluded that L-band integration with TLS-derived parameters shows great potential for the assessment of forest areas with very high biomass. The uncertainty can be mitigated using different machine learning algorithms and increasing the number of variables to train the model.

Author Contributions: Methodology, conceptualization, data analysis, writing, result interpretation: A.S. (Arunima Singh); Writing: S.K.P.K.; conceptualization, methodology: S.N.; writing—review and editing: H.P.; uncertainty analysis of results: S.G., A.S. (Ankur Srivastava) and N.K. helped in APC for the publication. All authors have read and agreed to the published version of the manuscript.

Funding: The research was not funded by any external sources. Only APC was provided by A.S. (Ankur Srivastava).

Data Availability Statement: Not applicable.

Acknowledgments: This research was undertaken as part of an M. Tech. dissertation for A.S. at the Indian Institute of Remote Sensing (IIRS), Dehradun, India. The authors also thank the Director and the Dean Academics of the IIRS for their continuous support and guidance. A.S. would like to acknowledge the late P. K. Champati ray for his valuable guidance. Uttarakhand Forest Department's support in the field data collection is duly acknowledged.

Conflicts of Interest: The authors declare no conflict of interest.

References

1. Houghton, R.A.; Hall, F.; Goetz, S.J. Importance of biomass in the global carbon cycle. *J. Geophys. Res. Biogeosci.* **2009**, *114*, G00E03. [CrossRef]
2. Brede, B.; Calders, K.; Lau, A.; Raumonen, P.; Bartholomeus, H.M.; Herold, M.; Kooistra, L. Non-destructive tree volume estimation through quantitative structure modelling: Comparing UAV laser scanning with terrestrial LIDAR. *Remote Sens. Environ.* **2019**, *233*, 111355. [CrossRef]
3. Silva, C.A.; Duncanson, L.; Hancock, S.; Neuenschwander, A.; Thomas, N.; Hofton, M.; Fatoyinbo, L.; Simard, M.; Marshak, C.Z.; Armston, J.; et al. Fusing simulated GEDI, ICESat-2 and NISAR data for regional aboveground biomass mapping. *Remote Sens. Environ.* **2021**, *253*, 112234. [CrossRef]
4. Kattenborn, T.; Leitloff, J.; Schiefer, F.; Hinz, S. Review on Convolutional Neural Networks (CNN) in vegetation remote sensing. *ISPRS J. Photogramm. Remote Sens.* **2021**, *173*, 24–49. [CrossRef]
5. Mangla, R.; Kumar, S.; Nandy, S. Random forest regression modelling for forest aboveground biomass estimation using RISAT-1 PolSAR and terrestrial LiDAR data. In Proceedings of the Lidar Remote Sensing for Environmental Monitoring XV, New Delhi, India, 4–7 April 2016; Singh, U.N., Sugimoto, N., Jayaraman, A., Seshasai, M.V.R., Eds.; SPIE: Bellingham, WA, USA, 2016; Volume 9879, p. 98790Q.
6. Ho Tong Minh, D.; Ndikumana, E.; Vieilledent, G.; McKey, D.; Baghdadi, N. Potential value of combining ALOS PALSAR and Landsat-derived tree cover data for forest biomass retrieval in Madagascar. *Remote Sens. Environ.* **2018**, *213*, 206–214. [CrossRef]

7. Leonardo, E.M.C.; Watt, M.S.; Pearse, G.D.; Dash, J.P.; Persson, H.J. Comparison of TanDEM-X InSAR data and high-density ALS for the prediction of forest inventory attributes in plantation forests with steep terrain. *Remote Sens. Environ.* **2020**, *246*, 111833. [CrossRef]
8. Montesano, P.M.; Nelson, R.F.; Dubayah, R.O.; Sun, G.; Cook, B.D.; Ranson, K.J.R.; Næsset, E.; Kharuk, V. The uncertainty of biomass estimates from LiDAR and SAR across a boreal forest structure gradient. *Remote Sens. Environ.* **2014**, *154*, 398–407. [CrossRef]
9. Peregon, A.; Yamagata, Y. The use of ALOS/PALSAR backscatter to estimate above-ground forest biomass: A case study in Western Siberia. *Remote Sens. Environ.* **2013**, *137*, 139–146. [CrossRef]
10. Santoro, M.; Wegmüller, U.; Askne, J. Forest stem volume estimation using C-band interferometric SAR coherence data of the ERS-1 mission 3-days repeat-interval phase. *Remote Sens. Environ.* **2018**, *216*, 684–696. [CrossRef]
11. Kushwaha, S.K.P.; Singh, A.; Jain, K.; Mokros, M. Optimum Number and Positions of Terrestrial Laser Scanner to derive DTM at Forest plot level. *Int. Arch. Photogramm. Remote Sens. Spat. Inf. Sci.* **2022**, *XLIII-B3-2*, 457–462. [CrossRef]
12. Liang, X.; Hyyppä, J.; Kaartinen, H.; Lehtomäki, M.; Pyörälä, J.; Pfeifer, N.; Holopainen, M.; Brolly, G.; Francesco, P.; Hackenberg, J.; et al. International benchmarking of terrestrial laser scanning approaches for forest inventories. *ISPRS J. Photogramm. Remote Sens.* **2018**, *144*, 137–179. [CrossRef]
13. Thapa, R.B.; Watanabe, M.; Motohka, T.; Shimada, M. Potential of high-resolution ALOS-PALSAR mosaic texture for aboveground forest carbon tracking in tropical region. *Remote Sens. Environ.* **2015**, *160*, 122–133. [CrossRef]
14. Santoro, M.; Cartus, O.; Fransson, J.E.S. Integration of allometric equations in the water cloud model towards an improved retrieval of forest stem volume with L-band SAR data in Sweden. *Remote Sens. Environ.* **2021**, *253*, 112235. [CrossRef]
15. Stovall, A.E.L.; Shugart, H.H. Improved biomass calibration and validation with terrestrial lidar: Implications for future LiDAR and SAR missions. *IEEE J. Sel. Top. Appl. Earth Obs. Remote Sens.* **2018**, *11*, 3527–3537. [CrossRef]
16. Gleason, C.J.; Im, J. Forest biomass estimation from airborne LiDAR data using machine learning approaches. *Remote Sens. Environ.* **2012**, *125*, 80–91. [CrossRef]
17. Mutanga, O.; Adam, E.; Cho, M.A. High density biomass estimation for wetland vegetation using worldview-2 imagery and random forest regression algorithm. *Int. J. Appl. Earth Obs. Geoinf.* **2012**, *18*, 399–406. [CrossRef]
18. Powell, S.L.; Cohen, W.B.; Healey, S.P.; Kennedy, R.E.; Moisen, G.G.; Pierce, K.B.; Ohmann, J.L. Quantification of live aboveground forest biomass dynamics with Landsat time-series and field inventory data: A comparison of empirical modeling approaches. *Remote Sens. Environ.* **2010**, *114*, 1053–1068. [CrossRef]
19. Dang, A.T.N.; Nandy, S.; Srinet, R.; Luong, N.V.; Ghosh, S.; Senthil Kumar, A. Forest aboveground biomass estimation using machine learning regression algorithm in Yok Don National Park, Vietnam. *Ecol. Inform.* **2019**, *50*, 24–32. [CrossRef]
20. Foody, G.M.; Boyd, D.S.; Cutler, M.E.J. Predictive relations of tropical forest biomass from Landsat TM data and their transferability between regions. *Remote Sens. Environ.* **2003**, *85*, 463–474. [CrossRef]
21. Mukesh; Manhas, R.K.; Tripathi, A.K.; Raina, A.K.; Gupta, M.K.; Kamboj, S.K. Sand and clay mineralogy of sal forest soils of the Doon Siwalik Himalayas. *J. Earth Syst. Sci.* **2011**, *120*, 123–144. [CrossRef]
22. Watham, T.; Patel, N.R.; Kushwaha, S.P.S.; Dadhwal, V.K.; Kumar, A.S. Evaluation of remote-sensing-based models of gross primary productivity over Indian sal forest using flux tower and MODIS satellite data. *Int. J. Remote Sens.* **2017**, *38*, 5069–5090. [CrossRef]
23. Singh, A.; Kushwaha, S.K.P.; Nandy, S.; Padalia, H. An approach for tree volume estimation using RANSAC and RHT algorithms from TLS dataset. *Appl. Geomat.* **2022**, *14*, 785–794. [CrossRef]
24. Singh, A.; Kushwaha, S.K.P.; Nandy, S.; Padalia, H. Novel Approach for Forest allometric eqaution modelling with RANSAC shape detection using Terrestrial Laser Scanner. *Int. Arch. Photogramm. Remote Sens. Spat. Inf. Sci.* **2022**, *XLVIII-4/W*, 133–138. [CrossRef]
25. Olofsson, K.; Holmgren, J.; Olsson, H. Tree stem and height measurements using terrestrial laser scanning and the RANSAC algorithm. *Remote Sens.* **2014**, *6*, 4323–4344. [CrossRef]
26. Rosich, B.; Meadows, P.J.; Monti-Guarnieri, A. ENVISAT ASAR Product Calibration and Product Quality Status. 2004. Available online: https://www.researchgate.net/publication/246078768_ENVISAT_ASAR_Product_Calibration_and_Product_Quality_Status (accessed on 19 December 2022).
27. Bergervoet, J.R.; van Campen, P.C.; van der Sanden, W.A.; de Swart, J.J. Phase shift analysis of 0–30 MeV pp scattering data. *Phys. Rev. C* **1988**, *38*, 15–50. [CrossRef]
28. Yamaguchi, Y.; Moriyama, T.; Ishido, M.; Yamada, H. Four-component scattering model for polarimetric SAR image decomposition. *IEEE Trans. Geosci. Remote Sens.* **2005**, *43*, 1699–1706. [CrossRef]
29. Haralick, R.M.; Dinstein, I.; Shanmugam, K. Textural Features for Image Classification. *IEEE Trans. Syst. Man Cybern.* **1973**, *SMC-3*, 610–621. [CrossRef]
30. Pope, K.O.; Rey-Benayas, J.M.; Paris, J.F. Radar remote sensing of forest and wetland ecosystems in the Central American tropics. *Remote Sens. Environ.* **1994**, *48*, 205–219. [CrossRef]
31. Dube, T.; Mutanga, O. Evaluating the utility of the medium-spatial resolution Landsat 8 multispectral sensor in quantifying aboveground biomass in uMgeni catchment, South Africa. *ISPRS J. Photogramm. Remote Sens.* **2015**, *101*, 36–46. [CrossRef]
32. Zhao, P.; Lu, D.; Wang, G.; Liu, L.; Li, D.; Zhu, J.; Yu, S. Forest aboveground biomass estimation in Zhejiang Province using the integration of Landsat TM and ALOS PALSAR data. *Int. J. Appl. Earth Obs. Geoinf.* **2016**, *53*, 1–15. [CrossRef]

33. Bouvet, A.; Mermoz, S.; Le Toan, T.; Villard, L.; Mathieu, R.; Naidoo, L.; Asner, G.P. An above-ground biomass map of African savannahs and woodlands at 25 m resolution derived from ALOS PALSAR. *Remote Sens. Environ.* **2018**, *206*, 156–173. [CrossRef]
34. Beyene, S.M.; Hussin, Y.A.; Kloosterman, H.E.; Ismail, M.H. Forest Inventory and Aboveground Biomass Estimation with Terrestrial LiDAR in the Tropical Forest of Malaysia. *Can. J. Remote Sens.* **2020**, *46*, 130–145. [CrossRef]
35. Liao, Z.; He, B.; Quan, X. Potential of texture from SAR tomographic images for forest aboveground biomass estimation. *Int. J. Appl. Earth Obs. Geoinf.* **2020**, *88*, 102049. [CrossRef]
36. Chowdhury, T.; Thiel, C.; Schmullius, C.; Stelmaszczuk-Górska, M. Polarimetric Parameters for Growing Stock Volume Estimation Using ALOS PALSAR L-Band Data over Siberian Forests. *Remote Sens.* **2013**, *5*, 5725–5756. [CrossRef]

Current Forestry Reports (2024) 10:281–297
https://doi.org/10.1007/s40725-024-00223-7

LiDAR Data Fusion to Improve Forest Attribute Estimates: A Review

Mattia Balestra[1] · Suzanne Marselis[2] · Temuulen Tsagaan Sankey[3] · Carlos Cabo[4] · Xinlian Liang[5] · Martin Mokroš[6,7,8] · Xi Peng[9] · Arunima Singh[7] · Krzysztof Stereńczak[10] · Cedric Vega[11] · Gregoire Vincent[12] · Markus Hollaus[13]

Accepted: 3 June 2024 / Published online: 21 June 2024

Abstract

Purpose of the Review Many LiDAR remote sensing studies over the past decade promised data fusion as a potential avenue to increase accuracy, spatial-temporal resolution, and information extraction in the final data products. Here, we performed a structured literature review to analyze relevant studies on these topics published in the last decade and the main motivations and applications for fusion, and the methods used. We discuss the findings with a panel of experts and report important lessons, main challenges, and future directions.

Recent Findings LiDAR fusion with other datasets, including multispectral, hyperspectral, and radar, is found to be useful for a variety of applications in the literature, both at individual tree level and at area level, for tree/crown segmentation, aboveground biomass assessments, canopy height, tree species identification, structural parameters, and fuel load assessments etc. In most cases, gains are achieved in improving the accuracy (e.g. better tree species classifications), and spatial-temporal resolution (e.g. for canopy height). However, questions remain regarding whether the marginal improvements reported in a range of studies are worth the extra investment, specifically from an operational point of view. We also provide a clear definition of "data fusion" to inform the scientific community on data fusion, combination, and integration.

Summary This review provides a positive outlook for LiDAR fusion applications in the decade to come, while raising questions about the trade-off between benefits versus the time and effort needed for collecting and combining multiple datasets.

Keywords Laser Scanner · Trees · Forest structure · Multispectral · Hyperspectral and Radar

Introduction

Forest ecosystems are often characterized in terms of structure, composition, and functions [1]. Light Detection and Ranging (LiDAR) remote sensing (RS) has substantially improved our understanding of forest structure around the world in recent decades [2–5]. LiDAR instruments provide explicit three-dimensional (3D) data that have enabled measurements of forest structure parameters such as canopy height, leaf area index, and diameter at breast height across different scales with unprecedented accuracy [6–8].

LiDAR data can be collected from a variety of sensors and platforms, resulting in a range of 3D data types (mostly point clouds), with different point densities, accuracies, and perspectives. Common LiDAR sensors can be mounted on different platforms including ground-based, both fixed and mobile [3, 9], airborne with unoccupied aerial vehicles (UAVs or drones), helicopters, and airplanes [10, 11], and space-based from satellites or the international space station [7, 12, 13]. The cross-scale LiDAR data collection has enabled many applications of tree and forest measurements, including forest inventories and biomass estimates [14, 15], species and habitat classification, biodiversity assessment [16, 17], forest fuel estimates [18] and detailed 3D reconstruction of trees [19, 20].

While LiDAR instruments have developed rapidly and extensively, the data continue to have limitations. For example, ground-based LiDAR data might not record all trees and tree tops due to occlusion [21]. Conversely, airborne and spaceborne LiDAR instruments can measure the top of the canopies and, in some cases, forest vertical structure, but rarely capture stems below canopies [22]. Moreover, LiDAR is specifically used to gather information on vegetation structure, but provides limited information on other important drivers of forest ecosystems, composition, and functioning. These limitations have resulted in a rapid increase in data fusion approaches, in which data from various instruments can be merged together (multi-sensor approach) to enhance the data and their application potential.

Extended author information available on the last page of the article

Various definitions of data fusion have been proposed [23, 24]. Here, we focus on multi-source or multi-sensor LiDAR data fusion, defined as "the merging of data or derived features from different sources (instruments/devices), of which at least one is LiDAR data, to improve the information content of the data sources and enable enhanced forest observations". Multi-sensor data fusion approaches have been deemed useful in overcoming measurement and sampling limitations from the original dataset to the final information extraction [25].

This review paper aims to summarize the current state-of-the-art LiDAR data fusion approaches for forest observations and identify main challenges that need to be addressed to move forward. We consider two levels of multi-sensor data fusion in this review: (1) data-level fusion, and (2) feature-level fusion. In data-level fusion, raw datasets from various sources are combined into one dataset or product (e.g. merging of two LiDAR point clouds, one collected with ground-based LiDAR and the other with unoccupied vehicle laser scanner (ULS)) [26]. In feature-level fusion, features extracted from various data sources individually are merged into new features or vectors (e.g. merging of structural parameters from LiDAR with coincident spectral parameters from hyperspectral (HS) data to derive a species classification) [27, 28].

This paper includes two major components. The first component provides a structured literature review on LiDAR data fusion addressing the following questions:

- What are the trends in LiDAR data fusion in the last decade?
- What are the main motivations and applications of LiDAR data fusion?
- What are the main methods used to perform data fusion?
- What are the main gains of LiDAR data fusion?

The literature review was then analyzed by a team of 11 international experts to address the following key questions:

- What is 'data fusion' and how should this term be used in our community?
- What are the most important lessons learned about data fusion in forest observations?
- What are the main challenges in data fusion for operational applications?
- What should the community focus on to move data fusion forward?

The experts in the team were assembled through the EU COST Action 3DForEcoTech; an EU initiative to bring together all experts on LiDAR data for forestry within the EU. An open call was held to solicit scientists interested in collaborating on this literature review. The final team was assembled to encompass all expertise required for addressing the key questions, including scientists with expertise on all types of LiDAR (mobile, terrestrial, airborne and spaceborne) and fusion with all common datasets assessed here (multispectral, hyperspectral, and radar).

Structured Literature Review Method

We used the Preferred Reporting Items for Systematic Reviews and Meta-Analyses (PRISMA) approach [29, 30]. The following search terms were used in the Web of Sciences database: LiDAR AND fus* (Topic) and forest* OR tree OR canop* (Topic) and structure OR height OR inventory (Topic). We included literature from the last decade between January 2014 - May 2023, published in English language, and with a publication status of 'article' or 'review article'. As defined in the introduction, we focused on multi-sensor data fusion. We did not consider studies that included a combination of two datasets from the same sensor collected at different times or at different locations. By limiting our search to only include the term 'data fusion' and no alternative search words, such as 'data integration' or 'data combination' (that may refer to the same process), we demonstrate how 'data fusion' is specifically used in the last decade. In the *Discussion* sub-section *Data fusion,* we further discuss the term 'data fusion' in relation to other terms with a potentially similar meaning in the LiDAR context.

Literature Search Results

The Web of Science query resulted in 664 papers (Fig. 1). Of these, 407 adhered to the eligibility criteria defined above (2014-2023, English, article or review). The abstracts of these 407 papers were screened by two independent reviewers, who decided whether to include or exclude a paper based on two criteria: (1) some aspect of trees/forest, relevant to forestry applications, was assessed, and all papers that solely studied crops, infrastructure or buildings were eliminated, and (2) the fusion must include LiDAR data.

Extracting Information from Literature

We developed a coding scheme to organize the information in the 151 papers in a comprehensive and understandable fashion that addressed the four main research questions. The coding scheme consisted of five main categories: general information, geographic location, survey area, data characteristics, and survey goals (Table 1). In the category 'general information', we included the most pertinent information, so the paper could be relocated for later analysis. In 'geographic location', we included information on the continent and country/countries of the study areas. Regarding 'survey area', we included survey scale (i.e. global or local) and forest stand (i.e. type of vegetation surveyed). In 'data characteristics', we included information on the LiDAR platform used, as well as the sensor's name and type. We also recorded the datasets that were fused with

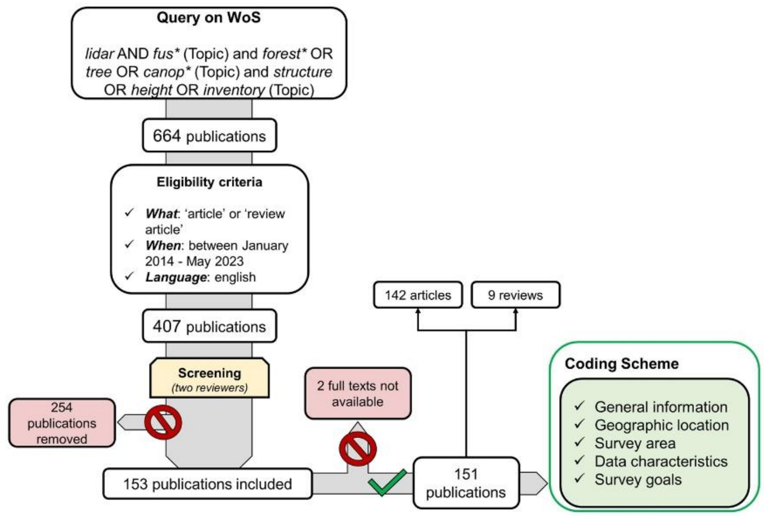

Fig. 1 Framework of structured literature review and coding scheme

Table 1 Categories and subjects included in the coding scheme for the structured literature review of the 151 selected papers

General information	Geographic Location	Survey area	Data characteristics	Survey goals
Authors	Continent	Survey scale	Type of LiDAR	Fusion application
Year	Country	Forest stand	Name of LiDAR sensor	Fusion aim
DOI			Type of fused sensor(s)	Fusion technique
Title			Name of fused sensor(s)	Fusion gain
Keywords				

the LiDAR dataset. Within 'survey goals', we included information on the application for which the fusion was used, the motivation (aim) for the fusion (e.g. increasing spatial resolution of data product), the type of method used to fuse the datasets, and reported gain of the fusion process.

Trends in Data Fusion Literature

The number of publications concerning LiDAR data fusion for forests demonstrates a slight general upward trend over the last 10 years, especially in 2022 (Fig. 2). LiDAR data from airborne platforms were most commonly used. These airborne platforms include both instruments mounted on UAVs and occupied aircrafts. Fusion with data from terrestrial platforms, including terrestrial laser scanners (TLSs) and mobile laser scanners (MLSs), seems to be emerging in recent years, starting in 2016. Generally, there has been a slightly increasing trend in the use of spaceborne LiDAR sensors, with satellite papers published in 2016 and 2017 employing data from ICESat/GLAS and the papers published after 2018 with data from ICESat-2 and GEDI.

LiDAR data can be fused with data collected from a similar platform (e.g. airborne-airborne) or a different platform (e.g. airborne-spaceborne). Fusion of airborne LiDAR and other airborne data types was the most common type of fusion encountered (45.4%), followed by fusion of LiDAR data from airborne and spaceborne devices (29.8%). Spaceborne LiDAR fused with data collected by other spaceborne sensors and airborne-terrestrial fusion had the same amount of publications (11.3%), whereas fusion of terrestrial LiDAR with other data from terrestrial platforms was found to be the least common (2.1%) (Table 2).

In terms of geographical representation (Fig. 3), studies from North America (38%), Europe (31%) and Asia (21%) represent 90% of the publications. The remaining 5% study Australia, and another 5% focus on Africa and South America together. In particular, our literature review found very few LiDAR data fusion studies in the southern hemisphere. This pattern is consistent with a review of the geographic distribution of authorship in remote sensing publications [31], documenting that four specific countries, the USA, Italy, Germany, and China, are over-represented, with almost no contributions from South America and Africa. Our literature

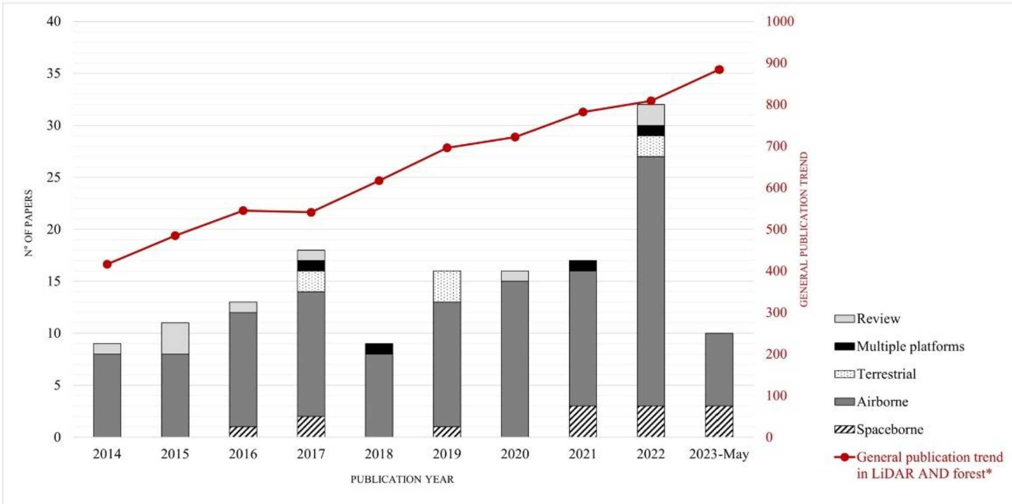

Fig. 2 Number of publications on LiDAR data fusion and general publication trend in LiDAR in forestry applications over the last decade. The shaded bars refer to the various LiDAR platforms. Multiple platforms indicates that LiDAR data from two (or more) different platforms was fused. Note 2023 only includes papers published until May

Table 2 Number of publications by platform, where at least one of the sensors is LiDAR

	LiDAR							Non-LiDAR sensors: Airborne				Non-LiDAR sensors: Spaceborne			Non-LiDAR sensors: UAV				Non-LiDAR sensors: Terr	Total per LiDAR type
	ALS	*SLS*	*ULS*	*TLS*	*MLS*	*HLS*	*BLS*	*HS*	*MS*	*RGB*	*SAR*	*HS*	*MS*	*SAR*	*HS*	*MS*	*RGB*	*T*	*TRGB*	
LiDAR *ALS*		1		3		2		24	21	9	2		31	6	1		1			101
LiDAR *SLS*			1										9	5						15
LiDAR *ULS*				7	1	1	4	3		1			1		4	2	1	1		26
LiDAR *TLS*																			1	1
LiDAR *MLS*																			1	1
Total per other type of sensor (non-LiDAR)								27	21	10	2		41	11	5	2	2	1	2	

LiDAR sensors used for data fusion include: *ALS* airborne laser scanner, *SLS* spaceborne laser scanner, *ULS* unoccupied aerial vehicle laser scanner, *TLS* terrestrial laser scanner, *MLS* mobile laser scanner, *HLS* handheld laser scanner, *BLS* backpack laser scanner. *Non-LiDAR* sensors used for data fusion with LiDAR include: *HS* hyperspectral, *MS* Multispectral, *RGB* red, green, and blue visible bands, *SAR* synthetic aperture radar, *T* thermal infrared, *TRGB* RGB+T.

sample demonstrates that most of the fusion studies in Asia are taking place in China alone, while other countries such as Iran, India, and Malaysia are studied just one time each.

Main Motivations and Applications of LiDAR Data Fusion

Motivations

Three main motivations for data fusion were found: (1) fusion of data across platforms can enhance spatial or temporal resolution of the data product. (2) two different LiDAR datasets can be fused to improve data density and/or overcome occlusion. For example, terrestrial and aerial point clouds are fused to better represent both the top and the bottom of the canopy, and to subsequently extract structural parameters more accurately [32, 33]. (3) fusion from the same platform primarily enriches the existing dataset with additional information, and these studies seek to add more information to the LiDAR dataset. For example, spectral data can be fused with LiDAR data to create a better estimate of aboveground biomass (AGB) or improve tree segmentation.

Applications

In the LiDAR data fusion literature, we find two main streams of applications, at the individual tree level (ITA - Individual Tree Approach) and at the area level (ABA

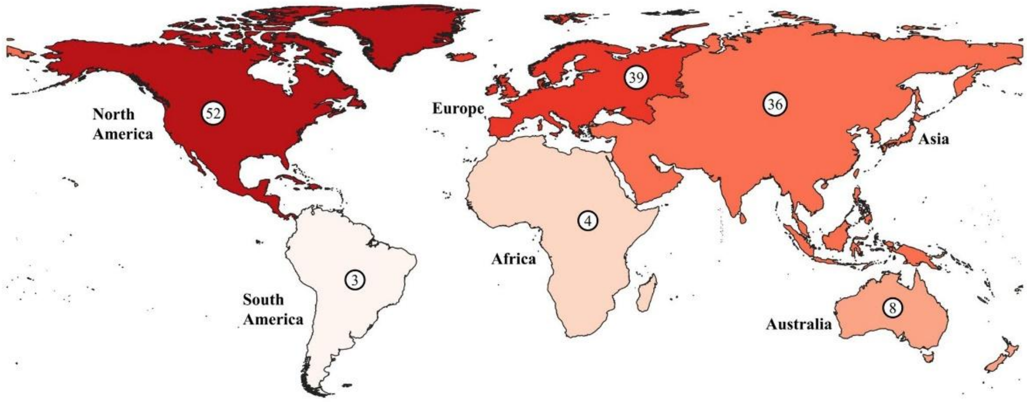

Fig. 3 Geographic distribution of study locations in the 142 case studies included in our literature sample

- Area-Based Approach). Among all papers reviewed, 27% focus on ITA, 50% on ABA, 17% on both ITA and ABA, and 6% are review papers. The main applications of LiDAR data fusion at these two levels are divided into seven categories:

1) Classification (tree species/land cover): 29.5% of the papers [27, 28, 34–73] encompassed land cover classification, specifically, forest type classification, classification of individual tree species or genus, and forest habitat mapping.
2) Growing stock volume / above-ground biomass: 17.7% of the papers [74–98] are studies in which data fusion was used to improve biomass estimates both at ABA and ITA levels.
3) Forest structure: 15.5% of the papers [11, 13, 32, 33, 99–115] include different datasets fused to improve the extraction of horizontal as well as vertical structure parameters beyond canopy height. This category includes individual tree biometric parameters such as crown diameter, crown length or base height. On an area-based level, the information derived includes mean crown length, number of vertical layers, gaps, crown coverage, stem density, basal area, DBH distribution etc. This category also includes assessment of post-fire forest structure and regeneration.
4) Tree height: 12.7% of the papers [116–133] include canopy height represented by different parameters such as mean height, quantiles, deviations etc. Data fusion was applied to generate better estimates of tree height at a single tree level or a stand level, mainly by fusing aerial LiDAR data with other LiDAR platforms.
5) Segmentation: 9.2 % of the papers [134–147] delineate individual tree crowns and identify locations of individual trees. In ABA, the segmentation includes delineation of homogeneous forest patches as well as forest stands.
6) Other: 9.1% of the papers [148–160] include a variety of applications, such as mapping the pigment distribution and quantifying taxonomic, functional, and phylogenetic diversity, tree age estimation etc.
7) Fuel load: 6.3% of the papers [161–169] include applications that deal with fuel load and forest fire modeling.

Methods for LiDAR Data Fusion

The methods used for LiDAR data fusion can generally be divided into two main categories. Data-level fusion studies typically merge datasets from different sensors during the pre-processing stage and before any formal classification or feature extraction occur, whereas feature-level fusion studies merge post-classification outputs and extracted features from disparate datasets to generate a new dataset. A third level, namely decision-level fusion, exists in the literature, but none of the papers in our literature sample fell into this category [170, 171].

Data-level Fusion

Among all papers we reviewed, 22% performed data-level fusion. Point cloud-to-cloud fusion can be achieved by combining, for example, airborne and terrestrial LiDAR datasets using the reference points acquired in both surveys [19]. TLS typically acquires detailed measurements at a plot-scale, while ULS can obtain measurements across a larger spatial extent at a landscape-scale [26]. The raw datasets can be fused using ground control points (GCPs) or by identifying similar features in the datasets [74, 100] using the same coordinate system acquired through GNSS or total stations. Other studies [26, 112, 162] used manual co-registration by identifying similar features such as the tallest tree, trees with large crowns, or tree locations. These features were used to guide the manual shifting process and to correctly co-register the two datasets. Defining appropriate key points for co-registration is challenging, especially in forest point clouds with few distinct objects, and can become even more complicated in plantation forests where trees share similar characteristics [32]. Some authors suggest using software tools to co-register point clouds based on key points [33] or the Iterative Closest Point (ICP) algorithm [140, 155, 172] in CloudCompare. The quality of the fused data depends on the forest conditions and the data characteristics, namely the number of terrestrial scans and distance of the scanners from the target [115, 173]. Another type of data-level fusion included LiDAR data fusion with spectral bands and indices, where spectral information was projected onto the point cloud [74, 113, 153] using, for example, CloudCompare [74] and FUSION software [113]. Reflective targets help the co-registration of terrestrial images and point clouds, enabling the merging of RGB pixel colors to point locations through co-registration [153].

Feature-level Fusion

A total of 78% of the papers performed feature-level fusion by merging post-classification outputs, rasterized LiDAR-derived products, extracted features, and spectral bands and indices to derive a final output. Feature-level fusion in this context can be broadly categorized into pixel-based fusion and object-based fusion [174]. Pixel-based fusion primarily occurs among airborne platforms and between airborne and satellite platforms, mostly combining LiDAR and spectral data. Many of these studies rasterized the LiDAR data to generate canopy height models (CHM) and digital terrain models (DTM) and layer-stacked these outputs with MS and HS bands as inputs for subsequent classification algorithms [28, 38, 54, 61, 149]. In most of these pixel-based fusion cases, the pre-processing takes place separately, after which they are combined. For example, hyperspectral data is processed in ENVI, while LiDAR data products are created separately. The combined data stack is then used for classifications often using machine learning methods [28]. Object-based fusion involves direct segmentation at both the individual tree scale and plot scale, followed by fusion based on various extracted features for the objects. For example, LiDAR data can be used to segment individual tree canopies, often using inverse watershed algorithms, and then features extracted from spectral data are added to those segments essentially creating a new vector-format data. The resulting spatial or vector format outputs were then used, for example, to classify tree species with machine learning methods [47, 66, 75, 102]. Most commonly, feature-level data fusion takes place in a coding environment, such as R packages to segment trees, or python for post-processing the datasets with machine learning algorithms. Readily available software solutions to process different types of data and combine the resulting features seem to be lagging behind.

Gains of LiDAR Data Fusion

To examine the gains that LiDAR data fusion brings for each of the application categories outlined above, we examined the studies that directly compared the performance of their methods with and without fusion.

Classification (Tree Species/Land Cover)

Species classification based exclusively on LiDAR data has proven effective in particular circumstances including when the set of species to be discriminated have contrasting silhouette or stature [45, 59] or when the segmentation addresses broad class separation between evergreen and deciduous species [34]. In our review, when a LiDAR dataset was compared to LiDAR fused with spectral information, overall classification accuracy increased by 41%, on average. Conversely, when they used fused datasets instead of spectral information alone, overall accuracy increased by a mere 10-14%. A few studies reported a beneficial effect of the combined use of LiDAR and spectral information by examining the importance of the various predictors in a Random Forest classification model [63]. Finally, in some cases, LiDAR only was used at the segmentation step to delineate tree crowns or stands [35, 66]. Vegetation height estimated from LiDAR data fused with MS and HS data enhances the overall accuracy of species classification [28]. However, this generally benefited object-level classification more than pixel-level classifications.

Growing Stock Volume and Biomass

Volume and/or AGB assessment requires structural and species information. While LiDAR data provide information about structure, fusion with optical data is often sought for species-specific estimates. Among the papers in this section, data fusion was performed mainly at the ITA (45%) and ABA (50%) levels, and much less at the landscape level (5%). Data fusion at tree-level mostly uses fusion of ground-based and airborne point clouds [77], addressing occlusion issues and enabling extraction of tree attributes such as DBH and total height with greater accuracy. For larger acquisitions in complex terrain, fusion of ULS, photogrammetric point clouds and MS images shows significant improvement in explained variance and error. For example, [75] fused

ULS and HS data at the individual tree level, increasing the R^2 from 0.75 to 0.89. In [81] (ABA), by fusing ALS and MS data, the authors reduced RMSE from 18.4% (LiDAR alone) and 19% (MS alone) to 16.8%. In [89] (ITA), by fusing RGB and MS data, the authors increased their R^2 from 0.77 to 0.81. Plot-level data fusion involved predominantly airborne or spaceborne data, which allowed larger scale assessment. While fusion with ALS mostly consists of combining continuous data over the area of interest [75, 88, 94, 95], applications with spaceborne data mostly consist of upscaling approaches [76, 81–83, 87]. In another study [94], fusing ALS and HS data increased R^2 from 0.81 to 0.87 for ITA and 0.65 to 0.84 for ABA. In [77] (ITA), the utilization of both TLS-based DBH and ULS-based tree height resulted in a reduced RMSE ranging from 8.6% to 12.7%. These RMSE values compare favorably to the RMSE values of 10.1% to 20.4% when exclusively using TLS and 30.3% to 76.9% when relying solely on ULS.

Forest Structure

The primary objective in fusing ground-based LiDAR with ULS and ALS data is to capitalize on the advantages of the ground-based LiDAR, which effectively capture the lower part of the trees, in combination with the strengths of airborne LiDAR, which accurately represent the crowns. In [26], fused TLS and ULS were used to measure tree height, crown projection area (CPA) and crown volume (CV). In estimating height, the RMSE with TLS and ULS alone was 0.30 m and 0.11 m, respectively, while the fused dataset RMSE was 0.05 m. In estimating CPA, the RMSE with TLS and ULS alone was 3.06 m^2 and 4.61 m^2, respectively, while the fused dataset RMSE was 0.46 m^2. Finally, for CV, the RMSE with TLS and ULS alone was 29.63 m^3 and 30.23 m^3, respectively, while the fused dataset RMSE was 8.30 m^3. Another study [32] that fused ground-based LiDAR and ULS observed significant R^2 improvements in tree height (9%), stem volume (5%), and crown volume estimates (18%). In [26, 33, 112, 115], there is a strong focus on co-registration issues before individual tree parameters were extracted. Furthermore, [33] achieved enhanced accuracy for DBH measurements through TLS and ULS data fusion: 2.1% compared to TLS alone and 20.7% compared to ULS alone for DBH. [113] fused ALS and MS data and reported improved R^2 when compared with ALS alone: quadratic mean diameter (from 0.5 to 0.64), basal area (from 0.53 to 0.73), tree height (from 0.92 to 0.94), stem density (from 0.29 to 0.30) and stand density index (from 0.72 to 0.82). Among the papers that use ALS and satellite data, [108] derive total volume and basal area by fusing LiDAR and topographic information (TI). Using LiDAR alone the R^2 is 0.67 for volume and 0.61 for basal area, while fusion with TI increased the R^2 to 0.74 and 0.69, respectively. MS-ALS-TI fusion increased the R^2 further to 0.85 and 0.84, respectively.

Tree Height

For tree height estimates, 50% of the papers focus on ITA, and 50% on ABA. For example, [126] spatial resolution of tree top height estimates was improved by fusing low-density ALS data with high resolution optical images by applying k-NN technique, which allowed tree height estimates for crowns that are not represented in the LiDAR data. In this paper, it is evident that a greater number of LiDAR points associated with tree crowns enhances the accuracy of tree top height estimation. With the fusion, they detected 97% of the total trees with an estimated tree-top mean absolute error of 2.45 m (measured error with LiDAR data alone was 3.70 m). In [122], the benefit of including LiDAR-derived topographic data for estimation of canopy heights from Tandem-X InSAR data is demonstrated. Furthermore, the use of the full-resolution DTM from Land, Vegetation, and Ice Sensor (LVIS) instead of the simulated GEDI DTM significantly decreased the RMSE from 4.6 m to 3.5 m, and the bias from 1.8 m to 1.3 m.

Segmentation

In a majority of the literature reviewed, data fusion was mainly used for single tree segmentation, using airborne data [135, 138, 143]. Segmentation challenges, especially for tree-level data, include georeferencing the data products and balancing data with different spatial resolution [138]. At the single-crown level, raw point clouds or point cloud-based metrics are easier to fuse than pixel-based information [139]. The results presented by [135] show a significant difference between fused data versus ALS alone: for low-density forests, the ITA method based on ALS alone correctly detects only 63% of trees, compared to 92% when fusing data from ALS and HS. For high-density forest, fusion detects 70% of the trees compared to 62% with ALS alone. In [137, 143], the authors fused ALS and MS data increasing their segmentation by 2-4% compared to ALS alone. In [138], fusion of ALS and HS increased their segmentation by 5% compared to single sensor accuracy.

Other

The 'other' applications included LiDAR data fusion studies focused on wetland/marsh areas, boreal forests and a natural disaster impact assessment [155, 156, 158]. For example, [158] fused airborne LiDAR with MS imagery to assess forest loss in a wetland zone. They document that forest/non-forest classification accuracy improved from 86-87% to 91-93%

demonstrating a small ~5% increase in accuracy due to the inclusion of LiDAR metrics. [155] demonstrated that their automatic ALS and TLS point cloud co-registration resulted in a denser point cloud, in which the stems and canopy of individual trees were better represented than in the single LiDAR datasets, but provided no quantitative improvement on retrieval of canopy/forest/tree information in a boreal forest. [156] developed a method to assess wind damage by fusing ALS and MS imagery. They conclude that adding the structural metrics from ALS to the spectral information provides estimates of structural damages that cannot be retrieved with spectral data alone.

Fuel Load

At a landscape-scale, multiple studies have documented that fusing ALS data with Landsat and Sentinel-2 satellite images improve total fuel estimates [168]. Specifically, [161] demonstrated that 24-32% of the remaining variability in surface fuels, uncharacterized by ALS data, can be explained by Landsat NDVI time-series. Furthermore, ALS data combined with Landsat time-series achieve both higher classification accuracy and lower prediction errors in post-fire snag classes, and shrub cover estimates [165]. Similarly, airborne MS image-derived NDVI metrics, when fused with ALS, further improved classification overall accuracy of the post-fire regeneration types at stand-scale by 10-50% [163]. Similar data fusion studies also predicted canopy fuel variables, such as canopy fuel load (kg/m^2), and surface fuel layers (including coarse woody debris biomass) with adjusted R^2 ranging between 0.55-0.94 [166]. At the ITA scale, post-fire changes in DBH and biomass can be estimated by fusing MLS data with ULS/ALS, where the below-canopy measurements are enabled by the MLS data [162]. However, a fusion of ALS and TLS data for ITA metrics was recently documented to offer no particular advantage over either sensor used alone [169].

Discussion

The information from the structured literature review was discussed by an international panel of experts in Leiden, the Netherlands, May 11-12, 2023. The panel consisted of 11 scientists with expertise across all LiDAR platforms and their fusion with other datasets across the full range of forestry applications.

What is 'Data Fusion' and How Should This Term Be Used?

Through the literature search, it became apparent that there was confusion regarding what should be considered data fusion. Specifically, we found that the terms 'data fusion', 'data combination' and 'data integration' are used in a confusing manner. For example, we recognize that there are studies that perform data-level or feature-level fusion without calling it as such, but instead commonly referring to it as data combination [175, 176], data registration [173] or data integration [177, 178]. However, we found that those terms are also commonly used for instances where data fusion as defined here is not actually appropriate. These include, for example, instances where one dataset is used to train a model that makes predictions based on another dataset, which would be considered calibration/validation studies [179–181]. We do find a few instances of those [118, 132] in our data-level and feature-level fusion examples, although there are very few of these cases.

Based on our literature review of papers that considered (multi-sensor) 'LiDAR data fusion', we define data- and feature-level data fusion as: *the merging of data or derived features from different sources, (instruments/devices) of which at least one is LiDAR, to improve the characteristics of the LiDAR dataset and/or enable enhanced forest observations.* The term 'data integration' can be reserved for decision-level data fusion, where datasets are only combined to come to a conclusion (decision), but they are not used to generate a new dataset or data product as inputs for classification etc [24, 182]. The term 'data combination' can be used to indicate the entire process that includes both data fusion starting at the pre-processing step through data integration at the decision-making step (Fig. 4).

It is important to note that we only focused on multi-source data fusion, while other instances of data fusion are ignored: multi-temporal data fusion (datasets repeatedly collected at different times with the same sensor), MS-LiDAR (MS data and LiDAR collected at the same time by the same instrument), and co-registration of data from the same instrument (e.g. strip adjustment of ALS data collection and co-registration of TLS point clouds acquired from various points of view to create a forest scene). These types of fusion, though beyond the scope of this review, can still be relevant for monitoring forest growth, species categorization, identifying tree locations and could be considered by practitioners.

What are the Most Important Lessons Learned About Data Fusion in Forest Observations?

Our review indicates that all common applications are improved using data fusion. Single tree *segmentation* can be improved by fusing spectral or 2.5D structural information from LiDAR data, especially in low-density forests. Results obtained with canopy height model for ITA were slightly improved when LiDAR data is fused with MS images. This application is likely to be more relevant at a local scale, where detailed information about individual trees is required. In

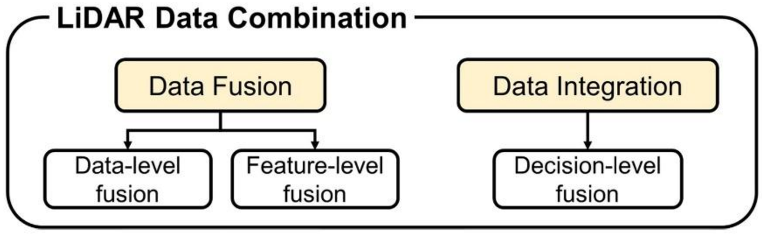

Fig. 4 Proposed conceptual framework defining data fusion, data integration, and data combination, which are ambiguously used in the literature

growing stock volume or above-ground biomass assessments, data fusion can improve model performance by improving tree species classification. These applications can be relevant at local to regional scales. The use of airborne and spaceborne data fusion expands the study areas to larger extents. *Tree height or canopy height* are correctly detected by LiDAR data alone, and there is no real need for LiDAR data fusion for further improvements, but data fusion can extend the spatial and temporal resolution of derived data products. LiDAR data fusion with spectral information, such as MS or HS data, improves *tree species classification* accuracy compared to using LiDAR data alone. While LiDAR alone can be effective in certain circumstances, combining LiDAR with spectral information enhances the accuracy of species classification models significantly. Fusion of ground-based LiDAR data with airborne LiDAR data improves the assessment of *forest structure* parameters, including tree density, crown diameter, stem density and stand volume. Fusion of ground-based and airborne LiDAR data allows the combination of strengths from both sources, capturing information above and below the canopy layer. LiDAR data fusion for *fuel load estimation* has been used for characterizing canopy and surface fuels. At a landscape scale, fusing LiDAR data with MS images enhances the total fuel estimates, classification accuracy of post-fire snag classes and prediction of canopy fuel variables. In summary, data fusion can further improve the accuracy of a resulting data product or application, and it can improve the spatial and/or temporal resolution of such data products, providing valuable information for practitioners. We note, though, that a lot of these gains are marginal. Therefore, it is important to further discuss the operationalization of these methods.

What are the Main Challenges in Data Fusion for Operational Applications?

We identified several challenges with operationalizing data fusion approaches. One fundamental challenge arises from the utilization of two distinct RS datasets to develop a particular solution. This necessitates acquiring multiple datasets, thereby increasing the overall cost, especially when combining data from independent acquisition platforms, such as ALS and HS data, or when dealing with large spatial extents. Although there are airborne systems available that allow simultaneous data collection from multiple sensors (e.g. LiDAR and MS image), data providers must subsequently process the acquired data, leading to additional costs. Data fusion is also a major challenge for the data user, as the effort required to process two or more RS datasets increases significantly. Consequently, separate processing steps must be developed for each dataset, increasing the overall processing time. Additionally, each step must be individually evaluated and quality-checked. To expedite processing, greater computing power becomes essential, which may be difficult to achieve, especially in practical applications. Moreover, the data processing demands specific expertise to ensure methodological correctness. Analysts may need to possess additional skills or collaborate with domain specialists to execute the analysis accurately. Both the processing time and the additional equipment and expertise required increase the cost of the analyses and can be a barrier. Another big challenge in data fusion is related to the data itself. Different data sources may have differences in resolution, accuracy, spatial or temporal coverage, which can affect the effectiveness of fusion techniques. If the quality of the data is low or the fusion process is not optimized, it might not add substantial benefits or may introduce additional uncertainties. A prevalent challenge in RS applications is the significant time lag between data collection (e.g., aerial flights) and the delivery of processed results to end users. The larger the surveyed area and the number of datasets fused, the longer it takes. IT also requires more validation and more rigorous accuracy assessment, which often reveals further deficiencies and errors that need to be addressed. This delay in information provision may render the data obsolete or limit its effectiveness in addressing situations with rapidly changing events, such as insect outbreaks or areas impacted by severe wind/fire damage.

What are the Priorities in Moving Data Fusion Forward?

We find that the RS community can further advance LiDAR data fusion enabling a wider range of applications from environmental monitoring and resource management to disaster responses. Several key areas should be a priority in propelling the applications and methodologies of LiDAR data fusion forward. First, our structured review shows that more studies on LiDAR data fusion are needed in the southern hemisphere to better understand the limitations and advantages of such applications in the extensive rainforests in the global south, which have been relatively underexplored compared to the northern hemisphere. The underrepresentation from the global south has important implications because these regions include a large majority of the tropical forests, where LiDAR fusion may have many benefits. For example, tropical forests typically include tall trees with several middle and understory layers of dense canopies, where TLS data fused with ALS data could fully characterize the forest structure. Secondly, even though improvements using data fusion for a variety of applications have been reported, compared to using LiDAR data alone, it is yet unclear to what extent these could be operationalized in a forestry setting. More information is required to properly balance the costs of additional data collection and processing, and the required expertise versus the benefits in accuracy or spatial and temporal resolution. Common data formats with metadata standards need to be established to develop interoperable algorithms among researchers to facilitate collaborations. As an example, variables that can be extracted from ALS point clouds are infinite and standardizing these variables is always a challenge. In [183], the authors suggested a list of 10 standard variables within 3 main classes (height, vertical variability, and cover) as a starting point to characterize the vegetation structure. Moreover, in [184], the authors recommend metrics such as the skewness or kurtosis or the coefficient of variation of vegetation height to describe vegetation structures. Both papers proposed that the data be made available in raster format to standardize subsequent studies or operations. Addressing sensor-specific biases, radiometric differences, and geometric distortions across different data sources is essential to harmonize fused datasets effectively. Moreover, it is necessary to develop robust methods to quantify and address uncertainties in data fusion processes, which will boost confidence in the final products. A rigorous validation and benchmarking of data fusion approaches with ground-based accuracy assessment and independent datasets are crucial. Finally, LiDAR data fusion studies should promote open data initiatives and foster collaboration among researchers, institutions, and data providers. This would facilitate access to diverse datasets and accelerate data fusion research, which will further enable data fusion methods and solutions that can operate in real-time especially for applications requiring quick and up-to-date information.

Conclusion

This paper presents a comprehensive review of LiDAR data fusion research for forest observations over the last decade. Our structured review indicates that there has been a slight upward trend in the number of publications on LiDAR data fusion for forestry observations and aerial platforms (both UAVs and airborne platforms) continue to be the most widely used option. We conclude that multi-sensor LiDAR data fusion has the potential to improve forest observations in a great variety of applications. Our team suggests a clear definition of the term "data fusion" to avoid confusion among the commonly used terms 'data fusion', 'data combination', and 'data integration'. The review further highlights that data fusion poses several challenges, including costs, computational effort, and processing times, variability in data quality, spatial resolution, and a need for specialized expertise. Therefore, practitioners must carefully weigh the potential benefits of LiDAR data fusion in relation to the actual need for such benefits and the accompanying cost.

Acknowledgements This article is based upon work from COST Action CA20118, supported by COST (European Cooperation in Science and Technology). Liang, X. would like to acknowledge the financial supports from the Natural Science Fund of China (32171789). Cabo, C. would like to acknowledge the support of the UK NERC project [NE/T001194/1]: 'Advancing 3D Fuel Mapping for Wildfire Behaviour and Risk Mitigation Modelling' and the Spanish Knowledge Generation project [PID2021-126790NB-I00]: 'Advancing carbon emission estimations from wildfires applying artificial intelligence to 3D terrestrial point clouds'

Author Contributions Conceptualization: H.M., M.S., B.M.; Data curation: M.S., B.M.; Formal analysis: M.S., B.M.; Funding acquisition: M.M., H.M., M.S.; Investigation: M.S., B.M.; Methodology: M.S., B.M.; Project administration: M.M, H.M.; Supervision: H.M., M.S.; Validation: H.M., M.S., B.M.; Visualization: B.M., S.T.; Writing - original draft: B.M., M.S., S.T., L.X., M.M, P.X., S.A., S.K., V.C., V.G., H.M. and Writing - review & editing: B.M., M.S., S.T., L.X., M.M, P.X., S.A., S.K., V.C., V.G., H.M., C.C.

Funding This work was supported by the COST Action 3DForEcoTech (CA20118). Natural Science Fund of China (32171789). UK NERC (NE/T001194/1). Spanish Knowledge Generation project (PID2021-126790NB-100).

Data Availability No datasets were generated or analysed during the current study.

Declarations

Human and Animal Rights and Informed Consent This article does not contain any studies with human or animal subjects performed by any of the authors.

Competing interests The authors declare no competing interests.

References

1. Franklin JF, Spies TA, Van Pelt R, et al. Disturbances and structural development of natural forest ecosystems with silvicultural implications, using Douglas-fir forests as an example. For Ecol Manag. 2002;155:399–423.
2. Wulder MA, White JC, Nelson RF, Næsset E, Ørka HO, Coops NC, Hilker T, Bater CW, Gobakken T. Lidar sampling for large-area forest characterization: a review. Remote Sens Environ. 2012;121:196–209.
3. Dassot M, Constant T, Fournier M. The use of terrestrial LiDAR technology in forest science: application fields, benefits and challenges. Ann For Sci. 2011;68:959–74.
4. Lim K, Treitz P, Wulder M, St-Onge B, Flood M. LiDAR remote sensing of forest structure. Prog Phys Geogr Earth Environ. 2003;27:88–106.
5. Dubayah RO, Drake JB. Lidar remote sensing for forestry. J For. 2000;98:44–6.
6. Simard M, Pinto N, Fisher JB, Baccini A. Mapping forest canopy height globally with spaceborne lidar. J Geophys Res Biogeosci. 2011; https://doi.org/10.1029/2011JG001708.
7. Dubayah R, Blair JB, Goetz S, et al. The global ecosystem dynamics investigation: High-resolution laser ranging of the Earth's forests and topography. Sci Remote Sens. 2020;1:100002.
8. Tang H, Dubayah R, Brolly M, Ganguly S, Zhang G. Large-scale retrieval of leaf area index and vertical foliage profile from the spaceborne waveform lidar (GLAS/ICESat). Remote Sens Environ. 2014;154:8–18.
9. Di Stefano F, Chiappini S, Gorreja A, Balestra M, Pierdicca R. Mobile 3D scan LiDAR: a literature review. Geomatics, Nat Hazards Risk. 2021;12:2387–429.
10. Kellner JR, Armston J, Birrer M, et al. New opportunities for forest remote sensing through ultra-high-density drone lidar. Surv Geophys. 2019;40:959–77.
11. Moran CJ, Kane VR, Seielstad CA. Mapping forest canopy fuels in thewestern united states with LiDAR-Landsat covariance. Remote Sens. 2020;12:1–37.
12. Narine LL, Popescu SC, Malambo L. Using ICESat-2 to estimate and map forest aboveground biomass: a first example. Remote Sens. 2020;12:1–16.
13. Nath B, Ni-Meister W. The interplay between canopy structure and topography and its impacts on seasonal variations in surface reflectance patterns in the boreal region of alaska—implications for surface radiation budget. Remote Sens. 2021; https://doi.org/10.3390/rs13163108.
14. Wallace L, Lucieer A, Watson C, Turner D. Development of a UAV-LiDAR system with application to forest inventory. Remote Sens. 2012;4:1519–43.
15. Duncanson L, Kellner JR, Armston J, et al. Aboveground biomass density models for NASA's Global Ecosystem Dynamics Investigation (GEDI) lidar mission. Remote Sens Environ. 2022; https://doi.org/10.1016/j.rse.2021.112845.
16. Simonson WD, Allen HD, Coomes DA. Applications of airborne lidar for the assessment of animal species diversity. Methods Ecol Evol. 2014;5:719–29.
17. Marselis SM, Abernethy K, Alonso A, et al. Evaluating the potential of full-waveform lidar for mapping pan-tropical tree species richness. Glob Ecol Biogeogr. 2020;29:1799–816.
18. Andersen HE, McGaughey RJ, Reutebuch SE. Estimating forest canopy fuel parameters using LIDAR data. Remote Sens Environ. 2005;94:441–9.
19. Balestra M, Tonelli E, Vitali A, Urbinati C, Frontoni E, Pierdicca R. Geomatic Data Fusion for 3D Tree Modeling: The Case Study of Monumental Chestnut Trees. Remote Sens. 2023; https://doi.org/10.3390/rs15082197.
20. Calders K, Adams J, Armston J, et al. Terrestrial laser scanning in forest ecology: Expanding the horizon. Remote Sens Environ. 2020;251:112102.
21. Liang X, Hyyppä J, Kaartinen H, Lehtomäki M, Pyörälä J, Pfeifer N, Holopainen M, Brolly G, Francesco P, Hackenberg J. International benchmarking of terrestrial laser scanning approaches for forest inventories. ISPRS J Photogramm Remote Sens. 2018;144:137–79.
22. Windrim L, Bryson M. Detection, segmentation, and model fitting of individual tree stems from airborne laser scanning of forests using deep learning. Remote Sens. 2020; https://doi.org/10.3390/RS12091469.
23. Schmitt M, Zhu XX. Data Fusion and Remote Sensing: an ever-growing relationship. IEEE Geosci Remote Sens Mag. 2016;4:6–23.
24. Zhang J. Multi-source remote sensing data fusion: status and trends. Int J Image Data Fusion. 2010;1:5–24.
25. Ghamisi P, Rasti B, Yokoya N, Wang Q, Hofle B, Bruzzone L, Bovolo F, Chi M, Anders K, Gloaguen R. Multisource and multitemporal data fusion in remote sensing: A comprehensive review of the state of the art. IEEE Geosci Remote Sens Mag. 2019;7:6–39.
26. Terryn L, Calders K, Bartholomeus H, et al. Quantifying tropical forest structure through terrestrial and UAV laser scanning fusion in Australian rainforests. Remote Sens Environ. 2022; https://doi.org/10.1016/j.rse.2022.112912.
27. Alonzo M, Bookhagen B, Roberts DA. Urban tree species mapping using hyperspectral and lidar data fusion. Remote Sens Environ. 2014;148:70–83.
28. Sankey T, Donager J, McVay J, Sankey JB. UAV lidar and hyperspectral fusion for forest monitoring in the southwestern USA. Remote Sens Environ. 2017;195:30–43.
29. Liberati A, Altman DG, Tetzlaff J, Mulrow C, Gøtzsche PC, Ioannidis JPA, Clarke M, Devereaux PJ, Kleijnen J, Moher D. The PRISMA statement for reporting systematic reviews and meta-analyses of studies that evaluate health care interventions: explanation and elaboration. Ann Intern Med. 2009;151:W-65–94.
30. Page MJ, McKenzie JE, Bossuyt PM, et al. The PRISMA 2020 statement: an updated guideline for reporting systematic reviews. Syst Rev. 2021;10:1–11.
31. Joyce KE, Nakalembe CL, Gómez C, Suresh G, Fickas K, Halabisky M, Kalamandeen M, Crowley MA. Discovering inclusivity in remote sensing: leaving no one behind. Front Remote Sens. 2022;3:1–6.
32. Fekry R, Yao W, Cao L, Shen X. Ground-based/UAV-LiDAR data fusion for quantitative structure modeling and tree parameter retrieval in subtropical planted forest. For Ecosyst. 2022;9:100065.
33. Panagiotidis D, Abdollahnejad A, Slavík M. 3D point cloud fusion from UAV and TLS to assess temperate managed forest structures. Int J Appl Earth Obs Geoinf. 2022;112:102917.
34. Hell M, Brandmeier M, Briechle S, Krzystek P. Classification of tree species and standing dead trees with lidar point clouds using two deep neural networks: PointCNN and 3DmFV-Net. PFG - J Photogramm Remote Sens Geoinf Sci. 2022;90:103–21.
35. Dutta D, Wang K, Lee E, Goodwell A, Woo DK, Wagner D, Kumar P. Characterizing vegetation canopy structure using airborne remote sensing data. IEEE Trans Geosci Remote Sens. 2017;55:1160–78.
36. Ruiz LÁ, Recio JA, Crespo-Peremarch P, Sapena M. An object-based approach for mapping forest structural types based on low-density LiDAR and multispectral imagery. Geocarto Int. 2018;33:443–57.
37. Sun Y, Xin Q, Huang J, Huang B, Zhang H. Characterizing tree species of a tropical wetland in Southern China at the individual

tree level based on convolutional neural network. IEEE J Sel Top Appl Earth Obs Remote Sens. 2019;12:4415–25.
38. Norton CL, Hartfield K, Collins CDH, van Leeuwen WJD, Metz LJ. Multi-temporal LiDAR and hyperspectral data fusion for classification of semi-arid woody cover species. Remote Sens. 2022; https://doi.org/10.3390/rs14122896.
39. Wernicke J, Seltmann CT, Wenzel R, Becker C, Körner M. Forest canopy stratification based on fused, imbalanced and collinear LiDAR and Sentinel-2 metrics. Remote Sens Environ. 2022; https://doi.org/10.1016/j.rse.2022.113134.
40. Hartling S, Sagan V, Maimaitijiang M. Urban tree species classification using UAV-based multi-sensor data fusion and machine learning. GIScience Remote Sens. 2021;58:1250–75.
41. Dash JP, Pearse GD, Watt MS, Paul T. Combining airborne laser scanning and aerial imagery enhances echo classification for invasive conifer detection. Remote Sens. 2017; https://doi.org/10.3390/rs9020156.
42. Onojeghuo AO, Onojeghuo AR. Object-based habitat mapping using very high spatial resolution multispectral and hyperspectral imagery with LiDAR data. Int J Appl Earth Obs Geoinf. 2017;59:79–91.
43. Yadav BKV, Lucieer A, Baker SC, Jordan GJ. Tree crown segmentation and species classification in a wet eucalypt forest from airborne hyperspectral and LiDAR data. Int J Remote Sens. 2021;42:7952–77.
44. Dechesne C, Mallet C, Le Bris A, Gouet-Brunet V. Semantic segmentation of forest stands of pure species combining airborne lidar data and very high resolution multispectral imagery. ISPRS J Photogramm Remote Sens. 2017;126:129–45.
45. Briechle S, Krzystek P, Vosselman G. Silvi-Net – A dual-CNN approach for combined classification of tree species and standing dead trees from remote sensing data. Int J Appl Earth Obs Geoinf. 2021;98:102292.
46. Yang J, Jones T, Caspersen J, He Y. Object-based canopy gap segmentation and classification: Quantifying the pros and cons of integrating optical and LiDAR data. Remote Sens. 2015;7:15917–32.
47. Plakman V, Janssen T, Brouwer N, Veraverbeke S. Mapping species at an individual-tree scale in a temperate forest, using sentinel-2 images, airborne laser scanning data, and random forest classification. Remote Sens. 2020;12:1–25.
48. Bigdeli B, Samadzadegan F, Reinartz P. Feature grouping-based multiple fuzzy classifier system for fusion of hyperspectral and LIDAR data. J Appl Remote Sens. 2014;8:083509.
49. Bigdeli B, Samadzadegan F, Reinartz P. Fusion of hyperspectral and LIDAR data using decision template-based fuzzy multiple classifier system. Int J Appl Earth Obs Geoinf. 2015;38:309–20.
50. Wu Q, Zhong R, Zhao W, Song K, Du L. Land-cover classification using GF-2 images and airborne lidar data based on Random Forest. Int J Remote Sens. 2019;40:2410–26.
51. Pervin R, Robeson SM, MacBean N. Fusion of airborne hyperspectral and LiDAR canopy-height data for estimating fractional cover of tall woody plants, herbaceous vegetation, and other soil cover types in a semi-arid savanna ecosystem. Int J Remote Sens. 2022;43:3890–926.
52. Dashti H, Poley A, Glenn NF, Ilangakoon N, Spaete L, Roberts D, Enterkine J, Flores AN, Ustin SL, Mitchell JJ. Regional scale dryland vegetation classification with an integrated lidar-hyperspectral approach. Remote Sens. 2019; https://doi.org/10.3390/rs11182141.
53. Su Y, Guo Q, Fry DL, Collins BM, Kelly M, Flanagan JP, Battles JJ. A vegetation mapping strategy for conifer forests by combining airborne LiDAR data and aerial imagery. Can J Remote Sens. 2016;42:1–15.
54. Hall EC, Lara MJ. Multisensor UAS mapping of plant species and plant functional Types in Midwestern Grasslands. Remote Sens. 2022; https://doi.org/10.3390/rs14143453.
55. Tong X, Li X, Xu X, Xie H, Feng T, Sun T, Jin Y, Liu X. A two-phase classification of urban vegetation using airborne LiDAR data and aerial photography. IEEE J Sel Top Appl Earth Obs Remote Sens. 2014;7:4153–66.
56. Jin H, Mountrakis G. Fusion of optical, radar and waveform LiDAR observations for land cover classification. ISPRS J Photogramm Remote Sens. 2022;187:171–90.
57. Torabzadeh H, Leiterer R, Hueni A, Schaepman ME, Morsdorf F. Tree species classification in a temperate mixed forest using a combination of imaging spectroscopy and airborne laser scanning. Agric For Meteorol. 2019;279:107744.
58. Esteban J, Fernández-Landa A, Tomé JL, Gómez C, Marchamalo M. Identification of silvicultural practices in mediterranean forests integrating landsat time series and a single coverage of als data. Remote Sens. 2021; https://doi.org/10.3390/rs13183611.
59. Trouvé R, Jiang R, Fedrigo M, White MD, Kasel S, Baker PJ, Nitschke CR. Combining environmental, multispectral, and LiDAR data improves forest type classification: a case study on mapping cool temperate rainforests and mixed forests. Remote Sens. 2023; https://doi.org/10.3390/rs15010060.
60. Kloiber SM, Macleod RD, Smith AJ, Knight JF, Huberty BJ. A semi-automated, multi-source data fusion update of a Wetland inventory for East-Central Minnesota, USA. Wetlands. 2015;35:335–48.
61. Sankey TT, McVay J, Swetnam TL, McClaran MP, Heilman P, Nichols M. UAV hyperspectral and lidar data and their fusion for arid and semi-arid land vegetation monitoring. Remote Sens Ecol Conserv. 2018;4:20–33.
62. Szostak M, Knapik K, Węzyk P, Likus-Cieślik J, Pietrzykowski M. Fusing Sentinel-2 imagery and ALS point clouds for defining LULC changes on reclaimed areas by afforestation. Sustain. 2019; https://doi.org/10.3390/su11051251.
63. Sun C, Cao S, Sanchez-Azofeifa GA. Mapping tropical dry forest age using airborne waveform LiDAR and hyperspectral metrics. Int J Appl Earth Obs Geoinf. 2019;83:101908.
64. Wan H, Tang Y, Jing L, Li H, Qiu F, Wu W. Tree species classification of forest stands using multisource remote sensing data. Remote Sens. 2021;13:1–24.
65. Parra A, Greenberg JA. Estimation of fractional plant lifeform cover for the conterminous United States using Landsat imagery and airborne LiDAR. IEEE Trans Geosci Remote Sens. 2022;60:1–14.
66. Zhang Z, Kazakova A, Moskal LM, Styers DM. Object-based tree species classification in urban ecosystems using LiDAR and hyperspectral data. Forests. 2016;7:1–16.
67. Tian X, Zhang X, Wu Y. Classification of planted forest species in southern China with airborne hyperspectral and LiDAR data. J For Res. 2020;25:369–78.
68. Feng B, Zheng C, Zhang W, Wang L, Yue C. Analyzing the role of spatial features when cooperating hyperspectral and LiDAR data for the tree species classification in a subtropical plantation forest area. J Appl Remote Sens. 2020;14:22213.
69. Verlič A, Đurić N, Kokalj Ž, Marsetič A, Simončič P, Oštir K. Tree species classification using worldview-2 satellite images and laser scanning data in a natural urban forest. Sumar List. 2014;138:477–88.
70. Szostak M, Pietrzykowski M, Likus-Cieslik J. Reclaimed area land cover mapping using Sentinel-2 imagery and LiDAR point clouds. Remote Sens. 2020; https://doi.org/10.3390/rs12020261.
71. Tang J, Liang J, Yang Y, Zhang S, Hou H, Zhu X. Revealing the structure and composition of the restored vegetation cover in semi-arid mine dumps based on LiDAR and hyperspectral images. Remote Sens. 2022; https://doi.org/10.3390/rs14040978.
72. Zhong H, Lin W, Liu H, Ma N, Liu K, Cao R, Wang T, Ren Z. Identification of tree species based on the fusion of UAV

hyperspectral image and LiDAR data in a coniferous and broad-leaved mixed forest in Northeast China. Front Plant Sci. 2022; https://doi.org/10.3389/fpls.2022.964769.
73. Fragoso-Campón L, Quirós E, Mora J, Gutiérrez Gallego JA, Durán-Barroso P. Overstory-understory land cover mapping at the watershed scale: accuracy enhancement by multitemporal remote sensing analysis and LiDAR. Environ Sci Pollut Res. 2020;27:75–88.
74. Lian X, Zhang H, Xiao W, Lei Y, Ge L, Qin K, He Y, Dong Q, Li L, Han Y. Biomass calculations of individual trees based on unmanned aerial vehicle multispectral imagery and laser scanning combined with terrestrial laser scanning in complex stands. Remote Sens. 2022;14:4715.
75. Qin H, Zhou W, Yao Y, Wang W. Estimating aboveground carbon stock at the scale of individual trees in subtropical forests using UAV LiDAR and hyperspectral data. Remote Sens. 2021;13:4969.
76. Chen A, Wang X, Zhang M, Guo J, Xing X, Yang D, Zhang H, Hou Z, Jia Z, Yang X. Fusion of LiDAR and multispectral data for aboveground biomass estimation in Mountain Grassland. Remote Sens. 2023;15:1–18.
77. Wang Y, Pyörälä J, Liang X, Lehtomäki M, Kukko A, Yu X, Kaartinen H, Hyyppä J. In situ biomass estimation at tree and plot levels: What did data record and what did algorithms derive from terrestrial and aerial point clouds in boreal forest. Remote Sens Environ. 2019;232:111309.
78. Fatoyinbo T, Armston J, Simard M, et al. The NASA AfriSAR campaign: Airborne SAR and lidar measurements of tropical forest structure and biomass in support of current and future space missions. Remote Sens Environ. 2021; https://doi.org/10.1016/j.rse.2021.112533.
79. Dalponte M, Frizzera L, Ørka HO, Gobakken T, Næsset E, Gianelle D. Predicting stem diameters and aboveground biomass of individual trees using remote sensing data. Ecol Indic. 2018;85:367–76.
80. Qi W, Saarela S, Armston J, Ståhl G, Dubayah R. Forest biomass estimation over three distinct forest types using TanDEM-X InSAR data and simulated GEDI lidar data. Remote Sens Environ. 2019;232:111283.
81. Ediriweera S, Pathirana S, Danaher T, Nichols D. Estimating above-ground biomass by fusion of LiDAR and multispectral data in subtropical woody plant communities in topographically complex terrain in North-eastern Australia. J For Res. 2014;25:761–71.
82. Campbell MJ, Dennison PE, Kerr KL, Brewer SC, Anderegg WRL. Scaled biomass estimation in woodland ecosystems: testing the individual and combined capacities of satellite multispectral and lidar data. Remote Sens Environ. 2021;262:112511.
83. Xi X, Han T, Wang C, Luo S, Xia S, Pan F. Forest above ground biomass inversion by fusing GLAS with optical remote sensing data. ISPRS Int J Geo-Information. 2016; https://doi.org/10.3390/ijgi5040045.
84. Chi H, Sun G, Huang J, Li R, Ren X, Ni W, Fu A. Estimation of forest aboveground biomass in Changbai Mountain region using ICESat/GLAS and Landsat/TM data. Remote Sens. 2017; https://doi.org/10.3390/rs9070707.
85. Hernando A, Puerto L, Mola-Yudego B, Manzanera JA, García-Abril A, Maltamo M, Valbuena R. Estimation of forest biomass components using airborne lidar and multispectral sensors. IForest. 2019;12:207–13.
86. de Almeida DRA, Broadbent EN, Ferreira MP, et al. Monitoring restored tropical forest diversity and structure through UAV-borne hyperspectral and lidar fusion. Remote Sens Environ. 2021; https://doi.org/10.1016/j.rse.2021.112582.
87. Shendryk Y. Fusing GEDI with earth observation data for large area aboveground biomass mapping. Int J Appl Earth Obs Geoinf. 2022;115:103108.
88. Gao L, Chai G, Zhang X. Above-ground biomass estimation of plantation with different tree species using airborne LiDAR and hyperspectral data. Remote Sens. 2022;14:1–18.
89. Huang R, Yao W, Xu Z, Cao L, Shen X. Information fusion approach for biomass estimation in a plateau mountainous forest using a synergistic system comprising UAS-based digital camera and LiDAR. Comput Electron Agric. 2022; https://doi.org/10.1016/j.compag.2022.107420.
90. Wang M, Im J, Zhao Y, Zhen Z. Multi-platform LiDAR for non-destructive individual aboveground biomass estimation for Changbai Larch (Larix olgensis Henry) using a hierarchical bayesian approach. Remote Sens. 2022; https://doi.org/10.3390/rs14174361.
91. Jiao Y, Wang D, Yao X, Wang S, Chi T, Meng Y. Forest emissions reduction assessment using optical satellite imagery and space LiDAR fusion for carbon stock estimation. Remote Sens. 2023;15:1–16.
92. Schreyer J, Tigges J, Lakes T, Churkina G. Using airborne LiDAR and QuickBird data for modelling urban tree carbon storage and its distribution-a case study of Berlin. Remote Sens. 2014;6:10636–55.
93. Benson ML, Pierce L, Bergen K, Sarabandi K. Model-based estimation of forest canopy height and biomass in the Canadian Boreal forest using radar, LiDAR, and optical remote sensing. IEEE Trans Geosci Remote Sens. 2021;59:4635–53.
94. Brovkina O, Novotny J, Cienciala E, Zemek F, Russ R. Mapping forest aboveground biomass using airborne hyperspectral and LiDAR data in the mountainous conditions of Central Europe. Ecol Eng. 2017;100:219–30.
95. Yan M, Xia Y, Yang X, Wu X, Yang M, Wang C, Hou Y, Wang D. Biomass estimation of subtropical arboreal forest at single tree scale based on feature fusion of Airborne LiDAR data and aerial images. Sustainability. 2023;15:1676.
96. Zhao Y, Ma Y, Quackenbush LJ, Zhen Z. Estimation of individual tree biomass in natural secondary forests based on ALS data and WorldView-3 imagery. Remote Sens. 2022; https://doi.org/10.3390/rs14020271.
97. Li S, Quackenbush LJ, Im J. Airborne lidar sampling strategies to enhance forest aboveground biomass estimation from Landsat imagery. Remote Sens. 2019; https://doi.org/10.3390/rs11161906.
98. Dhanda P, Nandy S, Kushwaha SPS, Ghosh S, Murthy YVNK, Dadhwal VK. Optimizing spaceborne LiDAR and very high resolution optical sensor parameters for biomass estimation at ICESat/GLAS footprint level using regression algorithms. Prog Phys Geogr Earth Environ. 2017;41:247–67.
99. Hardiman BS, Gough CM, Butnor JR, Bohrer G, Detto M, Curtis PS. Coupling fine-scale root and canopy structure using ground-based remote sensing. Remote Sens. 2017;9:1–13.
100. Pyörälä J, Saarinen N, Kankare V, Coops NC, Liang X, Wang Y, Holopainen M, Hyyppä J, Vastaranta M. Variability of wood properties using airborne and terrestrial laser scanning. Remote Sens Environ. 2019;235:111474.
101. Shamsoddini A, Trinder JC, Turner R. Paired-data fusion for improved estimation of pine plantation structure. Int J Remote Sens. 2015;36:1995–2009.
102. Kandare K, Dalponte M, Ørka HO, Frizzera L, Næsset E. Prediction of species-specific volume using different inventory approaches by fusing airborne laser scanning and hyperspectral data. Remote Sens. 2017;9:1–19.
103. Maack J, Lingenfelder M, Weinacker H, Koch B. Modelling the standing timber volume of Baden-Württemberg—a large-scale approach using a fusion of Landsat, airborne LiDAR and

National Forest inventory data. Int J Appl Earth Obs Geoinf. 2016;49:107–16.
104. Terryn L, Calders K, Bartholomeus H, et al. Quantifying tropical forest structure through terrestrial and UAV laser scanning fusion in Australian rainforests. Remote Sens Environ. 2022; https://doi.org/10.1016/j.rse.2022.112912.
105. Mohammadi J, Shataee S, Namiranian M, Næsset E. Modeling biophysical properties of broad-leaved stands in the hyrcanian forests of Iran using fused airborne laser scanner data and ultraCam-D images. Int J Appl Earth Obs Geoinf. 2017;61:32–45.
106. Lang M, Gulbe L, Traškovs A, Stepčenko A. Assessment of different estimation algorithms and remote sensing data sources for regional level wood volume mapping in hemiboreal mixed forests. Balt For. 2016;22:283–96.
107. Zhu Y, Jeon S, Sung H, Kim Y, Park C, Cha S, Jo HW, Lee WK. Developing uav-based forest spatial information and evaluation technology for efficient forest management. Sustain. 2020;12:1–17.
108. Lahssini K, Teste F, Dayal KR, Durrieu S, Ienco D, Monnet JM. Combining LiDAR metrics and sentinel-2 imagery to estimate basal area and wood volume in complex forest environment via neural networks. IEEE J Sel Top Appl Earth Obs Remote Sens. 2022;15:4337–48.
109. Hawryło P, Wezyk P. Predicting growing stock volume of scots pine stands using Sentinel-2 satellite imagery and airborne image-derived point clouds. Forests. 2018; https://doi.org/10.3390/f9050274.
110. Gao S, Zhang Z, Cao L. Individual tree structural parameter extraction and volume table creation based on near-field lidar data: a case study in a subtropical planted forest. Sensors. 2021; https://doi.org/10.3390/s21238162.
111. Manzanera JA, García-Abril A, Pascual C, Tejera R, Martín-Fernández S, Tokola T, Valbuena R. Fusion of airborne LiDAR and multispectral sensors reveals synergic capabilities in forest structure characterization. GIScience Remote Sens. 2016;53:723–38.
112. Qi Y, Coops NC, Daniels LD, Butson CR. Comparing tree attributes derived from quantitative structure models based on drone and mobile laser scanning point clouds across varying canopy cover conditions. ISPRS J Photogramm Remote Sens. 2022;192:49–65.
113. Valbuena R, Hernando A, Manzanera JA, Martínez-Falero E, García-Abril A, Mola-Yudego B. Most similar neighbor imputation of forest attributes using metrics derived from combined airborne LIDAR and multispectral sensors. Int J Digit Earth. 2018;11:1205–18.
114. Apostol B, Petrila M, Lorenţ A, Ciceu A, Gancz V, Badea O. Species discrimination and individual tree detection for predicting main dendrometric characteristics in mixed temperate forests by use of airborne laser scanning and ultra-high-resolution imagery. Sci Total Environ. 2020;698:134074.
115. Paris C, Kelbe D, Van Aardt J, Bruzzone L. A novel automatic method for the fusion of ALS and TLS LiDAR data for robust assessment of tree crown structure. IEEE Trans Geosci Remote Sens. 2017;55:3679–93.
116. Su Y, Ma Q, Guo Q. Fine-resolution forest tree height estimation across the Sierra Nevada through the integration of spaceborne LiDAR, airborne LiDAR, and optical imagery. Int J Digit Earth. 2017;10:307–23.
117. Wang Q, Ni-Meister W. Forest canopy height and gaps from multiangular BRDF, assessed with Airborne LiDAR Data (Short Title: Vegetation Structure from LiDAR and Multiangular Data). Remote Sens. 2019; https://doi.org/10.3390/rs11212566.
118. Denbina M, Simard M, Hawkins B. Forest height estimation using multibaseline PolInSAR and sparse lidar data fusion. IEEE J Sel Top Appl Earth Obs Remote Sens. 2018;11:3415–33.
119. Qi W, Lee SK, Hancock S, Luthcke S, Tang H, Armston J, Dubayah R. Improved forest height estimation by fusion of simulated GEDI Lidar data and TanDEM-X InSAR data. Remote Sens Environ. 2019;221:621–34.
120. Lee WJ, Lee CW. Forest canopy height estimation using multiplatform remote sensing dataset. J Sensors. 2018; https://doi.org/10.1155/2018/1593129.
121. Xie Y, Fu H, Zhu J, Wang C, Xie Q. A LiDAR-Aided multibaseline PolInSAR method for forest height estimation: with emphasis on dual-baseline selection. IEEE Geosci Remote Sens Lett. 2020;17:1807–11.
122. Qi W, Dubayah RO. Combining Tandem-X InSAR and simulated GEDI lidar observations for forest structure mapping. Remote Sens Environ. 2016;187:253–66.
123. Dorado-Roda I, Pascual A, Godinho S, Silva CA, Botequim B, Rodríguez-Gonzálvez P, González-Ferreiro E, Guerra-Hernández J. Assessing the accuracy of gedi data for canopy height and aboveground biomass estimates in mediterranean forests. Remote Sens. 2021; https://doi.org/10.3390/rs13122279.
124. Zhao Y, Im J, Zhen Z, Zhao Y. Towards accurate individual tree parameters estimation in dense forest: optimized coarse-to-fine algorithms for registering UAV and terrestrial LiDAR data. GIScience Remote Sens. 2023;60:2197281.
125. Luo Y, Qi S, Liao K, Zhang S, Hu B, Tian Y. Mapping the forest height by fusion of ICESat-2 and multi-source remote sensing imagery and topographic information: a case study in Jiangxi Province, China. Forests. 2023; https://doi.org/10.3390/f14030454.
126. Paris C, Bruzzone L. A three-dimensional model-based approach to the estimation of the tree top height by fusing low-density LiDAR data and very high resolution optical images. IEEE Trans Geosci Remote Sens. 2015;53:467–80.
127. Pourshamsi M, Garcia M, Lavalle M, Balzter H. A machine-learning approach to PolInSAR and LiDAR data fusion for improved tropical forest canopy height estimation using NASA AfriSAR campaign data. IEEE J Sel Top Appl Earth Obs Remote Sens. 2018;11:3453–63.
128. Herrero-Huerta M, Felipe-García B, Belmar-Lizarán S, Hernández-López D, Rodríguez-Gonzálvez P, González-Aguilera D. Dense canopy height model from a low-cost photogrammetric platform and LiDAR data. Trees - Struct Funct. 2016;30:1287–301.
129. Malambo L, Popescu S, Liu M. Landsat-scale regional forest canopy height mapping using ICESat-2 along-track heights: case study of Eastern Texas. Remote Sens. 2023; https://doi.org/10.3390/rs15010001.
130. Liu X, Su Y, Hu T, Yang Q, Liu B, Deng Y, Tang H, Tang Z, Fang J, Guo Q. Neural network guided interpolation for mapping canopy height of China's forests by integrating GEDI and ICESat-2 data. Remote Sens Environ. 2022;269:112844.
131. Chen H, Cloude SR, White JC. Using gedi waveforms for improved tandem-x forest height mapping: a combined sinc + legendre approach. Remote Sens. 2021;13:1–12.
132. Wang C, Elmore AJ, Numata I, Cochrane MA, Lei S, Hakkenberg CR, Li Y, Zhao Y, Tian Y. A framework for improving Wall-to-Wall Canopy Height Mapping by Integrating GEDI LiDAR. Remote Sens. 2022;14:1–24.
133. Swetnam TL, Gillan JK, Sankey TT, McClaran MP, Nichols MH, Heilman P, McVay J. Considerations for achieving cross-platform point cloud data fusion across different dryland ecosystem structural states. Front Plant Sci. 2018;8:1–13.
134. Yang W, Liu Y, He H, Lin H, Qiu G, Guo L. Airborne LiDAR and photogrammetric point cloud fusion for extraction of urban tree metrics according to street network segmentation. IEEE Access. 2021;9:97834–42.

135. La HP, Eo YD, Chang A, Kim C. Extraction of individual tree crown using hyperspectral image and LiDAR data. KSCE J Civ Eng. 2014;19:1078–87.
136. Li Y, Chai G, Wang Y, Lei L, Zhang X. ACE R-CNN: an attention complementary and edge detection-based instance segmentation algorithm for individual tree species identification using UAV RGB images and LiDAR data. Remote Sens. 2022; https://doi.org/10.3390/rs14133035.
137. Zhen Z, Quackenbush LJ, Zhang L. Impact of tree-oriented growth order in marker-controlled region growing for individual tree crown delineation using airborne laser scanner (ALS) data. Remote Sens. 2013;6:555–79.
138. Aubry-Kientz M, Laybros A, Weinstein B, Ball J, Jackson T, Coomes D, Vincent G. Multisensor data fusion for improved segmentation of individual tree crowns in dense tropical forests. IEEE J Sel Top Appl Earth Obs Remote Sens. 2021;14:3927–36.
139. Sumbul G, Cinbis RG, Aksoy S. Multisource region attention network for fine-grained object recognition in remote sensing imagery. IEEE Trans Geosci Remote Sens. 2019;57:4929–37.
140. Guan H, Zhang J, Ma Q, et al. A novel framework to automatically fuse Multiplatform LiDAR data in forest environments based on tree locations. IEEE Trans Geosci Remote Sens. 2020;58:2165–77.
141. Dian Y, Pang Y, Dong Y, Li Z. Urban tree species mapping using airborne LiDAR and hyperspectral data. J Indian Soc Remote Sens. 2016;44:595–603.
142. Man Q, Dong P, Yang X, Wu Q, Han R. Automatic extraction of grasses and individual trees in urban areas based on airborne hyperspectral and LiDAR data. Remote Sens. 2020;12:1–22.
143. Arenas-Corraliza I, Nieto A, Moreno G. Automatic mapping of tree crowns in scattered-tree woodlands using low-density LiDAR data and infrared imagery. Agrofor Syst. 2020;94:1989–2002.
144. Lee JH, Biging GS, Fisher JB. An individual tree-based automated registration of aerial images to lidar data in a forested area. Photogramm Eng Remote Sens. 2016;82:699–710.
145. Zahidi I, Yusuf B, Hamedianfar A, Shafri HZM, Mohamed TA. Object-based classification of QuickBird image and low point density LIDAR for tropical trees and shrubs mapping. Eur J Remote Sens. 2015;48:423–46.
146. O'Neil-Dunne J, MacFaden S, Royar A. A versatile, production-oriented approach to high-resolution tree-canopy mapping in urban and suburban landscapes using GEOBIA and data fusion. Remote Sens. 2014;6:29.
147. Kandare K, Ørka HO, Dalponte M, Næsset E, Gobakken T. Individual tree crown approach for predicting site index in boreal forests using airborne laser scanning and hyperspectral data. Int J Appl Earth Obs Geoinf. 2017;60:72–82.
148. Yin S, Zhou K, Cao L, Shen X. Estimating the horizontal and vertical distributions of pigments in canopies of Ginkgo plantation based on UAV-Borne LiDAR, hyperspectral data by coupling PROSAIL model. Remote Sens. 2022; https://doi.org/10.3390/rs14030715.
149. Kamoske AG, Dahlin KM, Read QD, Record S, Stark SC, Serbin SP, Zarnetske PL. Towards mapping biodiversity from above: Can fusing lidar and hyperspectral remote sensing predict taxonomic, functional, and phylogenetic tree diversity in temperate forests? Glob Ecol Biogeogr. 2022;31:1440–60.
150. Bulluck L, Lin B, Schold E. Fine resolution imagery and LIDAR-derived canopy heights accurately classify land cover with a focus on shrub/sapling cover in a mountainous landscape. Remote Sens. 2022; https://doi.org/10.3390/rs14061364.
151. Polewski P, Yao W, Cao L, Gao S. Marker-free coregistration of UAV and backpack LiDAR point clouds in forested areas. ISPRS J Photogramm Remote Sens. 2019;147:307–18.
152. Li W, Cao S, Campos-Vargas C, Sanchez-Azofeifa A. Identifying tropical dry forests extent and succession via the use of machine learning techniques. Int J Appl Earth Obs Geoinf. 2017;63:196–205.
153. Dandois JP, Baker M, Olano M, Parker GG, Ellis EC. What is the point? Evaluating the structure, color, and semantic traits of computer vision point clouds of vegetation. Remote Sens. 2017;9:1–20.
154. Xi Z, Hopkinson C, Rood SB, Barnes C, Xu F, Pearce D, Jones E. A lightweight leddar optical fusion scanning system (Fss) for canopy foliage monitoring. Sensors (Switzerland). 2019; https://doi.org/10.3390/s19183943.
155. Dai W, Yang B, Liang X, Dong Z, Huang R, Wang Y, Li W. Automated fusion of forest airborne and terrestrial point clouds through canopy density analysis. ISPRS J Photogramm Remote Sens. 2019;156:94–107.
156. Gopalakrishnan R, Packalen P, Ikonen VP, Räty J, Venäläinen A, Laapas M, Pirinen P, Peltola H. The utility of fused airborne laser scanning and multispectral data for improved wind damage risk assessment over a managed forest landscape in Finland. Ann For Sci. 2020; https://doi.org/10.1007/s13595-020-00992-8.
157. Peters D, Niemann O, Skelly R. Remote sensing of ecosystem structure: Fusing passive and active remotely sensed data to characterize a deltaic wetland landscape. Remote Sens. 2020;12:1–25.
158. Powell EB, Laurent KAS, Dubayah R. Lidar-imagery fusion reveals rapid coastal forest loss in delaware bay consistent with marsh migration. Remote Sens. 2022; https://doi.org/10.3390/rs14184577.
159. De Lima LC, Ramezani M, Borges P, Brunig M. Air-ground collaborative localisation in forests using lidar canopy maps. IEEE Robot Autom Lett. 2023;8:1818–25.
160. Kacic P, Hirner A, Da Ponte E. Fusing sentinel-1 and-2 to model gedi-derived vegetation structure characteristics in gee for the paraguayan chaco. Remote Sens. 2021;13:1–17.
161. Bright BC, Hudak AT, Meddens AJH, Hawbaker TJ, Briggs JS, Kennedy RE. Prediction of forest canopy and surface fuels from lidar and satellite time series data in a bark beetle-affected forest. Forests. 2017;8:1–22.
162. Qi Y, Coops NC, Daniels LD, Butson CR. Assessing the effects of burn severity on post-fire tree structures using the fused drone and mobile laser scanning point clouds. Front Environ Sci. 2022;10. https://doi.org/10.3389/fenvs.2022.949442.
163. Martín-Alcón S, Coll L, De Cáceres M, Guitart L, Cabré M, Just A, González-Olabarría JR. Combining aerial LiDAR and multispectral imagery to assess postfire regeneration types in a Mediterranean forest. Can J For Res. 2015;45:856–66.
164. Marino E, Ranz P, Tomé JL, Noriega MÁ, Esteban J, Madrigal J. Generation of high-resolution fuel model maps from discrete airborne laser scanner and Landsat-8 OLI: a low-cost and highly updated methodology for large areas. Remote Sens Environ. 2016;187:267–80.
165. Vogeler JC, Yang Z, Cohen WB. Mapping post-fire habitat characteristics through the fusion of remote sensing tools. Remote Sens Environ. 2016;173:294–303.
166. Braziunas KH, Abendroth DC, Turner MG. Young forests and fire: using lidar–imagery fusion to explore fuels and burn severity in a subalpine forest reburn. Ecosphere. 2022;13:1–20.
167. Liu M, Popescu S. Estimation of biomass burning emissions by integrating ICESat-2, Landsat 8, and Sentinel-1 data. Remote Sens Environ. 2022;280:113172.
168. Domingo D, de la Riva J, Lamelas MT, García-Martín A, Ibarra P, Echeverría M, Hoffrén R. Fuel type classification using airborne laser scanning and sentinel 2 data in mediterranean forest affected by wildfires. Remote Sens. 2020;12:1–22.
169. Rocha KD, Silva CA, Cosenza DN, et al. Crown-level structure and fuel load characterization from airborne and terrestrial laser

scanning in a longleaf pine (Pinus palustris Mill.) forest ecosystem. Remote Sens. 2023; https://doi.org/10.3390/rs15041002.
170. Zhang L, Zhang L, Du B. Deep learning for remote sensing data: a technical tutorial on the state of the art. IEEE Geosci Remote Sens Mag. 2016;4:22–40.
171. Zhang S, Meng X, Liu Q, Yang G, Sun W. Feature-decision level collaborative fusion network for hyperspectral and LiDAR classification. Remote Sens. 2023;15:4148.
172. Tai H, Xia Y, Yan M, Li C, Kong XL. Construction of artificial forest point clouds by laser SLAM technology and estimation of carbon storage. Appl Sci. 2022; https://doi.org/10.3390/app122110838.
173. Pohjavirta O, Liang X, Wang Y, Kukko A, Pyörälä J, Hyyppä E, Yu X, Kaartinen H, Hyyppä J. Automated registration of wide-baseline point clouds in forests using discrete overlap search. For Ecosyst. 2022;9:100080.
174. Dalponte M, Ørka HO, Ene LT, Gobakken T, Næsset E. Tree crown delineation and tree species classification in boreal forests using hyperspectral and ALS data. Remote Sens Environ. 2014;140:306–17.
175. Arjasakusuma S, Kusuma SS, Phinn S. Evaluating variable selection and machine learning algorithms for estimating forest heights by combining lidar and hyperspectral data. ISPRS Int J Geo-Information. 2020; https://doi.org/10.3390/ijgi9090507.
176. Machala M, Zejdová L. Forest mapping through object-based image analysis of multispectral and LiDAR aerial data. Eur J Remote Sens. 2014;47:117–31.
177. Anderson JE, Plourde LC, Martin ME, Braswell BH, Smith ML, Dubayah RO, Hofton MA, Blair JB. Integrating waveform lidar with hyperspectral imagery for inventory of a northern temperate forest. Remote Sens Environ. 2008;112:1856–70.
178. Guan H, Li J, Chapman M, Deng F, Ji Z, Yang X. Integration of orthoimagery and lidar data for object-based urban thematic mapping using random forests. Int J Remote Sens. 2013;34:5166–86.
179. Potapov P, Li X, Hernandez-Serna A, Tyukavina A, Hansen MC, Kommareddy A, Pickens A, Turubanova S, Tang H, Silva CE. Mapping global forest canopy height through integration of GEDI and landsat data. Remote Sens Environ. 2021;253:112165.
180. Hudak AT, Lefsky MA, Cohen WB, Berterretche M. Integration of lidar and Landsat ETM+ data for estimating and mapping forest canopy height. Remote Sens Environ. 2002;82:397–416.
181. Latifi H, Fassnacht F, Koch B. Forest structure modeling with combined airborne hyperspectral and LiDAR data. Remote Sens Environ. 2012;121:10–25.
182. Zhang M, Li W, Tao R, Li H, Du Q. Information fusion for classification of hyperspectral and LiDAR data using IP-CNN. IEEE Trans Geosci Remote Sens. 2021;60:1–12.
183. Moudrý V, Cord AF, Gábor L, et al. Vegetation structure derived from airborne laser scanning to assess species distribution and habitat suitability: The way forward. Divers Distrib. 2023;29:39–50.
184. Kissling WD, Shi Y. Which metrics derived from airborne laser scanning are essential to measure the vertical profile of ecosystems? Divers Distrib. 2023;29:1315–20.

Publisher's Note Springer Nature remains neutral with regard to jurisdictional claims in published maps and institutional affiliations.

5. Discussions

5.1 Summary of addressed knowledge gaps and objectives

The mapping of selected forest structural indicators is crucial for assessing forest productivity and maintaining the ecosystem functioning. The accuracy and precision of mapping these selected structural indicators vary greatly from different methodological approaches. The thesis addressed the knowledge gaps in the accuracy and precision of mapping selected structural indicators using TLS and MLS. The key features and objectives of the thesis are explained as follows:

a) Objective 1 is addressed as a review based on understanding the use and reliability of TLS and MLS for mapping selected forest structural indicators (DBH, tree height, Stem volume, AGB). A thorough review was also done to understand the role of LiDAR in tree parameter retrieval and its application in forestry.

b) Objectives 1 are addressed in paper I as another review focused on LiDAR data fusion with other data sources. The review addressed the main gains in LiDAR data fusion with other data. The current trend and opinion on LiDAR data fusion.

c) Objectives 2 and 4 are addressed in papers III and IV. A study was conducted on the estimation of AGB using TLS and ALOS PALSAR L-band data to resolve the saturation of biomass value with L-band. Machine learning algorithms were used to address this challenge, and it was found that biomass saturation can be resolved with better reference data training and machine learning approaches with the integration of TLS and ALOS PALSAR data.

d) Objective 2 is addressed as in paper III and II; an approach of the estimation of tree parameters (DBH, tree height, and stem volume) using RHT and RANSAC algorithms. A comparison study was conducted using TLS, MLS, and Photogrammetry to see these technologies' significant importance and potential in mapping individual tree dimensions, specifically DBH.

e) Currently, occlusion is one of the main challenges in LiDAR data acquisition in the forest environment, especially processing and analysis of the data, which makes it tricky to get the best accurate results. So, the investigation was done to propose a methodology to mitigate this challenge. This was addressed in paper V.

f) The investigation also focused on the role of revolutionary devices (iPhone 12 Pro and iPad Pro) in measuring DBH. Moreover, it also aimed at tree species' relevance and significance with DBH and algorithms. This was addressed in the paper III and VI.

g) Objective 3 is addressed as a paper VII, the benchmarking study was done on all the possible software solutions for processing LiDAR data (TLS and MLS). Benchmarking the point cloud processing software solutions was done to propose the best solution considering the tree parameters estimation and ease of applicability. A detailed user manual and documentation were prepared so to provide an overview of the current software solutions to the end users.

The objectives and thesis are structured based on the hypothesis that is answered as follows:

a) **Question**: The use of static and mobile laser scanning will significantly advance, mainly in the field of mapping trees' positions and dimensions. In contrast, mapping a wide range of tree parameters remains understudied.

Answer: In this context, software solutions were tested and installed considering a wide range of tree parameters. The mapping of tree parameters was conducted in paper VII during the testing and installation of the software solutions to benchmark the point cloud processing solutions. The results showed the potential to map those parameters using one of the benchmarking algorithms.

b) **Question**: Options for mapping the parameters can be substantially improved by the fusion of different data sources (e.g., point clouds with images)

Answer: Several options are available for mapping tree parameters by the fusion of different data sources; these have been clarified and found in the review conducted in the paper I. The potential of increasing the accuracy and precision of the tree parameters (AGB) with the integration of TLS and ALOS PALSAR data is shown in paper IV.

c) **Question**: Terrestrial laser scanning will provide more accurate and reliable data with lower estimation errors than mobile laser scanning.

Answer: TLS proved to be a more reliable and efficient device for accurately estimating tree parameters than MLS. A study was conducted and proved in paper II.

d) **Question**: Mobile laser scanning will be more efficient during the data acquisition and provide the required accuracy.

Answer: Irrespective of accuracy, MLS proved to be the most efficient device for data acquisition, with satisfactory accuracy for estimating a few tree parameters (especially DBH). This was examined as part of papers II and VI.

The thesis objectives were addressed and elaborated in the mentioned papers and explained briefly in the above sections of the thesis.

5.2 Summary of Used Methodological Approaches

A thorough Literature review on the Web of Science was conducted to understand the current state-of-the-art application of TLS and MLS in the estimation of tree metrics and forestry. A systematic review was done on Web of Science and Scopus to find the existing scientific literature and synthesize the current options for mapping variables of high ecological relevance using TLS and MLS. In the second review, PRISMA approach was utilized with the most suitable keywords at Web of Science which are mentioned in table 1.

The literature review was based on the LiDAR data fusion and its prospective role in forestry. Regarding this, an experiment was done to estimate ABG with the integration of variables derived from TLS and ALOS PALSAR using machine learning approaches RF and ANN to resolve the biomass saturation issues in L-band, for which TLS scanning was done on 13 plots. RF and ANN were trained at the LiDAR footprint using the TLS derived tree parameters and features extracted from the ALOS data at the LiDAR footprints

Occlusion is one of the main concerns during the scanning of forest plots. TLS is an efficient device to give detailed information about the vegetation, especially the canopy of the tree as it can penetrate deep into the canopy. However, the scanned data could have some voids due to different plot sizes, tree densities, and tree structure. Multiple scan positions were done to quantify these voids and analyze the occlusion in the canopy. These scans were combined into different combinations to get an overview of the number of canopy top points present in each scan combination. Based on these combinations, the most suitable combination was suggested for the same forest structure and density.

An experiment was also done on the estimation of tree parameters (DBH, tree height, and Stem volume) using algorithms such as RANSAC and RHT. Moreover, DBH was also estimated using three software tools such as rTLS, RANSAC , and ForestScanner application ,further statistical evaluation was done to find out the significance of tree species in the estimation of DBH.

A comparative analysis was also done between TLS, MLS, and photogrammetry to assess the performance and potential in the ease of data collection, tree parameter estimation, tree detection rate, and time required to collect the data. A cylinder-based algorithm was used to estimate the DBH.

Later, a benchmarking of 24-point cloud processing algorithms focused on forestry applications was done. A comprehensive and user-friendly database was prepared for the end users. This database illustrates the elaborative information on each of the algorithms mentioning different useful forestry parameters. The identified algorithms were tested, installed and a user manual was prepared for general use focusing on the user with no or little programming background. This manual is included in the web platform of the 3DForEcotech Cost Action Project (https://3dforecotech.eu/database/).

5.2.1 Limitations of the methodological approaches

The methodological approaches for the literature review were only focused on the review and articles and did not consider the conference proceedings. Some of the instances of data fusion were ignored during the review. Multi-temporal data fusion, multi-spectral LiDAR data, co-registration of data from the same instrument (strip adjustment of ALS data collection and co-registration of TLS point clouds acquired from various points of view to create a forest scene). These can still be relevant to forest monitoring, species classification, and tree localization.

Another review was conducted on the point cloud processing software solutions to prepare and avail a list of potential software solutions that focused on forestry application. The current methodology for review only works for 24 software solutions; however, the point cloud processing software and algorithms are updated and included every now and then. So, another review needs to be conducted on these updated versions of software, and other upcoming solutions. The review procedure only included the point clouds acquired using terrestrial devices; there is a limitation in the considered point cloud data formats for point clouds. The categories used for the output level have not mentioned all the features (tree parameters) concerning the forest studies.

In paper II, the comparative analysis of close-range technologies (TLS, iPad, PLS_{hh} , MultiCam) has been done. The methodology includes testing these devices on the performance within the forest stands, focusing on tree detection, DBH estimation, and overall performance. The methodology did not include other tree parameters or forest metrics. The study area chosen has 8 plots (25 x 25 m). The methodology neither considers different stand structures nor forest environments. The methodology applies to the same forest stand structure as it is mentioned in the study, and the results may vary in different forest stand structure environments. Moreover, depending on the devices used for the scanning of the forest plots, the accuracy and precision of the final output may vary because there are different ranges of terrestrial laser scanners (TLS) and mobile laser scanners (MLS) available with different technical features and capability of scanning are different compared to each other.

Furthermore, tree parameter extraction can be subjective depending on the methodological approach. In Paper III, tree parameters (DBH, tree height) were mainly focused, and RANSAC and RHT were used to estimate DBH and tree height. However, the conceptual framework did not consider another potential algorithm to serve the purpose. Other tree parameters were not included in the methodology. The number of plots established was 13, so the results may vary with the increase in the number of plots, scanning scheme, and forest type. The scanning scheme and forest stand structure are highly subjective when estimating tree parameters (especially DBH and tree height) because of the possibility of occlusion. The accuracy and precision of the DBH and tree height may change depending on the scanner. For instance, in paper VI, the tree was scanned with an iPhone 12 Pro to estimate DBH. The software tools that were used for DBH estimation were RANSAC (CloudCompare plugin), ForestScanner application, and rTLS. The forest stand was different. So, the DBH estimate achieved different accuracy. The precision and accuracy of these tree parameters are highly important for further estimation of stem volume and above-ground biomass.

In paper IV, forest above-ground estimation was used using TLS and ALOS PALSAR data. Two machine learning algorithms (RF and ANN) were used. The study was done in 13 plots. The conceptual framework of this study may vary depending on the study location, machine learning algorithms, and datasets used. This study aimed to mitigate the challenge of biomass saturation with the L-band of ALOS PALSAR data. The study works well in the tropical forest and was not tested in other forest conditions or types. The biomass saturation varies depending on the SAR data; different bands have different saturation levels. The results may also change with the different scanning schemes because it highly affects the occlusion rate in the forest plots.

The scanning scheme and position of scanners in the plots can change the entire output of the study, considering the forest stand structure and density. The number of points acquired in the forest plots may vary with different scanning schemes and so the estimated tree parameters. The quantification and assessment of the number of points acquired in the top of tree canopy using TLS was focused on paper V. The methodology can only work for the same forest stand structure and has not been tried in other forest types. The scan combinations may vary and will be different depending on the number and locations of scan positions in the forest plot. The study also does not consider the variation of DSM at each pixel, including canopy top points, points above branches, and surface points in non-canopy regions.

5.3 Key findings

The systematic review based on LiDAR data fusion reveals the confusion between the terms 'data fusion', 'data combination', and 'data integration'. For instance, the studies focused on data-level or feature-level fusion using the term data combination (Arjasakusuma et al., 2020; Machala & Zejdová, 2014), data registration (Pohjavirta et al., 2022), or data integration (Anderson et al., 2008; Guan et al., 2013); therefore, to avoid confusion, the definition was set to LiDAR data fusion as "Enhancement of forest observation and LiDAR characteristics using features derived from different data sources and merging of data of which at least one dataset is LiDAR". Data integration terms should be used when only features and characteristics from the data sources are used to train and enhance the model's efficiency. They are not used to generating new datasets. The data combination term should be used when the data fusion is done at the pre-processing steps and data integration is done at the decision-making step.

This review survey shows that precision forestry is oriented towards automated terrestrial point cloud processing. The precise measurement of individual trees including diameter, height, and location, is almost possible and mirrors the meticulous information as compared to traditional forest inventory. Besides the prevalence of automatic point cloud processing solutions, there is a gap to exploit the potential of terrestrial point clouds among practitioners fully. However, some software solutions utilize some complex metrics to unveil more information about the data; perhaps a broader utilization is required to thrive the full potential of these datasets. Furthermore, these datasets have the capability not only to recognize the basic forest structure but also to analyze some advanced variables such as canopy characterization, volumetric assessment, and habitat monitoring.

The most important glance from papers III, IV, and VI is the utilization of different conceptual approaches for the estimation of tree parameters (DBH, tree height, stem volume). Different datasets were used and tested on different locations mostly to ensure the potential and accuracy of the outputs. The tree parameters estimation accuracy is highly subjective to the scanner used for the collection of point cloud, forest type and stand structure, algorithm, or software tools used for the estimation. The precision error can also be dependent on the operator of the device. However, the most important finding from papers III and VI is the best performance of estimation of DBH by RANSAC and ForestScanner (iPhone-based application). Also, the iPhone showed the potential to estimate DBH with an R^2 of 0.976, equal to the R^2 of 0.976 achieved using RANSAC. The RMSE and rRMSE (%) observed were 2.58cm and 7.25 for ForestScanner. Also, The RMSE and rRMSE calculated for RANSAC were 2.19 and 6.15cm. There are so many tools available for this purpose, so perhaps benchmarking of the tools is required to get the most robust tool for ease of estimation of DBH. Other studies focus on the estimation of DBH using MLS with the comparison of 3 algorithms, namely RANSAC, Monte Carlo, and optimum circle and found good results with RMSE 5.31 cm and 1.23 cm of bias (Pérez-Martín et al., 2021).The other study on the DBH estimation was done using the RANSAC algorithm, which tested 71 trees and found a promising outcome. The RMSE calculated was 0.7 cm, and 2.27 % was the relative error. This shows the potential application of RANSAC in the estimation of DBH (Zhou et al., 2019).This study showed that the number of points fitting a circle does not affect the RANSAC algorithm. LiDAR-based iPad Pro efficiently estimated accurate DBH and distance between each tree. So, these low-cost technologies can accurately estimate a few tree parameters(Çakir et al., 2021).

Apart from this, statistical analysis was done to determine the significance of these devices on the estimation of DBH of different tree species and a significant relation was found between tree species and DBH. In paper IV, the biomass saturation issue was resolved at L-band ALOS PALSAR data by integrating it with tree parameters estimated using TLS. The R^2 value obtained for predicted biomass using RF is 0.94 and RMSE of 59.72 ton ha^{-1}. The RMSEcv and RMSE% obtained were 0.15 and 15.92, respectively. However, the statistical evaluation reveals the values obtained for R^2, RMSE, %RMSE, and RMSEcv are 0.77, 98.46 ton ha^{-1}, 26.0, and 0.26, respectively. The biomass range improved was 122.46 to 581.89 ton ha^{-1} using RF with the uncertainty of 15.75 to 85.14 ton ha^{-1}. These results were compared with a study and found that the LiDAR data is more reliable in estimating biomass and significantly improves the biomass saturation with intact precision and accuracy of the predicted biomass with correlation (R^2) value of 0.98 and RMSE of 0.08 Mg (Beyene et al., 2020; Chowdhury et al., 2013; Liao et al., 2020).

The most important finding in paper II was the best performance of TLS in the quality of point cloud and tree detection rate (90 %) compared to iPad (64.5 -87.5%), PLS_{hh} (55.6-74.3%), and MultiCam (57.1-74.3%), respectively. TLS achieved the highest accuracy in the estimation of DBH with an RMSE of 2 cm compared to other devices. Nevertheless, iPad achieved the closest accuracy to TLS with RMSE 2.6 to 3.4 cm. Furthermore, the time required to complete the scan of the plot is 40 mins (TLS), 10 mins (PLS_{hh}), 15 mins (iPad), and 8 mins (MultiCam). So, $PLS_{hh,}$ the tree detection rate achieved was 57-100% (Balenović et al., 2021). The highest tree detection rate (100%) was found with a DBH threshold of 10 cm (Bauwens et al., 2016), and 90.9 % to 95 % for a 5 cm or less DBH threshold; however, on the contrary, 57 % tree detection rate was achieved with the distance between the scanning strips of 15 m. The rate was increased to 94 % by changing the distance from 15 to 10 cm (Chen et al., 2019; Gollob et al., 2020; Perugia et al., 2019).

The top canopy surface point extraction in paper V was statistically evaluated, and it was found that the most reliable combination of all the 9 scan positions was Four Sides Centre with Centre Scans ($FSC_{W}CS$) compared to All Nine Scan (ANS). The rRMSE % obtained for TLS_Plot 1 was 0.14 to 2.48 %, whereas 0.096 to 1.22 % for TLS_Plot2. So, the study showed that using different scan combinations of TLS scan positions, the quantity assessment of point clouds can be done for forest plots. This approach will eventually help to assess and detect the probability of occurring occlusions while scanning a forest plot.

6. International Collaborations and Achievements

Strong international collaborations were established as a part of this thesis. Papers I and VII were mainly done in collaboration with scientists from very high university rankings. The collaborations were part of the 3DForEcoTech Cost Action project. Most of the datasets used in this thesis were associated with the collaborators.

Virtual mobility was done under the 3DForEcoTech project, and the mobility outcome was paper VII. A list of 24 algorithms was prepared, installed, and tested, and an intensive guideline and protocol were developed and made available on the project website (https://3dforecotech.eu/database/). The web portal is like in figure 30.

Moreover, the extended achievement of virtual mobility, a hackathon was organized to benchmark software solutions for processing close-range forest point clouds. It happened on 25-29 September, 2023, at TU Wien (Austria) https://3dforecotech.eu/activities/hackathon-a-benchmark-of-software-solutions-for-processing-close-range-forest-point-clouds/ . The outcome of hackathon will further lead to a publication in peer reviewed journal.

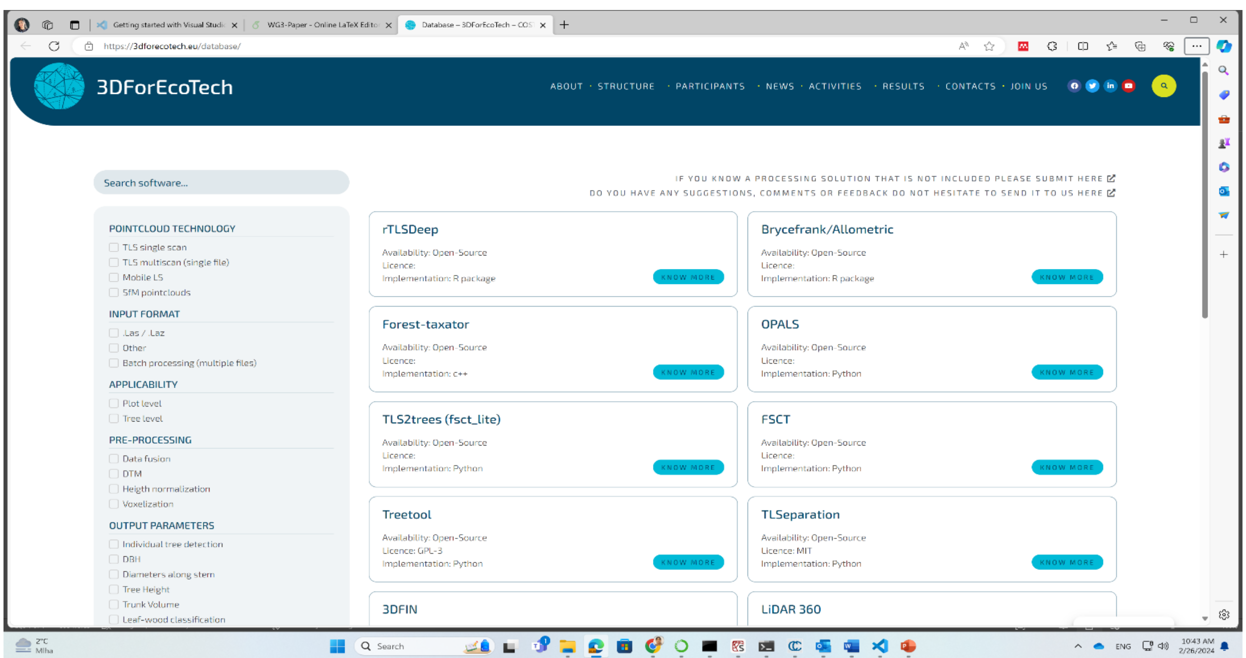

Figure 29: The webpage of the 3DForEcotech Cost Action project

7. Conclusions and Recommendations

The dissertation mainly focuses on utilizing TLS and MLS for mapping structural indicators in the forest and the significance of these indicators. The focus was to use the TLS and MLS technology to estimate tree parameters (structural indicators) using different software solutions or data integration. The thesis outcome was delivered in the respective studies described in papers I, II, III, IV, V, VI, and VII. The overall conclusion derived from all the papers is that the TLS is the most precise device for mapping structural indicators. However, in the analysis of the paper, I highlighted the data fusion technique and the literal meaning of data fusion, data integration, and data combination. Also, the proper use of these terminologies. The significance of the impact of the data fusion of the forestry application.

Paper II mentioned the comparative analysis of close-range technology (TLS, PLS_{hh}, iPad, MultiCam) for the tree detection rate and DBH estimation using different scanning trajectories and found that the TLS is more precise than other devices, perhaps iPad works closely to TLS, and it shows more potential in the estimation of DBH and tree detection rate. However, TLS and PLS_{hh} proved to have more potential to acquire point clouds with more range. So, it would be necessary to use these devices for the estimation of other tree parameters such as tree height. Moreover, the methodology can also be tested in different forest types and with more tree parameters.

In paper III, stem volume estimation was done using TLS point cloud. The stem volume was estimated and compared using RANSAC and RHT. RANSAC proved to be the best algorithm to estimate DBH with higher accuracy, and so stem volume. These algorithms have the potential to do the modeling of stem volume, preferably including more plots and trees. The current methodology needs to be tested in different forest types as well. The DBH estimation is very fast and accurate with the iPhone 12 Pro. The statistical analysis found that the in-built algorithm in the iPhone 12 pro-ForestScanner application is precise and close to RANSAC. So, this can be used for the estimation of DBH in the mentioned forest type and tree species. A significant relation was found between the tree species and DBH. More species and different forest types can also be tested using iPhone 12 pro to test the outcomes of paper VI.

Above-ground forest biomass was estimated using TLS and ALOS PALSAR data. The study proved that the biomass saturation using L-band SAR data can be mitigated with the integration of ALOS and TLS datasets. Also, RF has the potential to predict biomass with the most accuracy. This kind of study relies on the data source and machine learning algorithms used. This is clearly described in paper IV. The methodology is also used for the other forest types and different stand structures. Also, the deep learning approach could also make a significant difference in the biomass saturation range.

In paper V, DSM was used to extract the canopy top points with nine scan combinations. The most suitable combination was the Four Sides Centre with Centre Scans (FSC_WCS) compared to All Nine Scan (ANS). However, the scan combinations are highly subjective to the number of scan positions in the forest plots, and this methodology only works with static LiDAR devices (TLS). So, for future work, replication of the same methodology on different scan combinations can be done using TLS in different forest types. Also, benchmarking can be done to establish different scan combinations of TLS and other devices to establish the most accurate scanning scheme for tree detection rate and DBH estimation with some more tree parameters relevant to the understanding of the function of forest ecosystems.

A benchmarking of 24-point cloud processing software solutions was using some selected tree parameters. These solutions were installed and tested with different computer configurations and a detailed user guide and technical protocol were prepared for the end users with respect to the type of analysis they are focused on. For future work, the point cloud processing software solutions need to be updated, and more solutions need to be tested and updated at the web portal of 3DForEcoTech website. The tree parameters and testing parameters can be elaborated and diversified to make the outcome of these software solutions more prevalent.

These kinds of studies are important to understand the functionality of the forest ecosystem and help mitigate several challenges due to environmental crises and climate change. The structural indicators play a crucial role in understanding the minute level of change in the forest structure.

8. References

Anderson, J. E., Plourde, L. C., Martin, M. E., Braswell, B. H., Smith, M.-L., Dubayah, R. O., Hofton, M. A., & Blair, J. B. (2008). Integrating waveform lidar with hyperspectral imagery for inventory of a northern temperate forest. *Remote Sensing of Environment, 112(4)*, 1856–1870.

Arjasakusuma, S., Kusuma, S. S., & Phinn, S. (2020). Evaluating variable selection and machine learning algorithms for estimating forest heights by combining lidar and hyperspectral data. *ISPRS International Journal of Geo-Information, 9(9)*. https://doi.org/10.3390/ijgi9090507

Ashcroft, M. B., Gollan, J. R., & Ramp, D. (2014). Creating vegetation density profiles for a diverse range of ecological habitats using terrestrial laser scanning. *Methods in Ecology and Evolution*, *5*(3), 263–272. https://doi.org/10.1111/2041-210X.12157

Astrup, R., Ducey, M. J., Granhus, A., Ritter, T., & von Lüpke, N. (2014). Approaches for estimating stand-level volume using terrestrial laser scanning in a single-scan mode. *Canadian Journal of Forest Research*, *44*(6), 666–676. https://doi.org/10.1139/cjfr-2013-0535

Balenović, I., Liang, X., Jurjević, L., Hyyppä, J., Seletković, A., & Kukko, A. (2021). Hand-Held Personal Laser Scanning. *Croatian Journal of Forest Engineering*, *42*(1), 165–183. https://doi.org/10.5552/crojfe.2021.858

Balvanera, P., Siddique, I., Dee, L., Paquette, A., Isbell, F., Gonzalez, A., Byrnes, J., O'Connor, M. I., Hungate, B. A., & Griffin, J. N. (2014). Linking biodiversity and ecosystem services: Current uncertainties and the necessary next steps. *BioScience, 64(1)*, 49–57. https://doi.org/10.1093/biosci/bit003

Bastianoni, S., Niccolucci, V., Pulselli, R. M., & Marchettini, N. (2012). Indicator and indicandum: "sustainable way" vs "prevailing conditions" in the Ecological Footprint. *Ecological Indicators*, *16*, 47–50. https://doi.org/10.1016/j.ecolind.2011.10.001

Bauwens, S., Bartholomeus, H., Calders, K., & Lejeune, P. (2016). Forest inventory with terrestrial LiDAR: A comparison of static and hand-held mobile laser scanning. *Forests*, *7*(6). https://doi.org/10.3390/f7060127

Béland, M., Baldocchi, D. D., Widlowski, J. L., Fournier, R. A., & Verstraete, M. M. (2014). On seeing the wood from the leaves and the role of voxel size in determining leaf area distribution of forests with terrestrial LiDAR. *Agricultural and Forest Meteorology*, *184*, 82–97. https://doi.org/10.1016/j.agrformet.2013.09.005

Belton, D., Moncrieff, S., & Chapman, J. (2013). Processing tree point clouds using Gaussian Mixture Models. *ISPRS Annals of the Photogrammetry, Remote Sensing and Spatial Information Sciences*, *2*(5W2), 43–48. https://doi.org/10.5194/isprsannals-II-5-W2-43-2013

Bergen, K. M., Goetz, S. J., Dubayah, R. O., Henebry, G. M., Hunsaker, C. T., Imhoff, M. L., Nelson, R. F., Parker, G. G., & Radeloff, V. C. (2009). Remote sensing of vegetation 3-D structure for biodiversity and habitat: Review and implications for lidar and radar spaceborne missions. Journal of Geophysical Research: *Biogeosciences, 114(4),* 1–13. https://doi.org/10.1029/2008JG000883

Beyene, S. M., Hussin, Y. A., Kloosterman, H. E., & Ismail, M. H. (2020). Forest Inventory and Aboveground Biomass Estimation with Terrestrial LiDAR in the Tropical Forest of Malaysia. *Canadian Journal of Remote Sensing, 46(2),* 130–145. https://doi.org/10.1080/07038992.2020.1759036

Bienert, A., Georgi, L., Kunz, M., Maas, H. G., & von Oheimb, G. (2018). Comparison and combination of mobile and terrestrial laser scanning for natural forest inventories. *Forests*, *8*(2), 1–25. https://doi.org/10.3390/f9070395

Bornand, A., Rehush, N., Morsdorf, F., Thürig, E., & Abegg, M. (2023). Individual tree volume estimation with terrestrial laser scanning: Evaluating reconstructive and allometric approaches. *Agricultural and Forest Meteorology*, *341*(August), 109654. https://doi.org/10.1016/j.agrformet.2023.109654

Bucksch, A., & Lindenbergh, R. (2008). CAMPINO - A skeletonization method for point cloud processing. *ISPRS Journal of Photogrammetry and Remote Sensing*, *63*(1), 115–127. https://doi.org/10.1016/j.isprsjprs.2007.10.004

Burt, A., Disney, M., & Calders, K. (2019). Extracting individual trees from lidar point clouds using treeseg. *Methods in Ecology and Evolution*, *10*(3), 438–445. https://doi.org/10.1111/2041-210X.13121

Çakir, G. Y., Post, C. J., Mikhailova, E. A., & Schlautman, M. A. (2021). 3D LiDAR Scanning of Urban Forest Structure Using a Consumer Tablet. *Urban Science*, *5(4)*. https://doi.org/10.3390/urbansci5040088

Calders, K., Adams, J., Armston, J., Bartholomeus, H., Bauwens, S., Bentley, L. P., Chave, J., Danson, F. M., Demol, M., Disney, M., Gaulton, R., Krishna Moorthy, S. M., Levick, S. R., Saarinen, N., Schaaf, C., Stovall, A., Terryn, L., Wilkes, P., & Verbeeck, H. (2020). Terrestrial laser scanning in forest ecology: Expanding the horizon. *Remote Sensing of Environment*, *251*(April), 112102. https://doi.org/10.1016/j.rse.2020.112102

Calders, K., Newnham, G., Burt, A., Murphy, S., Raumonen, P., Herold, M., Culvenor, D., Avitabile, V., Disney, M., Armston, J., & Kaasalainen, M. (2015). Nondestructive estimates of above-ground biomass using terrestrial laser scanning. *Methods in Ecology and Evolution*, *6*(2), 198–208. https://doi.org/10.1111/2041-210X.12301

Carpenter, S. R., Mooney, H. A., Agard, J., Capistrano, D., Defries, R. S., Díaz, S., Dietz, T., Duraiappah, A. K., Oteng-Yeboah, A., Pereira, H. M., Perrings, C., Reid, W. V, Sarukhan, J., Scholes, R. J., & Whyte, A. (2009). *Science for managing ecosystem services: Beyond the Millennium Ecosystem Assessment*. www.pnas.orgcgidoi10.1073pnas.0808772106

Cartus, O., Santoro, M., Wegmuller, U., Labriere, N., & Chave, J. (2022). Sentinel-1 Coherence for Mapping Above-Ground Biomass in Semiarid Forest Areas. *IEEE Geoscience and Remote Sensing Letters*, *19*. https://doi.org/10.1109/LGRS.2021.3071949

Chen, S., Liu, H., Feng, Z., Shen, C., & Chen, P. (2019). Applicability of personal laser scanning in forestry inventory. *PLoS ONE*, *14*(2), 1–22. https://doi.org/10.1371/journal.pone.0211392

Chen, Y., Zhu, X., Yebra, M., Harris, S., & Tapper, N. (2016). Strata-based forest fuel classification for wild fire hazard assessment using terrestrial LiDAR. *Journal of Applied Remote Sensing*, *10*(4), 046025. https://doi.org/10.1117/1.jrs.10.046025

Choi, C., Pardini, M., Heym, M., & Papathanassiou, K. P. (2021). Improving Forest Height-To-Biomass Allometry with Structure Information: A Tandem-X Study. *IEEE Journal of Selected Topics in Applied Earth Observations and Remote Sensing*, *14*, 10415–10427. https://doi.org/10.1109/JSTARS.2021.3116443

Chowdhury, T., Thiel, C., Schmullius, C., & Stelmaszczuk-Górska, M. (2013). Polarimetric Parameters for Growing Stock Volume Estimation Using ALOS PALSAR L-Band Data over Siberian Forests. *Remote Sensing, 5(11)*, 5725–5756. https://doi.org/10.3390/rs5115725

Dale, V. H., & Beyeler, S. C. (2001). Challenges in the development and use of ecological indicators. *Ecological Indicators, 1*(1), 3–10. https://doi.org/10.1016/S1470-160X(01)00003-6

de Jesus, J. B., & Kuplich, T. M. (2020). Applications of sar data to estimate forest biophysical variables in Brazil. *Cerne*, *26*(1), 88–97. https://doi.org/10.1590/01047760202026012656

Del Perugia, B., Giannetti, F., Chirici, G., & Travaglini, D. (2019). Influence of scan density on the estimation of single-tree attributes by hand-held mobile laser scanning. *Forests*, *10*(3), 277.

Espelta, J. M., Cruz-Alonso, V., Alfaro-Sánchez, R., Hampe, A., Messier, C., & Pino, J. (2020). Functional diversity enhances tree growth and reduces herbivory damage in secondary broadleaf forests, but does not influence resilience to drought. *Journal of Applied Ecology*, *57*(12), 2362–2372. https://doi.org/10.1111/1365-2664.13728

Fleck, S., Mölder, I., Jacob, M., Gebauer, T., Jungkunst, H. F., & Leuschner, C. (2011). Comparison of conventional eight-point crown projections with LIDAR-based virtual crown projections in a temperate old-growth forest. *Annals of Forest Science*, *68*(7), 1173–1185. https://doi.org/10.1007/s13595-011-0067-1

Forsman, M., Holmgren, J., & Olofsson, K. (2016). Tree stem diameter estimation from mobile laser scanning using line-wise intensity-based clustering. *Forests*, *7*(9). https://doi.org/10.3390/f7090206

Gan, Y., Wang, Q., & Song, G. (2024). Non-Destructive Estimation of Deciduous Forest Metrics: Comparisons between UAV-LiDAR, UAV-DAP, and Terrestrial LiDAR Leaf-Off Point Clouds Using Two QSMs. *Remote Sensing*, *16*(4), 1–15. https://doi.org/10.3390/rs16040697

Gao, T., Nielsen, A. B., & Hedblom, M. (2015). Reviewing the strength of evidence of biodiversity indicators for forest ecosystems in Europe. *Ecological Indicators*, *57*, 420–434. https://doi.org/10.1016/j.ecolind.2015.05.028

Girardeau-Montaut, D. (2015). *CloudCompare version 2.6.1. user manual*. 181. http://www.danielgm.net/cc/

Godinho Cassol, H. L., De Oliveira E Cruz De Aragão, L. E., Moraes, E. C., De Brito Carreiras, J. M., & Shimabukuro, Y. E. (2021). Quad-pol Advanced Land Observing Satellite / Phased Array L-band Synthetic Aperture Radar-2 (ALOS/PALSAR-2) data for modelling secondary forest above-ground biomass in the central Brazilian Amazon. *International Journal of Remote Sensing*, *42*(13), 4989–5013. https://doi.org/10.1080/01431161.2021.1903615

Gollob, C., Ritter, T., & Nothdurft, A. (2020). Forest inventory with long range and high-speed personal laser scanning (PLS) and simultaneous localization and mapping (SLAM) technology. *Remote Sensing*, *12*(9), 1509.

Gonzalez de Tanago, J., Lau, A., Bartholomeus, H., Herold, M., Avitabile, V., Raumonen, P., Martius, C., Goodman, R. C., Disney, M., Manuri, S., Burt, A., & Calders, K. (2018). Estimation of above-ground biomass of large tropical trees with terrestrial LiDAR. *Methods in Ecology and Evolution*, *9*(2), 223–234. https://doi.org/10.1111/2041-210X.12904

Grisetti, G., Stachniss, C., & Burgard, W. (2007). Improved techniques for grid mapping with Rao-Blackwellized particle filters. *IEEE Transactions on Robotics*, *23*(1), 34–46. https://doi.org/10.1109/TRO.2006.889486

Guan, H., Li, J., Chapman, M., Deng, F., Ji, Z., & Yang, X. (2013). Integration of orthoimagery and lidar data for object-based urban thematic mapping using random forests. *International Journal of Remote Sensing, 34(14)*, 5166–5186.

Guarnieri, A., Pirotti, F., & Vettore, A. (2012). Comparison of Discrete Return and Waveform Terrestrial Laser Scanning for Dense Vegetation Filtering. *The International Archives of the Photogrammetry, Remote Sensing and Spatial Information Sciences*, *XXXIX-B7*(August), 511–516. https://doi.org/10.5194/isprsarchives-xxxix-b7-511-2012

Hackenberg, J., Spiecker, H., Calders, K., Disney, M., & Raumonen, P. (2015). SimpleTree - An efficient open source tool to build tree models from TLS clouds. *Forests*, *6*(11), 4245–4294. https://doi.org/10.3390/f6114245

Hallé, F., Oldeman, R. A. A., & Tomlinson, P. B. (1978). Opportunistic tree architecture. In *Tropical trees and forests* (pp. 269–331). Springer.

Hauglin, M., Astrup, R., Gobakken, T., & Næsset, E. (2013). Estimating single-tree branch biomass of Norway spruce with terrestrial laser scanning using voxel-based and crown dimension features. *Scandinavian Journal of Forest Research*, *28*(5), 456–469. https://doi.org/10.1080/02827581.2013.777772

Hess, W., Kohler, D., Rapp, H., & Andor, D. (2016). Real-time loop closure in 2D LIDAR SLAM. *2016 IEEE International Conference on Robotics and Automation (ICRA)*, 1271–1278.

Hofman, J., Bartholomeus, H., Calders, K., Van Wittenberghe, S., Wuyts, K., & Samson, R. (2014). On the relation between tree crown morphology and particulate matter deposition on urban tree leaves: A ground-based LiDAR approach. *Atmospheric Environment*, *99*(2014), 130–139. https://doi.org/10.1016/j.atmosenv.2014.09.031

Hofman, J., Bartholomeus, H., Janssen, S., Calders, K., Wuyts, K., Van Wittenberghe, S., & Samson, R. (2016). Influence of tree crown characteristics on the local PM10 distribution inside an urban street canyon in Antwerp (Belgium): A model and experimental approach. *Urban Forestry and Urban Greening*, *20*(2016), 265–276. https://doi.org/10.1016/j.ufug.2016.09.013

Hristov, N. I., Nikolaidis, D., Hubel, T. Y., & Allen, L. C. (2019). Estimating Overwintering Monarch Butterfly Populations Using Terrestrial LiDAR Scanning. *Frontiers in Ecology and Evolution*, *7*(July). https://doi.org/10.3389/fevo.2019.00266

Huang, H., Li, Z., Gong, P., Cheng, X., Clinton, N., Cao, C., Ni, W., & Wang, L. (2011). Automated methods for measuring DBH and tree heights with a commercial scanning lidar. *Photogrammetric Engineering and Remote Sensing*, *77*(3), 219–227. https://doi.org/10.14358/PERS.77.3.219

Hyyppä, E., Kukko, A., Kaijaluoto, R., White, J. C., Wulder, M. A., Pyörälä, J., Liang, X., Yu, X., Wang, Y., Kaartinen, H., Virtanen, J. P., & Hyyppä, J. (2020a). Accurate derivation of stem curve and volume using backpack mobile laser scanning. *ISPRS Journal of Photogrammetry and Remote Sensing*, *161*(November 2019), 246–262. https://doi.org/10.1016/j.isprsjprs.2020.01.018

Hyyppä, E., Kukko, A., Kaijaluoto, R., White, J. C., Wulder, M. A., Pyörälä, J., Liang, X., Yu, X., Wang, Y., Kaartinen, H., Virtanen, J. P., & Hyyppä, J. (2020b). Accurate derivation of stem curve and volume using backpack mobile laser scanning. *ISPRS Journal of Photogrammetry and Remote Sensing*, *161*(January), 246–262. https://doi.org/10.1016/j.isprsjprs.2020.01.018

Ji, Y., Huang, J., Ju, Y., Guo, S., & Yue, C. (2020). Forest structure dependency analysis of L-band SAR backscatter. *PeerJ*, *8*. https://doi.org/10.7717/peerj.10055

Jiang, T., Zhang, Q., Liu, S., Liang, C., Dai, L., Zhang, Z., Sun, J., & Wang, Y. (2023). LWSNet: A Point-Based Segmentation Network for Leaf-Wood Separation of Individual Trees. *Forests*, *14*(7). https://doi.org/10.3390/f14071303

Jurjevic, L., Gašparovic, M., Liang, X., & Balenovic, I. (2021). Assessment of close-range remote sensing methods for dtm estimation in a lowland deciduous forest. *Remote Sensing*, *13*(11). https://doi.org/10.3390/rs13112063

Kankare, V., Holopainen, M., Vastaranta, M., Puttonen, E., Yu, X., Hyyppä, J., Vaaja, M., Hyyppä, H., & Alho, P. (2013). Individual tree biomass estimation using terrestrial laser scanning. *ISPRS Journal of Photogrammetry and Remote Sensing*, *75*, 64–75. https://doi.org/10.1016/j.isprsjprs.2012.10.003

Karila, K., Yu, X., Vastaranta, M., Karjalainen, M., Puttonen, E., & Hyyppä, J. (2019). TanDEM-X digital surface models in boreal forest above-ground biomass change detection. *ISPRS Journal of Photogrammetry and Remote Sensing*, *148*, 174–183. https://doi.org/10.1016/j.isprsjprs.2019.01.002

Khati, U., & Singh, G. (2022). Combining L-band Synthetic Aperture Radar backscatter and TanDEM-X canopy height for forest aboveground biomass estimation. *Frontiers in Forests and Global Change*, *5*. https://doi.org/10.3389/ffgc.2022.918408

Knoke, T., Hahn, A., & Schneider, T. (2010). Linking Inventory and Forest Optimisation: Information and decision-making in forest management. *European Journal of Forest Research*, *129(5)*, 771–775. https://doi.org/10.1007/s10342-010-0398-8

Kohlbrecher, S., Von Stryk, O., Meyer, J., & Klingauf, U. (2011). A flexible and scalable SLAM system with full 3D motion estimation. *2011 IEEE International Symposium on Safety, Security, and Rescue Robotics*, 155–160.

Konolige, K., Grisetti, G., Kümmerle, R., Burgard, W., Limketkai, B., & Vincent, R. (2010). Efficient sparse pose adjustment for 2D mapping. *2010 IEEE/RSJ International Conference on Intelligent Robots and Systems*, 22–29.

Korom, A., Syukur, M. S., Jawan, A., Suratman, M. N., Jalloh, M. B., Jamian, M. A. H., & Abd Latif, Z. (2022). Understanding forest degradation-a review of forest structure indicators. *Borneo Akademika*, *6(1)*, 115–125.

Krisanski, S., Taskhiri, M. S., Aracil, S. G., Herries, D., Muneri, A., Gurung, M. B., Montgomery, J., & Turner, P. (2021). Forest structural complexity tool—an open source, fully-automated tool for measuring forest point clouds. *Remote Sensing*, *13*(22). https://doi.org/10.3390/rs13224677

Kukko, A., Kaartinen, H., Hyyppä, J., & Chen, Y. (2012). Multiplatform mobile laser scanning: Usability and performance. *Sensors*, *12*(9), 11712–11733.

Kukko, A., Kaijaluoto, R., Kaartinen, H., Lehtola, V. V., Jaakkola, A., & Hyyppä, J. (2017). Graph SLAM correction for single scanner MLS forest data under boreal forest canopy. *ISPRS Journal of Photogrammetry and Remote Sensing*, *132*, 199–209. https://doi.org/10.1016/j.isprsjprs.2017.09.006

Lau, A., Bentley, L. P., Martius, C., Shenkin, A., Bartholomeus, H., Raumonen, P., Malhi, Y., Jackson, T., & Herold, M. (2018). Quantifying branch architecture of tropical trees using terrestrial LiDAR and 3D modelling. *Trees - Structure and Function*, *32*(5), 1219–1231. https://doi.org/10.1007/s00468-018-1704-1

Liang, X., Kankare, V., Hyyppä, J., Wang, Y., Kukko, A., Haggrén, H., Yu, X., Kaartinen, H., Jaakkola, A., Guan, F., Holopainen, M., & Vastaranta, M. (2016). Terrestrial laser scanning in forest inventories. *ISPRS Journal of Photogrammetry and Remote Sensing*, *115*, 63–77. https://doi.org/10.1016/j.isprsjprs.2016.01.006

Liang, X., Kukko, A., Balenovic, I., Saarinen, N., Junttila, S., Kankare, V., Holopainen, M., Mokros, M., Surovy, P., Kaartinen, H., Jurjevic, L., Honkavaara, E., Nasi, R., Liu, J., Hollaus, M., Tian, J., Yu, X., Pan, J., Cai, S., … Hyyppa, J. (2022). Close-Range Remote Sensing of Forests: The state of the art, challenges, and opportunities for systems and data acquisitions. *IEEE Geoscience and Remote Sensing Magazine, 10(3)*, 32–71. https://doi.org/10.1109/MGRS.2022.3168135

Liang, X., Kukko, A., Hyyppä, J., Lehtomäki, M., Pyörälä, J., Yu, X., Kaartinen, H., Jaakkola, A., & Wang, Y. (2018). In-situ measurements from mobile platforms: An emerging approach to address the old challenges associated with forest inventories. *ISPRS Journal of Photogrammetry and Remote Sensing*, *143*, 97–107.

Liang, X., Litkey, P., Hyyppä, J., Kaartinen, H., Vastaranta, M., & Holopainen, M. (2012). Automatic stem mapping using single-scan terrestrial laser scanning. *IEEE Transactions on Geoscience and Remote Sensing*, *50*(2), 661–670. https://doi.org/10.1109/TGRS.2011.2161613

Liu, B., Chen, S., Huang, H., & Tian, X. (2022). Tree Species Classification of Backpack Laser Scanning Data Using the PointNet++ Point Cloud Deep Learning Method. *Remote Sensing*, *14*(15). https://doi.org/10.3390/rs14153809

Liao, Z., He, B., & Quan, X. (2020). Potential of texture from SAR tomographic images for forest aboveground biomass estimation. *International Journal of Applied Earth Observation and Geoinformation, 88*, 102049. https://doi.org/10.1016/j.jag.2020.102049

Machala, M., & Zejdová, L. (2014). Forest mapping through object-based image analysis of multispectral and LiDAR aerial data. *European Journal of Remote Sensing, 47(1)*, 117–131.

Małaszek, M., Zembrzuski, A., & Gajowniczek, K. (2022). Foresttaxator: a Tool for Detection and Approximation of Cross-Sectional Area of Trees in a Cloud of 3D Points. *Machine Graphics and Vision*, *31*(1–4), 19–48. https://doi.org/10.22630/MGV.2022.31.1.2

Marchi, N., Pirotti, F., & Lingua, E. (2018). Airborne and terrestrial laser scanning data for the assessment of standing and lying deadwood: Current situation and new perspectives. *Remote Sensing*, *10*(9). https://doi.org/10.3390/rs10091356

Marselis, S. M., Tang, H., Armston, J. D., Calders, K., Labrière, N., & Dubayah, R. (2018). Distinguishing vegetation types with airborne waveform lidar data in a tropical forest-savanna mosaic: A case study in Lopé National Park, Gabon. *Remote Sensing of Environment*, *216*(January), 626–634. https://doi.org/10.1016/j.rse.2018.07.023

Melin, M., Matala, J., Mehtätalo, L., Tiilikainen, R., Tikkanen, O. P., Maltamo, M., Pusenius, J., & Packalen, P. (2014). Moose (Alces alces) reacts to high summer temperatures by utilizing thermal shelters in boreal forests - an analysis based on airborne laser scanning of the canopy structure at moose locations. *Global Change Biology*, *20(4)*, 1115–1125. https://doi.org/10.1111/gcb.12405

Mengesha, T., Hawkins, M., & Nieuwenhuis, M. (2015). Validation of terrestrial laser scanning data using conventional forest inventory methods. *European Journal of Forest Research*, *134*(2), 211–222. https://doi.org/10.1007/s10342-014-0844-0

Mohite, J., Sawant, S., Pandit, A., Sakkan, M., Pappula, S., & Parmar, A. (2024). Forest aboveground biomass estimation by GEDI and multi-source EO data fusion over Indian forest. *International Journal of Remote Sensing*, *45*(4), 1304–1338. https://doi.org/10.1080/01431161.2024.2307944

Moskal, L. M., & Zheng, G. (2012). Retrieving forest inventory variables with terrestrial laser scanning (TLS) in urban heterogeneous forest. *Remote Sensing*, *4*(1), 1–20. https://doi.org/10.3390/rs4010001

Muhojoki, J., Hakala, T., Kukko, A., Kaartinen, H., & Hyyppä, J. (2024). Comparing positioning accuracy of mobile laser scanning systems under a forest canopy. *Science of Remote Sensing*, *9*(February). https://doi.org/10.1016/j.srs.2024.100121

Mur-Artal, R., Montiel, J. M. M., & Tardos, J. D. (2015). ORB-SLAM: A Versatile and Accurate Monocular SLAM System. *IEEE Transactions on Robotics*, *31*(5), 1147–1163. https://doi.org/10.1109/TRO.2015.2463671

Murino, V., & Puppo, E. (2015). Image Analysis and Processing – ICIAP 2015: 18th International Conference Genoa, Italy, September 7–11, 2015 Proceedings, Part I. *Lecture Notes in Computer Science (Including Subseries Lecture Notes in Artificial Intelligence and Lecture Notes in Bioinformatics)*, *9279*, 343–353. https://doi.org/10.1007/978-3-319-23231-7

Narvaes, I. da S., Santos, J. R. dos, Bispo, P. da C., Graça, P. M. de A., Guimarães, U. S., & Gama, F. F. (2023). Estimating Forest Above-Ground Biomass in Central Amazonia Using Polarimetric Attributes of ALOS/PALSAR Images. *Forests*, *14*(5). https://doi.org/10.3390/f14050941

Palace, M., Sullivan, F. B., Ducey, M., & Herrick, C. (2016). Estimating Tropical Forest Structure Using a Terrestrial Lidar. *Plos One*, *11*(4), e0154115. https://doi.org/10.1371/journal.pone.0154115

Pérez-Martín, E., Medina, S. L. C., Herrero-Tejedor, T., Pérez-Souza, M. A., de Mata, J. A., & Ezquerra-Canalejo, A. (2021). Assessment of tree diameter estimation methods from mobile laser scanning in a historic garden. *Forests, 12(8)*, 1–17. https://doi.org/10.3390/f12081013

Perugia, B. Del, Giannetti, F., Chirici, G., & Travaglini, D. (2019). Influence of scan density on the estimation of single-tree attributes by hand-held mobile laser scanning. *Forests, 10(3)*, 1–13. https://doi.org/10.3390/f10030277

Petrie, G., & Toth, C. K. (2017). Terrestrial laser scanners. In *Topographic Laser Ranging and Scanning* (pp. 87–128). CRC Press.

Pierzchała, M., Giguère, P., & Astrup, R. (2018). Mapping forests using an unmanned ground vehicle with 3D LiDAR and graph-SLAM. *Computers and Electronics in Agriculture*, *145*(January), 217–225. https://doi.org/10.1016/j.compag.2017.12.034

Pirotti, F., Guarnieri, A., & Vettore, A. (2013). Ground filtering and vegetation mapping using multi-return terrestrial laser scanning. *ISPRS Journal of Photogrammetry and Remote Sensing*, *76*, 56–63. https://doi.org/10.1016/j.isprsjprs.2012.08.003

Pohjavirta, O., Liang, X., Wang, Y., Kukko, A., Pyörälä, J., Hyyppä, E., Yu, X., Kaartinen, H., & Hyyppä, J. (2022). Automated registration of wide-baseline point clouds in forests using discrete overlap search. *Forest Ecosystems, 9*, 100080.

Pueschel, P., Newnham, G., Rock, G., Udelhoven, T., Werner, W., & Hill, J. (2013). The influence of scan mode and circle fitting on tree stem detection, stem diameter and volume extraction from terrestrial laser scans. *ISPRS Journal of Photogrammetry and Remote Sensing*, *77*, 44–56. https://doi.org/10.1016/j.isprsjprs.2012.12.001

Ratajczak, Z., Carpenter, S. R., Ives, A. R., Kucharik, C. J., Ramiadantsoa, T., Stegner, M. A., Williams, J. W., Zhang, J., & Turner, M. G. (2018). Abrupt Change in Ecological Systems: Inference and Diagnosis. *Trends in Ecology and Evolution*, *33*(7), 513–526. https://doi.org/10.1016/j.tree.2018.04.013

Rocchini, D., Salvatori, N., Beierkuhnlein, C., Chiarucci, A., de Boissieu, F., Förster, M., Garzon-Lopez, C. X., Gillespie, T. W., Hauffe, H. C., He, K. S., Kleinschmit, B., Lenoir, J., Malavasi, M., Moudrý, V., Nagendra, H., Payne, D., Šímová, P., Torresani, M., Wegmann, M., & Féret, J. B. (2021). From local spectral species to global spectral communities: A benchmark for ecosystem diversity estimate by remote sensing. *Ecological Informatics*, *61*(November 2020). https://doi.org/10.1016/j.ecoinf.2020.101195

Ryding, J., Williams, E., Smith, M. J., & Eichhorn, M. P. (2015). Assessing handheld mobile laser scanners for forest surveys. *Remote Sensing*, *7*(1), 1095–1111.

Santoro, M., Cartus, O., Fransson, J. E. S., & Wegmüller, U. (2019). Complementarity of X-, C-, and L-band SAR backscatter observations to retrieve forest stem volume in boreal forest. *Remote Sensing*, *11*(13). https://doi.org/10.3390/rs11131563

Shao, J., Zhang, W., Mellado, N., Wang, N., Jin, S., Cai, S., Luo, L., Lejemble, T., & Yan, G. (2020). SLAM-aided forest plot mapping combining terrestrial and mobile laser scanning. *ISPRS Journal of Photogrammetry and Remote Sensing*, *163*(May 2019), 214–230. https://doi.org/10.1016/j.isprsjprs.2020.03.008

Sinha, S., Mohan, S., Das, A. K., Sharma, L. K., Jeganathan, C., Santra, A., Santra Mitra, S., & Nathawat, M. S. (2020). Multi-sensor approach integrating optical and multi-frequency synthetic aperture radar for carbon stock estimation over a tropical deciduous forest in India. *Carbon Management*, *11*(1), 39–55. https://doi.org/10.1080/17583004.2019.1686931

Solberg, S., Bollandsås, O. M., Gobakken, T., Næsset, E., Basak, P., & Duncanson, L. I. (2024). Biomass Change Estimated by TanDEM-X Interferometry and GEDI in a Tanzanian Forest. *Remote Sensing*, *16*(5). https://doi.org/10.3390/rs16050861

Srinivasan, S., Popescu, S. C., Eriksson, M., Sheridan, R. D., & Ku, N. W. (2014). Multi-temporal terrestrial laser scanning for modeling tree biomass change. *Forest Ecology and Management*, *318*, 304–317. https://doi.org/10.1016/j.foreco.2014.01.038

Stein, A., Gerstner, K., & Kreft, H. (2014). Environmental heterogeneity as a universal driver of species richness across taxa, biomes and spatial scales. *Ecology Letters*, *17(7)*, 866–880. https://doi.org/10.1111/ele.12277

Stobo-Wilson, A. M., Murphy, B. P., Cremona, T., Carthew, S. M., & Levick, S. R. (2021). Illuminating den-tree selection by an arboreal mammal using terrestrial laser scanning in northern Australia. *Remote Sensing in Ecology and Conservation*, *7*(2), 154–168. https://doi.org/10.1002/rse2.177

Stovall, A. E. L., MacFarlane, D. W., Crawford, D., Jovanovic, T., Frank, J., & Brack, C. (2023). Comparing mobile and terrestrial laser scanning for measuring and modelling tree stem taper.

Forestry: An International Journal of Forest Research, *96*(5), 705–717. https://doi.org/10.1093/forestry/cpad012

Stovall, A. E. L., Vorster, A., Anderson, R., & Evangelista, P. (2023). Developing nondestructive species-specific tree allometry with terrestrial laser scanning. *Methods in Ecology and Evolution*, *14*(1), 280–290. https://doi.org/10.1111/2041-210X.14027

Tamiminia, H., Salehi, B., Mahdianpari, M., Beier, C. M., & Johnson, L. (2022). Evaluating pixel-based and object-based approaches for forest above-ground biomass estimation using a combination of optical, sar, and an extreme gradient boosting model. *ISPRS Annals of the Photogrammetry, Remote Sensing and Spatial Information Sciences*, *5*(3), 485–492. https://doi.org/10.5194/isprs-Annals-V-3-2022-485-2022

Terryn, L., Calders, K., Åkerblom, M., Bartholomeus, H., Disney, M., Levick, S., Origo, N., Raumonen, P., & Verbeeck, H. (2023). Analysing individual 3D tree structure using the R package ITSMe. *Methods in Ecology and Evolution*, *14*(1), 231–241. https://doi.org/10.1111/2041-210X.14026

Toivonen, J., Kangas, A., Maltamo, M., Kukkonen, M., & Packalen, P. (2023). Assessing biodiversity using forest structure indicators based on airborne laser scanning data. *Forest Ecology and Management*, *546*(September), 121376. https://doi.org/10.1016/j.foreco.2023.121376

Trochta, J., Kruček, M., Vrška, T., & Kraâl, K. (2017). 3D Forest: An application for descriptions of three-dimensional forest structures using terrestrial LiDAR. *PLoS ONE*, *12*(5), 1–17. https://doi.org/10.1371/journal.pone.0176871

Tupinambá-Simões, F., Pascual, A., Guerra-Hernández, J., Ordóñez, C., de Conto, T., & Bravo, F. (2023). Assessing the Performance of a Handheld Laser Scanning System for Individual Tree Mapping—A Mixed Forests Showcase in Spain. *Remote Sensing*, *15*(5). https://doi.org/10.3390/rs15051169

Turner, W., Spector, S., Gardiner, N., Fladeland, M., Sterling, E., & Steininger, M. (2003). Remote sensing for biodiversity science and conservation. *Trends in Ecology and Evolution*, *18(6)*, 306–314. https://doi.org/10.1016/S0169-5347(03)00070-3

Using, M., Laser, T., & Data, S. (2023). Volume Estimation of Stem Segments Based on a Tetrahedron Model Using Terrestrail Laser Scanning Data. *Remote Sensing*, *15*(20), 5060. https://doi.org/https://doi.org/10.3390/rs15205060

Vandendaele, B., Martin-Ducup, O., Fournier, R. A., Pelletier, G., & Lejeune, P. (2022). Mobile Laser Scanning for Estimating Tree Structural Attributes in a Temperate Hardwood Forest. *Remote Sensing*, *14*(18). https://doi.org/10.3390/rs14184522

Vatandaşlar, C., & Abdikan, S. (2022). Carbon stock estimation by dual-polarized synthetic aperture radar (SAR) and forest inventory data in a Mediterranean forest landscape. *Journal of Forestry Research*, *33*(3), 827–838. https://doi.org/10.1007/s11676-021-01363-3

Velasco Pereira, E. A., Varo Martínez, M. A., Ruiz Gómez, F. J., & Navarro-Cerrillo, R. M. (2023). Temporal Changes in Mediterranean Pine Forest Biomass Using Synergy Models of ALOS PALSAR-Sentinel 1-Landsat 8 Sensors. *Remote Sensing*, *15*(13). https://doi.org/10.3390/rs15133430

Verbeeck, H., Bauters, M., Jackson, T., Shenkin, A., Disney, M., & Calders, K. (2019). Time for a Plant Structural Economics Spectrum. *Frontiers in Forests and Global Change*, *2*(August), 1–5. https://doi.org/10.3389/ffgc.2019.00043

Wang, D. (2020). Unsupervised semantic and instance segmentation of forest point clouds. *ISPRS Journal of Photogrammetry and Remote Sensing*, *165*(November 2019), 86–97. https://doi.org/10.1016/j.isprsjprs.2020.04.020

Wang, F., Sun, Y., Jia, W., Li, D., Zhang, X., Tang, Y., & Guo, H. (2023). A Novel Approach to Characterizing Crown Vertical Profile Shapes Using Terrestrial Laser Scanning (TLS). *Remote Sensing*, *15*(13). https://doi.org/10.3390/rs15133272

Wu, Y., Mao, Z., Guo, L., Li, C., & Deng, L. (2023). Forest Volume Estimation Method Based on Allometric Growth Model and Multisource Remote Sensing Data. *IEEE Journal of Selected Topics in Applied Earth Observations and Remote Sensing*, *16*, 8900–8912. https://doi.org/10.1109/JSTARS.2023.3313251

Wu, Z., Yao, F., Zhang, J., Ma, E., Yao, L., & Dong, Z. (2024). Genetic Programming Guided Mapping of Forest Canopy Height by Combining LiDAR Satellites with Sentinel-1/2, Terrain, and Climate Data. *Remote Sensing*, *16*(1). https://doi.org/10.3390/rs16010110

Xi, Z., Hopkinson, C., & Chasmer, L. (2016). Automating plot-level stem analysis from terrestrial laser scanning. *Forests*, *7*(11), 1–20. https://doi.org/10.3390/f7110252

Xu, D., Wang, H., Xu, W., Luan, Z., & Xu, X. (2021). LiDAR applications to estimate forest biomass at individual tree scale: Opportunities, challenges and future perspectives. *Forests*, *12*(5), 1–19. https://doi.org/10.3390/f12050550

You, L., Sun, Y., Liu, Y., Chang, X., Jiang, J., Feng, Y., & Song, X. (2023). Tree Skeletonization with DBSCAN Clustering Using Terrestrial Laser Scanning Data. *Forests*, *14*(8), 1–17. https://doi.org/10.3390/f14081525

Yu, X., Liang, X., Hyyppä, J., Kankare, V., Vastaranta, M., & Holopainen, M. (2013). Stem biomass estimation based on stem reconstruction from terrestrial laser scanning point clouds. *Remote Sensing Letters*, *4*(4), 344–353. https://doi.org/10.1080/2150704X.2012.734931

Yurtseven, H., Çoban, S., Akgül, M., & Akay, A. O. (2019). Individual tree measurements in a planted woodland with terrestrial laser scanner. *Turkish Journal of Agriculture and Forestry*, *43*(2), 192–208. https://doi.org/10.3906/tar-1805-5

Zeybek, M., & Vatandaşlar, C. (2021). An automated approach for extracting forest inventory data from individual trees using a handheld mobile laser scanner. *Croatian Journal of Forest Engineering*, *42*(3), 515–528. https://doi.org/10.5552/crojfe.2021.1096

Zhang, J., & Singh, S. (2014). LOAM: Lidar Odometry and Mapping in Real-time. *Robotics: Science and Systems*, *2*(9).

Zhang, T., Lin, H., Long, J., Zheng, H., Ye, Z., & Liu, Z. (2023). Evaluating the Sensitivity of Polarimetric Features Related to Rotation Domain and Mapping Chinese Fir AGB Using Quad-Polarimetric SAR Images. *Remote Sensing*, *15*(6). https://doi.org/10.3390/rs15061519

Zheng, S., Wang, J., Rizos, C., Ding, W., & El-Mowafy, A. (2023). Simultaneous Localization and Mapping (SLAM) for Autonomous Driving: Concept and Analysis. *Remote Sensing*, *15(4)*, 1–41. https://doi.org/10.3390/rs15041156

Zhong, L., Cheng, L., Xu, H., Wu, Y., Chen, Y., & Li, M. (2017). Segmentation of Individual Trees from TLS and MLS Data. *IEEE Journal of Selected Topics in Applied Earth Observations and Remote Sensing*, *10*(2), 774–787. https://doi.org/10.1109/JSTARS.2016.2565519

Zhou, S., He, G., Kang, F., Li, W., Kan, J., & Zheng, Y. (2019). Extracting diameter at breast height with a handheld mobile liDAR system in an outdoor environment. *Sensors (Switzerland), 19(14)*. https://doi.org/10.3390/s19143212